

# **Functional nanofibres for regenerative medicine**

Dissertation zur Erlangung des naturwissenschaftlichen Doktorgrades der  
Julius-Maximilians-Universität Würzburg

vorgelegt von

Diplom-Chemiker

**Karl-Heinz Heffels**

aus Geilenkirchen

Würzburg 2012



Eingereicht bei der Fakultät für Chemie und Pharmazie am

\_\_\_\_\_

Gutachter der schriftlichen Arbeit

1. Gutachter: \_\_\_\_\_

2. Gutachter: \_\_\_\_\_

Prüfer des öffentlichen Promotionskolloquiums

1. Prüfer: \_\_\_\_\_

2. Prüfer: \_\_\_\_\_

3. Prüfer: \_\_\_\_\_

Datum des öffentlichen Promotionskolloquiums

\_\_\_\_\_

Doktorurkunde ausgehändigt am

\_\_\_\_\_



***“I do not know what I may appear to the world,  
but to myself I seem to have been only like a boy playing on the sea-shore,  
and diverting myself in now and then finding a smoother pebble or a prettier shell than  
ordinary, whilst the great ocean of truth lay all undiscovered before me.”***

Sir Isaac Newton, 1642–1727



# Table of contents

<b>List of abbreviations</b>			VIII
<b>CHAPTER</b>	<b>1</b>	Introduction	1
<b>CHAPTER</b>	<b>2</b>	State of the art	5
	<b>I</b>	<b>Material development</b>	
<b>CHAPTER</b>	<b>3</b>	Development and characterisation of ECM mimicking fibres	35
<b>CHAPTER</b>	<b>4</b>	Functionalised fibres for advanced ECM mimicry	69
	<b>II</b>	<b><i>In vitro</i> examination</b>	
<b>CHAPTER</b>	<b>5</b>	Response of human dermal fibroblasts to RGD-functionalised fibres	89
<b>CHAPTER</b>	<b>6</b>	Interaction and differentiation of chondrocytes on electrospun fibres modified with cartilage derived peptides	101
<b>CHAPTER</b>	<b>7</b>	Immune response of monocytes and macrophages on 2D and 3D hydrogel surfaces and fibres based on NCO-sP(EO- <i>stat</i> -PO)	137
	<b>III</b>	<b><i>In vivo</i> examination</b>	
<b>CHAPTER</b>	<b>8</b>	<i>In vivo</i> Biocompatibility of NCO-sP(EO- <i>stat</i> -PO)/PLGA/Prolene®-meshes for the treatment of diaphragmatic hernias	153
<b>Summary</b>			167
<b>Zusammenfassung</b>			170
<b>Acknowledgement</b>			174
<b>List of publications</b>			176
<b>Conferences</b>			177
<b>Curriculum Vitae</b>			179

## List of abbreviations

%	percent
$(n_e)_{soln}$	entanglement number
°	degree
°C	degrees centigrade
∅	average
μL	microliter
μm	micrometre
μS	micro Siemens
27E10	pro-inflammatory marker of macrophages
2D	two-dimensional
3D	three-dimensional
Å	Ångstrom
BSA	bovine serum albumin
$c^*$	critical chain overlap concentration
CA	contact angle
CD163	cluster of differentiation 163
cDNA	complementary DNA
$C_e$	entanglement concentration
cm	centimetre
D	chondrocytes originating from the "deep zone" of articular cartilage
DAPI	2-(4-amidinophenyl)-1H-indole-6-carboxamide
dl/g	inherent viscosity
DMF	N,N-dimethylformamide
DMMB	1,9-dimethylmethylen blue
DMSO	dimethyl sulfoxide
DNA	desoxyribonucleic acid
dsDNA	double stranded desoxyribonucleic acid
ECM	extracellular matrix
EDTA	2,2',2'',2'''-(Ethane-1,2-diyldinitrilo)tetraacetic acid
e-field	electric field



EHD	electrohydrodynamics
ELISA	Enzyme Linked Immunosorbent Assay
e-PTFE	expanded poly(tetrafluor ethylene)
FBS	foetal bovine serum
FCS	foetal calf serum
FDA	Food and Drug Administration
FITC	fluorescein isothiocyanate
GAG	glycosaminoglycan
GPC	gel permeation chromatography
GRGDS	peptide glycine-arginine-glycine-aspartic acid-serine
GRGES	peptide glycine-arginine-glycine-glutamic acid-serine
h	hour
hdF	human dermal fibroblasts
HEPES	2-[4-(2-hydroxyethyl)piperazin-1-yl]ethanesulfonic acid
HPLC	high performance liquid chromatography
HV	high voltage
Hz	Hertz
i.e.	that is
IPDI	isophorone diisocyanate
IQR	interquartile range
kDa	kilo Dalton
kGy	kilo Gray
kN	kilo Newton
kV	kilo Volt
LDL	low-density lipoprotein
m	meter
M	chondrocytes originating from the "middle zone" of articular cartilage
M1	pro-inflammatory macrophage phenotype
M2	healing macrophage phenotype
MARCO	scavenger receptor with collageneous structure
mg	milligram
min	minute

## List of abbreviations

---

mL	millilitre
mm	millimetre
MMP	matrix metalloproteinase
$M_n$	number average molecular weight
mN	milli Newton
mol	unit of the amount of substance n
mRNA	messenger RNA
ms	milliseconds
$M_w$	weight average molecular weight
n	amount of substance
NA	neutraavidin
NaCl	sodium chloride
NCO	isocyanate group
ng	nanogram
NH <sub>2</sub>	amino group
nm	nanometre
Pa	Pascal
PBE	phosphate buffered EDTA
PBS	phosphate buffered saline
PCL	poly(caprolactone)
PDI	poly dispersity index
PEG	poly(ethylene glycol)
PEO	poly(ethylene oxide)
PFB	pentafluorobenzaldehyde
pg	picogram
PGA	poly(glycolic acid)
pH	negative decadic logarithm of H <sup>+</sup> ion concentration
pI	isoelectric point of a protein
PLA	poly(lactide acid)
PLGA	poly(lactide-co-glycolide)
PMMA	poly(methyl methacrylate)
PP	poly(propylene)

PRG4	proteoglycan 4, lubricin
PS	polystyrene
PVA	poly(vinyl alcohol)
PVC	poly(vinyl chloride)
PVP	poly(vinyl pyrrolidone)
qRT-PCR	quantitative real-time polymerase chain reaction
r.h.	relative humidity
RGD	peptide arginine-glycine-aspartic acid
RNA	ribonucleic acid
rpm	revolutions per minute
s	second
S	chondrocytes originating from the "superficial zone" of articular cartilage
SA	streptavidin
SDS	sodium dodecyl sulphate
SEM	scanning electron microscopy
TCPS	tissue culture polystyrene
TE	tissue engineering
TFA	trifluoro acetic acid
Tg	glass transition temperature
THF	tetrahydrofuran
UV	ultraviolet
v/v	volume per volume
w/v	weight per volume
wrt	with relation to
wt	weight
XPS	X-ray Photoelectron Spectroscopy
$\gamma$	surface tension
$\epsilon$	porosity
$\epsilon_r$	dielectric constant
$\rho_{\text{mesh}}$	mesh density
$\bar{c}$	mean coverage, defined as the expected numbers of fibres covering a point in the plane of the network



# CHAPTER 1

---

## Scope and structure of the thesis

Polymers of all kind are part of the everyday life of mankind. Since the 1950s the superior properties of polymers gave rise to their tremendous use in fields as diverse as: construction; the automotive industry; household aids; packaging; and medicine. This list can be continued and it is obvious that without forfeiting a high quality of life, daily life cannot be imagined without these materials. Focusing on the medical sector, we find examples such as: blood bags made from poly(vinyl chloride) (PVC) [1]; hernia meshes made from expanded poly(tetrafluor ethylene) (e-PTFE) [2] and poly propylene [3]; or degradable surgical sutures made from aliphatic polyesters such as poly(lactide-co-glycolide) (PLGA) [4]. These materials play an important role in the development of modern medical treatments and supporting therapies for various diseases.

During the last two decades medical research has moved on from biomaterial-only treatments to cell supported approaches [5, 6]. The term “regenerative medicine” was coined with this development and one aspect of this approach, a new interdisciplinary research field called “tissue engineering” (TE) was established [7]. These approaches seek to exceed a mere “tissue repair” strategy in medical treatment, which focuses on the “replacement of lost tissue by granulation tissue which matures to form scar tissue” [8]. The concept of “regeneration” includes an endpoint to a healing process which incorporates restoration of tissue to fully functional organs [9]. To pursue this aim, cells (preferably

pluripotent stem cells) are used to differentiate and grow into the desired tissue with or without the help of a support scaffold that contains the cell suspension. Various definitions on “regenerative medicine” have been proposed. Most of them are lengthy as they try to encompass the topic in its entirety [10-12]. Mason and Dunnill created a simple and concise, but comprehensive, definition that captures this continuously evolving field: “*Regenerative medicine replaces or regenerates human cells, tissue or organs, to restore or establish normal function*” [13]. Successful TE requires collaboration between a diverse range of research fields from chemistry, materials science and biology to biomedical engineering, medical, veterinary and transplantation sciences. The first step in the development of scaffold-based TE concepts involves the selection of an appropriate material that is processed into a structural scaffold. In combination with viable cells and eventually biomolecules a so-called tissue-engineered construct (TEC) results. The goal is for implantation of the TEC *in vivo* to replace or regenerate lost or damaged tissue. Before a TEC may finally be marketed, extensive *in vitro* biocompatibility tests, animal studies and clinical trials have to be passed [7].

This thesis describes the development and characterisation of a fibrous scaffold for TE purposes. The target of the design of the scaffold structure is to mimic characteristic cell environment features found in soft tissues, including: the presence of fibres such as hyaluronan, glycosaminoglycans and proteins [14]. The electro-hydrodynamic process of electrospinning proved to be a suitable means to generate fibrous polymeric materials, regardless of their functionality, which mimic these structures [15].

The first part of the dissertation (**Development and characterisation of ECM mimicking fibres**) focuses on the development and characterisation of a fibrous network (scaffold) produced by electrospinning (**Chapter 3**). The choice of the deployed polymers determines their functionality and interaction with proteins and cells. **Chapter 4** explores both passive interactions such as protein adsorption and active interaction possibilities by selective chemical functionalisation of the electrospun fibres.

An easy functionalisation method, developed in Chapter 4, is widely used in the second part “***In vitro* studies of NCO-sP(EO-stat-PO) based scaffolds**” of this thesis. Here, the biological interactions of cells with functionalised and non-functionalised fibres are investigated *in vitro*. Each chapter focuses on a specific cell type and reports on the observed cell adhesion,

migration and biochemical signalling of the cells. **Chapter 5** proves the concept of cell-fibre interactions with primary human dermal fibroblasts adhering to RGD-modified fibres. Furthermore, a correlation is discovered between the magnitude of fibre functionalisation and cell-scaffold interactions. A possible application of the fibrous scaffolds in cartilage regeneration is examined in **Chapter 6**. Primary human chondrocytes are cultured on scaffolds with different fibre modifications, mimicking the extracellular environment of superficial chondrocytes. Cell morphology and mRNA expression are used to characterize cell re-differentiation. The success of a TEC does not only depend on the optimal interaction between the targeted cell type and the scaffold, moreover the immunologic response largely affects the fate of an implant. Hence, the immune response of macrophages on electrospun fibres is analysed in **Chapter 7**. The cytokine release depending on the substrate morphology, comparing two-dimensional and three-dimensional situations, was monitored and correlated to a pro-inflammatory or healing phenotype of macrophages.

In the last part of the thesis (***In vivo* studies of NCO-sP(EO-stat-PO) based scaffolds**) the acquired knowledge is incorporated into the *in vivo* treatment of a diaphragmatic hernia. A stepwise development from a non-degradable polypropylene macrofibrous mesh to an airtight construct of macrofibres and nanofibres is presented in **Chapter 8**. Finally, these scaffolds are investigated in a rabbit model to test the *in vivo* compatibility of the scaffolds.

## References

- [1] Carmen R., 'The Selection of Plastic Materials for Blood Bags', *Transfusion Medicine Reviews*, 7, **1993**, 1-10.
- [2] Maximo D., 'Hernia Repair with Expanded Polytetrafluoroethylene', *The American Journal of Surgery*, 163, **1992**, 422-424.
- [3] Cobb W. S., Kercher K. W. and Heniford B. T., 'The Argument for Lightweight Polypropylene Mesh in Hernia Repair', *Surgical Innovation*, 12, **2005**, 63-69.
- [4] Middleton J. C. and Tipton A. J., 'Synthetic Biodegradable Polymers as Orthopedic Devices', *Biomaterials*, 21, **2000**, 2335-2346.
- [5] Niklason L. E., 'Replacement Arteries Made to Order', *Science*, 286, **1999**, 1493-1494.
- [6] Hutmacher D. W., 'Scaffolds in Tissue Engineering Bone and Cartilage', *Biomaterials*, 21, **2000**, 2529-2543.
- [7] Foundation N. S., 'The Emergence of Tissue Engineering as a Research Field', (U.S.A, 2004).
- [8] Walter J. B., Talbot, I C, Gardner, H A, *General Pathology (7th Edition)* (NY, USA: Churchill Livingstone, 1996).
- [9] Yannas I. V., *Tissue and Organ Regeneration in Adults* Springer Publishing, 2007).
- [10] Haseltine W. A., 'The Emergence of Regenerative Medicine: A New Field and a New Society', *e-biomed: The Journal of Regenerative Medicine*, 2, **2001**, 17-23.
- [11] Mironov V., Visconti R. and Markwald R., 'What Is Regenerative Medicine? Emergence of Applied Stem Cell and Developmental Biology', *Expert Opinion on Biological Therapy*, 4, **2004**, 773-781.
- [12] Greenwood H. L., Thorsteinsdottir H., Perry G., Renihan J., Singer P. and Daar A., 'Regenerative Medicine: New Opportunities for Developing Countries', *International Journal of Biotechnology*, 8, **2006**, 60-77.
- [13] Mason C. and Dunnill P., 'A Brief Definition of Regenerative Medicine', *Regenerative Medicine*, 3, **2008**, 1-5.
- [14] Aumailley M. and Gayraud B., 'Structure and Biological Activity of the Extracellular Matrix', *Journal of Molecular Medicine*, 76, **1998**, 253-265.
- [15] Li W. J., Laurencin C. T., Caterson E. J., Tuan R. S. and Ko F. K., 'Electrospun Nanofibrous Structure: A Novel Scaffold for Tissue Engineering', *Journal of Biomedical Materials Research*, 60, **2002**, 613-621.



# CHAPTER 2

---

## State of the Art

### 1 Electrohydrodynamics

Processes involving charged particles are omnipresent in nature. Phenomena such as charge separation when water particles hit obstacles were observed by Lenard as early as 1892 [1-3]. Spindrift and charged particles from sea surf are similar examples [4]. The opposite effect, when surface charges cause particle spraying, occurs on tree needles or leaves: the wax coated leaves emanate aerosol particles that are seen as a blue haze above forests [5]. All these environmental phenomena are examples of “electrohydrodynamics” (EHD) that can be defined as the study of dynamics of electrically charged liquids. When subject to an electric field, the transport and distribution of charges within a liquid generate stresses that cause it to move. Following the first observations of liquid spraying between 1600 and 1900 [6-8], the first systematic studies on EHD were performed by John Zeleny at the beginning of the 20<sup>th</sup> century [9, 10]. He described electrostatic spraying (electrospraying) phenomena of predominantly Newtonian fluids with electrified surfaces and linked the nature of solvent, high voltage and flow rate to the spray.

In contrast to Newtonian fluids, viscoelastic fluids may form fibres on the basis of the same EHD principle. Formhals was the first to patent the process in 1934 to prepare “artificial threads” out of cellulose acetate [11]. More patents followed with methods to continuously collect spun fibres. On the basis of the fibrous product the terminology of electrostatic

spinning or simply “electrospinning” evolved. Theoretical knowledge about jet formation and process control was not gained until several decades later when Vonnegut and Neubauer revisited these phenomena [12]. After their observations on different spraying modes, G.I. Taylor investigated the deformation of a charged droplet to a cone in the 1960s [13, 14]. Since then several cone- and jet-modes were characterised in EHD processes [15] and models were proposed to describe the phenomena [16-18].

Interest in the EHD processes of electro spraying and especially electrospinning has risen dramatically during the last two decades, beginning with a series of papers from Reneker *et al.* [19-23]. The wide spread possibilities for applications of electrospun fibres such as the production of non-woven fabrics, non-wetting fibres in ordinary textiles, filtration membranes or wound dressings has propelled scientific interest in this widely unexplored field. Nowadays, various polymeric materials [24] have been spun and find applications as smart textiles [25], sensors and actuators [26-29], optoelectronics [30, 31], piezoelectric energy generators [32] and in energy storage [33]. In the biological-medical field the use of electrospun fibres as scaffolds for TE [34-38] and as drug delivery devices [39, 40] is being pursued. The design of such TE scaffolds requires knowledge about desired fibre morphology and functionality which will be addressed in chapter 3. The following paragraphs will focus on the EHD process of “electrospinning”, providing details on the mechanisms and influence of process parameters which control fibre production.

## **2 Electrospinning process**

The essential elements required to produce nanofibres using electrostatic forces are depicted in Figure 1. They consist of a polymer solution or melt, a capillary or “spinneret” through which the fluid is pumped, a high voltage source and a grounded target. A syringe pump can be used to provide constant flow at a defined speed or alternatively, gravity or pressurised gas may be used to force polymer solutions through the capillary. The fluid is charged with either positive or negative polarity by immersing an electrode into the solution or by contacting the spinneret if a metal needle is used. Pendant droplets emerging from the spinneret tip are deformed as the effect of like charges in the liquid increases. The deformation is influenced by two competing forces: surface tension favours spherical shapes with small surface areas whereas coulomb repulsion results in large surface areas. With rising charge the droplet deforms into a conical shape. As the electrostatic forces exceed the

surface tension of the liquid a jet is initiated at the apex of the meniscus. The path of the jet is sketched in Figure 2.

The jet is accelerated towards a grounded or oppositely charged target in a straight line until an electrically driven bending instability occurs. The jet thins along its path, leading to increasing charge density on the surface. The mutual repulsion of like charges on the surface of the jet causes it to bend, resulting in the observed “whipping” process [41]. In contrast to multiple threads observed in electrostatic spraying [14], the use of high speed cameras has revealed that the jet does not split, rather it remains coherent while bending and turning rapidly [42, 43].

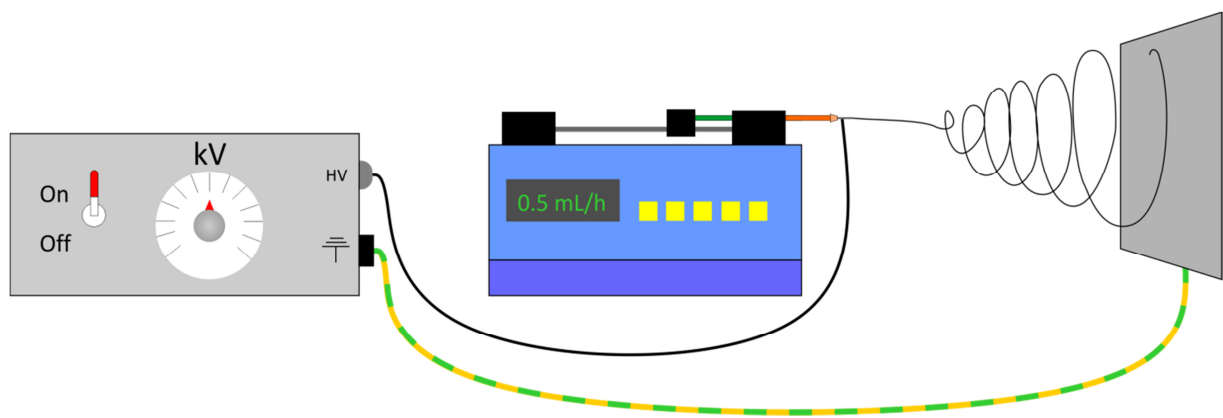


**Figure 1:** A simple Electrospinning setup consisting of a syringe pump, high voltage (HV) generator and a grounded collector.

The jet is subject to several opposing forces that influence the morphology of the resulting fibres. Surface tension tends to reduce the free surface energy by minimizing the jet surface area. Whereas Newtonian liquid jets without electric forces tend to break up into droplets [44] due to “Rayleigh instabilities”, viscoelastic jets generate beads-on-strings or uniform fibres as a result of slower jet breakup or no breakup at all. While extensional stresses towards the collector due to the electric field stabilise the jet and suppress the Rayleigh instability, additional conducting instabilities arise [45]. Two modes were reported by Hohman *et al.*: an axisymmetric conducting instability and a non-axisymmetric whipping instability [42]. Which of these dominate depends largely on the material properties of the fluid and on the process parameters. Theoretical calculations by Saville conclude that in sufficiently high electric fields the whipping instability dominates as observed in the majority of electrospinning experiments [46]. Figure 3 images the three instability phenomena.

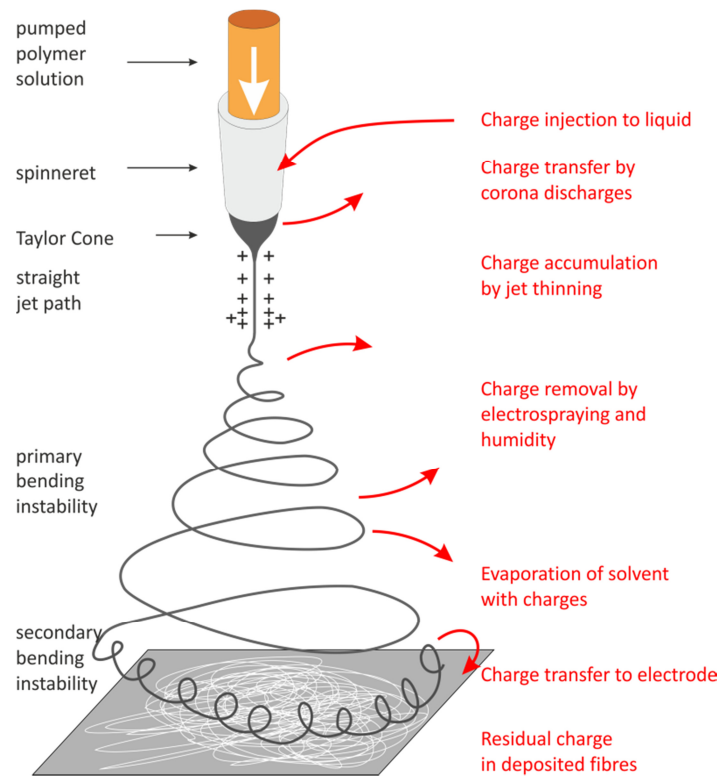


**Figure 2:** In the electrospinning process a pumped polymer solution is charged inside a spinneret. The pendant droplet deforms into a conical shape (Taylor cone) and a jet emerges when the electrostatic forces outbalance the surface tension. The jet evolves from a straight path to a whipping motion. Several “bending instabilities” can superimpose each other.

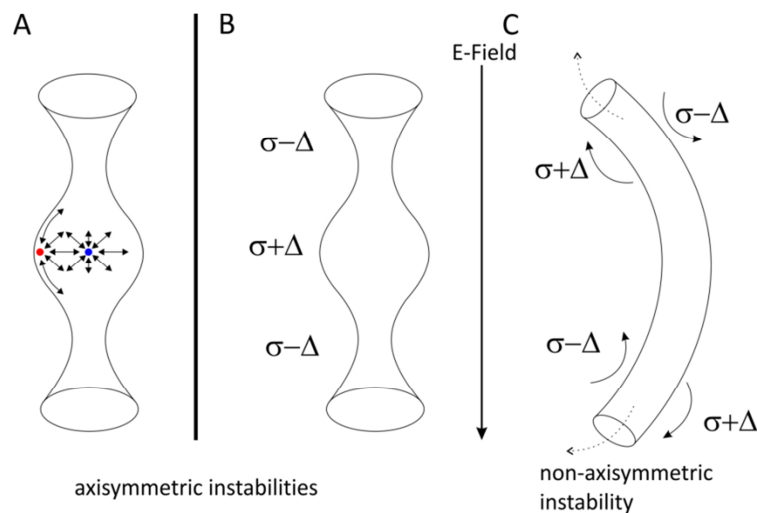


**Figure 3:** Instability processes during electrospinning. A) Rayleigh instability due to surface tension forces that exceed electrostatic forces and cause beading on fibres. Molecules in the bulk of the jet are equally surrounded by attractive forces from neighbouring molecules whereas molecules at the air-liquid interface are pulled inward, reducing the overall surface. B) Axisymmetric instability similar to A) but caused by inhomogeneous surface charge ( $\sigma$ ) distribution. C) Non-axisymmetric instability caused by inhomogeneous surface charge distribution that leads to the characteristic bending and whipping process. Figure was modified from reference [47] with permission from Elsevier.

As a consequence of the spiralling motion, the jet travels a longer distance before it is deposited, enabling sufficient time to be stretched due to non-axisymmetric whipping, resulting in small cross-sectional diameters on the nanometre scale [48]. The jet solidifies by two possible processes: firstly, conventional evaporation of the solvent as a function of partial pressures in the air and at the fluid surface. Secondly, ion evaporation being an electrostatically assisted ejection of ionised solvent in the whipping region of the jet [49]. The latter mechanism is associated with corona discharges and often leads to beaded fibre morphologies [48, 50].

Solidified fibres may be collected on a variety of targets ranging from stationary plates, rotating mandrels to liquid surfaces such as water. The final application of fibres generally determines the type of collector.

## **2.1 Parameters influencing electrospinning**

Though the electrospinning setup is easily assembled, the parameters that influence fibre production can be classed into three categories: “solution parameters”, “process parameters” and “ambient parameters” [19]. Important solution properties are viscosity, surface tension and conductivity. The first of these can be manipulated by the polymer concentration and its molecular weight. The dipole moment and dielectric constant of the solvent used are decisive factors in determining surface tension and conductivity. Secondly, the size and morphology of the electrospun product can be influenced by process parameters such as applied voltage, spinneret to collector distance, flow rate as well as spinneret design and collector geometry [51]. The third set of parameters involves air humidity, temperature and air velocity [52]. The parameters and their effects on fibre morphology are summarised in Table 1.

**Table 1:** List of parameters and their influences on the fibre morphology. The table was modified from reference [51] with permission from Elsevier.

Parameter	Effect on fibre morphology
Viscosity (polymer concentration) ↑	Fibre diameter ↑ (from beads to beaded fibres to smooth fibres)
Surface tension ↑	Number of beaded fibres and beads ↑
Solvent volatility ↑	Fibres exhibit microtexture (pores on fibre surfaces)
Solution conductivity ↑	Fibre diameter ↓
Applied voltage ↑	Fibre diameter ↓ initially, then ↑ (not monotonic)
Spinneret to collector distance ↑	Fibre diameter ↓ (beaded morphologies occur if the distance between the capillary and collector is too short)
Flow rate ↑	Fibre diameter (beaded morphologies occur if the flow rate is too high)
Temperature ↑	Fibre diameter ↓ then ↑
Humidity ↑	Fibre diameter ↓ (pores on fibre surfaces)

### 2.1.1 Solution parameters

It is crucial that the spinning solution features appropriate properties for a continuously running electrospinning experiment. Surface tension and viscosity are required to be balanced to maintain a stable jet and homogeneous fibre formation. These parameters will set boundaries for a range of fibre morphologies which can be modified by changing process parameters.

#### 2.1.1.1 Viscosity

The balance between viscosity and surface tension determines if electrospayed particles, electrospun fibres or no product is formed during the EHD process. The polymer concentration is a decisive factor for solution viscosity but its influence will vary for specific polymer – solvent combinations. Studies by various groups allow some general statements to be drawn [21, 53-62]. It was found that low polymer concentrations lead to particle

formation while higher concentrations permit fibre formation (Figure 4). The intermediate region shows beaded fibres with a continuous change in morphology from particles to homogeneous fibres [63].

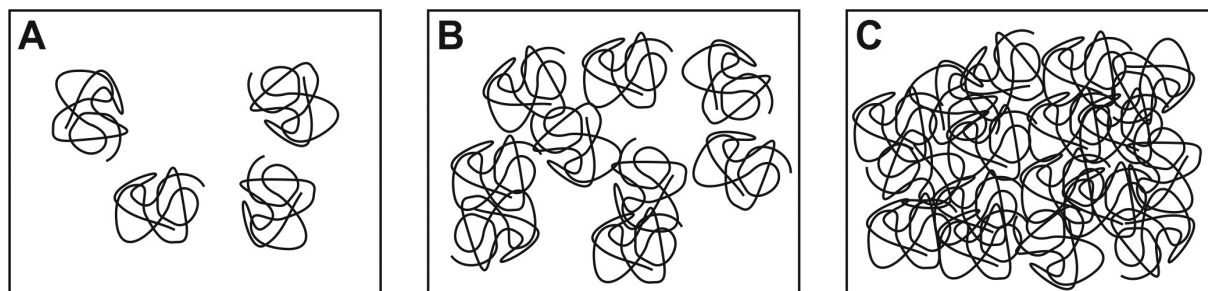


**Figure 4:** The number of entanglements in polymer solutions is directly correlated with the polymer concentration. Electrospinning of A would result in beads; B would lead to beaded fibres. The number of entanglements in C is large enough to prepare electrospun fibres with this solution. Figure was modified from reference [61] with permission from Elsevier.

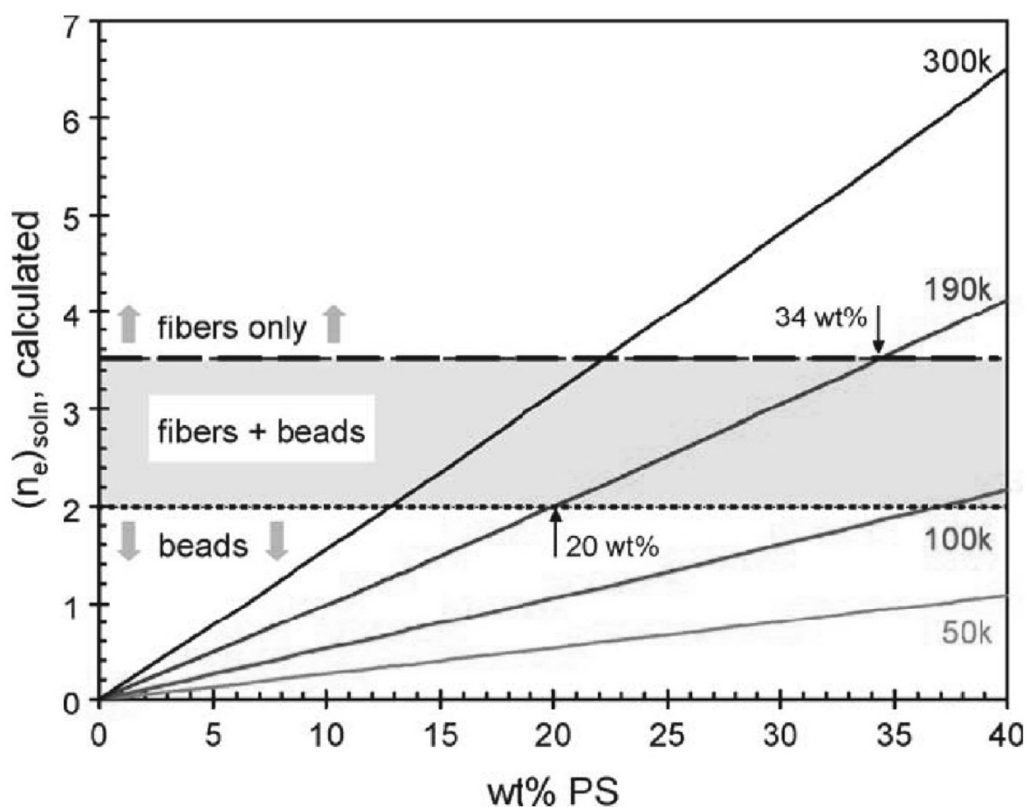


**Figure 5:** The calculated entanglement number  $(n_e)_{soln}$  of different polystyrene samples in tetrahydrofuran, representing the viscosity, versus the concentration. Reprinted from reference [63] with permission from Elsevier.

The degree of chain entanglements is the predominant cause of this effect. Below a critical chain overlap concentration  $c^*$ , polymer solutions will result in electrospaying only. The jet is not stable and splits into droplets as a result of the Rayleigh instability. For concentrations around  $c^*$  beads with incipient fibres and beaded fibres occur. Axisymmetric instabilities still govern the process but increased viscosity reduces the adaption speed of the spinning solution. McKee *et al.* determined a concentration of 2-2.5 times the entanglement concentration ( $C_e$ ) that is necessary for uniform fibre formation [64].  $C_e$  was defined by Colby *et al.* as an onset of entanglements in polymer solutions and can be identified by a higher viscosity increase with concentration due to constrained chain motion and couplings [65, 66]. Extremely high concentrations and viscosities prevent a stable jet from forming and instead globular fibres or macrobeads are formed. In Figure 5 an example of the change in fibre morphology as a function of viscosity is presented.

### 2.1.1.2 Surface tension

Surface tension describes the cohesive forces between liquid molecules. For molecules in the bulk of the liquid balanced attractive forces in all directions apply. However, for surface molecules, net inward forces remain which contract the liquid into a conformation with minimal surface area that is commonly spherical. In the case of electrostatic processes this appears as a Rayleigh instability and forces the solvent/polymer jet to break up into droplets [67, 68]. Viscoelastic polymers are not prone to undergo rapid deformation, countering the surface tension forces which favour spherical shapes. Fong *et al.* investigated the effect of reducing surface tension forces by adding ethanol to poly(ethylene oxide) (PEO) in an aqueous solution. They observed a transition in morphology from beaded to smooth fibres for solutions with high to low surface tension, respectively [21].

### 2.1.1.3 Solvent volatility

Besides an adequate balance between viscosity and surface tension the solvating media needs to be volatile for fibre or particle formation. Discrete structures are achieved when the solvent completely evaporates from the jet as it moves from the nozzle to the collector. Residual solvent may lead to conglomerated fibres with flattened morphologies [48]. Megelski *et al.* demonstrated the difference in fibre morphology of polystyrene fibres spun from THF/DMF solutions. Whereas highly volatile solvents such as tetrahydrofuran (THF) led to porous fibres with a 20-40% increase in surface area, N,N-dimethylformamide (DMF)



solutions yielded smooth fibres without microstructures [69]. During the solidification process a vapour-induced phase separation occurs with a non-solvent from the atmosphere (water) penetrating the polymer solution. As the diffusion into the polymer solution is slow a fibre skin forms. For highly volatile solvents the atmosphere around the moving fibre jet is saturated with solvents and thus minimises non-solvent penetration. Consequently, a homogeneous fibre skin does not form and allows the development of porous fibre surface structures.

#### *2.1.1.4 Conductivity*

Conductivity determines the charge carrying capacity in a jet and hence influences the tensile forces exerted on the jet by the electric field. Higher stresses on the jet induced by higher conductivities generally result in reduced fibre diameters. The increased amount of charge forces the jet to elongate as a consequence of coulombic repulsion. These forces act against surface tension, thus suppressing the Rayleigh instability favouring formation of non-beaded fibres. The inherent conductivities of common solvents are in the range of 0.1 to 0.01  $\mu\text{S}/\text{cm}$  and do not significantly increase by the addition of polymers. Salt additives in electrospinning solutions create migrating ions in solution that transport charges and contribute to higher conductivities [70]. Zhang and co-workers decreased the fibre diameter of poly(vinyl alcohol) (PVA) fibres by 25 % while adding 0.2 % NaCl instead of 0.05 % into the spinning solution [58]. Besides salt concentration the size of ionic radii are important factors as well. Charge density and ion mobility are higher for small ions such as sodium and chloride producing smaller fibres (210 nm diameter) compared to potassium phosphate additives where fibres of 1000 nm in diameter were achieved [54].

#### **2.1.2 Process parameters**

The process parameters initiate and control any electrospinning or electro spraying experiment. As these parameters are linked with secondary, indirect parameters their adjustment is challenging. The applied voltage creates an electric field whose strength depends on the distance between spinneret and collector. Furthermore, a certain voltage is related to a feed rate that supplies sufficient solution to form a stable jet.

### 2.1.2.1 Applied voltage

To activate EHD processes, charge is required. This is provided by connected voltage generators. Typically applied voltages in electrospinning experiments range from 8 to 25 kV. For aqueous solutions a minimum voltage of 6 kV was needed to induce electrospinning as stated by Taylor [14]. Deitzel *et al.* investigated the PEO/water system in respect to jet initiation and cone formation. Their experiments revealed a Taylor cone formation on a pendant drop at low field strengths of 0.3 kV/cm. For voltages of 9 kV (0.6 kV/cm) the size of this droplet receded into the capillary resulting in a jet emanating from the tip of the spinneret. Even higher voltages caused a jet formation within the capillary producing mainly fibres decorated with beads [53]. Similar results were found by Shin *et al.* where a water/PEO jet emanated directly from a capillary at electric field strength of 1 kV/cm. It seems likely that the flow rate was too low to supply enough solution for a stable jet [47]. When glycerol was used as the solvent, the group observed smaller cones but these were not receding into the spinneret [71]. The change in cone formation depending on the field strength is depicted in Figure 6. Comparing two solutions of the same polymer but different concentration showed a predominantly beaded fibre formation for field strengths below 2 kV/cm for the 15 (w/v)% poly(desaminotyrosyl-tyrosine ethyl ester carbonate) solution. Smooth fibres formed at higher field strengths.

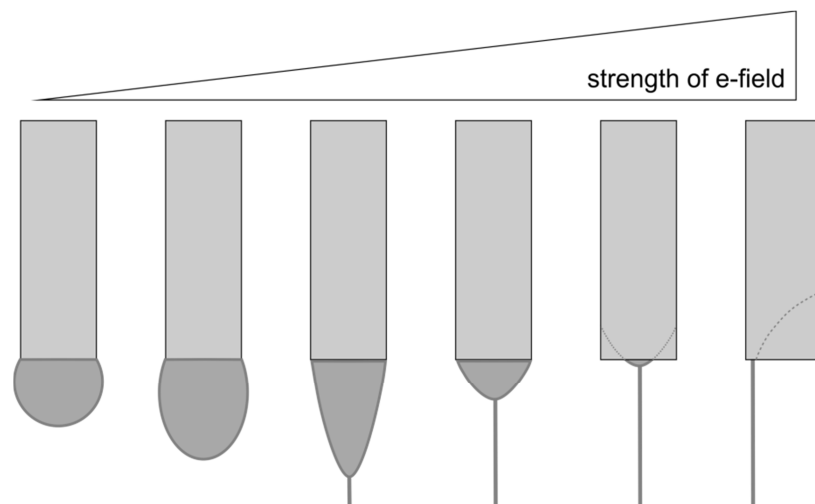


**Figure 6:** Morphological deformation of pendant droplets to cones and emerging jets with increasing electrical field strength.

### 2.1.2.2 Spinneret – collector distance

As described above, the distance between jet formation and fibre collection is connected to the applied voltage due to the field strength. Common electrospinning setups operate up to a distance of 30 cm. Unlimited distance is an unrealistic scenario as the jet will deviate to an unintended target or the required voltage reaches values where corona discharge effects take place and prevent a homogeneous spinning behaviour [50]. As a process parameter the distance determines how far the jet movement can evolve until the spinning product is collected. Generally the diameter decreases with increasing distance [19]. At very close distances, eventually still in the linear motion of the jet, fibre thinning from 19  $\mu\text{m}$  to 9  $\mu\text{m}$  has been observed for distances of 1 and 3.5 cm, respectively [72]. “Near Field Electrospinning” relies similarly on close distances to achieve a controlled fibre deposition from solution. Bisht *et al.* required field strengths of 2 - 3 kV/cm to deposit poly(ethylene oxide).

### 2.1.2.3 Flow rate

The flow rate is used to describe the speed at which the solution is delivered to the electrospinning process. As the Taylor cone shape recedes into the capillary with increasing voltage, the flow rate can be adjusted to generate a constant cone on the capillary tip. If the cone vanishes into the spinneret there is insufficient solution to replace the ejected fibre jet [14]. Thicker fibres are generally produced with higher flow rates as published by Megelski *et al.* [69]. Furthermore, an increasing number in bead defects on fibres has been observed at high flow rates as the solvent cannot evaporate completely before fibres are collected. As a consequence ribbon-like, flattened and “coalescent” fibres may result.

### 2.1.2.4 Spinneret design

In the most simple electrospinning setup a single blunt-tip stainless steel capillary is used. Common inner diameters range from 0.3 to 0.8 mm allowing viscous solutions to pass through the spinneret, but are still small enough to prevent premature solvent evaporation in the pendant droplet or cone. This would impact on the jet formation and eventually prevent the development of a stable spinning condition. With single capillaries, single polymer solutions [73] as well as polymer blends have been processed [74]. If polymer blends need to be electrospun with special solvents that are immiscible, side-by-side configurations [75, 76] or coaxial capillaries can be used [77-81]. The latter design is widely

used to create drug carrying fibres and particles for drug delivery purposes. High drug loadings are achieved when the outer capillary provides the particle or fibre generating solution, whereas the inner nozzle is loaded with a highly concentrated drug solution that does not necessarily form particles or fibres.

The relatively small scale of a typical electrospinning setup is advantageous for laboratory use. However, this is a major drawback for industrial use of this technique. Few companies exist that build electrospinning machines or sell fibres [82]. The two main approaches to up-scale the process are either to use multiple cannulas or electrodes without capillaries. The interactions of several spinnerets next to each other have been assessed by Theron *et al.*, where with a linear nozzle setup coulombic repulsions were observed between neighbouring jets [83]. The repulsive interactions were observed best for the distal spinnerets as the spinning direction diverted from the neighbouring jets.

Needleless electrospinning allows high throughput and is a promising candidate for industrial use [84-88]. The main advantage is that multiple jets develop through self-organizing effects in conductive liquids as soon as the electric field intensity exceeds a threshold [89]. The necessary voltages typically range from 30 to 80 kV. Recently a study by Liu presented a needleless electrospinning setup. Here, popping gas bubbles on a solvent surface generate jets and lead to fibre production [90].

### 2.1.2.5 Collector design

A variety of target designs have been explored to collect electrospun fibres. A simple and straight-forward setup involves a stationary conductive plate onto which non-woven meshes are deposited. Rotating drums with sufficient speed can lead to aligned fibres as well as the gap-method with two metal plates [91] (Figure 7). The choice of collector geometry largely depends on the application the fibres are intended for. More extraordinary examples use rings [92], rotating wire cages [93], collectors with conductive patterns [94, 95] and even an oppositely charged jet has been tested as spinning target [96]. An extensive review on this topic was published by Teo and Ramakrishna discussing various electrospinning designs [97].

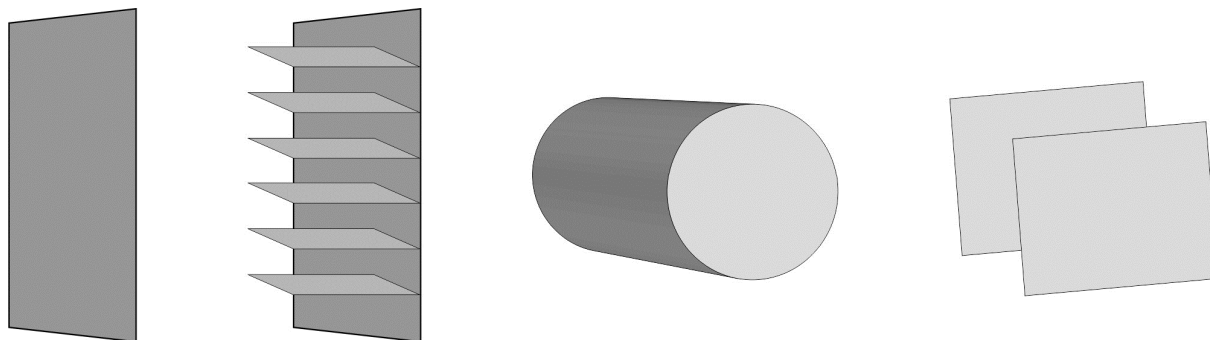


**Figure 7:** Various kinds of collectors: A metal plate / aluminium foil, plate with ribs, a drum, two separated plates for aligned fibre collection.

### 2.1.3 Ambient parameters

Ambient parameters cover the surrounding relative humidity and temperature at which the experiments are performed. The volatility of solvents changes with temperature and impacts on the fibre solidification process. De Vrieze and co-workers spun poly(vinylpyrrolidone) (PVP) at 10, 20 and 30 °C and observed indiscrete, fused fibres for low temperatures. The partial pressure of solvent ethanol is lower for 10 °C than at higher temperatures, therefore it takes longer to evaporate and fibres still containing ethanol are collected. For the influence on fibre diameter two effects compete: firstly, increased evaporation time enables longer jet thinning and results in thinner diameter fibres. At high temperatures the fibre solidification is faster but solution viscosity decreases as a consequence of increased polymer chain mobility [98]. Similar results were gained by Mit-uppatham *et al.* who spun polyamide-6 fibres at temperatures ranging from 25 to 60 °C [99].

The effect of humidity on fibre formation was investigated by De Vrieze *et al.* on PVP/ethanol solutions. They observed smaller fibre diameters for higher humidity and suggested that jet solidification was retarded due to absorption of water. Tripatanasuwan *et al.* published similar results on PEO fibres spun from aqueous solutions [100]. In the case where water was a non-solvent for the polymer a porous microstructure within the fibre skin was observed [69, 101].

## 2.2 Fibre properties

A characteristic of electrospinning is the ability to customise fibre size and morphology over a wide range. The resulting fibres generally have a large surface to volume ratio, making them suitable for surface dependant applications such as filtration, drug delivery or

scaffolding in TE approaches. Additionally, the non-woven mats feature porosities between 60 and more than 90 %, which is advantageous for cell infiltration.

Besides the influence of the fibrous morphology on the material properties, the type of polymer determines greatly the performance of the fibre in any application. For TE applications several prerequisites on material properties have to be met to ensure a successful use in *in vitro* and *in vivo* conditions.

### 3 Biomaterials

The microfibrils and nanofibrils made by electrospinning offer versatile application possibilities as stated earlier. Among these, their use as TE scaffolds is promising and intensely investigated [38]. Various tissues and cell types have been addressed by many research groups in combination with a broad range of polymers ranging from natural polymers such as collagen [102, 103], fibrinogen [104], silk [105-107], elastin [108] and hyaluronan [109] to synthetic polymers such as poly( $\epsilon$ -caprolactone) (PCL) [110], poly(lactic acid) (PLA) [111], poly(glycolic acid) (PGA) [112] and PLGA [38]. Commonly these are referred to as “Biomaterials”, being “... *substances that have been engineered to take a form which, alone or as part of a complex system, are used to direct, by control of interactions with components of living systems, the course of any therapeutic or diagnostic procedure, in human or veterinary medicine*” as stated by Williams [113]. One of the aims of regenerative medicine is to restore form and function to damaged tissues by using structural support scaffolds. Therefore the applied materials must be biocompatible and biodegradable so that native tissue may replace the implanted medical device.

#### 3.1 Biocompatibility

The most important property of a biomaterial is that it must be “biocompatible”. At first, the term qualifies a material not to have toxic or injurious effects on biological systems but furthermore it includes desired positive interactions between the host tissue and the biomaterial. The definition of Williams describes biocompatibility as “... *the ability of a biomaterial to perform its desired function with respect to a medical therapy, without eliciting any undesirable local or systemic effects in the recipient or beneficiary of that therapy, but generating the most appropriate beneficial cellular or tissue response in that specific situation, and optimizing the clinically relevant performance of that therapy*” [114]. It

is important to ensure the biocompatibility of a biomaterial before it is widely used in medical applications. Therefore, extensive *in vitro*, *in vivo* and human clinical trials have to be passed before the investigated material is approved to be used for medical devices [115]. Undesired immune responses such as foreign body reactions easily lead to implant rejection within the first 2-3 weeks after implantation [116, 117].

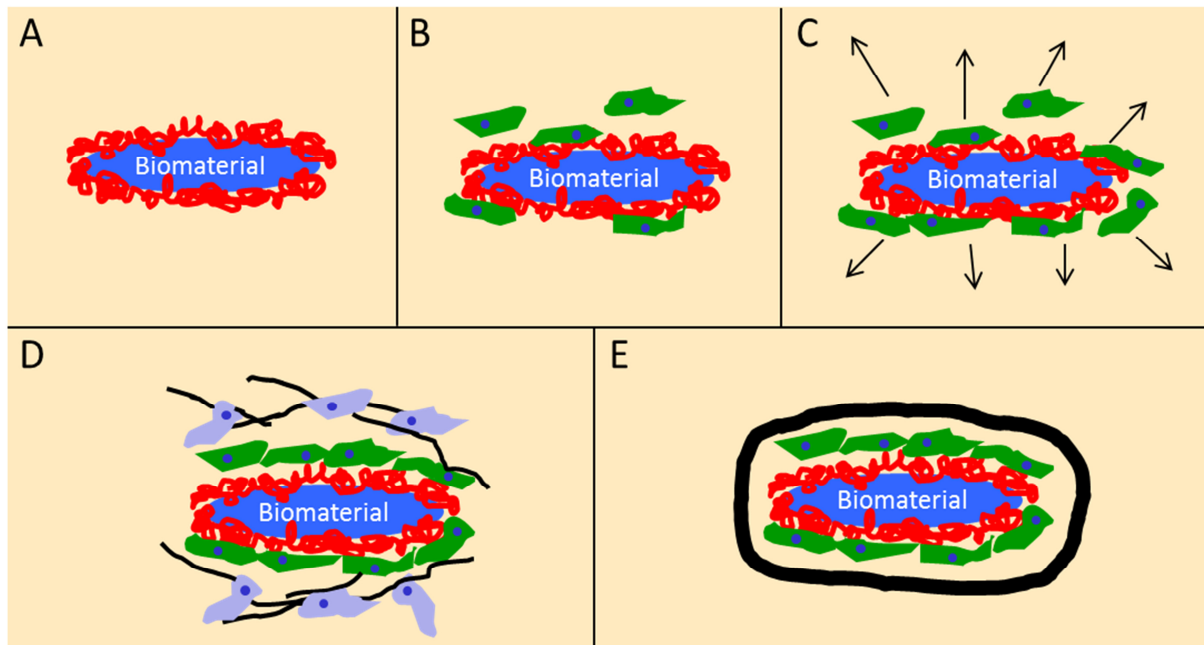


**Figure 8:** The fate of implanted biomaterials in the case of an implant failure with capsule formation: A) Proteins unspecifically adsorb to the biomaterial surface. B) Macrophages examine the material and try to digest it. C) If the device is too big, the cells communicate with other cells for support. D) Cells from the connective tissue such as fibroblasts synthesise collagen fibres around the implant. E) A dense capsule of collagen surrounds the material and prevents interaction with the organism. The figure was modified from reference [118] with permission from Elsevier.

The interaction at the interface between a medical device and the surrounding tissue is decisive for the host response. As an example, the cascade that runs during a foreign body reaction is presented in Figure 8: immediately after implantation a material is in contact with body fluids containing hundreds of proteins which unspecifically adhere to the material surface [118, 119]. Immune cells analyse and try to digest the foreign material as a means to protect the organism. If the device is too large to be ingested, the macrophages and neutrophils fuse together to become giant cells that surround the material causing a chronic inflammation. Communication signals call other cells such as fibroblasts from the connective

tissue. These produce collagen fibres, creating a capsule around the implant. Finally the “biomaterial” is encapsulated with collagen and cannot interact with the organism anymore [118]. While this natural process is favourable to provide protection against the undesired inclusion of foreign materials in the body following injury; on the other hand it is one of the major challenges for medical treatments using implants.

To circumvent this natural foreign body response, the prevention of unspecific protein adsorption needs to be addressed. The first step in this cascade is that proteins adsorb on material surfaces due to material properties such as wettability, surface charge and structure [120]. The adsorbed proteins denature and densely cover the material surface [121]. Thus, the cells cannot sense the material surface anymore and subsequent cell attachment is rather a consequence of the protein layer than of the material properties [117, 122]. Controlling the mentioned biomaterial properties would result in preventing unspecific protein adsorption and hence foreign body reactions.

### **3.2 Biodegradation**

The approach of TE relies on scaffolds that at first support wound healing but are replaced by newly formed tissue as therapy progresses. Biodegradable materials tackle the major issue that biostable materials face: that is the mostly unknown long term biocompatibility which is associated with revision surgeries and thus unnecessary costs and pain for the patient. By applying a material that can be decomposed and resorbed these problems can be avoided in an elegant way [123]. It is obvious that the same biocompatibility requirements apply for degradation products as well as for the original material, which summarised include: non-toxicity; acceptable shelf life; matching degradation time and appropriate mechanical properties to the regeneration process; and lastly they must be able to be metabolised and resorbed by the organism [124].

Today, polymeric materials are widely used in biomedical applications with tailored degradation properties [125]. This is a benefit of their inherent properties such as material chemistry, molecular weight, solubility, hydrophilicity/hydrophobicity and water absorption, which can influence their degradation profile. The key feature of degradable polymers are their hydrolytically or enzymatically unstable bonds, where if cleaved, induces polymer erosion [126]. Enzymatic degradation applies mostly for natural polymers and depends largely on the availability of the respective enzymes which are associated to the



implantation site. In contrast, synthetic polymers with hydrolytically cleavable bonds show less dependency on site-to-site and patient-to-patient variations [126].

Polymers range from fast degrading polyanhydrides to slowly degrading polyesters and to almost inert urethanes (Figure 9).

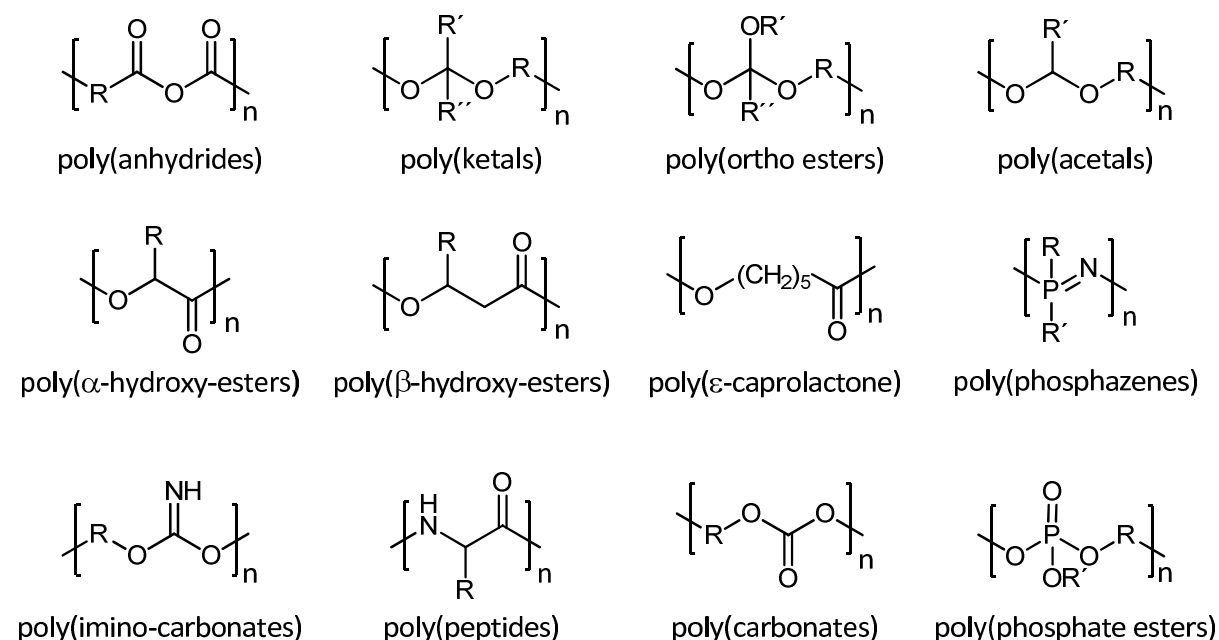


**Figure 9:** Hydrolysable polymers for drug release and TE.

The time scale in which a polymer decomposes determines its suitability for use in medical applications [127]. Poly( $\alpha$ -hydroxy esters) have been intensely studied because the available degradation times range from a few weeks up to a few years. Adjusting the degradation profile can be simply achieved by varying copolymer compositions of polylactide and polyglycolide, where the first applications as surgical sutures and bone screws date more than 30 years back [128, 129].

The mechanism of degradation of polyesters relies on chain scission, resulting in oligomers and monomers that can diffuse out of the material. Here two main patterns are found that depend on the diffusion speed of water into the polymer bulk, versus chain scission speed and accompanied debris erosion. For polymers with very hydrolytically labile bonds and faster chain scission than water intrusion, we find a “surface erosion” pattern. Therefore, degradation occurs only at the outermost polymer layers. The opposite called “bulk erosion” takes place for polymers where the bulk is completely penetrated by water before significant

chain degradation occurs. Which of these degradation types applies depends largely on the chemical bonds but also on the size of the material [130]. Figure 10 schematically describes the erosion patterns.

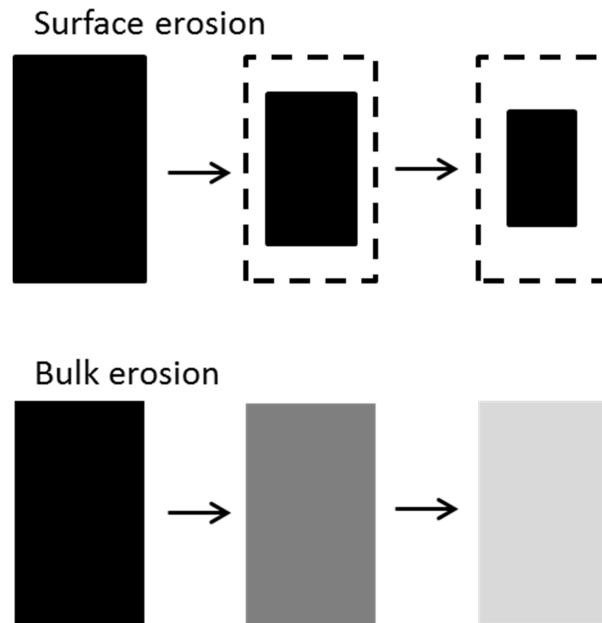


**Figure 10:** Erosion mechanisms of hydrolytically degradable polymers. Surface degradation is observed when water protrusion into the bulk along with polymer chain scission is slower than mass loss from the device surface. The figure was modified from reference [130] with permission from Elsevier.

For bulk eroding polymers such as poly( $\alpha$ -hydroxy esters), autocatalytic effects have been observed during degradation experiments. Each chain scission results in a free acid that contributes to a pH reduction. As the chain scission reaction is catalysed by acids, the degradation rate increases within the bulk [131, 132]. Due to this effect, Therin *et al.* observed materials with only a shell left around a completely dissolved core [133, 134]. Moreover, once the trapped acid is released from its confinement a local pH drop in the adjacent tissue may cause inflammation and be detrimental to the regeneration process.

Returning to electrospun fibrous scaffolds made from polylactide and/or polyglycolide, these negative effects are minimised because fibre dimensions of less than one micrometre prevent the accumulation of large amounts of acid within the fibres [111, 135].

Before beginning to design scaffolds for TE, the medical-biological aspect of cells and their environment should be understood, as presented in the following paragraphs.

## 4 Cells and tissues

“Tissue” can be defined as *“an aggregate of cells in an organism that have similar structure and function”* [136] and can be distinguished into four main types: muscle, nerve, epithelial and connective tissue. Muscle tissue generates forces and induces motion. It is subdivided into smooth muscle (inner lining of organs), skeletal muscle (connecting bones) and cardiac muscle (heart). Nerve cells communicate and transmit information between the peripheral and central nervous system through the neural tissue. Epithelial tissue covers surfaces (skin, airways, etc.) and acts as a barrier, protecting the organism from microorganisms, injury and fluid loss. Apart from these tissues with close cell-cell contact, connective tissue is comprised of cells, separated by a fibrous hydrogel that is called “extracellular matrix” (ECM). It has, as the name states, a “connective” function by providing structural support to other tissues and connecting them. Typical examples are bone, cartilage and adipose tissue. Furthermore, blood and lymphatic tissue including monocytes and macrophages can be classed as connective tissue.

### 4.1 Extracellular matrix

Connective tissues are largely comprised of non-living material which surrounds and is expressed by cells within each tissue [137]. The main components are polysaccharides, proteins and water which together form a hydrogel with an inner fibrous structure. Three types of macromolecules can be found in the ECM that differ in structure and function. Firstly, there are highly hydrated proteoglycans which provide a space filling function and resist compressive forces. Proteoglycans consist of a protein core chain onto which glycosaminoglycans (GAGs) are covalently attached. The side chains (GAGs) are polysaccharides consisting of a disaccharide repeating unit. The latter is comprised of a uronic acid (glucuronate or iduronate) and a modified hexose such as N-acetylgalactosamine or N-acetylglucosamine. Highly negatively charged, these polymers have an extended conformation that contributes to their viscosity and low compressibility in solution. The second type of biomacromolecules in the ECM are protein fibres that provide structural support to resident cells. The most prominent representative of this class is collagen type I with its fibrillar structure [137]. Functional glycoproteins with linking properties are the third macromolecular group that is expressed by cells into the ECM. Examples are fibronectin and

laminin which act as anchors to cells, connecting them to collagen fibres for support [138, 139].

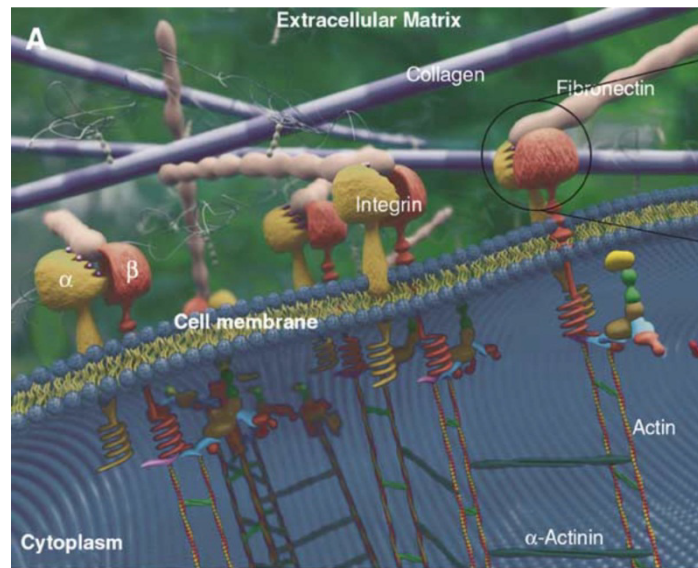


**Figure 11:** Schematic illustration of cell-matrix interaction (picture reproduced from ref. [140] with permission from Elsevier).

Within this framework, cells are supplied with nutrients, growth factors and sites for adhesion. Therefore, they are able to survive, migrate, differentiate and proliferate [139, 141, 142]. It is an evolving environment that is continually degraded and rebuilt by the resident cells [137, 143], which is a crucial function for tissue growth and repair [144, 145].

#### 4.2 Cell - ECM interactions

To maintain a functional tissue, cells must interact with their surrounding matrix [146]. When anchorage dependent cells adhere to external structures it influences their morphology and induces cell spreading. This spreading is decisive for DNA synthesis and proliferation of fibroblasts (an anchorage dependent cell type) [147]. In contrast, round cells which have no or wrong adhesion signals cannot survive and often induce a controlled cell death [148, 149]. A very common adhesion mechanism is the key-lock principle where peptide sequences of the ECM are recognised by transmembrane cell proteins. Besides other cell receptors, integrins are a class of transmembrane proteins that are expressed by many human cell types [143, 150, 151].

Integrins consist of two non-covalently associated subunits ( $\alpha$  and  $\beta$  subunits) that form a binding site in the extracellular space [151]. Special binding ligands can adhere to the binding site and induce a conformation change of the protein complex. On the inside of cells these

signals are forwarded to actin fibres that are responsible for the cell morphology and movement [146, 150, 152]. Figure 11 B shows the binding process and interaction with the actin skeleton of a cell. Depending on the subunit combination, several different protein sequences can be detected. A prominent example is the tripeptide sequence “arginine-glycine-aspartic acid” (RGD). It can be found in various proteins such as fibronectin, vitronectin, fibrinogen laminin and collagen [153-155] and is a major cell adhesion promoting sequence [156].

With a view to developing an artificial fibrous scaffold intended to support tissue regrowth it is crucial that cell adhesion markers are present and accessible for cells. The dense fibrous network can only function as a supporting framework with these binding sequences.

## **5 Tissue engineering**

The term “tissue engineering” comprises the creation of tissues through cultivation of cells. The term first appeared 25 years ago on a National Science Foundation Conference, where it was defined as “...*the application of the principles and methods of engineering and the life sciences toward the fundamental understanding of structure-function relationships in normal and pathological mammalian tissues and the development of biological substitutes to restore, maintain, or improve functions.*” [157]. Since then this research field evolved that requires the combined expertise of biology, biotechnology, chemistry, material sciences and medicine.

The method relies on explanting cells, cultivating them and then reimplanting these cells into a patient. During cell cultivation, adequate scaffolds should be used to allow cell growth in three dimensions analogous to the original native tissue [158]. The tissues grown in vitro are finally reimplanted, incorporated into the scaffolds. A TE scaffold should be resorbable to ensure that patients are exposed to foreign materials only for a limited time, as visualised in Figure 12.

Since the rediscovery of electrospinning as a means to produce non-woven fibrous networks, such scaffolds have been used to grow cells on. A significant amount of literature describes engineering tissues with biodegradable electrospun fibres [38]. Various tissues have been addressed such as neural [159], bone [160], cartilage [161], skin [162] and blood vessel [163-165] tissues.

Before a TE scaffold is designed some fundamental decisions need to be made, which are directed by the ultimate application of the scaffold. Firstly, either a natural or synthetic material should be chosen. Although natural materials (collagen, hyaluronan, chitosan, alginate etc.) feature inherent biocompatibility and biofunctional adhesion anchors, they are disadvantaged by batch-to-batch variability and limited possibilities for modification.

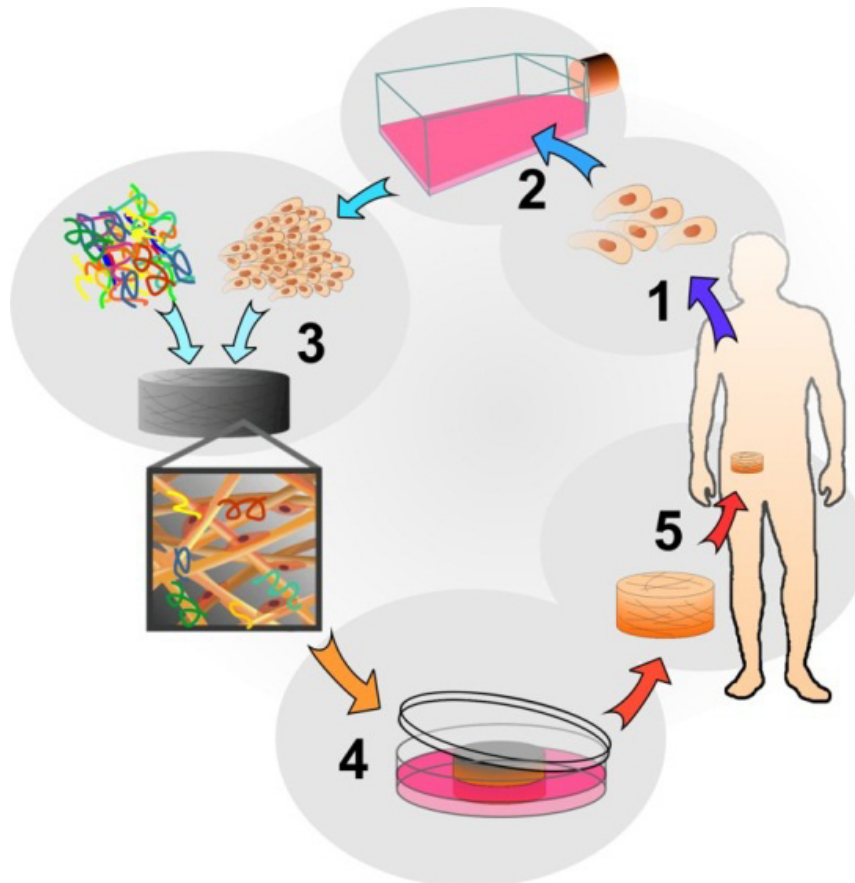


**Figure 12:** The tissue engineering approach: 1) Cells are explanted from a human, 2) cultivated and expanded in vitro, 3) and seeded into a scaffold. Growth factors or other suitable additives promote cell growth within the scaffold. 4) The cell-scaffold construct is finally reimplanted into the host tissue 5) to support the regeneration of damaged or diseased tissue. Image taken from <http://biomed.brown.edu/Courses/BI108/BI1082007Groups/group12/TEModelLarge.jpg>

Furthermore, restrictions may arise due to the risk of immunogenicity and disease transfer. Instead, synthetic materials offer more control over structural properties, their degradation profile and a lower immunogenic risk. The scaffold architecture and stiffness should match the natural cell environment in design and strength [148].

Secondly, a consequent decision concerns the presence or absence of adhesion markers as well as inductive signals. Natural polymers such as collagen naturally contain adhesion

sequences. For “inert” molecules such as poly(ethylene glycol) (PEG), chemical modifications open various possibilities to include bioactive elements. Means to enhance synthetic polymers and fibrous scaffolds in terms of surface chemistry and functionality have been examined but published methods are mainly based on multi step procedures following electrospinning [166]. For example, to transform hydrophobic fibres into hydrophilic materials via surface graft polymerisation takes several steps: reactive groups are generated via plasma treatment or UV-irradiation, then polymerisations are performed or natural polymers are linked to electrospun fibres in a secondary step [167-170].

Finally, the seeding with cells should be considered during scaffold design. Two seeding methods exist either in a “from the top” manner on a prefabricated scaffold or the cells can be integrated during scaffold formation [171].

TE is a promising field of research showing promise to enhance medical treatments in the future. In this thesis a scaffold treatment approach is developed on the basis of PLGA and a functional, star-shaped PEG prepolymer (Chapter 3 + 4). Fabricated non-wovens are exposed to various cell types such as fibroblasts (Chapter 5), chondrocytes (Chapter 6) and macrophages (Chapter 7) and their interaction is monitored. In Chapter 8, the fibres are used for the treatment of a diaphragmatic hernia, tested in a rabbit model *in vivo*.

## 6 References

- [1] Lenard P., 'Über Die Elektrizität Der Wasserfälle', *Annalen der Physik*, 46, **1892**, 584.
- [2] Lenard P., 'Über Wasserfallelektrizität Und Über Die Oberflächenbeschaffenheit Der Flüssigkeiten', *Annalen der Physik*, 352, **1915**, 463-524.
- [3] Laakso L., Hirsikko A., Groenholm T., Kulmala M., Luts A. and Parts T. E., 'Waterfalls as Sources of Small Charged Aerosol Particles', *Atmospheric Chemistry and Physics*, 7, **2007**, 2271-2275.
- [4] Reiter R., 'Charges on Particles of Different Size from Bubbles of Mediterranean Sea Surf and from Waterfalls', *J. Geophys. Res.*, 99, **1994**, 10807-10812.
- [5] Fish B. R., 'Electrical Generation of Natural Aerosols from Vegetation', *Science*, 175, **1972**, 1239-1240.
- [6] Gilbert W., 'De Magnete, Magnetisque Corporibus, Et De Magno Magnete Tellure', **1600**.
- [7] Rayleigh J. W. S., 'On the Conditions of Instability of Electrified Drops, with Applications to the Electric Discharge from Liquid Points', *Proc. R. Soc.*, 29, **1879**, 71-83.
- [8] Bose G. M., *Recherches Sur La Causa Et Sur La Veritable Theorie Del'electricite* (Wittenberg, 1745).
- [9] Zeleny J., 'The Electrical Discharge from Liquid Points, and a Hydrostatic Method of Measuring the Electric Intensity at Their Surfaces', *Physical Review*, 3, **1914**, 69-91.
- [10] Zeleny J., 'Instability of Electrified Liquid Surfaces', *Physical Review*, 10, **1917**, 1-6.
- [11] Formhals A., 'Process and Apparatus for Preparing Artificial Threads', (United States: Richard, Schreiber Gastell, Anton, Formhals, 1934).
- [12] Vonnegut B. and Neubauer R. L., 'Production of Monodisperse Liquid Particles by Electrical Atomization', *Journal of Colloid Science*, 7, **1952**, 616-622.
- [13] Taylor G., 'Disintegration of Water Drops in an Electric Field', *Proceedings of the Royal Society of London. Series A. Mathematical and Physical Sciences*, 280, **1964**, 383-397.
- [14] Taylor G., 'Electrically Driven Jets', *Proceedings of the Royal Society of London. A. Mathematical and Physical Sciences*, 313, **1969**, 453-475.
- [15] Cloupeau M. and Prunet-Foch B., 'Electrohydrodynamic Spraying Functioning Modes: A Critical Review', *Journal of Aerosol Science*, 25, **1994**, 1021-1036.
- [16] Saville D. A., 'Electrohydrodynamics: The Taylor-Melcher Leaky Dielectric Model', *Annual Review of Fluid Mechanics*, 29, **1997**, 27-64.
- [17] Grace J. M. and Marijnissen J. C. M., 'A Review of Liquid Atomization by Electrical Means', *Journal of Aerosol Science*, 25, **1994**, 1005-1019.
- [18] Marginean I., Parvin L., Heffernan L. and Vertes A., 'Flexing the Electrified Meniscus: The Birth of a Jet in Electrosprays', *Analytical Chemistry*, 76, **2004**, 4202-4207.
- [19] Doshi J. and Reneker D. H., 'Electrospinning Process and Applications of Electrospun Fibers', *Journal of Electrostatics*, 35, **1995**, 151-160.
- [20] Reneker D. H. and Chun I., 'Nanometre Diameter Fibres of Polymer, Produced by Electrospinning', *Nanotechnology*, 7, **1996**, 216-223.
- [21] Fong H., Chun I. and Reneker D. H., 'Beaded Nanofibers Formed During Electrospinning', *Polymer*, 40, **1999**, 4585-4592.
- [22] Yarin A. L., Koombhongse S. and Reneker D. H., 'Taylor Cone and Jetting from Liquid Droplets in Electrospinning of Nanofibers', *Journal of Applied Physics*, 90, **2001**, 4836-4846.
- [23] Yarin A. L., Koombhongse S. and Reneker D. H., 'Bending Instability in Electrospinning of Nanofibers', *Journal of Applied Physics*, 89, **2001**, 3018-3026.
- [24] Ramakrishna Seeram; Fujihara Kazutoshi; Teo Wee-Eong L. T.-C., Ma Zuwei, *An Introduction to Electrospinning and Nanofibers* (Singapore: World Scientific Publishing Oc. Pte. Ltd., 2005).
- [25] Lee S. and Obendorf S. K., 'Use of Electrospun Nanofiber Web for Protective Textile Materials as Barriers to Liquid Penetration', *Textile Research Journal*, 77, **2007**, 696-702.
- [26] Liu H., Kameoka J., Czaplewski D. A. and Craighead H. G., 'Polymeric Nanowire Chemical Sensor', *Nano Letters*, 4, **2004**, 671-675.
- [27] Hahm J.-i. and Lieber C. M., 'Direct Ultrasensitive Electrical Detection of DNA and DNA Sequence Variations Using Nanowire Nanosensors', *Nano Letters*, 4, **2003**, 51-54.
- [28] Kameoka J., Verbridge S. S., Liu H., Czaplewski D. A. and Craighead H. G., 'Fabrication of Suspended Silica Glass Nanofibers from Polymeric Materials Using a Scanned Electrospinning Source', *Nano Letters*, 4, **2004**, 2105-2108.



- [29] Medina-Castillo A. L., Fernández-Sánchez J. F. and Fernández-Gutiérrez A., 'One-Step Fabrication of Multifunctional Core-Shell Fibres by Co-Electrospinning', *Advanced Functional Materials*, 21, **2011**, 3488-3495.
- [30] Kumar E. N., Jose R., Archana P. S., Vijila C., Yusoff M. M. and Ramakrishna S., 'High Performance Dye-Sensitized Solar Cells with Record Open Circuit Voltage Using Tin Oxide Nanoflowers Developed by Electrospinning', *Energy & Environmental Science*, 5, **2012**, 5401-5407.
- [31] Di Benedetto F., Camposeo A., Pagliara S., Mele E., Persano L., Stabile R., Cingolani R. and Pisignano D., 'Patterning of Light-Emitting Conjugated Polymer Nanofibres', *Nat Nano*, 3, **2008**, 614-619.
- [32] Chang C., Tran V. H., Wang J., Fuh Y.-K. and Lin L., 'Direct-Write Piezoelectric Polymeric Nanogenerator with High Energy Conversion Efficiency', *Nano Letters*, 10, **2010**, 726-731.
- [33] Li X., Cao Q., Wang X., Jiang S., Deng H. and Wu N., 'Preparation of Poly(Vinylidene Fluoride)/Poly(Methyl Methacrylate) Membranes by Novel Electrospinning System for Lithium Ion Batteries', *Journal of Applied Polymer Science*, 122, **2011**, 2616-2620.
- [34] Li M., Mondrinos M. J., Gandhi M. R., Ko F. K., Weiss A. S. and Lelkes P. I., 'Electrospun Protein Fibers as Matrices for Tissue Engineering', *Biomaterials*, 26, **2005**, 5999-6008.
- [35] Kumbar S. G., James R., Nukavarapu S. P. and Laurencin C. T., 'Electrospun Nanofiber Scaffolds: Engineering Soft Tissues', *Biomedical Materials*, 3, **2008**.
- [36] Chew S. Y., Wen Y., Dzenis Y. and Leong K. W., 'The Role of Electrospinning in the Emerging Field of Nanomedicine', *Current Pharmaceutical Design*, 12, **2006**, 4751-4770.
- [37] Brun P., Ghezzi F., Roso M., Danesin R., Palù G., Bagno A., Modesti M., Castagliuolo I. and Dettin M., 'Electrospun Scaffolds of Self-Assembling Peptides with Poly(Ethylene Oxide) for Bone Tissue Engineering', *Acta Biomaterialia*, 7, **2011**, 2526-2532.
- [38] Ashammakhi N., Ndreu A., Yang Y., Ylikauppila H. and Nikkola L., 'Nanofiber-Based Scaffolds for Tissue Engineering', *European Journal of Plastic Surgery*, 35, **2012**, 135-149.
- [39] Luu Y. K., Kim K., Hsiao B. S., Chu B. and Hadjiargyrou M., 'Development of a Nanostructured DNA Delivery Scaffold Via Electrospinning of Plga and Pla-Peg Block Copolymers', *Journal of Controlled Release*, 89, **2003**, 341-353.
- [40] Zeng J., Xu X., Chen X., Liang Q., Bian X., Yang L. and Jing X., 'Biodegradable Electrospun Fibers for Drug Delivery', *Journal of Controlled Release*, 92, **2003**, 227-231.
- [41] Reneker D. H., Yarin A. L., Fong H. and Koombhongse S., 'Bending Instability of Electrically Charged Liquid Jets of Polymer Solutions in Electrospinning', *Journal of Applied Physics*, 87, **2000**, 4531-4547.
- [42] Shin Y. M., Hohman M. M., Brenner M. P. and Rutledge G. C., 'Electrospinning: A Whipping Fluid Jet Generates Submicron Polymer Fibers', *Applied Physics Letters*, 78, **2001**, 1149-1151.
- [43] Peter K B., 'Electrostatic Spinning of Acrylic Microfibers', *Journal of Colloid and Interface Science*, 36, **1971**, 71-79.
- [44] Rayleigh J. W. S., *Phil. Mag.*, 14, **1882**, 184.
- [45] Bousfield D. W., Keunings R., Marrucci G. and Denn M. M., 'Nonlinear Analysis of the Surface Tension Driven Breakup of Viscoelastic Filaments', *Journal of Non-Newtonian Fluid Mechanics*, 21, **1986**, 79-97.
- [46] Saville D. A., 'Stability of Electrically Charged Viscous Cylinders', *Physics of Fluids*, 14, **1971**, 1095-1099.
- [47] Shin Y. M., Hohman M. M., Brenner M. P. and Rutledge G. C., 'Experimental Characterization of Electrospinning: The Electrically Forced Jet and Instabilities', *Polymer*, 42, **2001**, 9955-9967.
- [48] Reneker D. H. and Yarin A. L., 'Electrospinning Jets and Polymer Nanofibers', *Polymer*, 49, **2008**, 2387-2425.
- [49] Higuera F. J., 'Ion Evaporation from the Surface of a Taylor Cone', *Physical Review E*, 68, **2003**, 016304.
- [50] Tripatanasuwan S. and Reneker D. H., 'Corona Discharge from Electrospinning Jet of Poly(Ethylene Oxide) Solution', *Polymer*, 50, **2009**, 1835-1837.
- [51] Sill T. J. and von Recum H. A., 'Electrospinning: Applications in Drug Delivery and Tissue Engineering', *Biomaterials*, 29, **2008**, 1989-2006.
- [52] Pham Q. P., Sharma U. and Mikos A. G., 'Electrospinning of Polymeric Nanofibers for Tissue Engineering Applications: A Review', *Tissue Engineering*, 12, **2006**, 1197-1211.
- [53] Deitzel J. M., Kleinmeyer J., Harris D. and Beck Tan N. C., 'The Effect of Processing Variables on the Morphology of Electrospun Nanofibers and Textiles', *Polymer*, 42, **2001**, 261-272.
- [54] Zong X., Kim K., Fang D., Ran S., Hsiao B. S. and Chu B., 'Structure and Process Relationship of Electrospun Bioabsorbable Nanofiber Membranes', *Polymer*, 43, **2002**, 4403-4412.
- [55] Kim H. S., Kim K., Jin H. J. and Chin I.-J., 'Morphological Characterization of Electrospun Nano-Fibrous Membranes of Biodegradable Poly(L-Lactide) and Poly(Lactide-Co-Glycolide)', *Macromolecular Symposia*, 224, **2005**, 145-154.

- [56] Son W. K., Youk J. H., Lee T. S. and Park W. H., 'The Effects of Solution Properties and Polyelectrolyte on Electrospinning of Ultrafine Poly(Ethylene Oxide) Fibers', *Polymer*, 45, **2004**, 2959-2966.
- [57] Koski A., Yim K. and Shivkumar S., 'Effect of Molecular Weight on Fibrous Pva Produced by Electrospinning', *Materials Letters*, 58, **2004**, 493-497.
- [58] Zhang C., Yuan X., Wu L., Han Y. and Sheng J., 'Study on Morphology of Electrospun Poly(Vinyl Alcohol) Mats', *European Polymer Journal*, 41, **2005**, 423-432.
- [59] Lee J. S., Choi K. H., Ghim H. D., Kim S. S., Chun D. H., Kim H. Y. and Lyoo W. S., 'Role of Molecular Weight of Atactic Poly(Vinyl Alcohol) (Pva) in the Structure and Properties of Pva Nanofabric Prepared by Electrospinning', *Journal of Applied Polymer Science*, 93, **2004**, 1638-1646.
- [60] Ding B., Kim H. Y., Lee S. C., Shao C. L., Lee D. R., Park S. J., Kwag G. B. and Choi K. J., 'Preparation and Characterization of a Nanoscale Poly(Vinyl Alcohol) Fiber Aggregate Produced by an Electrospinning Method', *Journal of Polymer Science Part B-Polymer Physics*, 40, **2002**, 1261-1268.
- [61] Gupta P., Elkins C., Long T. E. and Wilkes G. L., 'Electrospinning of Linear Homopolymers of Poly(Methyl Methacrylate): Exploring Relationships between Fiber Formation, Viscosity, Molecular Weight and Concentration in a Good Solvent', *Polymer*, 46, **2005**, 4799-4810.
- [62] Jarusuwannapoom T., Hongrojjanawiwat W., Jitjaicham S., Wannatong L., Nithitanakul M., Pattamaprom C., Koombhongse P., Rangkupan R. and Supaphol P., 'Effect of Solvents on Electrospinnability of Polystyrene Solutions and Morphological Appearance of Resulting Electrospun Polystyrene Fibers', *European Polymer Journal*, 41, **2005**, 409-421.
- [63] Shenoy S. L., Bates W. D., Frisch H. L. and Wnek G. E., 'Role of Chain Entanglements on Fiber Formation During Electrospinning of Polymer Solutions: Good Solvent, Non-Specific Polymer-Polymer Interaction Limit', *Polymer*, 46, **2005**, 3372-3384.
- [64] McKee M. G., Wilkes G. L., Colby R. H. and Long T. E., 'Correlations of Solution Rheology with Electrospun Fiber Formation of Linear and Branched Polyesters', *Macromolecules*, 37, **2004**, 1760-1767.
- [65] Colby R. H., Fetters L. J., Funk W. G. and Graessley W. W., 'Effects of Concentration and Thermodynamic Interaction on the Viscoelastic Properties of Polymer Solutions', *Macromolecules*, 24, **1991**, 3873-3882.
- [66] Graessley W. W., 'Polymer Chain Dimensions and the Dependence of Viscoelastic Properties on Concentration, Molecular Weight and Solvent Power', *Polymer*, 21, **1980**, 258-262.
- [67] Zuo W., Zhu M., Yang W., Yu H., Chen Y. and Zhang Y., 'Experimental Study on Relationship between Jet Instability and Formation of Beaded Fibers During Electrospinning', *Polymer Engineering & Science*, 45, **2005**, 704-709.
- [68] Magarvey R. H. and Outhouse L. E., 'Note on the Break-up of a Charged Liquid Jet', *Journal of Fluid Mechanics*, 13, **1962**, 151-157.
- [69] Megelski S., Stephens J. S., Chase D. B. and Rabolt J. F., 'Micro- and Nanostructured Surface Morphology on Electrospun Polymer Fibers', *Macromolecules*, 35, **2002**, 8456-8466.
- [70] You Y., Lee S. J., Min B. M. and Park W. H., 'Effect of Solution Properties on Nanofibrous Structure of Electrospun Poly(Lactic-Co-Glycolic Acid)', *Journal of Applied Polymer Science*, 99, **2006**, 1214-1221.
- [71] Hohman M. M., Shin M., Rutledge G. and Brenner M. P., 'Electrospinning and Electrically Forced Jets. II. Applications', *Physics of Fluids*, 13, **2001**, 2221-2236.
- [72] Jaeger R., Bergshoef M. M., Batlle C. M. I., Schönherr H. and Julius Vancso G., 'Electrospinning of Ultra-Thin Polymer Fibers', *Macromolecular Symposia*, 127, **1998**, 141-150.
- [73] Tan E. P. S., Ng S. Y. and Lim C. T., 'Tensile Testing of a Single Ultrafine Polymeric Fiber', *Biomaterials*, 26, **2005**, 1453-1456.
- [74] Stitzel J., Liu J., Lee S. J., Komura M., Berry J., Soker S., Lim G., Van Dyke M., Czerw R., Yoo J. J. and Atala A., 'Controlled Fabrication of a Biological Vascular Substitute', *Biomaterials*, 27, **2006**, 1088-1094.
- [75] Gupta P. and Wilkes G. L., 'Some Investigations on the Fiber Formation by Utilizing a Side-by-Side Bicomponent Electrospinning Approach', *Polymer*, 44, **2003**, 6353-6359.
- [76] Roh K.-H., Martin D. C. and Lahann J., 'Biphasic Janus Particles with Nanoscale Anisotropy', *Nat Mater*, 4, **2005**, 759-763.
- [77] Zhang Y. Z., Wang X., Feng Y., Li J., Lim C. T. and Ramakrishna S., 'Coaxial Electrospinning of (Fluorescein Isothiocyanate-Conjugated Bovine Serum Albumin)-Encapsulated Poly(E-Caprolactone) Nanofibers for Sustained Release', *Biomacromolecules*, 7, **2006**, 1049-1057.
- [78] Jiang H., Hu Y., Li Y., Zhao P., Zhu K. and Chen W., 'A Facile Technique to Prepare Biodegradable Coaxial Electrospun Nanofibers for Controlled Release of Bioactive Agents', *Journal of Controlled Release*, 108, **2005**, 237-243.

- [79] Jiang H., Hu Y., Zhao P., Li Y. and Zhu K., 'Modulation of Protein Release from Biodegradable Core–Shell Structured Fibers Prepared by Coaxial Electrospinning', *Journal of Biomedical Materials Research Part B: Applied Biomaterials*, 79B, **2006**, 50-57.
- [80] Yarin A. L., 'Coaxial Electrospinning and Emulsion Electrospinning of Core–Shell Fibers', *Polymers for Advanced Technologies*, 22, **2011**, 310-317.
- [81] Shih Y.-H., Yang J.-C., Li S.-H., Yang W.-C. V. and Chen C.-C., 'Bio-Electrospinning of Poly(L-Lactic Acid) Hollow Fibrous Membrane', *Textile Research Journal*, 82, **2012**, 602-612.
- [82] Collins G., Federici J., Imura Y. and Catalani L. H., 'Charge Generation, Charge Transport, and Residual Charge in the Electrospinning of Polymers: A Review of Issues and Complications', *Journal of Applied Physics*, 111, **2012**, 044701-044718.
- [83] Theron S. A., Yarin A. L., Zussman E. and Kroll E., 'Multiple Jets in Electrospinning: Experiment and Modeling', *Polymer*, 46, **2005**, 2889-2899.
- [84] Yarin A. L. and Zussman E., 'Upward Needleless Electrospinning of Multiple Nanofibers', *Polymer*, 45, **2004**, 2977-2980.
- [85] Miloh T., Spivak B. and Yarin A. L., 'Needleless Electrospinning: Electrically Driven Instability and Multiple Jetting from the Free Surface of a Spherical Liquid Layer', *Journal of Applied Physics*, 106, **2009**, 114910-114918.
- [86] Miller-Chou B. A. and Koenig J. L., 'A Review of Polymer Dissolution', *Progress in Polymer Science*, 28, **2003**, 1223-1270.
- [87] Wang X., Niu H., Lin T. and Wang X., 'Needleless Electrospinning of Nanofibers with a Conical Wire Coil', *Polymer Engineering & Science*, 49, **2009**, 1582-1586.
- [88] Lu B., Wang Y., Liu Y., Duan H., Zhou J., Zhang Z., Wang Y., Li X., Wang W., Lan W. and Xie E., 'Superhigh-Throughput Needleless Electrospinning Using a Rotary Cone as Spinneret', *Small*, 6, **2010**, 1612-1616.
- [89] Lukas D., Sarkar A. and Pokorny P., 'Self-Organization of Jets in Electrospinning from Free Liquid Surface: A Generalized Approach', *Journal of Applied Physics*, 103, **2008**, 084309-084307.
- [90] Liu Y., Dong L., Fan J., Wang R. and Yu J.-Y., 'Effect of Applied Voltage on Diameter and Morphology of Ultrafine Fibers in Bubble Electrospinning', *Journal of Applied Polymer Science*, 120, **2011**, 592-598.
- [91] Baker S. C., Atkin N., Gunning P. A., Granville N., Wilson K., Wilson D. and Southgate J., 'Characterisation of Electrospun Polystyrene Scaffolds for Three-Dimensional In Vitro Biological Studies', *Biomaterials*, 27, **2006**, 3136-3146.
- [92] Dalton P. D., Klee D. and Moller M., 'Electrospinning with Dual Collection Rings', *Polymer*, 46, **2005**, 611-614.
- [93] Murugan R. and Ramakrishna S., 'Design Strategies of Tissue Engineering Scaffolds with Controlled Fiber Orientation', *Tissue Engineering*, 13, **2007**, 1845-1866.
- [94] Aussawasathien D., Dong J. H. and Dai L., 'Electrospun Polymer Nanofiber Sensors', *Synthetic Metals*, 154, **2005**, 37-40.
- [95] Zhang K., Wang X., Jing D., Yang Y. and Zhu M., 'Bionic Electrospun Ultrafine Fibrous Poly(L-Lactic Acid) Scaffolds with a Multi-Scale Structure', *Biomedical Materials*, 4, **2009**, 035004.
- [96] Wee-Eong T., Ryuji I. and Seeram R., 'Technological Advances in Electrospinning of Nanofibers', *Science and Technology of Advanced Materials*, 12, **2011**, 013002.
- [97] Teo W. E. and Ramakrishna S., 'A Review on Electrospinning Design and Nanofibre Assemblies', *Nanotechnology*, 17, **2006**, R89.
- [98] De Vrieze S., Van Camp T., Nelvig A., Hagström B., Westbroek P. and De Clerck K., 'The Effect of Temperature and Humidity on Electrospinning', *Journal of Materials Science*, 44, **2009**, 1357-1362.
- [99] Mit-uppatham C., Nithitanakul M. and Supaphol P., 'Ultrafine Electrospun Polyamide-6 Fibers: Effect of Solution Conditions on Morphology and Average Fiber Diameter', *Macromolecular Chemistry and Physics*, 205, **2004**, 2327-2338.
- [100] Tripatanasuwan S., Zhong Z. and Reneker D. H., 'Effect of Evaporation and Solidification of the Charged Jet in Electrospinning of Poly(Ethylene Oxide) Aqueous Solution', *Polymer*, 48, **2007**, 5742-5746.
- [101] Casper C. L., Stephens J. S., Tassi N. G., Chase D. B. and Rabolt J. F., 'Controlling Surface Morphology of Electrospun Polystyrene Fibers: Effect of Humidity and Molecular Weight in the Electrospinning Process', *Macromolecules*, 37, **2003**, 573-578.
- [102] Matthews J. A., Wnek G. E., Simpson D. G. and Bowlin G. L., 'Electrospinning of Collagen Nanofibers', *Biomacromolecules*, 3, **2002**, 232-238.
- [103] Venugopal J., Ma L. L., Yong T. and Ramakrishna S., 'In Vitro Study of Smooth Muscle Cells on Polycaprolactone and Collagen Nanofibrous Matrices', *Cell Biology International*, 29, **2005**, 861-867.

- [104] Wnek G. E., Carr M. E., Simpson D. G. and Bowlin G. L., 'Electrospinning of Nanofiber Fibrinogen Structures', *Nano Letters*, 3, **2003**, 213-216.
- [105] Jin H. J., Fridrikh S. V., Rutledge G. C. and Kaplan D. L., 'Electrospinning Bombyx Mori Silk with Poly(Ethylene Oxide)', *Biomacromolecules*, 3, **2002**, 1233-1239.
- [106] Jin H. J., Chen J. S., Karageorgiou V., Altman G. H. and Kaplan D. L., 'Human Bone Marrow Stromal Cell Responses on Electrospun Silk Fibroin Mats', *Biomaterials*, 25, **2004**, 1039-1047.
- [107] Zhu J., Shao H. and Hu X., 'Morphology and Structure of Electrospun Mats from Regenerated Silk Fibroin Aqueous Solutions with Adjusting Ph', *International Journal of Biological Macromolecules*, 41, **2007**, 469-474.
- [108] Boland E. D., Matthews J. A., Pawlowski K. J., Simpson D. G., Wnek G. E. and Bowlin G. L., 'Electrospinning Collagen and Elastin: Preliminary Vascular Tissue Engineering', *Frontiers in Bioscience*, 9, **2004**, 1422-1432.
- [109] Liu Y., Ma G., Fang D., Xu J., Zhang H. and Nie J., 'Effects of Solution Properties and Electric Field on the Electrospinning of Hyaluronic Acid', *Carbohydrate Polymers*, 83, **2011**, 1011-1015.
- [110] Li W.-J., Tuli R., Okafor C., Derfoul A., Danielson K. G., Hall D. J. and Tuan R. S., 'A Three-Dimensional Nanofibrous Scaffold for Cartilage Tissue Engineering Using Human Mesenchymal Stem Cells', *Biomaterials*, 26, **2005**, 599-609.
- [111] Kim K., Yu M., Zong X. H., Chiu J., Fang D. F., Seo Y. S., Hsiao B. S., Chu B. and Hadjiargyrou M., 'Control of Degradation Rate and Hydrophilicity in Electrospun Non-Woven Poly(D,L-Lactide) Nanofiber Scaffolds for Biomedical Applications', *Biomaterials*, 24, **2003**, 4977-4985.
- [112] Li W. J., Laurencin C. T., Catterson E. J., Tuan R. S. and Ko F. K., 'Electrospun Nanofibrous Structure: A Novel Scaffold for Tissue Engineering', *Journal of Biomedical Materials Research*, 60, **2002**, 613-621.
- [113] Williams D. F., 'On the Nature of Biomaterials', *Biomaterials*, 30, **2009**, 5897-5909.
- [114] Williams D. F., 'On the Mechanisms of Biocompatibility', *Biomaterials*, 29, **2008**, 2941-2953.
- [115] Peppas N. and Langer R., 'New Challenges in Biomaterials', *Science*, 263, **1994**, 1715-1720.
- [116] Anderson J. M., 'Biological Responses to Materials', *Annual Review of Materials Research*, 31, **2001**, 81-110.
- [117] Puleo D. A. and Nanci A., 'Understanding and Controlling the Bone-Implant Interface', *Biomaterials*, 20, **1999**, 2311-2321.
- [118] Castner D. G. and Ratner B. D., 'Biomedical Surface Science: Foundations to Frontiers', *Surface Science*, 500, **2002**, 28-60.
- [119] Ratner B. D. and Bryant S. J., 'Biomaterials: Where We Have Been and Where We Are Going', *Annual Review of Biomedical Engineering*, 6, **2004**, 41-75.
- [120] Altankov G., Grinnell F. and Groth T., 'Studies on the Biocompatibility of Materials: Fibroblast Reorganization of Substratum-Bound Fibronectin on Surfaces Varying in Wettability', *Journal of Biomedical Materials Research*, 30, **1996**, 385-391.
- [121] Ostuni E., Yan L. and Whitesides G. M., 'The Interaction of Proteins and Cells with Self-Assembled Monolayers of Alkanethiolates on Gold and Silver', *Colloids and Surfaces B: Biointerfaces*, 15, **1999**, 3-30.
- [122] Wilson C. J., Clegg R. E., Leavesley D. I. and Pearcy M. J., 'Mediation of Biomaterial-Cell Interactions by Adsorbed Proteins: A Review', *Tissue Engineering*, 11, **2005**, 1-18.
- [123] Nair L. S. and Laurencin C. T., 'Biodegradable Polymers as Biomaterials', *Progress in Polymer Science (Oxford)*, 32, **2007**, 762-798.
- [124] Lloyd A. W., 'Interfacial Bioengineering to Enhance Surface Biocompatibility', *Medical device technology*, 13, **2002**, 18-21.
- [125] Vert M., 'Aliphatic Polyesters: Great Degradable Polymers That Cannot Do Everything', *Biomacromolecules*, 6, **2005**, 538-546.
- [126] Katti D. S., Lakshmi S., Langer R. and Laurencin C. T., 'Toxicity, Biodegradation and Elimination of Polyanhydrides', *Advanced Drug Delivery Reviews*, 54, **2002**, 933-961.
- [127] Rosen H. B. K., J.; Leong, K.; Langer, R.;, 'Bioerodible Polymers for Controlled Release Systems', in *Controlled Release Systems: Fabrication Technology Vol. 2*, ed. by D. Hsieh (Boca Raton: CRC Press, 1988), pp. 83-110.
- [128] Benicewicz B. C. and Hopper P. K., 'Polymers for Absorbable Surgical Sutures .1', *Journal of Bioactive and Compatible Polymers*, 5, **1990**, 453-472.
- [129] Leenslag J. W., Pennings A. J., Bos R. R. M., Rozema F. R. and Boering G., 'Resorbable Materials of Poly(L-Lactide). Vi. Plates and Screws for Internal Fracture Fixation', *Biomaterials*, 8, **1987**, 70-73.

- [130] Siepmann J. and Göpferich A., 'Mathematical Modeling of Bioerodible, Polymeric Drug Delivery Systems', *Advanced Drug Delivery Reviews*, 48, **2001**, 229-247.
- [131] Li S., Garreau H. and Vert M., 'Structure-Property Relationships in the Case of the Degradation of Massive Poly(A-Hydroxy Acids) in Aqueous Media', *Journal of Materials Science: Materials in Medicine*, 1, **1990**, 198-206.
- [132] Vert M., Li S. and Garreau H., 'More About the Degradation of La/Ga-Derived Matrices in Aqueous Media', *Journal of Controlled Release*, 16, **1991**, 15-26.
- [133] Li S. M., 'Hydrolytic Degradation Characteristics of Aliphatic Polyesters Derived from Lactic and Glycolic Acids', *Journal of Biomedical Materials Research*, 48, **1999**, 342-353.
- [134] Therin M., Christel P., Li S., Garreau H. and Vert M., 'In Vivo Degradation of Massive Poly(A-Hydroxy Acids): Validation of in Vitro Findings', *Biomaterials*, 13, **1992**, 594-600.
- [135] Cui W. G., Li X. H., Zhou S. B. and Weng J., 'Degradation Patterns and Surface Wettability of Electrospun Fibrous Mats', *Polymer Degradation and Stability*, 93, **2008**, 731-738.
- [136] 'Definition of "Tissue"', 2012) <<http://www.biology-online.org/dictionary/Tissue>>.
- [137] Aumailley M. and Gayraud B., 'Structure and Biological Activity of the Extracellular Matrix', *Journal of Molecular Medicine*, 76, **1998**, 253-265.
- [138] Tanzer M. L., 'Current Concepts of Extracellular Matrix', *Journal of Orthopaedic Science*, 11, **2006**, 326-331.
- [139] Geiger B., Bershadsky A., Pankov R. and Yamada K. M., 'Transmembrane Extracellular Matrix-Cytoskeleton Crosstalk', *Nature Reviews Molecular Cell Biology*, 2, **2001**, 793-805.
- [140] Tirrell M., Kokkoli E. and Biesalski M., 'The Role of Surface Science in Bioengineered Materials', *Surface Science*, 500, **2002**, 61-83.
- [141] Alberts B. J., A.; Lewis, J., *Molecular Biology of the Cell* (New York: Garland Science, 2002).
- [142] Ma Z. W., Kotaki M., Inai R. and Ramakrishna S., 'Potential of Nanofiber Matrix as Tissue-Engineering Scaffolds', *Tissue Engineering*, 11, **2005**, 101-109.
- [143] Franz S., Rammelt S., Scharnweber D. and Simon J. C., 'Immune Responses to Implants – a Review of the Implications for the Design of Immunomodulatory Biomaterials', *Biomaterials*, 32, **2011**, 6692-6709.
- [144] Lu P., Takai K., Weaver V. M. and Werb Z., 'Extracellular Matrix Degradation and Remodeling in Development and Disease', *Cold Spring Harbor Perspectives in Biology*, 3, **2011**.
- [145] Raeber G. P., Lutolf M. P. and Hubbell J. A., 'Molecularly Engineered Peg Hydrogels: A Novel Model System for Proteolytically Mediated Cell Migration', *Biophysical Journal*, 89, **2005**, 1374-1388.
- [146] Gumbiner B. M., 'Cell Adhesion: The Molecular Basis of Tissue Architecture and Morphogenesis', *Cell*, 84, **1996**, 345-357.
- [147] Folkman J. and Moscona A., 'Role of Cell Shape in Growth Control', *Nature*, 273, **1978**, 345-349.
- [148] Discher D. E., Janmey P. and Wang Y.-I., 'Tissue Cells Feel and Respond to the Stiffness of Their Substrate', *Science*, 310, **2005**, 1139-1143.
- [149] Gilmore A. P., 'Anoikis', *Cell Death and Differentiation*, 12, **2005**, 1473-1477.
- [150] Hynes R. O., 'Integrins - Versatility, Modulation, and Signaling in Cell-Adhesion', *Cell*, 69, **1992**, 11-25.
- [151] Hynes R. O., 'Integrins: A Family of Cell Surface Receptors', *Cell*, 48, **1987**, 549-554.
- [152] Clark E. and Brugge J., 'Integrins and Signal Transduction Pathways: The Road Taken', *Science*, 268, **1995**, 233-239.
- [153] Buck C. A. and Horwitz A. F., 'Cell-Surface Receptors for Extracellular-Matrix Molecules', *Annual Review of Cell Biology*, 3, **1987**, 179-205.
- [154] Plow E. F., Haas T. A., Zhang L., Loftus J. and Smith J. W., 'Ligand Binding to Integrins', *Journal of Biological Chemistry*, 275, **2000**, 21785-21788.
- [155] Ruoslahti E., 'Rgd and Other Recognition Sequences for Integrins', *Annual Review of Cell and Developmental Biology*, 12, **1996**, 697-715.
- [156] Pierschbacher M. D. and Ruoslahti E., 'Cell Attachment Activity of Fibronectin Can Be Duplicated by Small Synthetic Fragments of the Molecule', *Nature*, 309, **1984**, 30-33.
- [157] Nerem R., 'Cellular Engineering', *Annals of Biomedical Engineering*, 19, **1991**, 529-545.
- [158] Schmidt-Rohlfing B., Tzioupis C., Menzel C. L. and Pape H. C., 'Tissue Engineering of Bone Tissue. Principles and Clinical Applications', *Unfallchirurg*, 112, **2009**, 785-794.
- [159] Cao H., Liu T. and Chew S. Y., 'The Application of Nanofibrous Scaffolds in Neural Tissue Engineering', *Advanced Drug Delivery Reviews*, 61, **2009**, 1055-1064.
- [160] Jang J.-H., Castano O. and Kim H.-W., 'Electrospun Materials as Potential Platforms for Bone Tissue Engineering', *Advanced Drug Delivery Reviews*, 61, **2009**, 1065-1083.

- [161] Li W. J., Chiang H., Kuo T. F., Lee H. S., Jiang C. C. and Tuan R. S., 'Evaluation of Articular Cartilage Repair Using Biodegradable Nanofibrous Scaffolds in a Swine Model: A Pilot Study', *Journal of tissue engineering and regenerative medicine*, 3, **2009**, 1-10.
- [162] Zhu X., Cui W., Li X. and Jin Y., 'Electrospun Fibrous Mats with High Porosity as Potential Scaffolds for Skin Tissue Engineering', *Biomacromolecules*, 9, **2008**, 1795-1801.
- [163] He W., Ma Z., Yong T., Teo W. E. and Ramakrishna S., 'Fabrication of Collagen-Coated Biodegradable Polymer Nanofiber Mesh and Its Potential for Endothelial Cells Growth', *Biomaterials*, 26, **2005**, 7606-7615.
- [164] Keun Kwon I., Kidoaki S. and Matsuda T., 'Electrospun Nano- to Microfiber Fabrics Made of Biodegradable Copolyesters: Structural Characteristics, Mechanical Properties and Cell Adhesion Potential', *Biomaterials*, 26, **2005**, 3929-3939.
- [165] He W., Yong T., Teo W. E., Ma Z. W. and Ramakrishna S., 'Fabrication and Endothelialization of Collagen-Blended Biodegradable Polymer Nanofibers: Potential Vascular Graft for Blood Vessel Tissue Engineering', *Tissue Engineering*, 11, **2005**, 1574-1588.
- [166] Yoo H. S., Kim T. G. and Park T. G., 'Surface-Functionalized Electrospun Nanofibers for Tissue Engineering and Drug Delivery', *Advanced Drug Delivery Reviews*, 61, **2009**, 1033-1042.
- [167] Turmanova S., Minchev M., Vassilev K. and Danev G., 'Surface Grafting Polymerization of Vinyl Monomers on Poly(Tetrafluoroethylene) Films by Plasma Treatment', *Journal of Polymer Research*, 15, **2008**, 309-318.
- [168] Mori M., Uyama Y. and Ikada Y., 'Surface Modification of Polyethylene Fiber by Graft Polymerization', *Journal of Polymer Science Part A: Polymer Chemistry*, 32, **1994**, 1683-1690.
- [169] Kou R.-Q., Xu Z.-K., Deng H.-T., Liu Z.-M., Seta P. and Xu Y., 'Surface Modification of Microporous Polypropylene Membranes by Plasma-Induced Graft Polymerization of A-Allyl Glucoside', *Langmuir*, 19, **2003**, 6869-6875.
- [170] Ma Z. W., Kotaki M., Yong T., He W. and Ramakrishna S., 'Surface Engineering of Electrospun Polyethylene Terephthalate (Pet) Nanofibers Towards Development of a New Material for Blood Vessel Engineering', *Biomaterials*, 26, **2005**, 2527-2536.
- [171] Kraehenbuehl T. P., Langer R. and Ferreira L. S., 'Three-Dimensional Biomaterials for the Study of Human Pluripotent Stem Cells', *Nat Meth*, 8, **2011**, 731-736.

## CHAPTER 3

---

### Development and characterisation of ECM mimicking fibres

To perform advanced tissue engineering (TE) tasks, scaffolds need to be developed that mimic native tissue surroundings as closely as possible. The applied biomaterials require passive features such as biocompatibility and biodegradability, but furthermore active interaction is desired to promote guided tissue regeneration. In this chapter the idea of an advanced fibrous scaffold is presented. The development of the production process of poly(D,L-lactide-*co*-glycolide) (PLGA) fibres containing NCO-sP(EO-*stat*-PO) prepolymers is described in detail and accompanied by observations of influences on solution and process parameters. The electrospun PLGA fibres were rendered highly hydrophilic once NCO-sP(EO-*stat*-PO) was included into the spinning solution. The fibres degraded under physiological conditions within 3 months and exhibited functional moieties for further modification.

---

Parts of this chapter represent a cooperative project with Dirk Grafahrend and have been published:

Grafahrend D., Heffels K. H., Beer M. V., Gasteier P., Moller M., Boehm G., Dalton P. D. and Groll J., 'Degradable Polyester Scaffolds with Controlled Surface Chemistry Combining Minimal Protein Adsorption with Specific Bioactivation', *Nature Materials*, 10, **2011**, 67-73.

## 1 Introduction

When artificial materials come into contact with complex biological fluids or living tissue, the initial contact plays a decisive role in determining the following interaction between the two systems. One key factor is the prevention of unspecific protein adsorption. If proteins can adsorb on a material surface in a non-specific way, they are recognised by their biological binding partners, thus initiating signal cascades and binding events that are neither controlled nor intended. In the case of biosensors and analytical devices this leads to a bad signal to noise ratio or even false signals, while for biomaterials the result may be inflammation, fibrous capsule formation, implant loosening or implant failure.

The general strategy to render surfaces inert towards proteins is to introduce a coating layer which prevents protein adsorption either thermodynamically, so that attractive surface interactions are overcompensated by repulsive interactions with the layer, or at least kinetically by creating a free energy barrier of sufficient height that cannot be overcome within relevant time scales [1]. One of the most successful materials used in this context is poly (ethylene oxide) (PEO). PEO is non-toxic, non-immunogenic and FDA approved for biomedical applications [2]. When linear PEO chains are grafted onto substrate surfaces they create a thin layer that minimises unspecific protein adsorption. Although the reasons for the remarkable non-fouling property of PEO are still not yet fully understood, experimentally, the grafting density and the chain length are the two essential control parameters by which the degree of protein resistance is governed [3-5]. When linear polymer chains are used, a high grafting density is difficult to achieve on non-model substrates due to steric hindrance of the chains at the interface. Thus, an alternative method has been developed that relies on star shaped PEO based prepolymers. The system consists of six-arm, star-shaped molecules with terminal reactive functional groups. The backbone consists of a statistical copolymer of ethylene oxide and propylene oxide in a ratio of 4: 1; each arm has a molecular mass of 2 kDa and is attached to a sorbitol core. Following the core-first method the stars are prepared by anionic polymerisation from sorbitol potassium salt as the initiator which ensures that the molecular mass distribution is small ( $PDI < 1.2$ ). The arms of the star molecules are initially terminated with OH and are functionalised with isophorone diisocyanate (IPDI) to yield isocyanate (NCO-) terminated star molecules [6]. The chemical composition of the NCO-sP(EO-*stat*-PO) system is shown in Figure 1. IPDI was



chosen as reagent since it provides different reactivities between its primary and secondary isocyanate groups in the molecule.

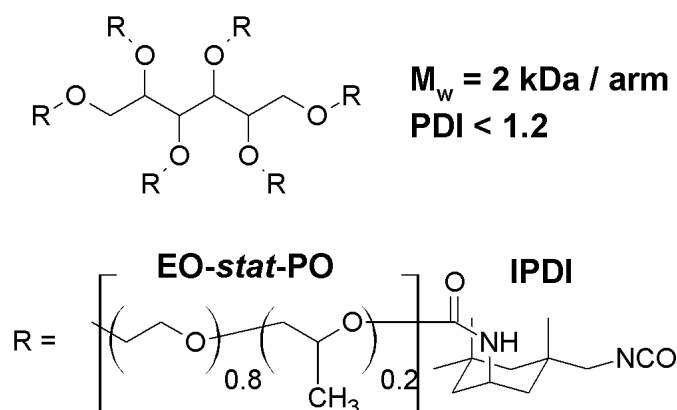


**Figure 1:** Chemical composition of the NCO-sP(EO-*stat*-PO) molecule.

In this way, the chemical attachment of the diisocyanate to the star molecules can be performed without a catalyst. In this condition, the secondary isocyanate groups are more reactive so that over 80% of the secondary isocyanates form secondary urethane bonds between the star molecules and IPDI, and the primary, less reactive aliphatic isocyanate groups remain as functional groups at the ends of the arms [6]. This is, besides a high excess of IPDI towards star molecules, helpful during synthesis to prevent oligomerisation. Furthermore, it results in a rather slow hydrolysis of the NCO-endgroups which allows the use of water as (co-)solvent for the prepolymers.

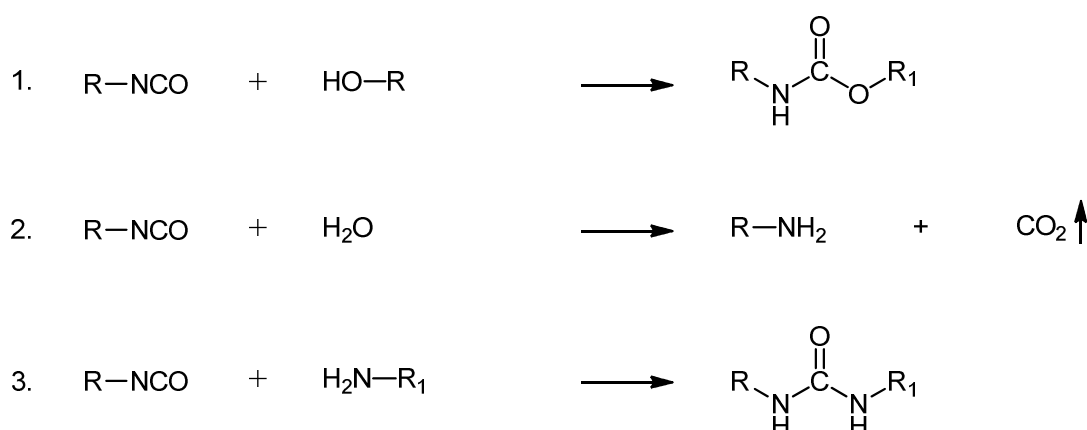


**Figure 2:** Various reactions of isocyanates. Intermolecular reactions of 2) and 3) result in a hydrogel network.

One particular advantage of the NCO-sP(EO-*stat*-PO) system is the change in reactivity from isocyanate groups (which are reactive towards amines and alcohols) to amine groups (which exhibit inverse reactivity) during the layer preparation and curing of the coating. This means a chemical orthogonality for the functionalisation of the layers. The NCO-sP(EO-*stat*-PO)

layers can be functionalised at three different stages of layer preparation: (i) reaction with the isocyanate groups of the NCO-sP(EO-*stat*-PO) molecules in solution before coating, (ii) reaction with the isocyanate groups in freshly prepared layers and (iii) reaction with the amine groups in the cross-linked layers. The preparation and characterisation of NCO-sP(EO-*stat*-PO) coatings, their functionalisation and resulting interaction with proteins and cells have been summarised in a review article [7].

The design of a scaffold for TE is adjusted to the demands of the type of tissue that should be regenerated. Focusing on soft tissues such as skin, muscles etc. highly flexible and porous scaffolds are required that support fast cell migration, vascularisation and the supply of nutrients [8]. Furthermore, suitable properties such as an adjustable degradation rate from a few weeks to several months cover the time frame in which the damaged tissue heals and fundamental support by a scaffold is not necessary anymore. The polymer family of aliphatic polyesters, mainly comprised of poly (lactic acid) (PLA), poly (glycolic acid) (PGA), copolymers of these and poly ( $\epsilon$ -caprolacton) (PCL), possess the desired properties required for soft TE [9]. Electrospun meshes made from poly (lactide-*co*-glycolide) (PLGA) have been examined *in vitro*, and good cell adhesion and proliferation was found [10]. Experiments with triblockcopolymers comprised of PLA, PLGA and PEG chains featured higher hydrophilicity, smaller contact angles and less *in vivo* adhesions [11].

In this chapter a one-step preparation method that combines a degradable polymer (PLGA) and a functional additive (NCO-sP(EO-*stat*-PO)) in a co-electrospinning setup is described. Observations on electrospinning phenomena as well as process optimisations and fibre characterisations are presented.

## 2 Experimental section

### 2.1 NCO-sP(EO-*stat*-PO) synthesis

A hydroxyl terminated six arm star shaped prepolymer consisting of an ethylene oxide and propylene oxide backbone (ratio 80:20) and a molecular weight of 12 kDa was transferred into an isocyanate terminated prepolymer with isophorone diisocyanate. The detailed synthesis is described by Götz *et al.* [6].

### 2.2 Electrospinning

Unless otherwise stated the electrospinning was performed with a solution of 6 w/v% NCO-sP(EO-*stat*-PO) and 28 w/v% PLGA RG 504 in a mixture of acetone, DMSO and acidic water. The spinning solution was prepared as follows: first, NCO-sP(EO-*stat*-PO) was dissolved in DMSO and consecutively mixed with an aqueous solution of trifluoroacetic acid (TFA) at a concentration of 20  $\mu$ L TFA per mL water. The solution was diluted with acetone, briefly mixed and finally PLGA was added and stirred for 10 min until a homogeneous solution was at hand. A common batch of such an electrospinning solution consisted of 143 mg PLGA, 30 mg NCO-sP(EO-*stat*-PO), 450  $\mu$ L acetone, 50  $\mu$ L DMSO and 10  $\mu$ L acidic water.

The solution was spun at a feed rate of 0.5 mL/h through a flat-tip stainless steel spinneret ( $\varnothing = 0.4 * 25$  mm) connected to a high-voltage power supply. An Eltex KNH34 (Germany) high voltage generator was utilised to charge the solutions at 13 kV while the collector remained grounded. The fibres were collected on aluminium foil at a distance of 160 mm. Varying targets were applied, depending on the further fibre processing. Rotating drums (10 cm wide, 6 cm diameter) were used to produce non-woven meshes. Small samples of fibres were spun on aluminium foil for the determination of fibre diameters.

### 2.3 Scanning electron microscopy and optical microscopy:

Fibre morphology was characterised using scanning electron microscopy (SEM) and optical microscopy (OM). For high-resolution images, the electrospun fibres were deposited onto SEM stubs. Unless otherwise stated, all samples were imaged with an S-4800 Ultra High Resolution Scanning Electron Microscope (Hitachi) using an accelerating voltage of 10 kV and a working distance of 10-15 mm. All samples for optical microscopy were collected on sP(EO-*stat*-PO) coated silicon wafers. Microscope images were taken with a Zeiss Stemi 2000-C. In

order to observe the presence of the fluorescent dyes on the fibre surface, images were taken with an exposure time of 20000 ms using an appropriate fluorescence filter. Green fluorescence was observed with an F41-26 filter provided by AHF Analysentechnik (Germany), whereas red fluorescence was documented by filterset 31 of Zeiss (Germany).

### **2.4 Fibre size determination**

The fibre diameter was determined by analysing three SEM-images of the respective sample. The open source program ImageJ was applied measuring at least 50 fibres for each sample. The data is presented in Box plots giving the lower quartile, median and upper quartile as box shape. The whiskers represent either a 1.5 fold interquartile range (IQR, range between upper and lower quartile) or the minimal or maximal values if they are within the 1.5 fold IQR. Outliers are given as crosses.

### **2.5 Rheology measurements**

The gelling behaviour of spinning solutions containing NCO-sP(EO-*stat*-PO) and PLGA were measured with a Rheometrics – Dynamic Stress Rheometer. At a constant sweep rate of 1 Hz the viscosity of the spinning solution was determined with a 25 mm plate geometry setup.

### **2.6 Conductivity measurements**

The conductivity of spinning solutions including 143 mg PLGA, 30 mg NCO-sP(EO-*stat*-PO) was measured with a ExStik®II Conductivity/TDS Meter(ExTech Instruments Corporation, USA). The solvent mixture ratios were DMSO: TFA/H<sub>2</sub>O (100: 2), acetone: TFA/H<sub>2</sub>O (100: 2) and acetone: DMSO: TFA/H<sub>2</sub>O (90: 10: 2). The amount of TFA is given in section 3.1.3.

### **2.7 Tensile tests**

The tensile tests were conducted using a Zwick/Roell Z010 (Ulm, Germany) static materials testing machine. An Xforce load cell of 1 kN measured the tensile forces on specimens clamped in screw grips. The dogbone specimens were 6 mm wide and 60 mm long with a gauge length of 25 mm. Testing was completed with the tensile grips moving at 50 mm/min. A standard test according to DIN EN ISO 527-1 was performed to acquire the maximal tensile force and mesh elongation.

## 2.8 Wettability studies

The wettability of electrospun fibre meshes was examined by contact angle measurements. Sessile drop measurements with a goniometer G40 (Krüss, Hamburg, Germany) were performed using the electrospun meshes as substrates. To achieve this, dense compact nonwoven meshes, collected on a grounded rotating drum, were cut into 25 · 15 mm pieces and fixed onto an object slide using two small stripes of adhesive tape at the sides of the sample. Droplets of water (5 µL) were deposited on the surfaces and the contour of the droplets was captured by a digital camera. Contact angles were calculated from three independent experiments. To allow comparison between sP(EO-*stat*-PO) containing nonwovens and PLGA meshes, images of the water droplets on electrospun fibre meshes were taken starting at the moment of contact in one second time intervals.

## 2.9 Degradation studies

Under physiological conditions mass loss as well as molecular weight changes were examined for electrospun PLGA and NCO-sP(EO-*stat*-PO)/PLGA nonwovens. Pieces of the nonwovens with a mass of 70 mg were incubated with 1.5 mL phosphate buffered saline (PBS) solution (pH 7.4). The samples were kept in 1.5 mL Eppendorf tubes on a Heidolph Polymax 1040 incubator (Germany) for 12 weeks at 37°C and a rotation speed of 150 s<sup>-1</sup>. The pH was checked weekly and in the case of alterations of more than 0.2 the buffer was exchanged. Samples were taken after 0, 1, 3, 7, 14, 21, 28, 35, 63 and 84 days. The samples were centrifuged at 10000 rpm for 5 min and then the buffer was carefully removed. Prior to weighing, the remaining samples were incubated 3 times for 20 min with distilled water to extract remaining PBS from the sample. After a second centrifugation the distilled water was removed and the samples were freeze-dried for 24 h. An average mass loss of three samples for each point in time was determined. The resulting molecular weights ( $M_w$ ,  $M_n$ ) and  $M_w/M_n$  (PDI) were determined by gel permeation chromatography (GPC). GPC measurements were carried out at 35°C using a high performance liquid chromatography pump (ERC HPLC 64200) and a refractive index detector (ERC 7215a). The eluting solvent was tetrahydrofuran (THF) (HPLC grade) with 250 mg/mL 2,6-di-*tert*-butyl-4-methylphenol and a flow rate of 1 mL/min. Five columns with MZ gel were applied. The first column was 50 mm long and the other four columns 300 mm long. The diameter of each column was eight mm, the diameter of the gel particles five mm, and the nominal pore widths were 50, 50, 100, 1000 and 10000 Å,

respectively. Poly (methyl methacrylate) (PMMA) standards were used for calibration purposes. Additionally SEM images were taken after 0, 7, 14, 21, 28, 35 and 42days of incubation in PBS.

### **2.10 XPS measurement**

X-ray photoelectron spectroscopy (XPS) analysis was performed using an X-Probe 206 spectrometer (Surface Science Instruments, USA). An aluminium anode was used as an X-ray source. The binding energies were referenced to hydrocarbon at 285.0 eV. The emission angle of electrons was set at 55° with respect to the sample normal, which results in an information depth of about 10 nm.

### 3 Results and discussion

#### 3.1 Solution parameters

##### 3.1.1 Single solvent electrospinning of PLGA

Initially the electrospinning behaviour of PLGA solutions in acetone was examined as this is the main component of the fibres. Therefore solutions of 9, 12.5, 16.8, 20, 25 and 30 wt% PLGA RG 504 in acetone were prepared and electrospun immediately. The resulting morphologies were observed under SEM. Figure 3 A-C show predominately electrospayed products where the PLGA is predominantly in a beaded form. With increasing concentration of PLGA the beads are flattened and the overall shape turns into “beaded fibres”, which is visualised in Figure 3 D.

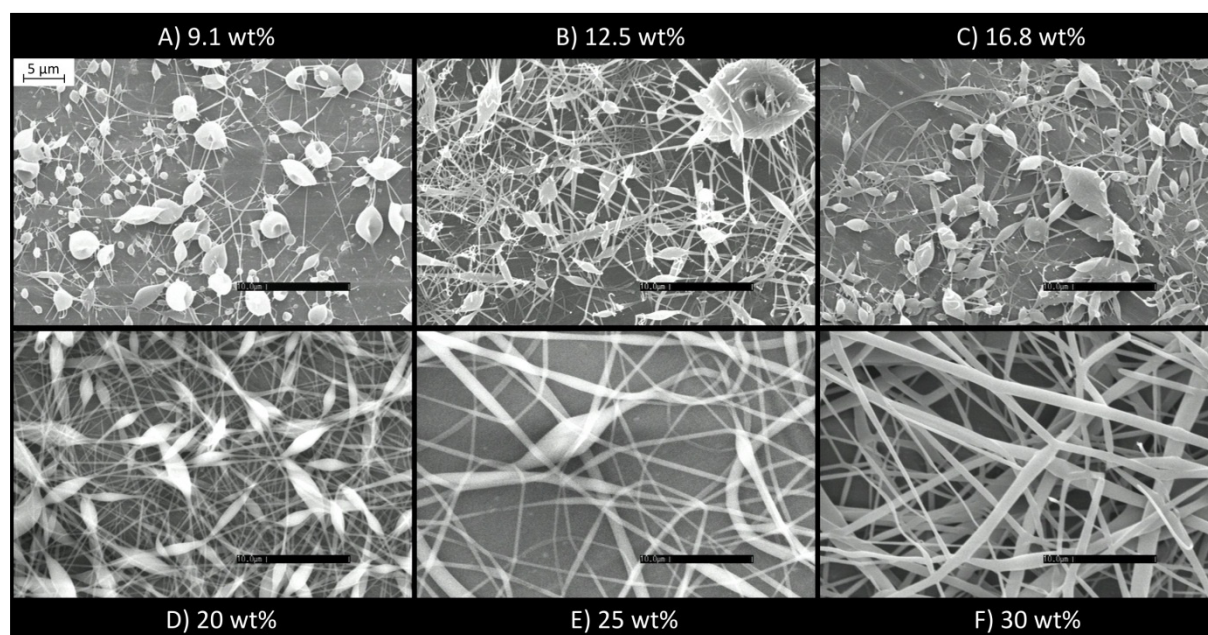


**Figure 3:** SEM-images of pure PLGA electrospun fibres. PLGA (RG504) was dissolved in acetone and electrospun. These pictures demonstrate that with increasing concentration the formation of beads and beaded fibres turns into smooth and regular fibres.

Spinning from solutions with concentrations of 25 and 30 wt% PLGA in acetone resulted in uniform fibres without beads (Figure 3 E-F). The difference between Figure 3 E and F is the increased fibre diameter in Figure 3 F, which can clearly be related to the higher concentration of PLGA. A comparison of fibres from 20 wt% to those from 30 wt% solutions shows an almost tenfold increase in fibre diameter from 250 nm to 2.3 μm. The fibre morphology improved significantly from 20 to 25 wt% solutions, while no further

improvement could be obtained with higher concentrations. The optimum concentration for electrospinning of PLGA from acetone was determined to be 25 wt%.

To summarise, dilute solutions with few entanglements lead to beads and beaded fibres, examples are displayed in Figure 3 A-D. Sufficient entanglements resulted in a stable jet and hence in uniform fibres, as shown in Figure 3 E and F. Thus the theoretical explanation of entanglements in polymer solutions and their corresponding electrospun products given in Chapter 2 can be used to explain the observed phenomena.

### 3.1.2 Dual component solution

#### 3.1.2.1 PLGA

With regard to advanced electrospinning options such as the inclusion of peptides or drugs (discussed in Chapter 4), pure acetone solutions did not provide acceptable results for most water soluble peptide sequences. Therefore, solvent additives featuring proper solubility for both PLGA and peptides were tested. Water, as a native solvent for peptides, is a non-solvent for PLGA: even 5 v/v% of water in acetone resulted in precipitation of PLGA rendering the solution not suitable for electrospinning. Instead, dimethyl sulfoxide (DMSO) as a polar, aprotic and nontoxic solvent featured not only good solvent properties for PLGA but also for a large amount of peptides and was miscible with acetone.

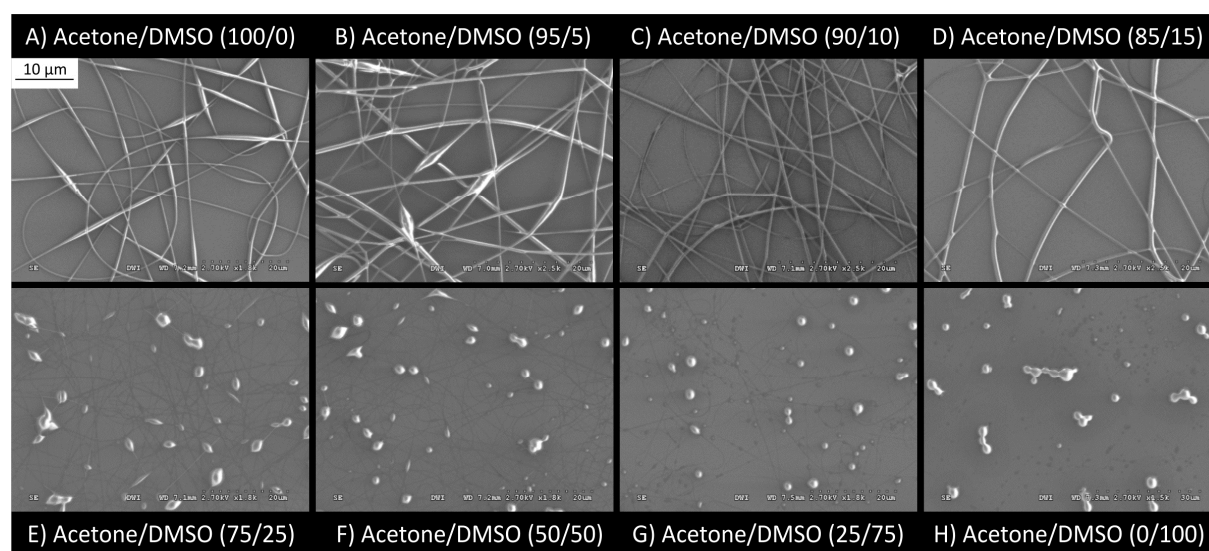


**Figure 4:** SEM-images of pure PLGA electrospun fibres. 25 w/v% PLGA (RG504) was dissolved in various acetone-DMSO mixtures and electrospun. Two transitions are observed: First, from spindle shaped fibres to smooth fibres at an acetone-DMSO ratio of 90:10; secondly to electrospayed particles as a consequence of the high surface tension of DMSO.



The spinning properties were tested in a series with pure PLGA fibres. Generally 25 w/v% PLGA solutions were examined with various acetone – DMSO mixtures.

Figure 4 displays the PLGA fibre morphologies spun from acetone – DMSO solutions. Starting with a 100% acetone solution the fibres featured spindle-like shapes. These defects are minimised at an additive concentration of 10 v/v% DMSO. Higher concentrations than 25% DMSO lead to predominantly beads-on-string morphologies with mostly inhomogeneous beads produced from 100% DMSO solutions.

Best results were achieved with a solvent composition of 90/10 v/v% acetone/DMSO and set as a “standard” for further investigations. These observations can be explained with respect to the dielectric constant DMSO and its surface tension (Table 1). Higher dielectric constants result in increased charging of the jet. The forces of the electric field exert more stress on the jet and lead to thinner diameters [12]. The surface tension of 43 mN/m compared to 23 mN/m for acetone caused an axisymmetric jet instability (Rayleigh instability) that gradually changed the fibre morphology from smooth fibres to beaded fibres and finally beads [13].

**Table 1:** Properties of applied solvents.

	dielectric constant $\epsilon_r$	surface tension $\gamma$ [ $10^{-3}$ N/m]	viscosity $\eta$ [ $10^{-3}$ Pa·s]	vapour pressure P [kPa (at 25°C)]	conductivity $\sigma$ [ $\mu$ S/cm]
acetone	20.7	23.3	0.36	24.6	0.2
DMSO	48	43	2.14	0.6	0.03
water	80.2	72.8	1.002	3.16	0.04

### 3.1.2.2 PLGA with functional NCO-sP(EO-stat-PO) additive

Transferring the gathered knowledge of PLGA electrospinning to an alternative, comprised of PLGA and the prepolymer additive “NCO-sP(EO-stat-PO)” resulted in homogeneous fibres spun from a solution of 25 w/v% PLGA and 5 w/v% NCO-sP(EO-stat-PO). The observed fibres had increased average diameters of 2.4  $\mu$ m compared to pure PLGA fibres with average diameters of 2.3  $\mu$ m. This change can be explained by the increased viscosity of the spinning solution [14]. The fibre formation process is solely based on chain entanglements within

PLGA molecules. Their inherent viscosity of 0.45 dl/g represents an average  $M_w$  of 45 kDa being long enough to form entanglements, whereas NCO-sP(EO-*stat*-PO) prepolymers of 12 kDa size and a six-arm geometry cannot contribute to the fibre formation process. The latter instead may form a hydrogel network after the electrospinning process but no crosslinking agents were present during the spinning process itself.

The viscosities of a 25 w/v % PLGA and a 25 w/v % PLGA with 5 w/v % NCO-sP(EO-*stat*-PO) solution were 0.145 Pa·s and 0.221 Pa·s, respectively. The setup of the rheology tests did not prevent acetone evaporation during the measurements, thus the viscosity of pure PLGA and PLGA/sP(EO-*stat*-PO) solutions increased during the course of the experiment. However, 15 minutes after mixing of the spinning components the viscosity of NCO-sP(EO-*stat*-PO) solutions started to increase significantly faster than pure PLGA solutions. This suggests a gel forming process within the prepolymer containing solution, as in contrast to a pure PLGA solution with no reactive groups, the isocyanates of the star polymer can form a dense hydrogel network in the presence of water. This finding agreed with the observation that electrospinning experiments were impaired after two hours when the solution turned into a gel.

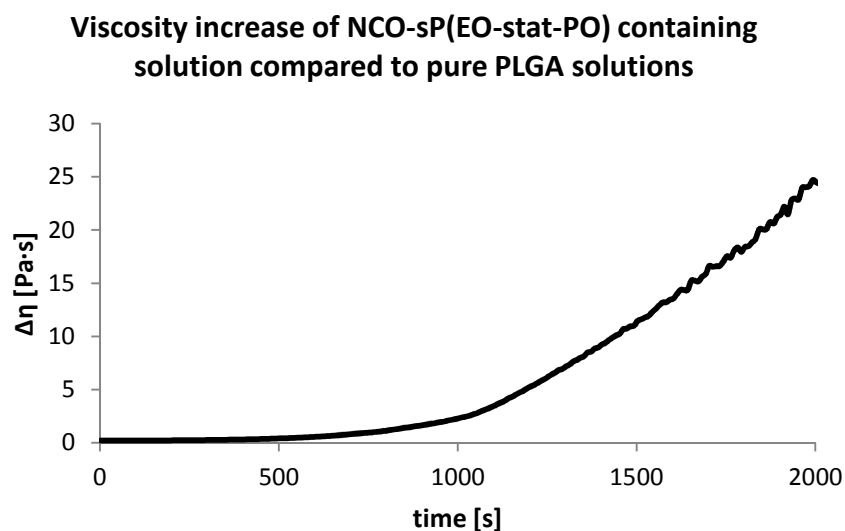


**Figure 5:** Increase of viscosity as a consequence of a hydrogel formation of NCO-sP(EO-*stat*-PO).

### 3.1.3 Conductive solvent additives

In addition to biocompatibility and specific functionality, fibres designed for ECM mimicry are recommended to possess similar morphology to natural ECM fibres. With relatively thick NCO-sP(EO-*stat*-PO)/PLGA fibres with 2.4  $\mu\text{m}$  average diameter compared to native

extracellular matrix fibres (100 nm diameter [15, 16]) there is still range for optimisation. The main characteristics that are decisive for electrospinning are the solution properties such as viscosity, surface tension and conductivity. Optimising these first, followed by an extensive variation and analysis of process parameters such as applied voltage, flow rate, spinneret to target distance and cannula size leads to the ability to control fibre diameters and morphologies with desired characteristics. The following paragraphs focus on adjusting the conductivity of the electrospinning solution followed by analysing the dependencies of the mentioned process parameters. With regard to future incorporation of peptides into spinning solutions, properly dissolved additives are crucial for reactions with isocyanates. Though some peptides may be solubilised in DMSO, most peptides and especially proteins need to be dissolved in water. In spite of PLGA precipitation in acetone solutions with more than 5 v/v% water, as a “minor” additive with less than 5 v/v %, water did not lead to precipitating PLGA. Therefore 2 v/v % water was mixed into the spinning solution. Small amounts of trifluoroacetic acid (TFA) were included as the strong acid significantly increased conductivity.

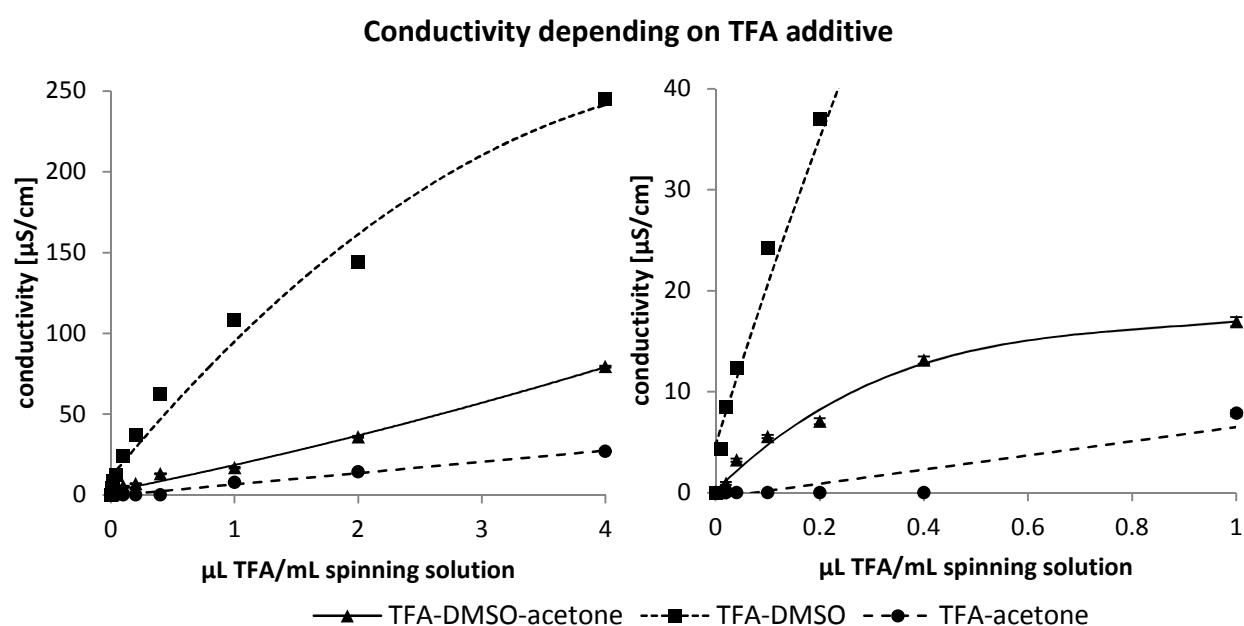


**Figure 6:** The conductivity of spinning solutions with DMSO and acetone show an initially strong increase in conductivity before a linear progression sets in.

The graphs in Figure 6 show the increase in conductivity depending on the amount of TFA in the spinning solution. As a complex solvent mixture is used, a linear relation between TFA

concentration and conductivity is only observed for concentrations above 0.1 % TFA in the spinning solution.

Figure 7 depicts the change in fibre diameter distribution which is dependent upon the amount of TFA.

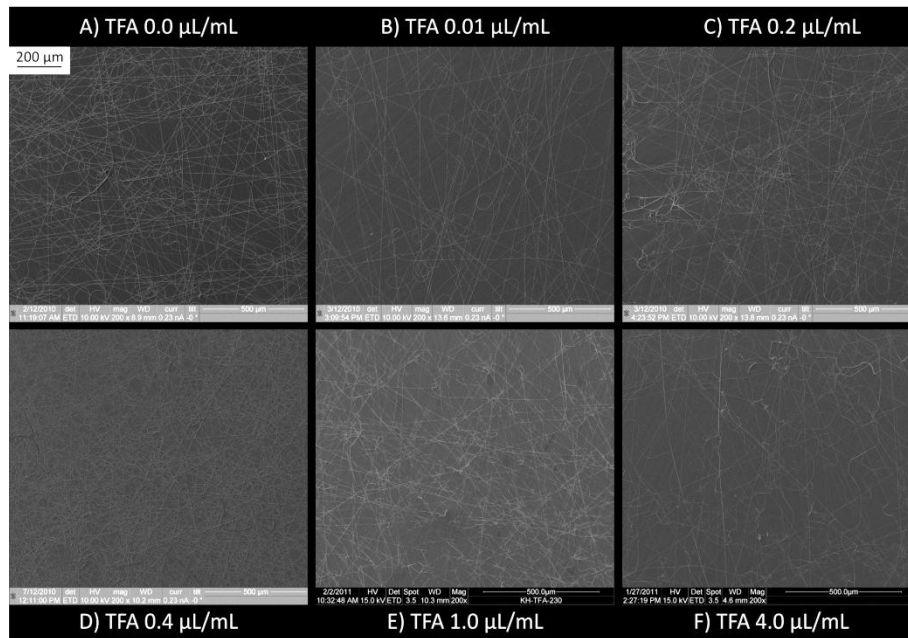


**Figure 7:** SEM-images of sP(EO-*stat*-PO)/PLGA electrospun fibres. Several spinning solutions were examined with varying TFA content. From A) to D) the fibre diameter is constantly decreasing, whereas for E) and F) inhomogeneities in the spinning behaviour increased, leading to a broader fibre size distribution.

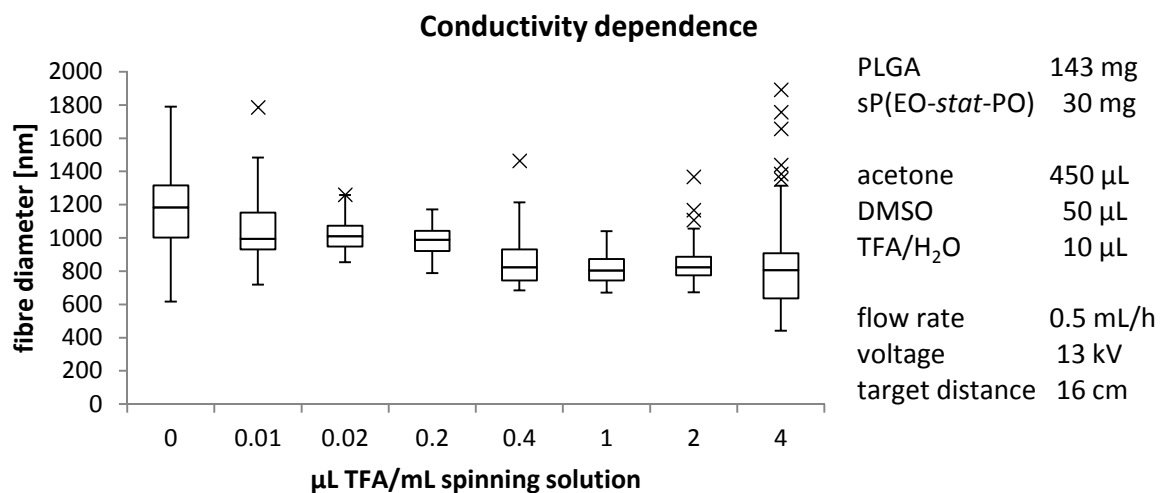


**Figure 8:** Boxplot of the fibre diameter distribution depending on the conductivity of the solution.

Already 0.02 µL TFA/mL spinning solution changed the fibre distribution from a broad distribution of  $1246 \pm 590$  nm without TFA to  $1011 \pm 95$  nm. In this series the smallest mean

diameter was found at 1.0  $\mu\text{L}$  TFA/mL spinning solution with  $821 \pm 97$  nm. In spite of the narrow fibre size distribution, SEM images reveal an inhomogeneous deposition pattern caused by strong bending instabilities [17]. Higher conductivities amplify this effect. Figure 7 displays the increasing inhomogeneity together with a broadening fibre size distribution. For the highest tested TFA content (4.0  $\mu\text{L}$  TFA/mL spinning solution) smallest fibre diameters were achieved at the cost of unsteady electrospinning behaviour and a wide fibre size distribution.

### 3.1.4 NCO-sP(EO-stat-PO) concentration influences

Various amounts of NCO-sP(EO-stat-PO) can be incorporated into PLGA fibres. Figure 9 depicts the changes in fibre morphology with increasing star polymer content in the fibres. A spinning solution consisting of acetone and DMSO produced wet fibres that were fused at a fibre composition of 75 % PLGA and 25 % NCO-sP(EO-stat-PO). Comparable solutions with higher conductivities due to the TFA additive generated discrete fibres with 30 % star molecules. The higher conductivity led to a stronger acceleration of the jet and induced a more pronounced whipping instability, giving more time for solvent evaporation and jet thinning.

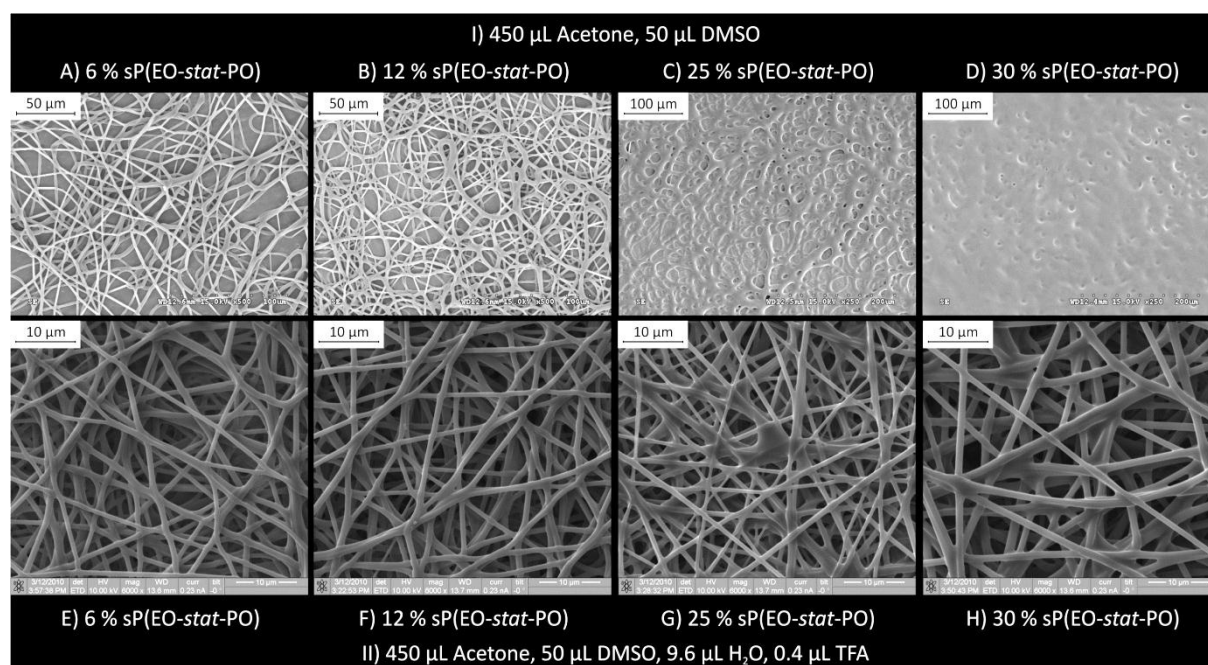


**Figure 9:** SEM images of NCO-sP(EO-stat-PO)/PLGA fibres, morphological differences depending on the NCO-sP(EO-stat-PO) content with or without TFA additive.

## 3.2 Process parameters

### 3.2.1 Voltage

The electric field between spinneret and grounded target is a governing parameter for the formation of a Taylor cone and jet initiation. It is influenced by the applied voltage and depending on its strength the fibre morphology changes as displayed in Figure 10. Below 8 kV no jet initiation was observed though the polymer solution droplet already changed from a spherical to a conical shape. At 8 kV, firstly a stable jet was observed which produced homogeneous fibres with little secondary bending instability. With increasing field strength jet instabilities were amplified.

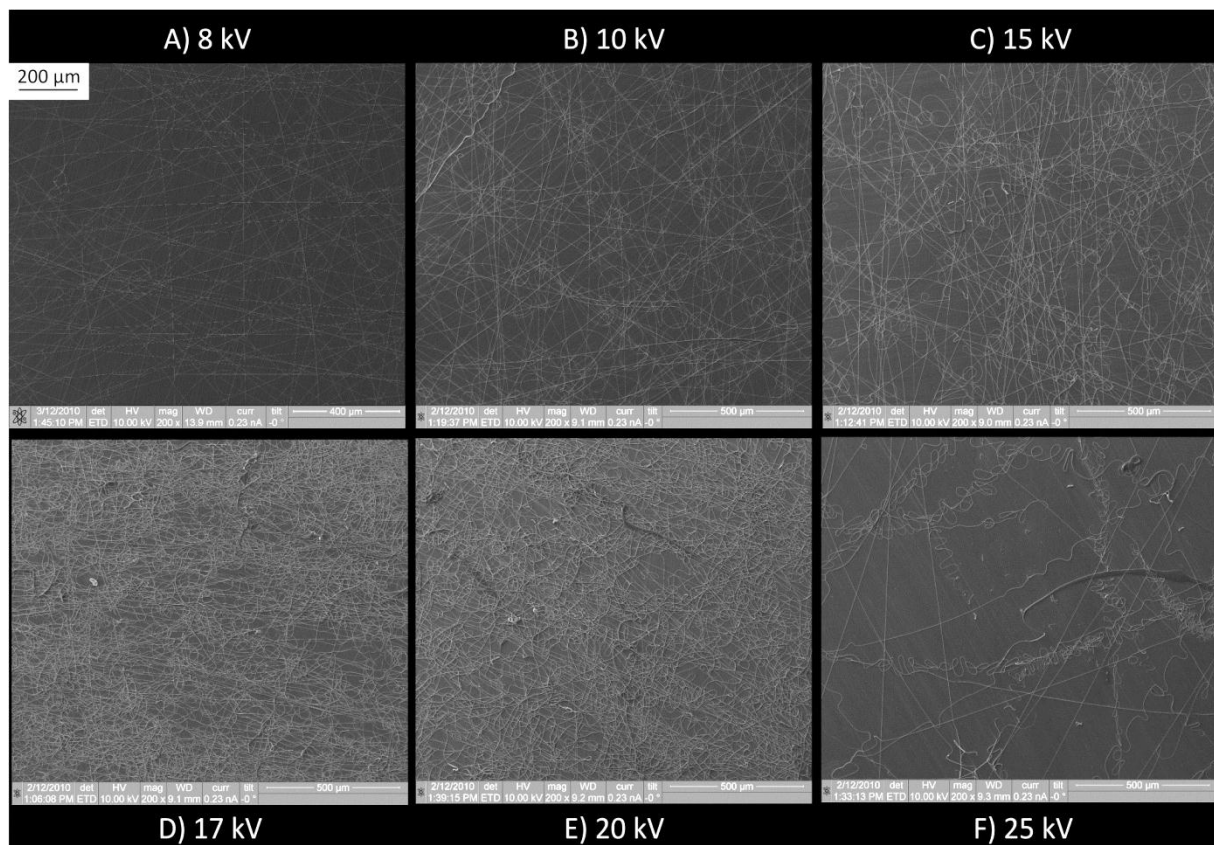


**Figure 10:** SEM-images of sP(EO-*stat*-PO)/PLGA electrospun fibres. A spinning solution with 0.4 μL/mL TFA was examined with respect to the applied voltage. With increasing voltage the fibre morphology changed from linear, straight fibres at 8 kV to curled fibres up to 20 kV. The bending instability increased in with higher charging. In F) the spinning process showed strong irregularities and inhomogeneous fibres were obtained.

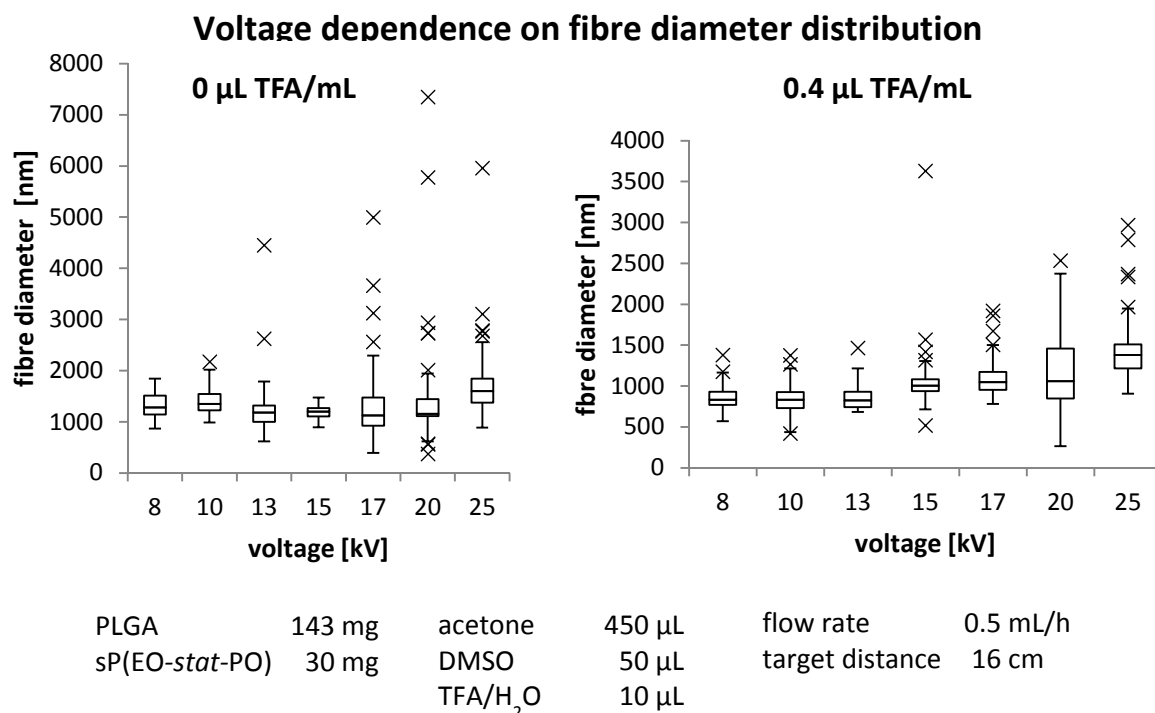


**Figure 11:** Boxplots of NCO-sP(EO-*stat*-PO)/PLGA fibre diameter distributions depending on voltage.

This can be seen with a pronounced coiling and at 25 kV in a “wriggling” pattern of deposited fibres. In the latter case there was no stable jet formation as it was ruptured as a consequence of a high acceleration through the electric field. Furthermore the diagrams indicate the stronger acceleration with an overall increase in fibre diameter and broader fibre size distribution for higher electric fields. A higher voltage leads to increased charging of the polymer solution. During the flight of the jet towards the target the charges condense on the fibre surface triggering secondary instabilities and jet buckling. The higher acceleration implies a faster jet speed towards the target, and consequently a shorter travel time and less time for jet thinning through solvent evaporation.

### 3.2.2 Collector distance

The process parameter of spinneret to collector distance is correlated with the applied voltage by the electric field strength. Here effects can be observed that support but also expand the statements from the last paragraph. Short collector distances such as 6 to 8 cm gave broad fibre size distributions around 1400 nm, whereas distances between 12 and 20 cm feature fibre sizes between 800 to 900 nm accompanied by a narrow distribution.

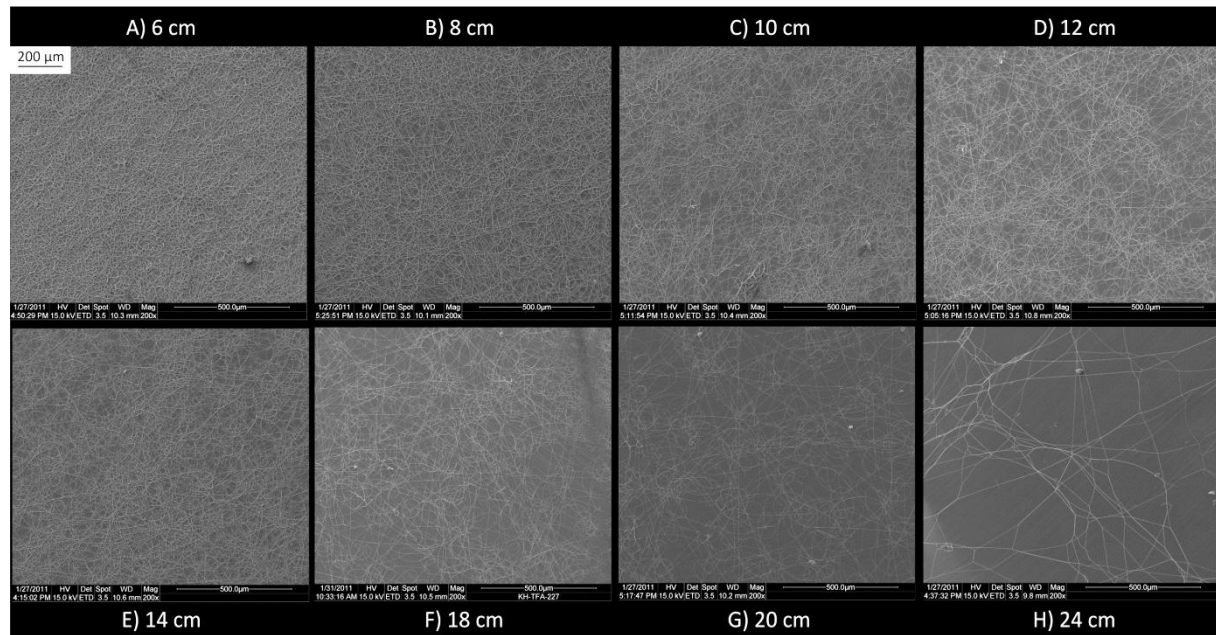


**Figure 12:** SEM-images of sP(EO-*stat*-PO)/PLGA electrospun fibres. A spinning solution with 0.4 μL/mL TFA was examined with respect to the spinneret to collector distance. Close distances of 6 to 8 cm resulted in thick fibres and a high deposition rate. Both decreased with increasing distance from the spinneret. At far distances H) 24 cm only few interconnected fibres were collected.

With relatively long tip to collector distances of 24 cm and more, the electrospinning jet lost stability due to low electric field strengths causing it to be attracted to the surrounding spinning chamber. At small distances the time of flight is short, with little time for jet thinning, though an intense jet whipping takes place due to the field strength of 2 kV/cm. For distances between 12 and 18 cm field strength and distance can be said to balance each other and similar spinning qualities can be observed. For greater distances the fibrous pattern becomes “branched” as soon as the field strength is insufficient to produce a stable jet towards the target. The SEM micrographs show electrospun fibres that were spun for 10 seconds each on an aluminium foil. The high collection density on samples with a spinneret to collector distance of 6 to 8 cm is a consequence of the small whipping range of the jet. Whereas the density of collected fibres decreases with increasing collector distance as the whipping radius also increases. With a relatively large collector distance of 24 cm, only a few fibres were deposited due to the relatively weak field strength (Figure 12 H).



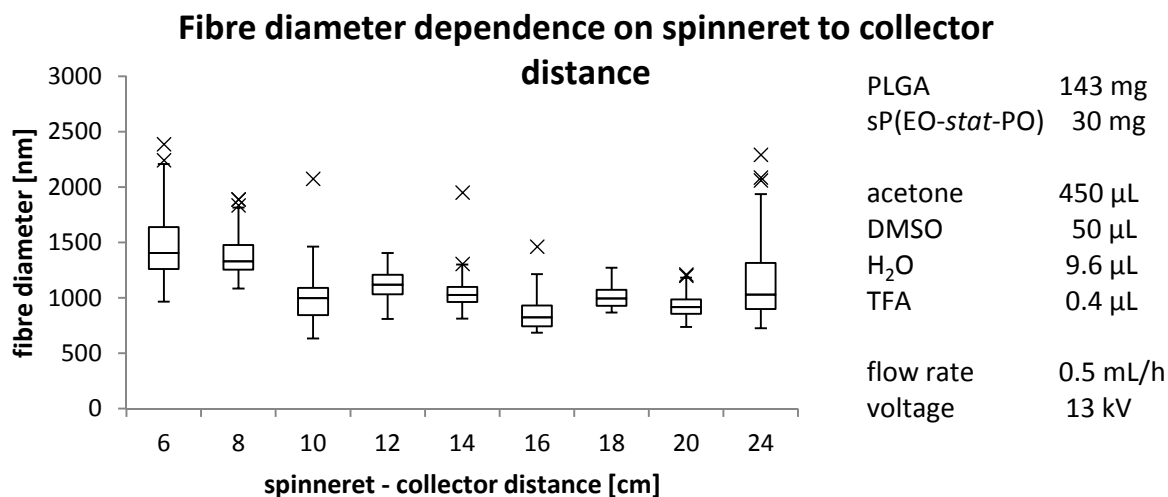


**Figure 13:** Boxplots of NCO-sP(EO-*stat*-PO)/PLGA fibre diameter distributions depending on the distance between spinneret and collector.

### 3.2.3 Flow rate

The flow rate can be set on the syringe pump to control the supply of polymer solution to the spinneret and additionally the production speed of fibres. Although its effect is not independent of parameters such as voltage and collector distance, changing the flow rate has a significant impact on fibre morphology. Figure 14 illustrates that a higher polymer solution flow rate through the spinneret will lead to larger diameter fibres. The characteristic deposition of fibres is more significantly influenced by jet buckling at lower flow rates, as seen by more coiling in Figure 14 A – D), whereas for higher flow rates the whipping radius is larger and the fibres appear almost straight. This effect is due to the diameter of the jet: the charge density is less on a larger diameter jet as it thins and condenses to form fibres. Therefore the primary jet instability, whipping, remains while secondary instabilities such as buckling and coiling are less frequent.

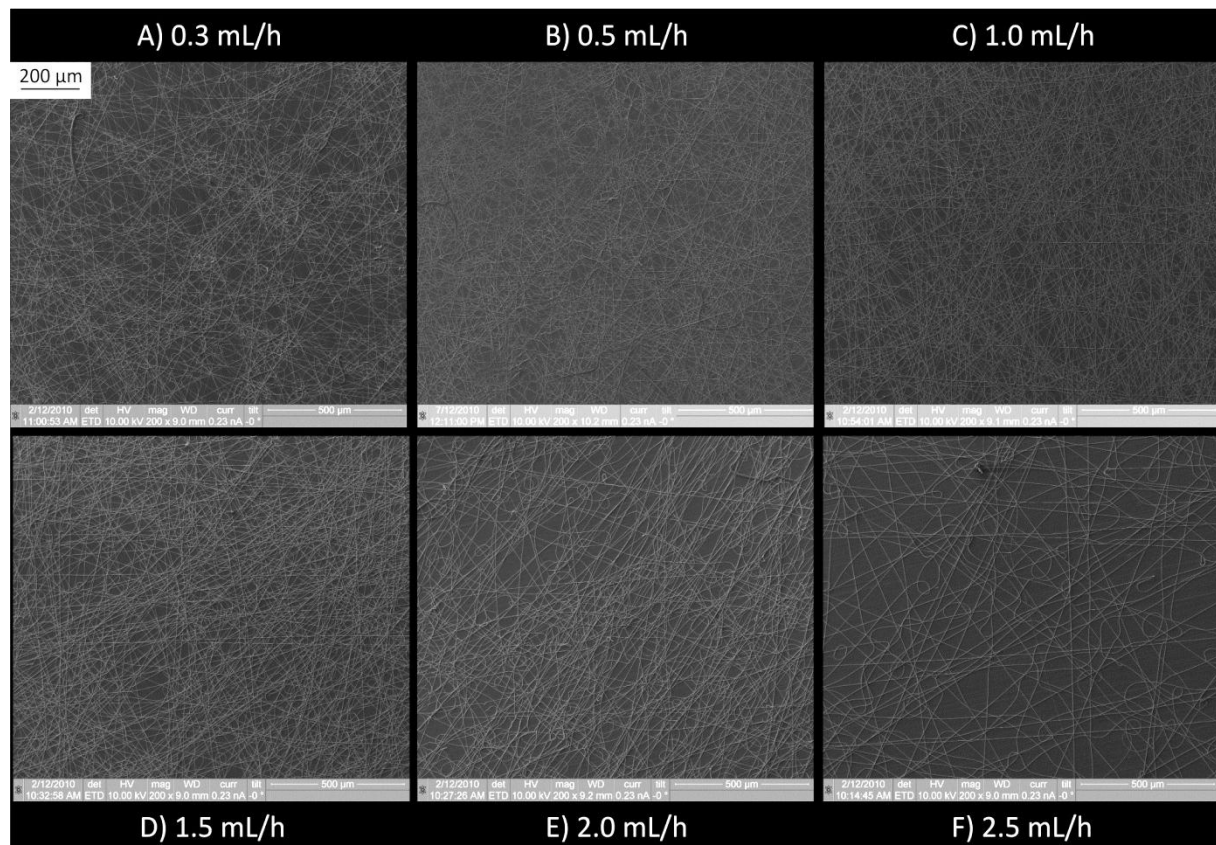


**Figure 14:** SEM-images of sP(EO-*stat*-PO)/PLGA electrospun fibres. A solution with 0.4 µL/mL TFA was spun at a varying flow rate but at a constant distance of 16 cm and with a voltage of 13 kV. The fibres showed a homogeneous morphology and exhibited larger diameters for higher flow rates.

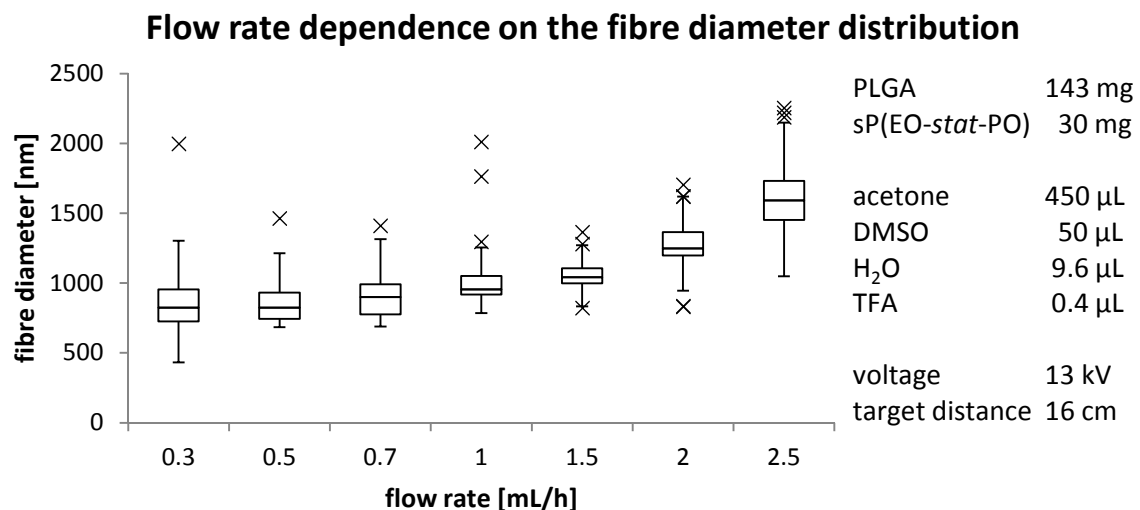


**Figure 15:** Boxplots of NCO-sP(EO-*stat*-PO)/PLGA fibre diameter distributions depending on the flow rate.

### 3.3 Ambient parameters

The process parameters were optimised at 20 °C and 40 % relative humidity. These conditions proved to be ideal for electrospinning PLGA and NCO-sP(EO-*stat*-PO)/PLGA fibres

from solutions consisting mainly of acetone and DMSO. Temperatures above 24 °C led to irregular spinning behaviour. Distinguishing features are jet breakup and solidifying droplets at the tip to the spinneret. Once a droplet with a solid shell was formed, new jet initiation was poor or prohibited. The reason for this phenomenon is an increased volatility of the solvent components with the largest contributor acetone.

At an increased relative humidity of 60 %, unstable spinning behaviours were also observed. Here the charged jet may be subject to discharging phenomena resulting in fewer forces that cause jet deformation and acceleration towards the collector. Here, an unstable spinning behaviour was observed that was associated with solvent evaporation at the droplet on the spinneret and subsequent prevention to form a new Taylor cone and jet.

### **3.4 Fibre properties**

Electrospun fibres should possess properties which meet the requirements for their intended use. In the field of TE important factors include adequate mechanical strength and flexibility so that the electrospun scaffolds can be handled during cell culture experiments and for implantation surgery [18]. Moreover, as the fibres only play an interim support role, they need to feature a degradation profile suitable for the targeted tissue and its related healing time. Besides the “passive” properties discussed in this chapter, scaffold functionality is examined in Chapter 4.

#### **3.4.1 Fibre strength**

Typical stress – strain curves of sP(EO-*stat*-PO)/PLGA fibres are given in Figure 16. The inherent properties of PLGA dominate the mechanical properties of the star polymer containing fibres. The maximal stress measured at fibre breakage was  $6.20 \pm 0.11$  MPa for PLGA fibres and  $5.48 \pm 0.62$  MPa for sP(EO-*stat*-PO)/PLGA fibres. The elongation was similar for both mesh types with  $50.5 \pm 13.5$  % for PLGA and  $53.4 \pm 21.5$  % for sP(EO-*stat*-PO)/PLGA meshes. The reported tensile strengths were in the range of 0.8 to 18.0 MPa and matched the strength required to culture dermal tissue [19-21]. Because the fibres are designed for a temporary scaffold application to support cells in damaged tissue, the meshes described above can be deemed to provide sufficient mechanical strength to withstand implantation and the tissue growth process [22].

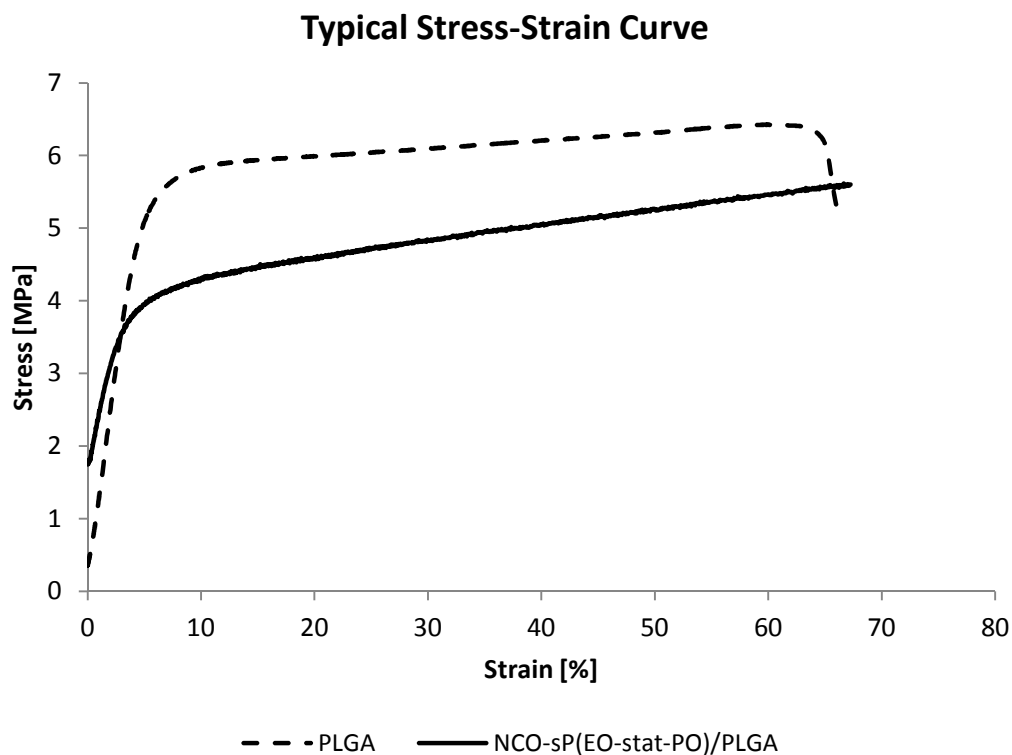


**Figure 16:** Representative stress-strain curves of PLGA and NCO-sP(EO-*stat*-PO)/PLGA fibres.

### 3.4.2 Fibre stability and deformation processes

Fibres made from NCO-sP(EO-*stat*-PO)/PLGA or pure PLGA are stable at ambient conditions (22°C, 50% r.h.) and can be stored for more than one year. This morphological stability changes with increasing temperature. In Figure 18, the reduction of electrospun mat sizes due to shrinkage is visualised depending on the temperature. Whereas no morphologic changes were observed at 22 °C either in a dry or wet state for NCO-sP(EO-*stat*-PO)/PLGA fibres, wet non-woven mats shrank at 37 °C to 60 % of their original length in both the x and y dimensions. The heat shrinkage effect enhanced with increasing temperature with biggest morphologic changes at 37 °C in a wetted state and 45 °C in dry atmosphere. For fibre mats kept in dry conditions the shrinkage gradually increased beginning at 37 °C up to 47 °C where 60 % of the original mesh size was reached. Along with shrinkage in the x-y dimensions, the fibre meshes grew in z-direction to 150 % of their original size. These observations were only made on fibre meshes spun on rotating drums. Fibres covalently attached to surfaces did not exhibit this shrinkage behaviour due to local fibre fixation.

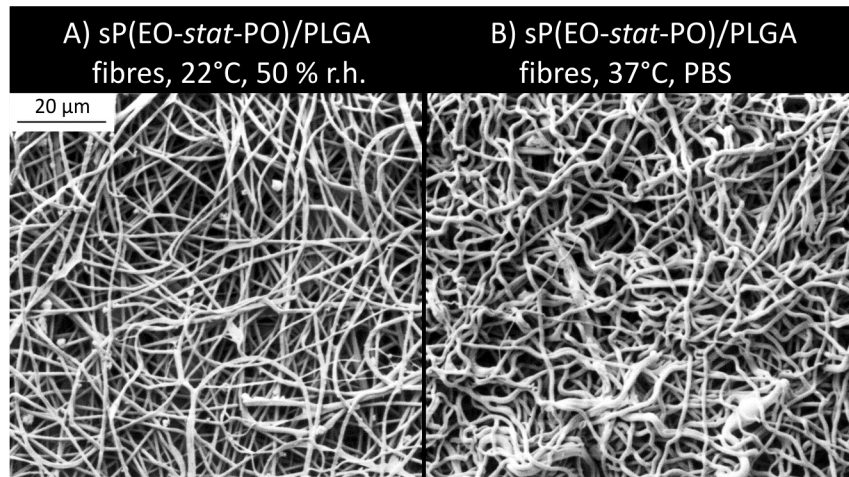


**Figure 17:** SEM images of NCO-sP(EO-stat-PO)/PLGA fibre meshes after 1 day of storage under A) ambient conditions or B) physiologic conditions.

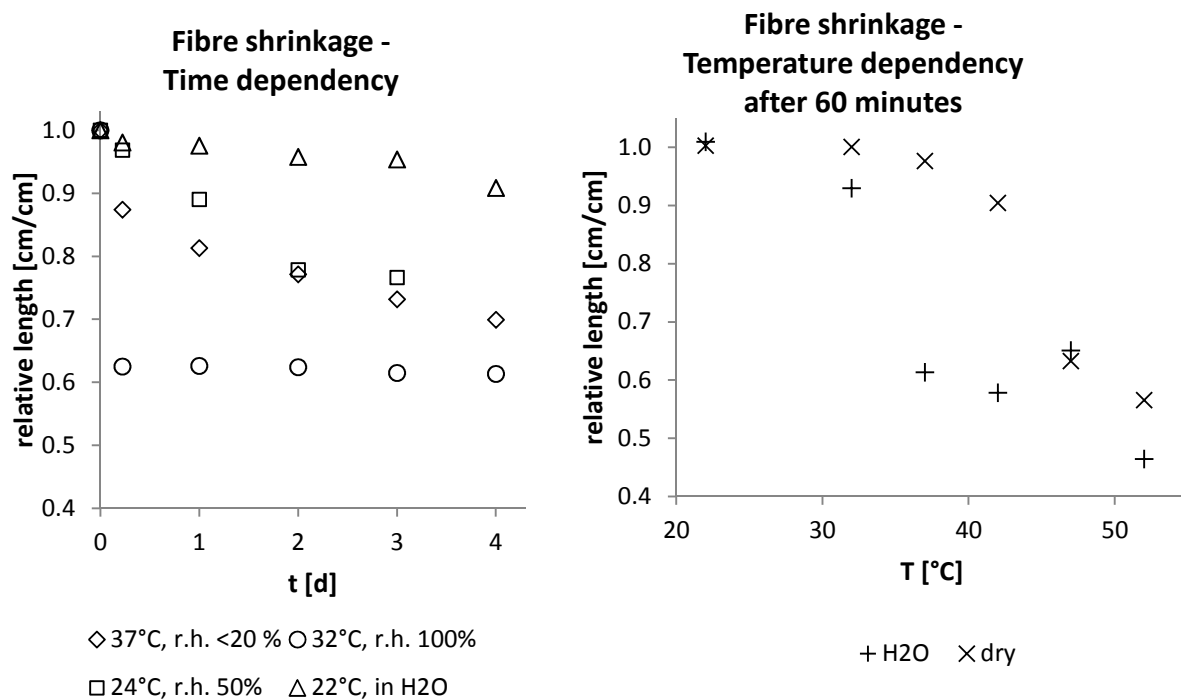


**Figure 18:** Diagrams of non-woven mesh shrinkage with time under various temperature and humidity conditions.

The phenomenon “heat shrinkage” points to an internal stress in polymer chains resulting from a relaxation process. Looking at the electrospinning process, a rapid solvent evaporation leads to polymer fibre formation. The polymer chains are stretched in the direction of the jet movement and entangle as a consequence of their coiled conformation in solution. This stretching results in oriented chains within amorphous domains containing

the entanglements. As solution electrospinning is generally performed at room temperature, well below typical glass transition temperatures ( $T_g$ ), polymers are solidified in an amorphous but oriented glassy state. At these temperatures the mobility of polymer chains is very limited but increases significantly around 45 – 50 °C, the glass transition region for PLGA. Here, oriented chains in amorphous regions relax and heat shrinkage is observed as described above with an associated reshaping process that led to an observed increase in mesh thickness. For elevated temperatures between glass transition and melting point further heat shrinkage takes place as stress is released in crystalline domains containing chain ends, defects and amorphous-crystalline interfaces [23].

The influence of water as a surrounding medium accelerates the heat shrinkage. Immersed in a liquid, the PLGA polymer chains can interact with the medium more directly. Penetrating the mesh accompanied with fibre swelling allows a direct heat transfer resulting in faster shrinkage. Shrinkage experiments, conducted at 37 °C, showed that even faster heat transfer is enabled with more hydrophobic solvents such as ethanol and isopropanol. In ethanol, sP(EO-*stat*-PO)/PLGA meshes shrank within 3 seconds to 40 % of their original size. Using Isopropanol as surrounding medium led to final mesh sizes of 46 % compared to untreated control samples.

### 3.4.3 Wettability studies

Sessile drop measurements were performed with a goniometer G40 using the electrospun meshes as substrates. It is known that PLGA fibre meshes are hydrophobic since the bulk contact angle of PLGA is around 80° [24]. In this study a water contact angle of 120° was measured on electrospun PLGA meshes, which is significantly higher than the value on bulk PLGA due to the roughness of the mesh [25]. Moreover, the water droplet remained unchanged on such a mesh for more than 30 min. In contrast, NCO-sP(EO-*stat*-PO) containing PLGA fibres are extremely hydrophilic. Upon contact with the mesh, a water droplet was immediately soaked into the mesh. Figure 19 shows a time series of a water droplet before contact, one second after contact and 5 seconds after contact on pure PLGA and on NCO-sP(EO-*stat*-PO)/PLGA fibre meshes. Compared to other studies where surface grafting of poly(methyl methacrylate) or gelation resulted in zero water contact angles [26, 27], this directly demonstrates the presence of NCO-sP(EO-*stat*-PO) molecules at the fibre surface.

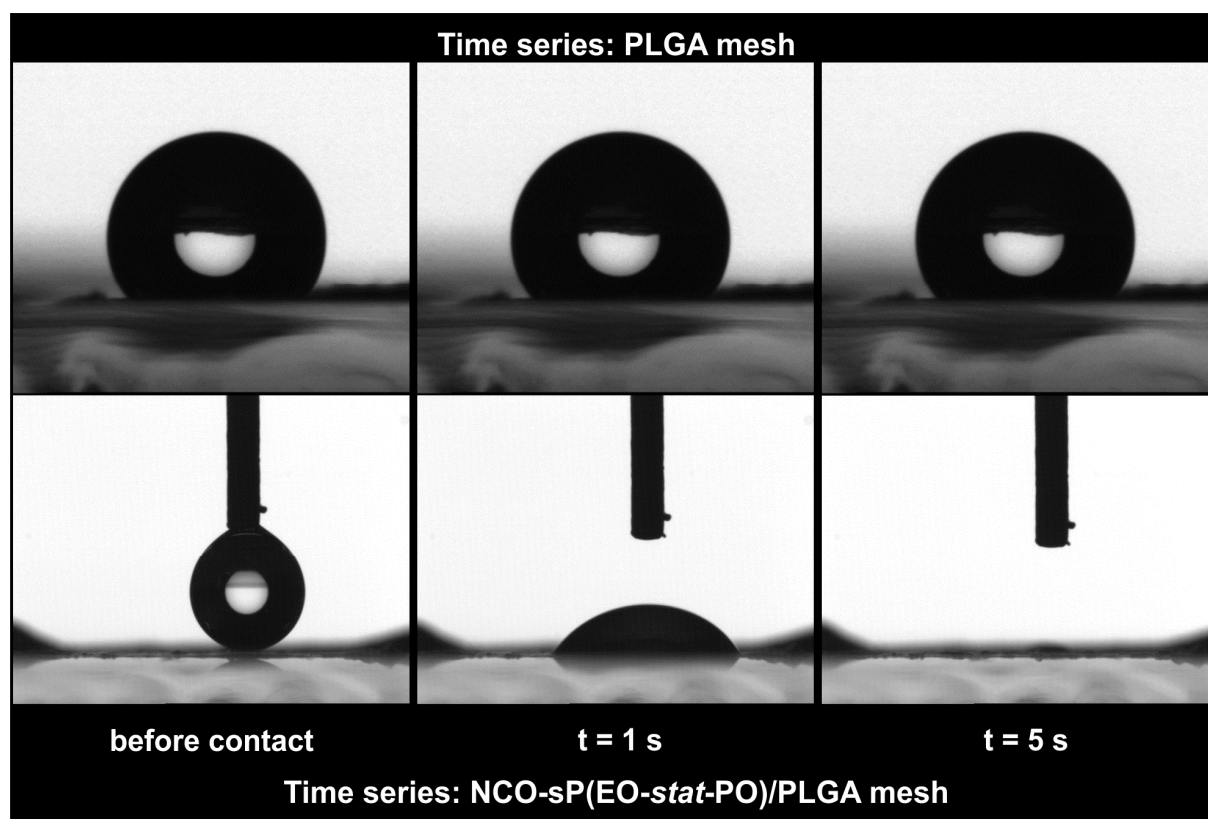


**Figure 19:** Contact angle measurements of a PLGA and a NCO-sP(EO-*stat*-PO)/PLGA non-woven. The PLGA mesh features a constant contact angle of  $120^\circ$  whereas any water droplet is soaked up by the PEG-containing mesh within seconds. Figure was reprinted from reference [28] with permission from Nature Publishing Group.

The mechanisms by which the hydrophilic star shaped molecules are enriched at the fibre surface are not absolutely clear. We hypothesise two probable mechanisms: first, the molecules surface segregate during the spinning process as an effect of solvent evaporation; or alternatively, electrostatic forces contribute to a surface segregation. A detailed discussion is given in paragraph 3.4.6.

### 3.4.4 Degradation studies

PLGA is a biodegradable material with hydrolytically cleavable ester linkages in the polymer backbone. The material degrades according to a bulk-degradation mechanism [29]. Thus, the transport rate of water into the fibres is crucial for the rate of degradation. In contrast to PLGA, the NCO-sP(EO-*stat*-PO) additive is a bioinert, non-degradable polyether. On the one hand, the reactive NCO-groups partly act as cross-linker for the PLGA chains, on the other hand the hydrophilic polyether backbone enables better wetting and better penetration of water into the fibres.

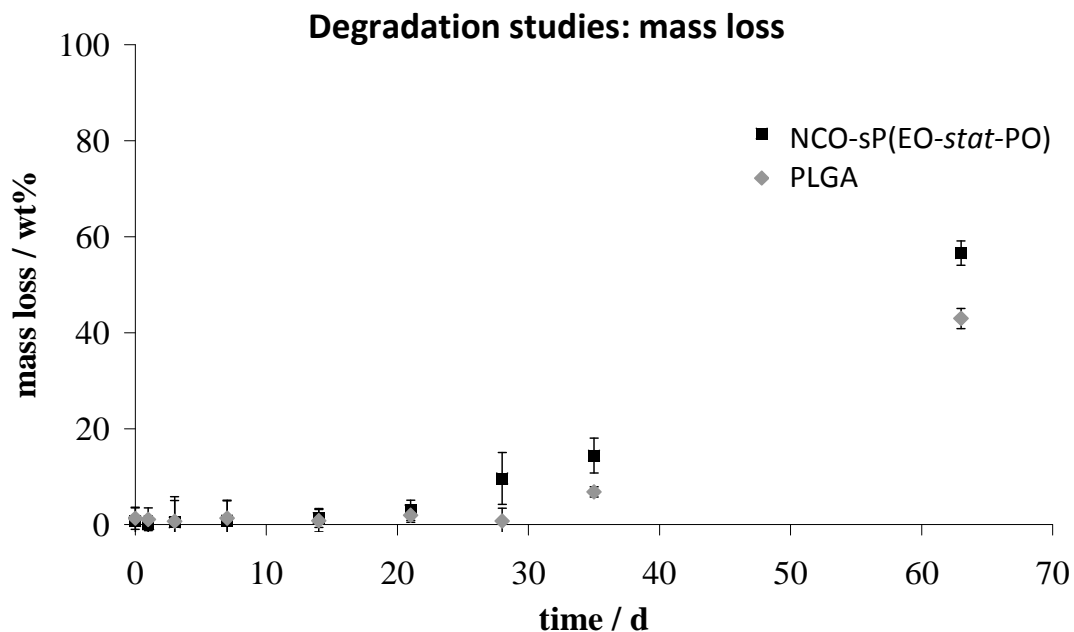


**Figure 20:** Degradation behaviour of PLGA and NCO-sP(EO-stat-PO)/PLGA meshes. Complete disintegration of the non-woven takes place within 3 months. Figure was reprinted from reference [28] with permission from Nature Publishing Group.

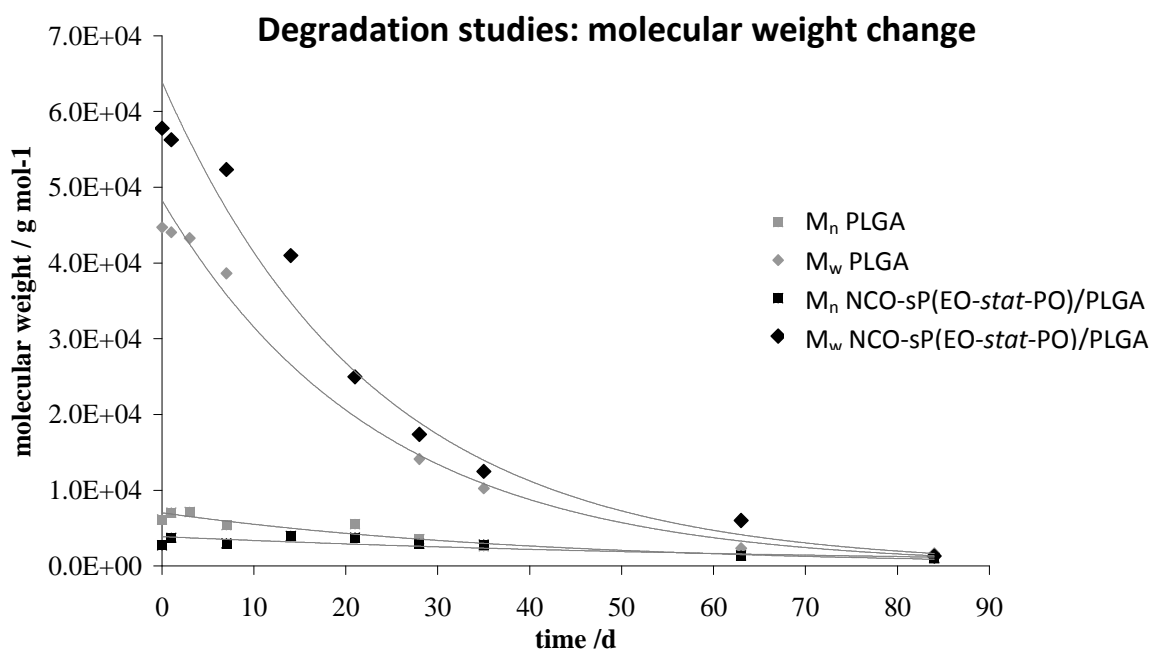


**Figure 21:** The change in molecular weight during 3 months of fibre degradation. Figure was reprinted from reference [28] with permission from Nature Publishing Group.

Figure 20 – Figure 21 show the mass loss and the change in molecular weight of pure PLGA fibres in comparison to NCO-sP(EO-stat-PO)/PLGA fibres. While the PLGA shows a weight



loss of 53 % after 9 weeks and a change in molecular weight from  $4.5 \cdot 10^4 \text{ g mol}^{-1}$  to  $2.3 \cdot 10^3 \text{ g mol}^{-1}$ , the NCO-sP(EO-*stat*-PO)/PLGA fibres reach a mass loss of 68 % after two

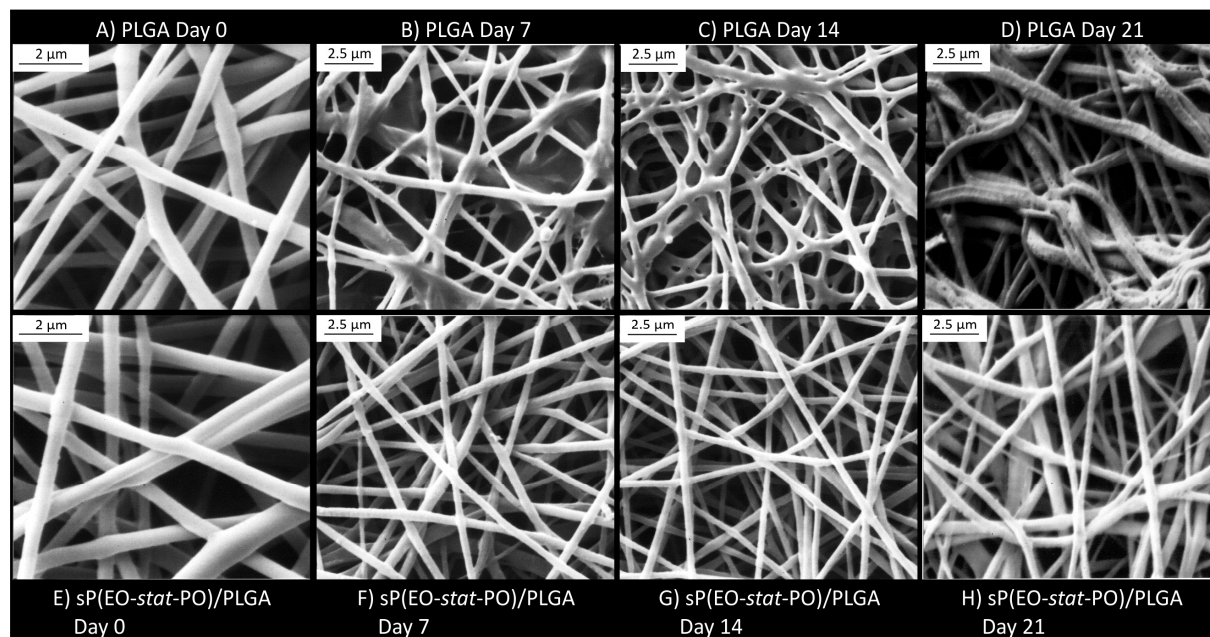


**Figure 22:** SEM images of morphological comparison between PLGA and sP(EO-*stat*-PO)/PLGA fibres after 0 to 21 days in PBS buffer at 37 °C.

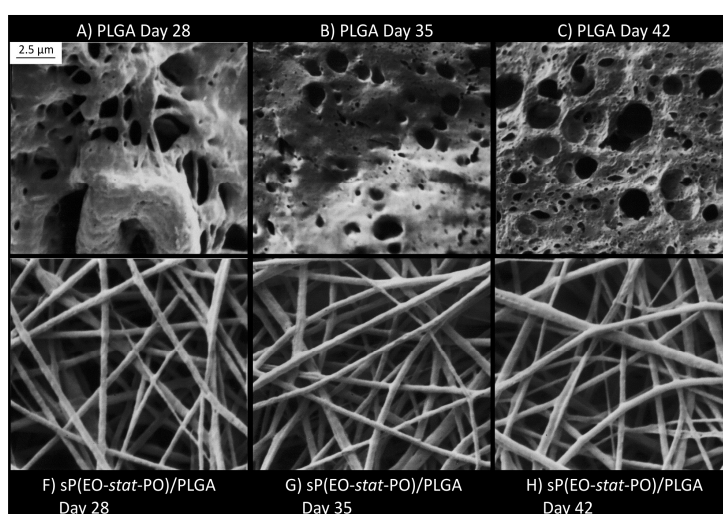


**Figure 23:** SEM images of morphological comparison between PLGA and sP(EO-*stat*-PO)/PLGA fibres after 28 to 63 days in PBS buffer at 37 °C.

months and a decrease in molecular weight from  $5.8 \cdot 10^4 \text{ g mol}^{-1}$  to  $6.0 \cdot 10^3 \text{ g mol}^{-1}$ . In fact, complete disintegration of the mesh was reached after 3 months. This demonstrates that the hydrophilicity which is introduced into the fibres upon addition of the polyether dominates the cross-linking effect and leads to an accelerated degradation of the material.

The morphological changes of PLGA and sP(EO-*stat*-PO)/PLGA fibres were monitored during degradation.

PLGA samples exhibited swelling and fibres merged within the first two weeks of degradation. After three and four weeks a significant number of pores were visible on the surface of the fibres. The degradation of PLGA is based on bulk erosion as described by Albertson *et al.* [9]. The formation of pores on the PLGA fibre surface correlates with the initiation of mass loss in the bulk degradation [30]. A similar morphological development has been observed on PLGA films by Ding *et al.* [31]. Star polymer containing fibres instead did not show swollen or merged fibres in the first weeks. The fibres were physically stable for six weeks without significant morphological changes for three weeks. Beginning with week four, small pores were visible on the fibre surface. Though a faster degradation rate was found for sP(EO-*stat*-PO) containing fibres, their morphological stability is surprising but can be explained by intermolecular bonds of NCO-sP(EO-*stat*-PO) forming a hydrogel network [32]. As the star molecules are mainly present on the fibre surface, (see paragraphs 3.4.3 and 3.4.6) the dense hydrogel network retards the disintegration of fibres through swelling.

### 3.4.5 XPS data

**Table 2** compares calculated XPS values of PLGA and PLGA/sP(EO-*stat*-PO) fibres with those measured. Additionally, XPS data of pure sP(EO-*stat*-PO) surfaces are given as reported and previously calculated [33, 34]. Importantly, the data given from Gopal *et al.* [35] includes amine-group determination of the pure sP(EO-*stat*-PO) layers by gas-phase derivatisation with pentafluorobenzaldehyde (PFB), so the spectra include F1s peaks.

Calculations for the sP(EO-*stat*-PO) surface are based on a statistical distribution of star molecules throughout the measurement volume. For calculating the atom per cent in the electrospun fibres, a mixture with PLGA (83% PLGA) was assumed which corresponds to the ratio taken for fibre preparation. The calculations from Groll *et al.* include a molecular layer model [34]. As contact angle of a previous study [32] and XPS measurements in Reference [34] point towards surface segregation of the star polymer endgroups to the layer surface, calculations were performed according to a model in which the star polymers are assembled in monomolecular layers, where some endgroups in the top layer of star molecules surface segregate. Different amounts of endgroup segregation and number of

**Table 2:** XPS data of PLGA fibres, NCO-sP(EO-*stat*-PO)/PLGA fibres and previously published values of pure

NCO-sP(EO-*stat*-PO) surfaces. Table was reprinted from reference [28] with permission from Nature Publishing Group.

		Atomic concentration / %			
		C 1s	O 1s	N 1s	F 1s
PLGA	calculated	56	44	0	0
	measured	62.22	37.78	0	0
17% NCO-sP(EO- <i>stat</i> -PO) 83% PLGA	calculated	56.34	43.58	0.07	0
	measured for standard fibre preparation conditions	71.04	27.82	1.14	0
	measured for water free fibre spinning	69.57	29.3	1.13	0
	(calc.)	69.41	29.28	1.31	0
NCO-sP(EO- <i>stat</i> -PO) surface	measured in [33]	70.8	27	2.2	0
	calculated in [35], including pentafluorbenzaldehyde (PFB)	70.0	26.6	2.4	1.0
	measured in [35], incl. PFB	70.5	25.6	2.1	1.2

layers in the measurement volume of the XPS were compared to the measurement data. The best fit is shown in **Table 2**. The deviation of PLGA measurements from the theoretical values have repeatedly been observed and are unclear. However, most importantly, measurements of PLGA/sP(EO-*stat*-PO) fibres point out a much more pronounced and significant deviation from the calculated expected value with a strong increase in C1s and decrease in O1s. Together with the much stronger N1s value, as expected from homogeneous distribution of the sP(EO-*stat*-PO) molecules in the PLGA, it demonstrates that the star shaped additive is enriched on the fibre surface. Moreover, a comparison of the XPS measurements of the fibres with data observed from pure sP(EO-*stat*-PO) coatings show that regarding C1s and O1s content, the spectra are very similar to the PLGA/sP(EO-*stat*-PO) fibres, indicating a pronounced enrichment of the star molecules at the fibre surface. However, the N1s peak is significantly stronger in the flat films. This has been interpreted as surface-segregation of the hydrophobic endgroup of the star molecules to the surface, resulting in an enrichment of endgroups and thus higher N1s peaks than expected. While this effect still contributes to the

surface enrichment of the star molecules on the fibres, some of the endgroups may act as hydrophobic anchors in the PLGA matrix. Hence, a lower degree of surface segregation leads to an atom per cent value that resembles statistic distribution of the endgroups on the star polymer modified fibres.

### 3.4.6 Surface segregation of sP(EO-*stat*-PO)

As mentioned above, surface-segregation of the hydrophobic endgroups contributes to the surface enrichment of the star polymers as the endgroups pull the hydrophilic arms with them. After solvent evaporation and solidification of the fibre, contact with water then causes the endgroups to bend back towards the hydrophobic fibre, and the polymer backbone dominates the wetting behaviour. However, since the endgroups only account for less than 3 wt% of the sP(EO-*stat*-PO) molecules, and especially since with this model, the PLGA should at least to a certain extent be located at the fibre surface, this model does not completely explain the dense and seemingly exclusive location of the star molecules at the fibre surface. Another important factor is the charge distribution in the polymer matrix, especially comparing PLGA and the sP(EO-*stat*-PO) polymers. In electrospinning, the Taylor cone and the electrospinning jet act as capacitor. As on any capacitor surface, the charges will be distributed on the surface of cone and fibre. The repelling nature of like charges tries to minimise the charge density. Jet elongation as one means has been discussed in Chapter 2, another possibility opens up in this case: as two polymers with different dielectric constants are spun ( $\epsilon_r(\text{PEO}) \approx 5$  [36];  $\epsilon_r(\text{PLGA}) \approx 2.5$  [37]), the charges are best shielded in the component with the higher dielectric constant. This may cause the more polar component (sP(EO-*stat*-PO)) to preferentially segregate to the fibre surface. This effect is further strengthened by the polar groups (urethane, urea, amine) associated with the star polymers that can act as charge carriers.

## 4 Conclusion

In this chapter a suitable scaffold for TE has been developed and characterised. It is comprised of a biodegradable polymer, PLGA, and a hydrophilic, isocyanate terminated star polymer. In a series of electrospinning experiments appropriate solvent compositions were found and in combination with adjustable process parameters the fibre dimensions can be set between 2.5  $\mu\text{m}$  and 700 nm. The additive NCO-sP(EO-*stat*-PO) renders the spun PLGA fibres hydrophilic as stable contact angles of 120° for PLGA fibres change to complete water uptake within seconds for the compound fibres. Together with full fibre degradation within 3 months these properties warrant the potential use of NCO-sP(EO-*stat*-PO)/PLGA fibres in soft TE. The surface segregation of the star molecules serves as a basis so that their isocyanate endgroups can be modified on the fibre surface. This allows specific cell targeting in further studies that are discussed in the following chapters.

## 5 References

- [1] Halperin A., 'Polymer Brushes That Resist Adsorption of Model Proteins: Design Parameters', *Langmuir*, 15, **1999**, 2525-2533.
- [2] Aumailley M. and Gayraud B., 'Structure and Biological Activity of the Extracellular Matrix', *Journal of Molecular Medicine*, 76, **1998**, 253-265.
- [3] Heo Y. J., Shibata H., Okitsu T., Kawanishi T. and Takeuchi S., 'Fluorescent Hydrogel Fibers for Long-Term in Vivo Glucose Monitoring', in *Solid-State Sensors, Actuators and Microsystems Conference (TRANSDUCERS), 2011 16th International*, (2011), pp. 2140-2143.
- [4] McPherson T., Kidane A., Szleifer I. and Park K., 'Prevention of Protein Adsorption by Tethered Poly(Ethylene Oxide) Layers: Experiments and Single-Chain Mean-Field Analysis', *Langmuir*, 14, **1998**, 176-186.
- [5] Unsworth L. D., Tun Z., Sheardown H. and Brash J. L., 'In Situ Neutron Reflectometry Investigation of Gold-Chemisorbed PEO Layers of Varying Chain Density: Relationship of Layer Structure to Protein Resistance', *Journal of Colloid and Interface Science*, 296, **2006**, 520-526.
- [6] Götz H., Beginn U., Bartelink C. F., Grünbauer H. J. M. and Möller M., 'Preparation of Isophorone Diisocyanate Terminated Star Polyethers', *Macromolecular Materials and Engineering*, 287, **2002**, 223-230.
- [7] Gasteier P., Reska A., Schulte P., Salber J., Offenhäusser A., Moeller M. and Groll J., 'Surface Grafting of PEO-Based Star-Shaped Molecules for Bioanalytical and Biomedical Applications', *Macromolecular Bioscience*, 7, **2007**, 1010-1023.
- [8] Discher D. E., Janmey P. and Wang Y.-I., 'Tissue Cells Feel and Respond to the Stiffness of Their Substrate', *Science*, 310, **2005**, 1139-1143.
- [9] Albertsson A. C. and Varma I. K., 'Aliphatic Polyesters: Synthesis, Properties and Applications', in *Advances in Polymer Science*, (2002), pp. 1-40.
- [10] Li W. J., Laurencin C. T., Cateforis E. J., Tuan R. S. and Ko F. K., 'Electrospun Nanofibrous Structure: A Novel Scaffold for Tissue Engineering', *Journal of Biomedical Materials Research*, 60, **2002**, 613-621.
- [11] Kim K., Yu M., Zong X. H., Chiu J., Fang D. F., Seo Y. S., Hsiao B. S., Chu B. and Hadjiargyrou M., 'Control of Degradation Rate and Hydrophilicity in Electrospun Non-Woven Poly(D,L-Lactide) Nanofiber Scaffolds for Biomedical Applications', *Biomaterials*, 24, **2003**, 4977-4985.
- [12] Theron S. A., Zussman E. and Yarin A. L., 'Experimental Investigation of the Governing Parameters in the Electrospinning of Polymer Solutions', *Polymer*, 45, **2004**, 2017-2030.
- [13] Fong H., Chun I. and Reneker D. H., 'Beaded Nanofibers Formed During Electrospinning', *Polymer*, 40, **1999**, 4585-4592.
- [14] McKee M. G., Wilkes G. L., Colby R. H. and Long T. E., 'Correlations of Solution Rheology with Electrospun Fiber Formation of Linear and Branched Polyesters', *Macromolecules*, 37, **2004**, 1760-1767.
- [15] Smith L. A. and Ma P. X., 'Nano-Fibrous Scaffolds for Tissue Engineering', *Colloids and Surfaces B: Biointerfaces*, 39, **2004**, 125-131.
- [16] Elsdale T. and Bard J., 'Collagen Substrata for Studies on Cell Behavior', *The Journal of Cell Biology*, 54, **1972**, 626-637.
- [17] Reneker D. H., Yarin A. L., Fong H. and Koombhongse S., 'Bending Instability of Electrically Charged Liquid Jets of Polymer Solutions in Electrospinning', *Journal of Applied Physics*, 87, **2000**, 4531-4547.
- [18] Baker S. C., Atkin N., Gunning P. A., Granville N., Wilson K., Wilson D. and Southgate J., 'Characterisation of Electrospun Polystyrene Scaffolds for Three-Dimensional in Vitro Biological Studies', *Biomaterials*, 27, **2006**, 3136-3146.
- [19] Barnes C. P., Sell S. A., Boland E. D., Simpson D. G. and Bowlin G. L., 'Nanofiber Technology: Designing the Next Generation of Tissue Engineering Scaffolds', *Advanced Drug Delivery Reviews*, 59, **2007**, 1413-1433.
- [20] He W., Ma Z., Yong T., Teo W. E. and Ramakrishna S., 'Fabrication of Collagen-Coated Biodegradable Polymer Nanofiber Mesh and Its Potential for Endothelial Cells Growth', *Biomaterials*, 26, **2005**, 7606-7615.
- [21] Duan B., Yuan X., Zhu Y., Zhang Y., Li X., Zhang Y. and Yao K., 'A Nanofibrous Composite Membrane of Piga-Chitosan/Pva Prepared by Electrospinning', *European Polymer Journal*, 42, **2006**, 2013-2022.

- [22] Chiu J. B., Liu C., Hsiao B. S., Chu B. and Hadjiargyrou M., 'Functionalisation of Poly(L-Lactide) Nanofibrous Scaffolds with Bioactive Collagen Molecules', *Journal of Biomedical Materials Research Part A*, 83A, **2007**, 1117-1127.
- [23] Fu B. X., Hsiao B. S., Chen G., Zhou J., Koyfman I., Jamiolkowski D. D. and Dormier E., 'Structure and Property Studies of Bioabsorbable Poly(Glycolide-co-Lactide) Fiber During Processing and in Vitro Degradation', *Polymer*, 43, **2002**, 5527-5534.
- [24] Khang G., Choe J.-H., Rhee J. M. and Lee H. B., 'Interaction of Different Types of Cells on Physicochemically Treated Poly(L-Lactide-co-Glycolide) Surfaces', *Journal of Applied Polymer Science*, 85, **2002**, 1253-1262.
- [25] Ma M., Mao Y., Gupta M., Gleason K. K. and Rutledge G. C., 'Superhydrophobic Fabrics Produced by Electrospinning and Chemical Vapor Deposition', *Macromolecules*, 38, **2005**, 9742-9748.
- [26] Ma Z. W., Kotaki M., Yong T., He W. and Ramakrishna S., 'Surface Engineering of Electrospun Polyethylene Terephthalate (Pet) Nanofibers Towards Development of a New Material for Blood Vessel Engineering', *Biomaterials*, 26, **2005**, 2527-2536.
- [27] Chua K.-N., Chai C., Lee P.-C., Tang Y.-N., Ramakrishna S., Leong K. W. and Mao H.-Q., 'Surface-Aminated Electrospun Nanofibers Enhance Adhesion and Expansion of Human Umbilical Cord Blood Hematopoietic Stem/Progenitor Cells', *Biomaterials*, 27, **2006**, 6043-6051.
- [28] Grafahrend D., Heffels K. H., Beer M. V., Gasteier P., Moller M., Boehm G., Dalton P. D. and Groll J., 'Degradable Polyester Scaffolds with Controlled Surface Chemistry Combining Minimal Protein Adsorption with Specific Bioactivation', *Nature Materials*, 10, **2011**, 67-73.
- [29] Park T. G., 'Degradation of Poly(Lactic-co-Glycolic Acid) Microspheres - Effect of Copolymer Composition', *Biomaterials*, 16, **1995**, 1123-1130.
- [30] Andriano K. P., Tabata Y., Ikada Y. and Heller J., 'In Vitro and in Vivo Comparison of Bulk and Surface Hydrolysis in Absorbable Polymer Scaffolds for Tissue Engineering', *Journal of Biomedical Materials Research*, 48, **1999**, 602-612.
- [31] Ding A. G. and Schwendeman S. P., 'Determination of Water-Soluble Acid Distribution in Poly(Lactide-co-Glycolide)', *Journal of Pharmaceutical Sciences*, 93, **2004**, 322-331.
- [32] Groll J., Ameringer T., Spatz J. P. and Moeller M., 'Ultrathin Coatings from Isocyanate-Terminated Star Peg Prepolymers: Layer Formation and Characterisation', *Langmuir*, 21, **2005**, 1991-1999.
- [33] Salber J., Grater S., Harwardt M., Hofmann M., Klee D., Dujic J., Huang J. H., Ding J. D., Kippenberger S., Bernd A., Groll J., Spatz J. P. and Moller M., 'Influence of Different Ecm Mimetic Peptide Sequences Embedded in a Nonfouling Environment on the Specific Adhesion of Human-Skin Keratinocytes and Fibroblasts on Deformable Substrates', *Small*, 3, **2007**, 1023-1031.
- [34] Groll J., Ademovic Z., Ameringer T., Klee D. and Moeller M., 'Comparison of Coatings from Reactive Star Shaped Peg-stat-Ppg Prepolymers and Grafted Linear Peg for Biological and Medical Applications', *Biomacromolecules*, 6, **2005**, 956-962.
- [35] Gopal R., Kaur S., Ma Z., Chan C., Ramakrishna S. and Matsuura T., 'Electrospun Nanofibrous Filtration Membrane', *Journal of Membrane Science*, 281, **2006**, 581-586.
- [36] Kumar M. and Sekhon S. S., 'Role of Plasticizer's Dielectric Constant on Conductivity Modification of Peo-Nh4f Polymer Electrolytes', *European Polymer Journal*, 38, **2002**, 1297-1304.
- [37] Liu S.-J., Chiou L.-Y. and Liao J.-Y., 'Ultralow Dielectric Property of Electrospun Polylactide-Polyglycolide Nanofibrous Membranes', *Japanese Journal of Applied Physics*, 50, **2011**.





# CHAPTER 4

---

## Functionalised fibres for advanced ECM mimicry

This chapter investigates the functionalisation of NCO-sP(EO-*stat*-PO)/PLGA electrospun fibres. Moreover, the behaviour in a biological environment is simulated through protein adsorption experiments using three model proteins. The NCO-sP(EO-*stat*-PO) prepolymers which are present on the fibre surfaces are known to be protein repellent as a consequence of their hydrophilic poly(ethylene oxide) (PEO) based backbone. Furthermore, the isocyanates are highly reactive towards thiols, amines and hydroxyl-groups, thus the fibres can be modified by various coupling techniques. After hydrolysis with water the reactivity changes from isocyanate-functional to amino-functional which opens further functionalisation possibilities. Therefore a stepwise and orthogonal modification using three different model-molecules is presented.

---

Parts of this chapter have been published:

Grafahrend D., Heffels K. H., Beer M. V., Gasteier P., Moller M., Boehm G., Dalton P. D. and Groll J., 'Degradable Polyester Scaffolds with Controlled Surface Chemistry Combining Minimal Protein Adsorption with Specific Bioactivation', *Nature Materials*, 10, **2011**, 67-73.

## 1 Introduction

In the previous chapter the fibres were examined in terms of their mechanical properties, wettability and surface composition using XPS measurements. However, interactions between the fibres and biological environments were also analysed, to predict possible material-organism interactions. These environments can be simulated through protein adsorption experiments, as once biomaterials are implanted into an organism they are initially in contact with proteins [1, 2]. The interaction and adhesion of proteins on biomaterial surfaces is based on hydrophobic interactions but can be minimised by using hydrophilic polymers, such as PEO, as surface coatings [3-6]. The protein repellent quality of PEO is influenced by a variety of properties such as the polymer chain length, density, hydration, conformation and functionalisation on the chain ends [5, 7, 8]. The interdependency of these factors makes it difficult to attribute the protein repellent effect to one property and unravel the non-fouling mechanism [9]. So the chain density influences polymer conformation and its degree of hydration [10, 11]. The theory attributes steric and hydration barriers as the main contributing factors to the properties of non-fouling materials [12].

Groll *et al.* used NCO-sP(EO-*stat*-PO) prepolymers ( $M_w = 3, 12$  and  $18$  kDa) as surface coatings and observed no protein adsorption of lysozyme and insulin [13]. The key factor in this study was the high grafting density as linear PEO ( $M_w = 30$  kDa) could suppress the adsorption of lysozyme, but the smaller insulin still adhered on the coated surfaces.

Besides the suppression of unspecific protein adsorption, reducing any undesired biomaterial-organism interaction, functionalising the material surface for tailored interactions is a crucial part in scaffold design [14, 15]. The isocyanate groups of NCO-sP(EO-*stat*-PO) open various possibilities to enhance any spun fibre with bioactive molecules such as recognition sites or drugs [16]. The aim of this study was to exploit the existing isocyanates and to create an up to threefold functionalisation without cross reactions of the additives used.

## 2 Experimental section

### 2.1 NCO-sP(EO-*stat*-PO) synthesis

A hydroxyl terminated six arm star shaped prepolymer consisting of an ethylene oxide and propylene oxide backbone (ratio 80:20) and a molecular weight of 12 kDa was transferred into an isocyanate terminated prepolymer with isophorone diisocyanate. The detailed synthesis was described by Götz *et al.* [17].

### 2.2 Preparation of NCO-sP(EO-*stat*-PO) coated surfaces

Both glass cover slips and silicon wafers were used for coating substrates. Prior to the coating process they were cleaned thoroughly in an ultrasonic bath, sequentially immersed in acetone, water and isopropanol and sonicated for 5 min each. Freshly UV/ozone activated substrates could be used for an aminosilylation with 0.3 mL of N-[3-(trimethoxysilyl)-propyl]ethylene diamine, filtered with a syringe filter of 0.02 µm pore size, in 50 mL dry toluene for 2 h under nitrogen atmosphere in a glove box. The aminosilylated wafers were washed thoroughly with and stored in dry toluene until further processing.

Immediately before applying a coating the glass cover slips were dried in a stream of nitrogen. A solution of 10 mg/mL NCO-sP(EO-*stat*-PO) was prepared in a mixture of water/THF (THF, dried over sodium, Prolabo, Darmstadt, Germany) (9/1, v/v). After 5 min the solution was filtered with a 0.2 µm syringe filter (Whatman, Dassel, Germany) and placed on the substrate. A spin coater “WS-400-B-6NPP/LITE” (Laurell Technologies, North Wales, USA) was applied for creating thin hydrogel films on the mentioned substrates. Efficient process parameters were rotation speeds of 2,500 rpm for 40 s with an acceleration time of 5 s. The resulting films featured thicknesses of 30 nm and were stored at ambient conditions before further use.

### 2.3 Electrospinning

Unless otherwise stated the electrospinning was performed with a solution of 6 w/v% NCO-sP(EO-*stat*-PO) and 28 w/v% PLGA RG 504 in a mixture of acetone, DMSO and acidic water. The spinning solution was prepared as follows: first, NCO-sP(EO-*stat*-PO) was dissolved in DMSO and consecutively mixed with an aqueous solution of trifluoroacetic acid (TFA) at a

concentration of 20  $\mu\text{L}$  TFA per mL water. The solution was diluted with acetone, briefly mixed and finally PLGA was added and stirred for 10 min until a homogeneous solution was at hand. A common batch of such an electrospinning solution consisted of 143 mg PLGA, 30 mg NCO-sP(EO-*stat*-PO), 450  $\mu\text{L}$  acetone, 50  $\mu\text{L}$  DMSO and 10  $\mu\text{L}$  acidic water. For functionalisation prior electrospinning 1 mg of biocytin was dissolved in DMSO and added to bulk NCO-sP(EO-*stat*-PO), any other procedure remained the same.

The solution was spun at a feed rate of 0.5 mL/h through a flat-tip stainless steel spinneret ( $\varnothing = 0.4 \cdot 25$  mm) connected to a high-voltage power supply. An Eltex KNH34 (Germany) high voltage generator was utilised to charge the solutions at 13 kV while the collector remained grounded. The fibres were collected on NCO-sP(EO-*stat*-PO) coated substrates fixed to a rotating mandrel in a distance of 160 mm for functionalisation experiments and on aluminium foil for scanning electron microscopy imaging.

### **2.4 Scanning electron microscopy and optical microscopy**

To investigate their morphology, the fibres were characterised by scanning electron microscopy (SEM) and optical microscopy. For high-resolution images, the electrospun fibres were deposited onto SEM stubs. Unless otherwise stated, all samples were imaged with an S-4800 Ultra High Resolution Scanning Electron Microscope (Hitachi) using an accelerating voltage of 10 kV and a working distance of 10-15 mm. All samples for optical microscopy were collected on sP(EO-*stat*-PO) coated silicon wafers. Microscope images were taken with a Zeiss Stemi 2000-C. In order to observe the presence of the fluorescent dyes on the fibre surface, images were taken with an exposure time of 20000 ms using an appropriate fluorescence filter. Green fluorescence was observed with an F41-26 filter provided by AHF Analysentechnik (Germany), whereas red fluorescence was documented by filterset 31 of Zeiss (Germany). Optical microscope images using a polarisation filter with an exposure time of 5 ms of the same sample section are shown in comparison to the fluorescence images. Representative images are presented in section 3.

### **2.5 Protein adsorption**

#### **2.5.1 Qualitative protein adsorption studies**

Three fluorescently labelled model proteins were used for protein adsorption tests. Stock solutions of bovine serum albumin (BSA) rhodamine red conjugate, streptavidin (SA) texas

red conjugate and neutravidin (NA) texas red conjugate were prepared with a concentration of 50 µg/mL in phosphate buffered saline (PBS). These stock solutions were stored at – 20°C and under exclusion of light. Prior to incubation with proteins the samples were pre-wetted in deionised water for 60 min. Consecutively, the substrates were incubated with 500 µL of the protein stock solution for 180 min, immersed 5 times for 20 min with PBS buffer and washed thoroughly with deionised water. The samples were dried in a stream of nitrogen and immediately used for optical/fluorescence microscopy.

### 2.5.2 Quantitative protein adsorption studies

Experiments were performed with non-woven meshes whose mass varied between 1 and 3 mg. The meshes were pre-wetted in pure water and then incubated with either 250 µL of a 50 µg/mL BSA rhodamin red conjugate solution for 180 min or 250 µL of a 50 µL/mL fluorescein isothiocyanate (FITC) labelled serum solution for 180 min. The samples were rinsed three times with PBS (pH 7.4) solution for 10 min each and subsequently washed with demineralised water. After drying in a light stream of N<sub>2</sub> the non-woven meshes were placed in 1 mL sodium dodecyl sulphate (SDS) solution for 1 h. SDS detached any adsorbed proteins from the fibre surface, thus the fluorescence of the proteins in solution was measured with a fluorescence spectrometer. A calibration curve gave the amount of protein per mL SDS solution.

To correlate the measured amount of proteins to the respective fibre surface, the fibre length and fibre surface was calculated based on a macroscopic non-woven mesh. For PLGA and NCO-sP(EO-*stat*-PO)/PLGA fibres two non-woven meshes were cut into a piece with homogeneous mesh thickness. The side lengths of the rectangular shapes were measured, the mesh thickness as well as fibre thickness was determined with SEM.

The density of the mesh ( $\rho_{mesh}$ ) is given by the mass ( $m$ ) – volume ( $V$ ) ratio:

$$\rho_{mesh} = \frac{m}{V} = \frac{m}{l \cdot w \cdot h}$$

To determine the void volume, i.e. the porosity  $\varepsilon$ , of the non-woven mesh, the apparent density was related to the bulk density of the fibre material:

$$\varepsilon = 1 - \frac{\rho_{mesh}}{\rho_{bulk}}$$

To calculate the fibre surface  $S$ , the fibre length has to be determined. The length  $\lambda$  is given by a cylinder with the base area of  $\pi \cdot r^2$  ( $r = \frac{\omega}{2}$ ) and the bulk volume of the non-woven mesh:

$$\lambda = \frac{(1 - \varepsilon) \cdot V}{\pi \cdot \left(\frac{\omega}{2}\right)^2}$$

The fibre surface is then given as

$$S = \pi \cdot \omega \cdot \lambda = \frac{\pi \cdot \omega \cdot (1 - \varepsilon) \cdot V}{\pi \cdot \frac{1}{4} \cdot \omega^2} = \frac{4 \cdot (1 - \varepsilon) \cdot V}{\omega}$$

For each measured fibre thickness  $\omega$  the theoretical fibre surface was calculated given with a mean value as well as standard deviation. The part of fibre surface which is in contact with other fibres was calculated with a model of Sampson *et al.* to less than 1 % of the total surface area. As this error is small compared to deviations through measuring inaccuracy it will be neglected in the calculation [18].

The fluorescence acquired with the spectrometer was calculated into a concentration  $c$  giving the mass of protein per mg non-woven mesh. Furthermore the amount of protein was correlated to the fibre surface of one milligram non-woven mesh.

$$c = \frac{m_{BSA}}{S}$$

The figures are given with deviations  $\sigma$  calculated with the error propagation method.

$$\sigma_c = \sqrt{\left(\frac{\partial c}{\partial m_{BSA}}\right)^2 \sigma_{m_{BSA}}^2 + \left(\frac{\partial c}{\partial S}\right)^2 \sigma_S^2}$$

In this case function  $c$  contains a division; hence the error propagation method results in a relation where the relative errors add.

$$\left(\frac{\sigma_c}{c}\right)^2 = \left(\frac{\sigma_{m_{BSA}}}{m_{BSA}}\right)^2 + \left(\frac{\sigma_S}{S}\right)^2$$

## 2.6 Fibre surface modification with glycidol

The fibres were immersed in 1 mg/mL glycidol solution in bicarbonate buffer for 60 min and rinsed with deionised water afterwards. The wetted fibres were immediately used in protein adsorption experiments described in paragraph 3.1.

## 2.7 Consecutive functionalisation

Electrospun fibres on NCO-sP(EO-*stat*-PO) coated glass cover slips were incubated 5 min after electrospinning with 0.05 mg/mL Alexa Fluor® 568 cadaverine in water for 15 min. After rinsing three times with deionised water the samples were incubated with 0.05 mg/mL Alexa Fluor® 488 succinimidyl ester in water for 2 h. After a second thorough rinsing with deionised water, streptavidin micro spheres with a diameter of 1.0 µm (Polysciences Inc.) should be bonded specifically onto the fibres. Therefore the fibres were immersed in 20 µL streptavidin labelled Latex beads, diluted with 980 µL deionised water for 60 min. Two types of latex beads were used during the study: once without green fluorescence and once labelled with FITC for easier visualisation purposes. The samples were rinsed thoroughly with deionised water and dried in a stream of nitrogen. The functionalised samples were examined with fluorescence and optical microscopy.

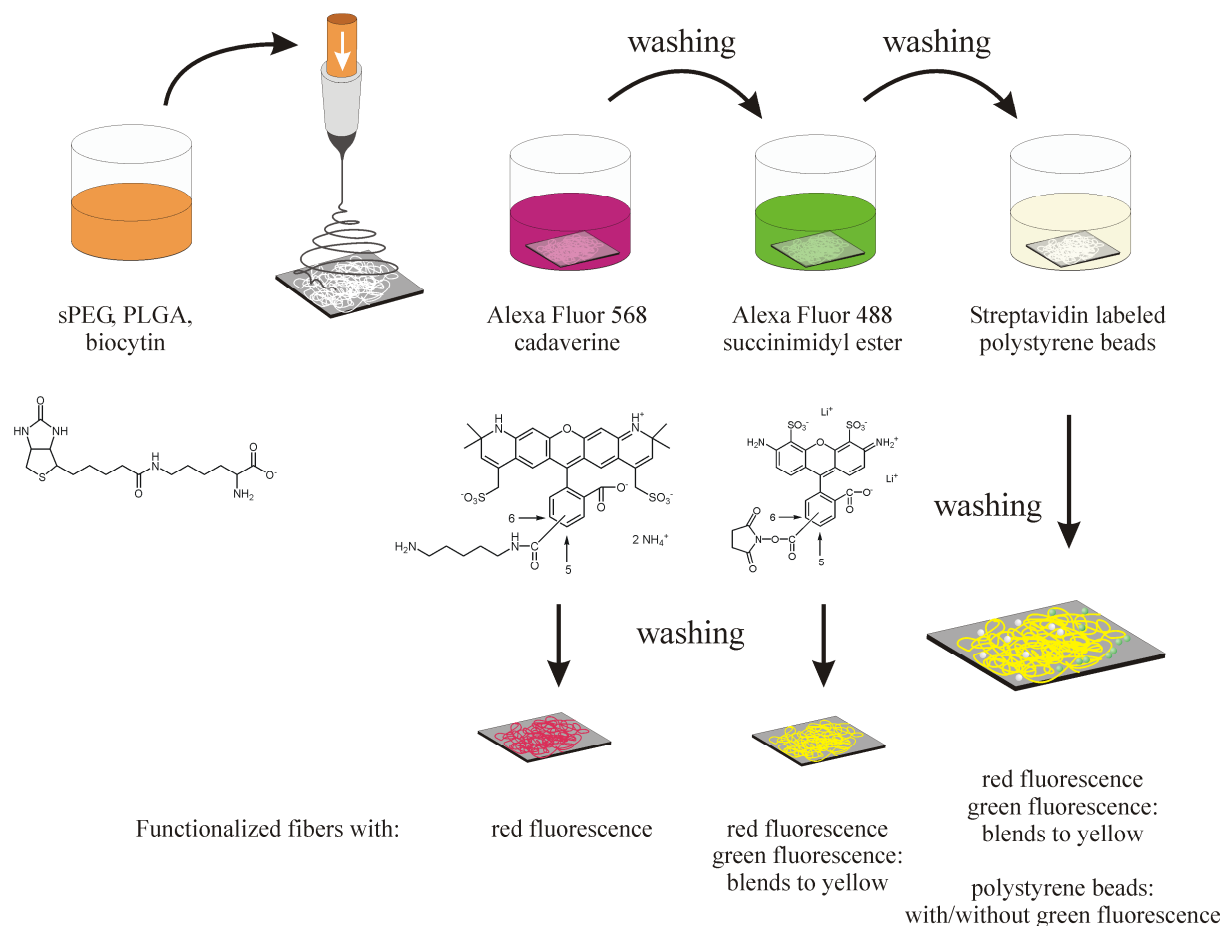


**Figure 1:** The experimental workflow of the consecutive functionalisation of NCO-sP(EO-*stat*-PO)/PLGA fibres.

### 3 Results and discussion

#### 3.1 Unspecific protein adsorption

PLGA has no protein repellent properties; hence in cell culture experiments cells can adhere to adsorbed proteins on the polymer surface [19]. The next building block towards highly specific, functional fibres is to render the PLGA fibre surface hydrophilic and protein repellent. PEO features both properties as it was used in block copolymers to enhance wetting abilities and to decrease unspecific protein adsorption [20].

##### 3.1.1 Qualitative protein adsorption studies

Fibre samples of PLGA and NCO-sP(EO-*stat*-PO)/PLGA were electrospun onto silicon wafers which were coated with an ultra-thin film of NCO-sP(EO-*stat*-PO). For PLGA fibres, freshly prepared films are used, so that NCO-groups on the target react with OH-groups of the PLGA that are present on the fibre surface. In case of the NCO-sP(EO-*stat*-PO)/PLGA fibres, completely hydrolysed films whose reactivity changed from isocyanate to amine can be used

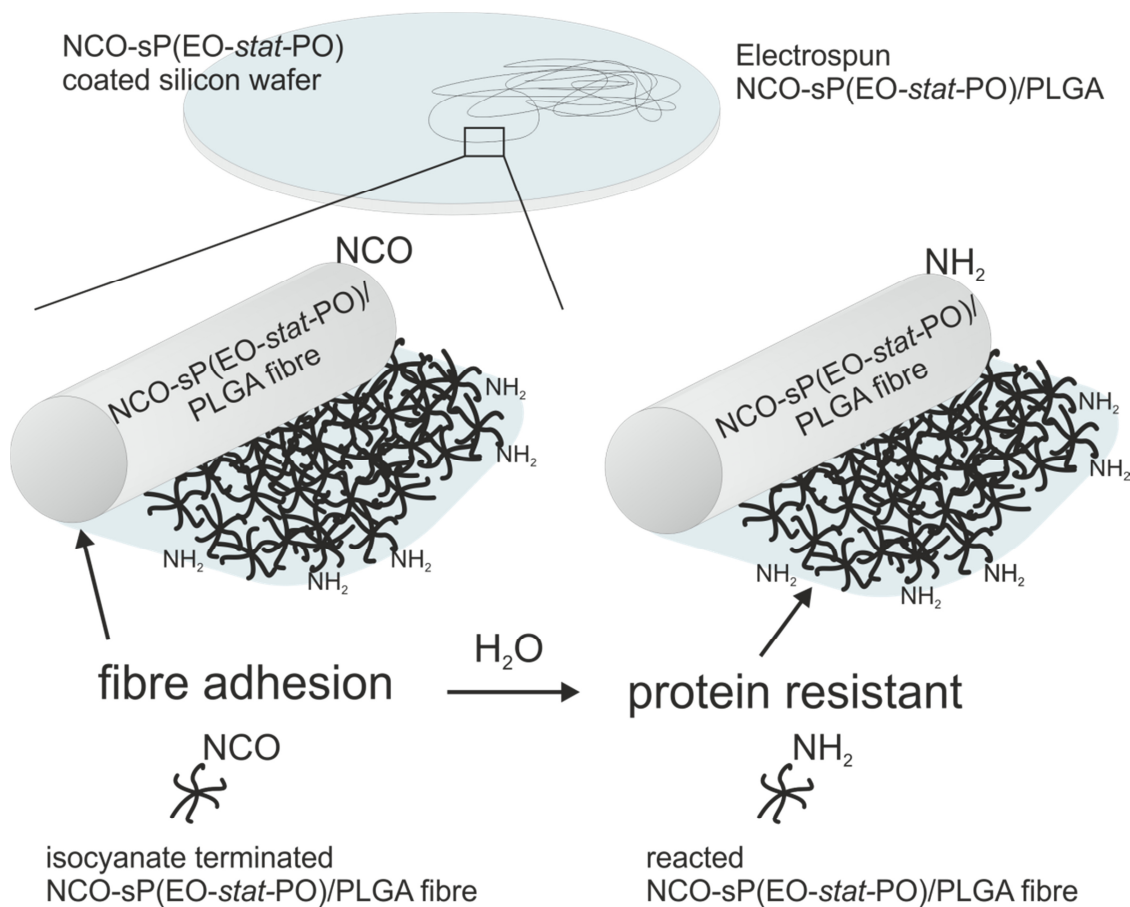


**Figure 2:** Schematic illustration of electrospun fibres on a NCO-sP(EO-*stat*-PO) coated surface. The fibre binds covalently onto the protein repellent surface.



as targets, since the fibres bear NCO-groups on the surface that can covalently attach to the  $\text{NH}_2$ -sP(EO-*stat*-PO) targets. In case of the NCO-sP(EO-*stat*-PO)/PLGA fibres, completely hydrolysed films can be used as targets, since the fibres bear NCO-groups on the surface (Figure 2).

After hydrolysis and partial aminolysis of the NCO-groups, in both cases a construct results where the substrate does not induce protein adsorption or cell adhesion and the fibres are covalently attached on this substrate. The fibre meshes can thus not lift off the substrate and float in the medium during cell culture or protein adsorption experiments. By this technique, protein adsorption and cell adhesion can exclusively be measured on the fibre surface.

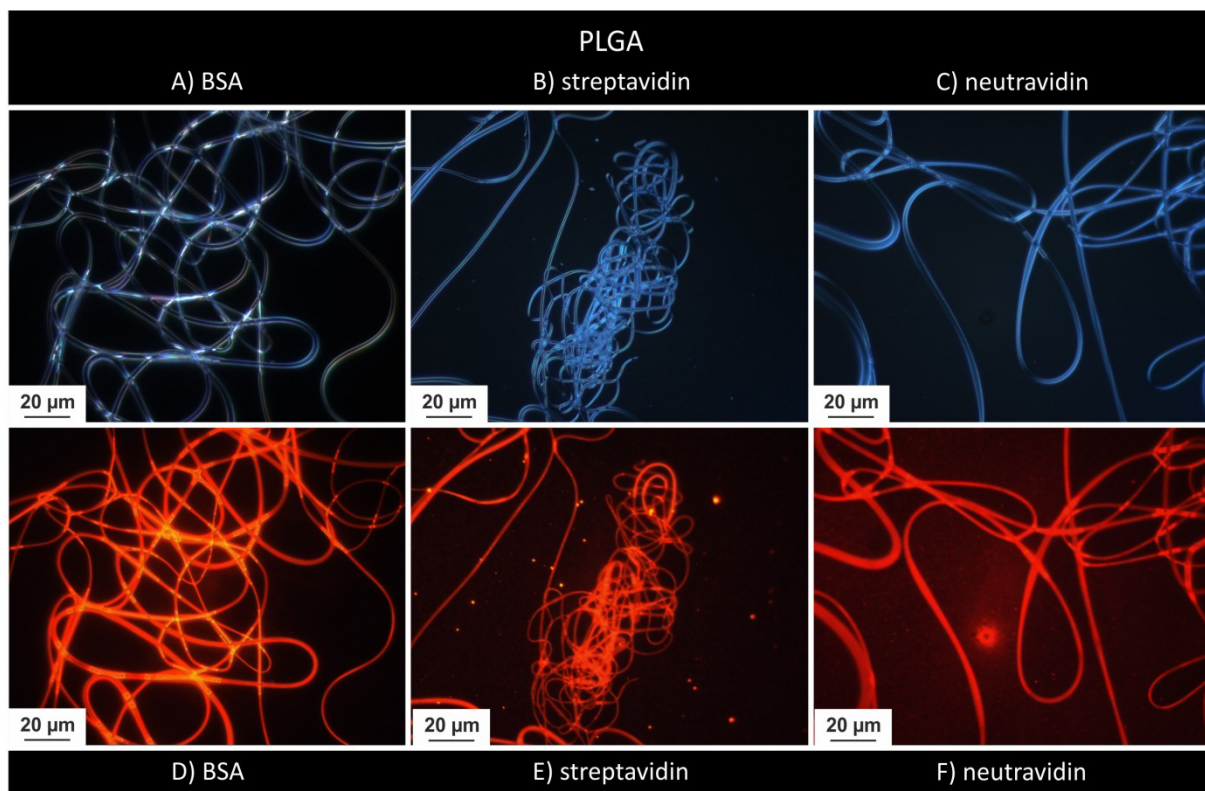


**Figure 3:** Protein adsorption on PLGA fibres with bovine serum albumin (BSA, pictures A and B), streptavidin (pictures C and D) and neutravidin (pictures E and F). A-C are dark field micrographs while D-F are fluorescent micrographs with an exposure time of 20000ms.

Those samples were incubated with protein solutions of bovine serum albumin, streptavidin and neutravidin. All proteins were labelled with a red fluorescent dye. Fibres consisting only of PLGA showed a homogeneous red fluorescence across all fibres in the case of any protein tested. The red fluorescence represents the dense and evenly distributed proteins on the fibre surface (Figure 3). Van der Waals attraction as well as hydrophobic interaction and other effects lead to this unspecific adsorption.

NCO-sP(EO-*stat*-PO)/PLGA fibres do not cause unspecific adsorption of BSA as displayed in Figure 4B. However, streptavidin and neutravidin could adsorb on the fibre surfaces as shown in Figure 4. The reason for this unexpected result is not completely clear.

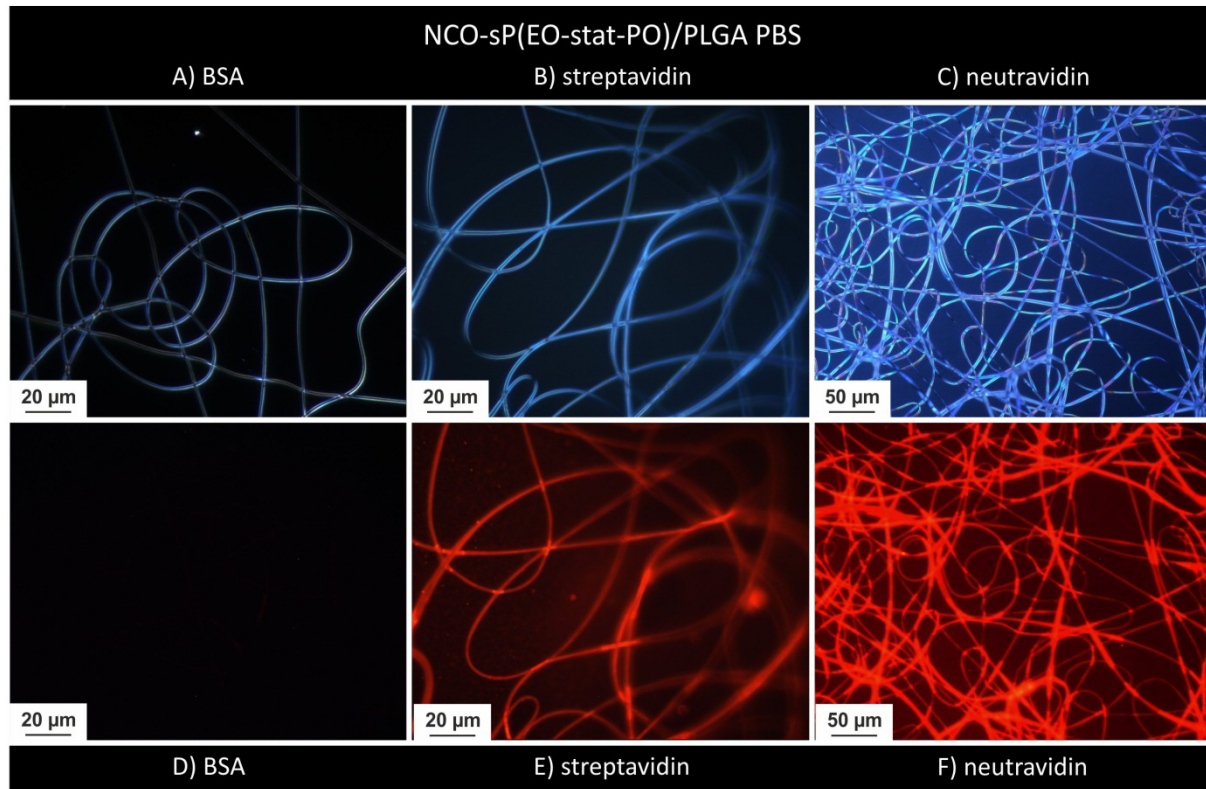


**Figure 4:** Protein adsorption on NCO-sP(EO-*stat*-PO)/PLGA fibres with bovine serum albumin (BSA, A and D), Streptavidin (B and E) and Neutravidin (C and F) in PBS buffer. A-C are dark field micrographs while D-F are fluorescent micrographs with an exposure time of 20000ms.

Insufficient density of NCO-sP(EO-*stat*-PO) on the fibre surface can be excluded, since the molecular weights of the proteins (BSA: 66 kDa, SA: 53 kDa, NA: 60 kDa) are very similar. Furthermore, SA and NA form dimers and tetramers in PBS puffer [13]. Weak interactions of proteins with PEO molecules have been predicted by Szleifer [21] and were experimentally observed for streptavidin by Sheth and Leckband [22].

Most probably, the adhesion of SA and NA is due to electrostatic interaction. The isoelectric point of BSA [23] [pI = 4.9] is more acidic than that of streptavidin [24] [pI = 6.4] and neutravidin [25] [pI = 6.3]. When the protein adsorption is performed at pH 9.4 (Figure 5), the adsorption of SA and NA is significantly reduced. The isoelectric point of a protein states at which pH-value the total charge of a protein is zero. If the environment's pH-value is above the pI, the protein will be charged negatively. A slightly negative charge may lead to stronger repellent forces towards amino groups of the NCO-sP(EO-*stat*-PO) modified PLGA fibres.

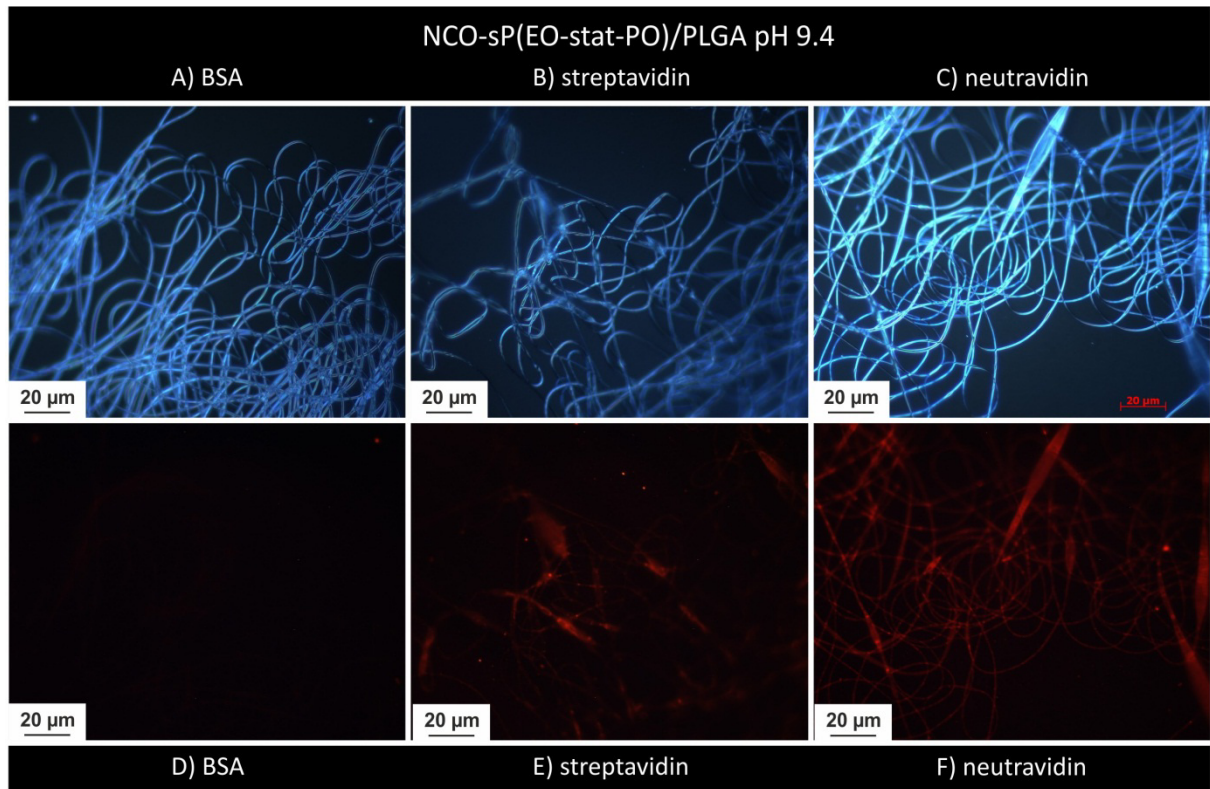


**Figure 5:** Protein adsorption on NCO-sP(EO-*stat*-PO)/PLGA fibres with bovine serum albumin (BSA, A and D), Streptavidin (B and E) and Neutravidin (C and F) in bicarbonate buffer. A-C are dark field micrographs while D-F are fluorescent micrographs with an exposure time of 20000ms.

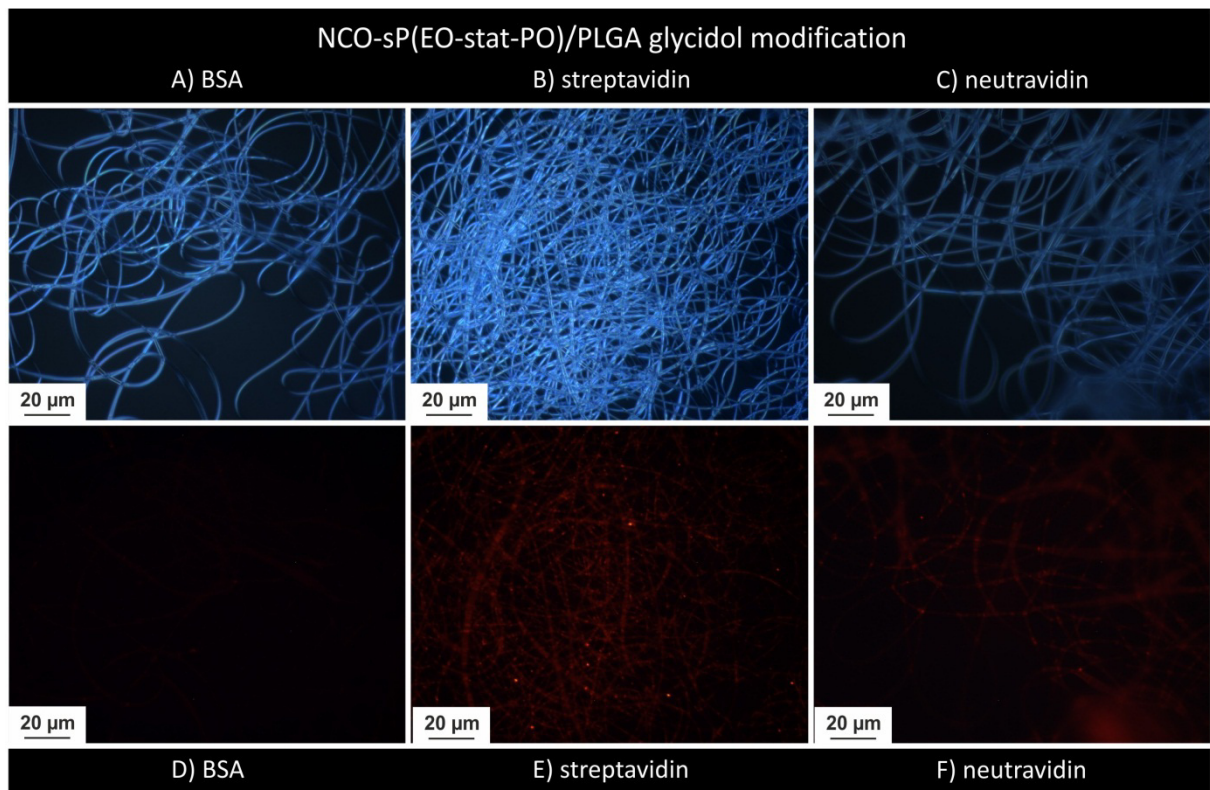


**Figure 6:** Protein adsorption on NCO-sP(EO-*stat*-PO)/PLGA fibres with bovine serum albumin (BSA, A and D), Streptavidin (B and E) and Neutravidin (C and F) in PBS buffer after glycidol treatment. A-C are dark field micrographs while D-F are fluorescent micrographs with an exposure time of 20000ms.

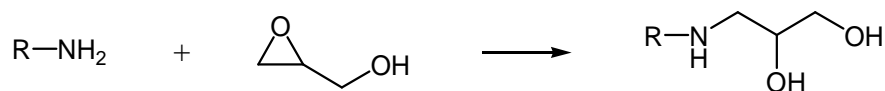


**Figure 7:** Reaction of glycidol with the terminal amino-groups of the NCO-sP(EO-*stat*-PO).

To underline the role of the amino groups in the unspecific adsorption of SA and NA, the NCO-sP(EO-*stat*-PO)/PLGA fibres were treated with glycidol. The reaction is schematically displayed in Figure 7. Such glycidol treated fibres generally prevented protein adsorption most effectively, with no adsorption of BSA and marginal adsorption of SA and NA (Figure 6). The glycidol treatment improves the non-fouling properties as  $NH_2$ -groups on the fibre surface are eliminated by reaction with glycidol which reduces the possibility for electrostatic interaction. In addition, the introduction of two alcohol groups at the rather hydrophobic IPDI-derived endgroup increases the hydrophilicity.

### 3.1.2 Quantitative protein adsorption studies

Quantitatively, the protein adsorption on PLGA scaffolds resulted in  $63.1 \pm 5.1$  ng BSA/cm<sup>2</sup> and in  $79.6 \pm 12.2$  ng serum/cm<sup>2</sup> fibre surface as presented in Figure 8. The fluorescent signal of the labelled proteins was approximately at the background level for 6.5 wt% to 25.9 wt% NCO-sP(EO-*stat*-PO) content in the examined fibres. On the fibre batch with 29.6 wt% NCO-sP(EO-*stat*-PO)  $3.4 \pm 2.0$  ng BSA and  $2.0 \pm 1.1$  ng serum adhered per square centimetre on the fibre surface. The minimised protein adsorption on fibre surfaces can be attributed to the presence of PEG chains of sP(EO-*stat*-PO) molecules. The hydrophilic nature of these polymers prevents hydrophobic interactions between fibre surface and proteins. Furthermore the PEG chains are highly hydrated and adhered proteins can be easily washed away.

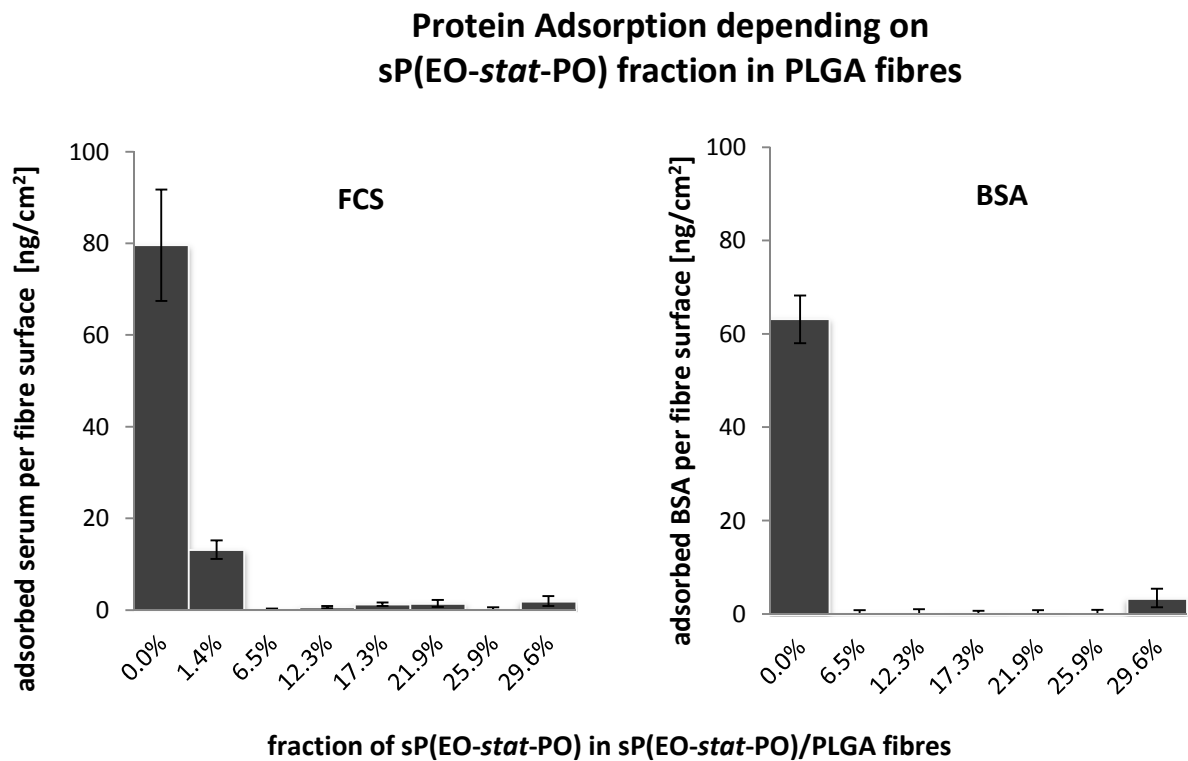


**Figure 8:** Quantitative protein adsorption on sP(EO-*stat*-PO)/PLGA fibres. Small amounts of the hydrophilic additive minimised the protein adsorption to less than 1 % compared to pure PLGA fibres.

### 3.2 Consecutive functionalisation

So far the designed PEG containing fibres proved to be inert to protein adsorption, thus unspecific cell adhesion is not expected for this fibre type. To render the electrospun fibres adhesive for specific cell types, signalling molecules were introduced on the fibre surface to be accessible for cells. In the following paragraphs three functionalisation approaches are presented that can be used to modify the fibre surface.

#### 3.2.1 NCO-functionalisation prior to electrospinning

Molecules that can react with isocyanates can be tethered to NCO-sP(EO-*stat*-PO) by mixing them into the spinning solution. The high reactivity of isocyanates to amines and thiols allows a covalent attachment prior to electrospinning. The surface segregation of the star polymers pulls any functionalised endgroups to the fibre surface. Here the investigated model peptide used in this one-step functionalisation method was biocytin, which was visualised by the specific adsorption of streptavidin [26]. The protein was either fluorescently labelled or adsorbed on a polystyrene bead with a diameter of 1  $\mu\text{m}$  to be visualised with fluorescence or optical microscopy. The biotinylated fibres were incubated

with glycidol to prevent any unspecific adsorption of SA, as shown in section 3.1.1. In the case of SA-coated PS beads, control tests showed that only with a specific biocytin – streptavidin bond the beads could be tethered to the fibres. No unspecific adsorption of beads to non-biotinylated fibres could be detected. Figure 9 demonstrates the specific binding of streptavidin to biocytin once fluorescently labelled and once coated on polystyrene beads.

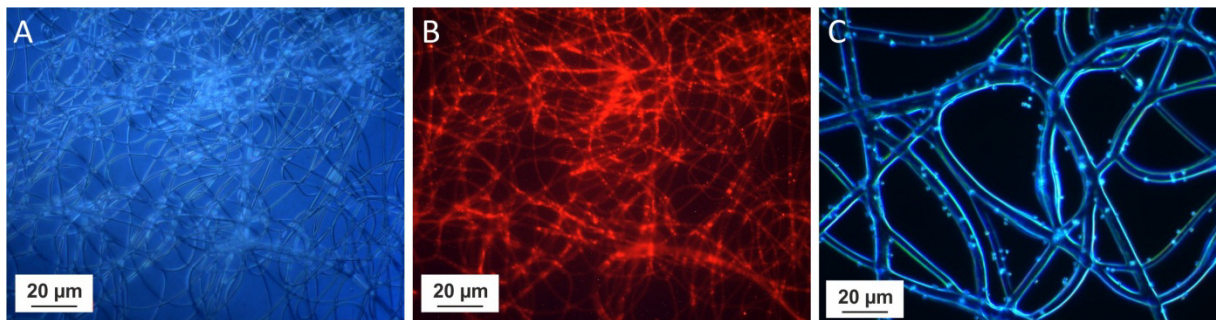


**Figure 9:** A and B show the specific binding of fluorescently labelled streptavidin to biotinylated NCO-sP(EO-*stat*-PO)/PLGA fibres after treatment with glycidol. Exposure time of B was 20000 ms. C represents the specific binding of streptavidin labelled polystyrene beads to biotinylated NCO-sP(EO-*stat*-PO)/PLGA fibres.

### 3.2.2 Functionalisation after electrospinning

The isocyanate groups on the fibre surface hydrolyse within a few hours after electrospinning. This gives time to attach isocyanate reactive molecules to the fibre surface by incubating the fibres in a respective aqueous solution. Functional groups such as amines or thiols have to be used as these functionalities exhibit a higher reactivity towards isocyanates than water. A third functionalisation possibility is accessible after hydrolysing isocyanates of NCO-sP(EO-*stat*-PO) to amines on the fibre surface. The amines can be used for functionalising fibres with active ester compounds such as a succinimidyl ester.

As the fibres have a very low intrinsic green and no red fluorescence the qualitative functionalisation after electrospinning was examined with two fluorescent dyes as model molecules. Alexa Fluor 568 cadaverine (red fluorescence) was used at a concentration of 0.05 mg/mL to functionalise isocyanates of as-spun fibres within two hours. The green dye Alexa Fluor 488 succinimidyl ester was immobilised to amine groups that are present on the fibre surface after hydrolysis of the isocyanates. Here, the fibres were incubated for two hours in a dye concentration of 0.05 mg/mL. The immobilisation was investigated using fluorescence imaging. Figure 10 demonstrates the difference in fluorescent intensity

comparing un-functionalised fibres with single functionalised fibres. The micrographs showed a strong red or green fluorescence indicating the successful reaction.

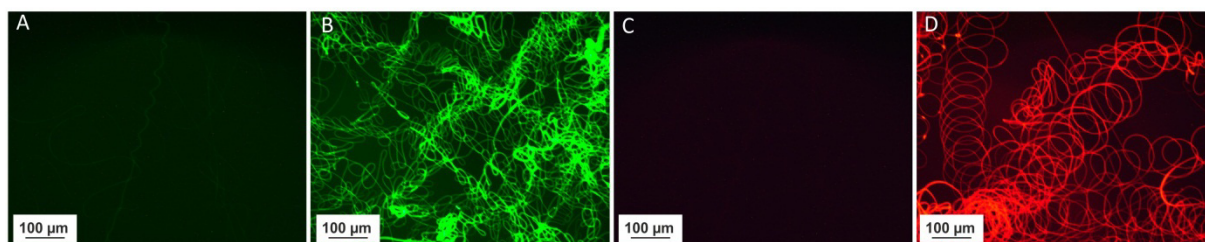


**Figure 10:** Fluorescence images of NCO-sP(EO-*stat*-PO)/PLGA fibres: A un-functionalised fibres and B with Alexa 488 succinimidyl ester functionalised fibres using a green filter set; C un-functionalised fibres and D with Alexa 568 cadaverine functionalised fibres using a red filter set. The exposure time of each micrograph was 20000 ms.

The workflow that was depicted in Figure 1 was applied to achieve double as well as triple functionalisation of electrospun fibres. The results of the dual functionalisations are presented in Figure 11. The top row with figures A – C displays the results of the pre-spinning modification with biocytin, visualised with SA coated and green fluorescence labelled PS beads and an additional post-spinning modification with an amine-reactive dye (also green fluorescence). The middle line D – F shows the best results with SA coated and green fluorescence labelled PS beads attached to the fibres and the red fluorescence of Alexa Fluor 568 cadaverine that was clearly detected at the fibre surface. In the bottom row with figures G – I two post-spinning modifications are displayed, visualised by the green and red fluorescence.

The micrographs in Figure 12 display the dye functionalised fibres. While single functionalisation yielded strong signals, the intensity of the respective signal is reduced with each additional functionalisation step performed on one sample. This is a consequence of a reduced number of functional groups that are available for the reaction as well as steric effects. However, Figure 12 demonstrates that, at a single substrate, all three steps of functionalisation can be performed and clearly detected. The green fluorescent SA-coated PS beads that attach to the biotin, the red fluorescence of the amino-functional dye that binds to the NCO-groups and the green fluorescence of the fibre that was introduced by reaction of the amino-reactive green fluorescence dye. The micrographs D – F of Figure 12 have been taken from an area of the sample where less PS beads have bound and the weaker fluorescence of the fibres can be visualised more clearly.

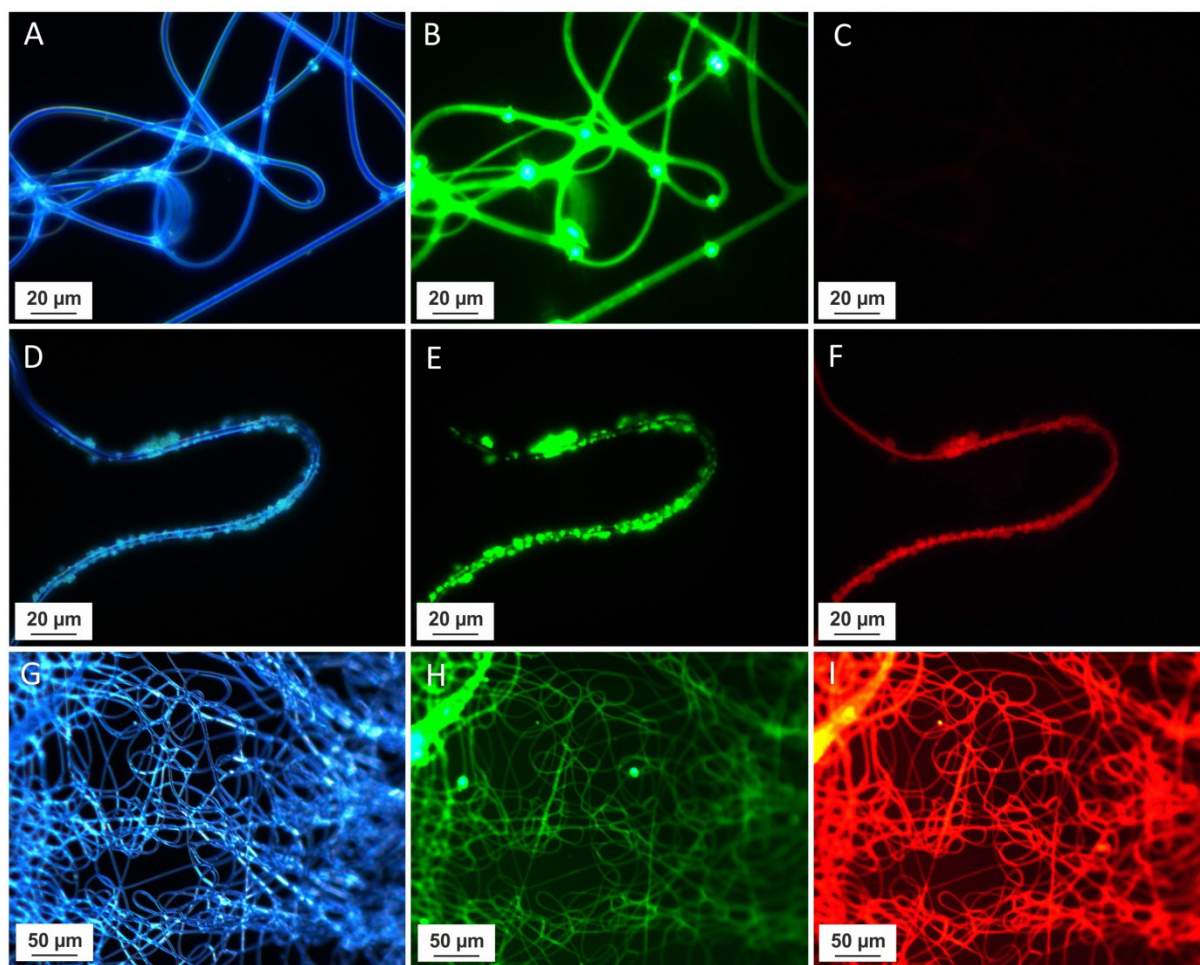


**Figure 11:** Dual functionalisations with: A – C: AF 488 + PS beads (labelled with green fluorescence) D – F: AF 568 with PS beads (labelled with green fluorescence) G – I: AF 488 + AF 568. The exposure time of B + C was 20000 ms, E = 1000 ms, F, H and I= 20000 ms.

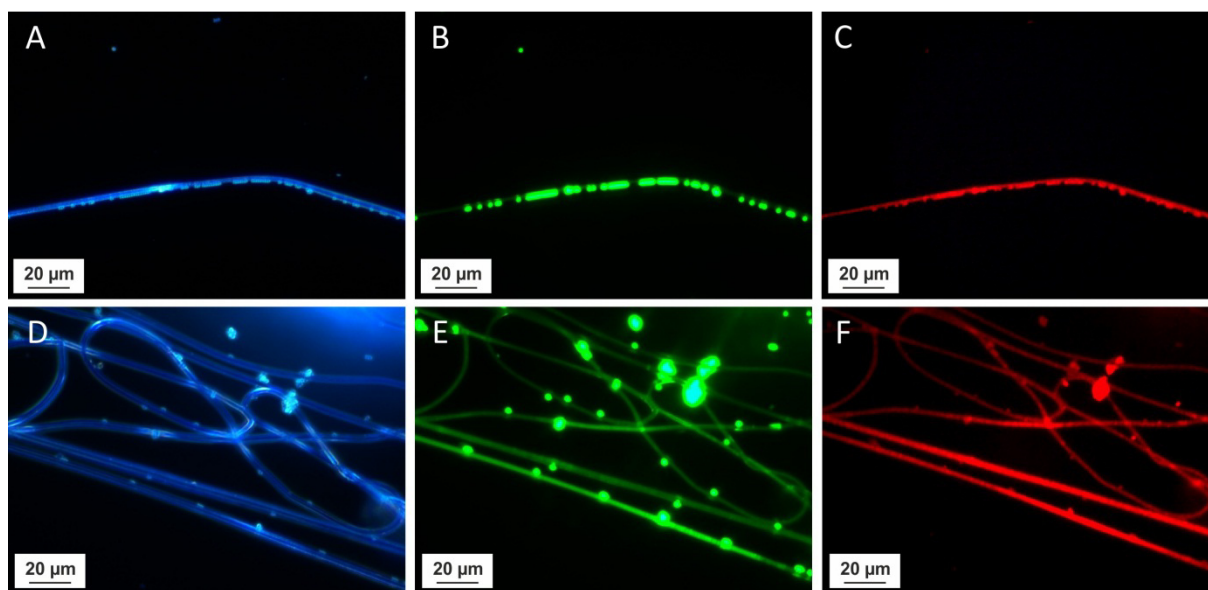


**Figure 12:** Triple functionalisation with Alexa Fluor 488 succinimidyl ester, Alexa Fluor 568 cadaverine and streptavidin labelled polystyrene beads (including green fluorescence). A + D are dark field micrographs, the exposure time of B and E was 1000 ms, C and F had an exposure time of 20000 ms.



## 4 Conclusion

In this chapter the adsorption behaviour of three model proteins (BSA, streptavidin and neutravidin) on NCO-sP(EO-*stat*-PO)/PLGA fibres has been presented. While the adsorption of BSA was negligible, SA and NA could adsorb on the fibres. However, after further treatment with glycidol the fibres exhibited protein repellent properties also towards the tested avidin derivatives. Quantitative studies with fluorescently labelled serum resulted in an adsorption reduced by more than 99 % for a sP(EO-*stat*-PO) content higher than 6.5 wt% in electrospun PLGA fibres. To control specific interactions between a scaffold and the biological environment a three-step orthogonal functionalisation procedure with model molecules such as an amino-functional red fluorescence dye, an amino-reactive green fluorescence dye and with streptavidin labelled and green fluorescent polystyrene beads has been performed. The exemplary experimental series demonstrated high signal intensities for single and two-step orthogonal modifications. A complete three-step functionalisation could also be performed, however the overall intensities of the signals were reduced. This proof-of-principle opens various possibilities to modify these fibres with bioactive components to address cells and guide tissue regeneration.

## 5 References

- [1] Castner D. G. and Ratner B. D., 'Biomedical Surface Science: Foundations to Frontiers', *Surface Science*, 500, **2002**, 28-60.
- [2] Horbett T. A., John L., Brash, *Proteins at Interfaces*. Vol. 343, *Acs Symposium Series*American Chemical Society, (1987), p. 720.
- [3] Kingshott P. and Griesser H. J., 'Surfaces That Resist Bioadhesion', *Current Opinion in Solid State and Materials Science*, 4, **1999**, 403-412.
- [4] Kingshott P., Thissen H. and Griesser H. J., 'Effects of Cloud-Point Grafting, Chain Length, and Density of Peg Layers on Competitive Adsorption of Ocular Proteins', *Biomaterials*, 23, **2002**, 2043-2056.
- [5] Malmsten M., Emoto K. and Van Alstine J. M., 'Effect of Chain Density on Inhibition of Protein Adsorption by Poly(Ethylene Glycol) Based Coatings', *Journal of Colloid and Interface Science*, 202, **1998**, 507-517.
- [6] Sofia S. J., Premnath V. and Merrill E. W., 'Poly(Ethylene Oxide) Grafted to Silicon Surfaces: Grafting Density and Protein Adsorption', *Macromolecules*, 31, **1998**, 5059-5070.
- [7] Morra M., 'On the Molecular Basis of Fouling Resistance', *Journal of Biomaterials Science, Polymer Edition*, 11, **2000**, 547-569.
- [8] Szeleifer I., 'Protein Adsorption on Surfaces with Grafted Polymers: A Theoretical Approach', *Biophysical Journal*, 72, **1997**, 595-612.
- [9] Unsworth L. D., Sheardown H. and Brash J. L., 'Protein-Resistant Poly(Ethylene Oxide)-Grafted Surfaces: Chain Density-Dependent Multiple Mechanisms of Action', *Langmuir*, 24, **2008**, 1924-1929.
- [10] Alexander S., 'Adsorption of Chain Molecules with a Polar Head a Scaling Description', *Journal de Physique*, 38, **1977**, 983-987.
- [11] Unsworth L. D., Tun Z., Sheardown H. and Brash J. L., 'Chemisorption of Thiolated Poly(Ethylene Oxide) to Gold: Surface Chain Densities Measured by Ellipsometry and Neutron Reflectometry', *Journal of Colloid and Interface Science*, 281, **2005**, 112-121.
- [12] Li L., Chen S., Zheng J., Ratner B. D. and Jiang S., 'Protein Adsorption on Oligo(Ethylene Glycol)-Terminated Alkanethiolate Self-Assembled Monolayers: The Molecular Basis for Nonfouling Behavior', *The Journal of Physical Chemistry B*, 109, **2005**, 2934-2941.
- [13] Groll J., Ademovic Z., Ameringer T., Klee D. and Moeller M., 'Comparison of Coatings from Reactive Star Shaped Peg-stat-Ppg Prepolymers and Grafted Linear Peg for Biological and Medical Applications', *Biomacromolecules*, 6, **2005**, 956-962.
- [14] Fittkau M. H., Zilla P., Bezuidenhout D., Lutolf M. P., Human P., Hubbell J. A. and Davies N., 'The Selective Modulation of Endothelial Cell Mobility on Rgd Peptide Containing Surfaces by Yigrs Peptides', *Biomaterials*, 26, **2005**, 167-174.
- [15] Sakiyama-Elbert S. E. and Hubbell J. A., 'Functional Biomaterials: Design of Novel Biomaterials', *Annual Review of Materials Research*, 31, **2001**, 183-201.
- [16] Elbert D. L., Pratt A. B., Lutolf M. P., Halstenberg S. and Hubbell J. A., 'Protein Delivery from Materials Formed by Self-Selective Conjugate Addition Reactions', *Journal of Controlled Release*, 76, **2001**, 11-25.
- [17] Götz H., Beginn U., Bartelink C. F., Grünbauer H. J. M. and Möller M., 'Preparation of Isophorone Diisocyanate Terminated Star Polyethers', *Macromolecular Materials and Engineering*, 287, **2002**, 223-230.
- [18] Eichhorn S. J. and Sampson W. W., 'Statistical Geometry of Pores and Statistics of Porous Nanofibrous Assemblies', *Journal of the Royal Society Interface*, 2, **2005**, 309-318.
- [19] Tjia J. S., Aneskievich B. J. and Moghe P. V., 'Substrate-Adsorbed Collagen and Cell Secreted Fibronectin Concertedly Induce Cell Migration on Poly(Lactide-Glycolide) Substrates', *Biomaterials*, 20, **1999**, 2223-2233.
- [20] Jeong J. H., Lim D. W., Han D. K. and Park T. G., 'Synthesis, Characterisation and Protein Adsorption Behaviors of Plga/Peg Di-Block Co-Polymer Blend Films', *Colloids and Surfaces B-Biointerfaces*, 18, **2000**, 371-379.
- [21] Szeleifer I., 'Protein Adsorption on Tethered Polymer Layers: Effect of Polymer Chain Architecture and Composition', *Physica A: Statistical Mechanics and its Applications*, 244, **1997**, 370-388.
- [22] Sheth S. R. and Leckband D., 'Measurements of Attractive Forces between Proteins and End-Grafted Poly(Ethylene Glycol) Chains', *Proceedings of the National Academy of Sciences*, 94, **1997**, 8399-8404.
- [23] Bertolatus J. A. and Hunsicker L. G., 'Glomerular Sieving of Anionic and Neutral Bovine Albumins in Proteinuric Rats', *Kidney International*, 28, **1985**, 467-476.

- [24] Skander M., Humbert N., Collot J., Gradinaru J., Klein G., Loosli A., Sauser J., Zocchi A., Gilardoni F. and Ward T. R., 'Artificial Metalloenzymes: (Strept)Avidin as Host for Enantioselective Hydrogenation by Achiral Biotinylated Rhodium-Diphosphine Complexes', *Journal of the American Chemical Society*, 126, **2004**, 14411-14418.
- [25] Vermette P., Gengenbach T., Divisekera U., Kambouris P. A., Griesser H. J. and Meagher L., 'Immobilisation and Surface Characterisation of Neutravidin Biotin-Binding Protein on Different Hydrogel Interlayers', *Journal of Colloid and Interface Science*, 259, **2003**, 13-26.
- [26] Weber P. C., Ohlendorf D. H., Wendoloski J. J. and Salemme F. R., 'Structural Origins of High-Affinity Biotin Binding to Streptavidin', *Science*, 243, **1989**, 85-88.



# CHAPTER 5

---

## Response of human dermal fibroblasts to RGD-functionalised fibres

The knowledge about fibre functionalisation from Chapter 4 is used in this chapter to address human dermal fibroblasts and induce selective cell binding to the fibres. A short peptide sequence, including the cell-adhesive tripeptide arginine-glycine-aspartic acid (RGD), has been used to functionalise fibres in a one-step fabrication process. Human dermal fibroblasts adhered selectively on functionalised fibres and did not show any interaction with control meshes. The amount of presented RGD-peptide influenced the adhesion strength of fibroblasts to fibre surfaces. More than a molar ratio of one GRGDS per ten sP(EO-*stat*-PO) molecules corresponding to the fibre weight did not lead to an increased adhesion and proliferation.

---

This chapter represents a cooperative project with Meike Beer.

Parts of this chapter have been published:

Grafahrend D., Heffels K. H., Beer M. V., Gasteier P., Moller M., Boehm G., Dalton P. D. and Groll J., 'Degradable Polyester Scaffolds with Controlled Surface Chemistry Combining Minimal Protein Adsorption with Specific Bioactivation', *Nature Materials*, 10, **2011**, 67-73.

## 1 Introduction

Fibroblasts are connective tissue cells and synthesise the main components of the extracellular matrix (ECM). Their activity becomes obvious during the process of wound healing. Usually two to five days after injury, while the inflammation is already diminishing, fibroblasts migrate from adjacent uninjured tissue into the wound site utilising fibrin fibres for adhesion and migration [1]. They secrete the ground substance comprised of collagen, proteoglycans and glycosaminoglycans that is the extracellular basis of the tissue. This newly formed ECM is different in composition to the original but serves wound closing, promoting a highly hydrated environment (by hyaluronan fibres) which permits cell migration through fibronectin fibres.

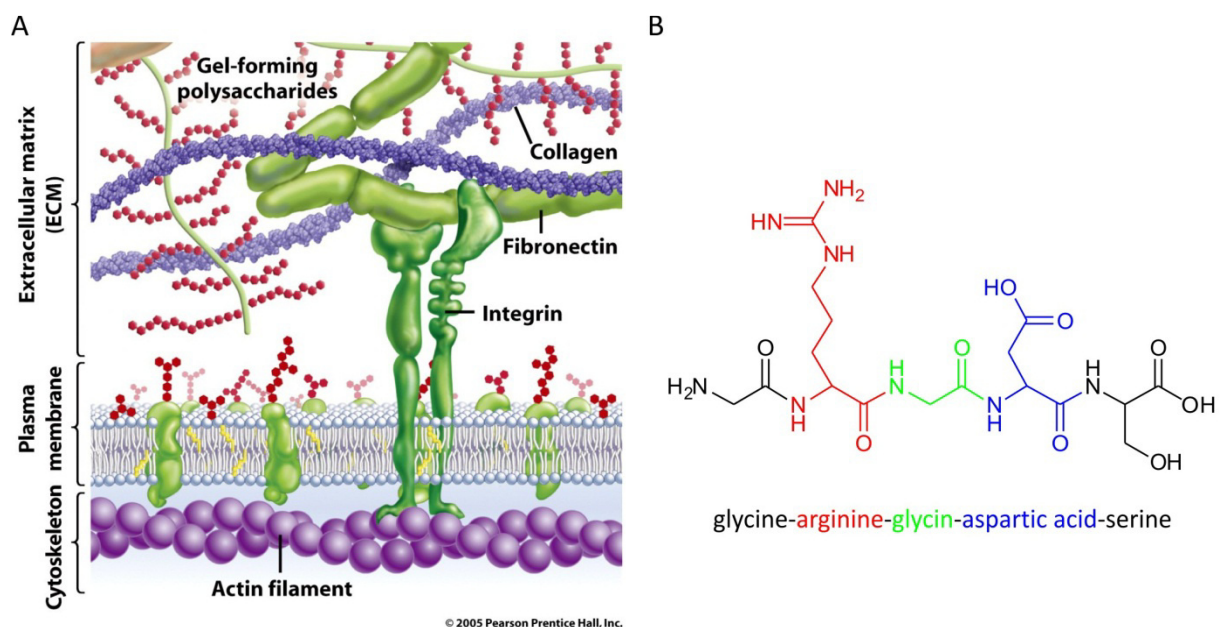


**Figure 1:** A) A transmembrane protein (Integrin) binds to ECM glycoproteins such as fibronectin that are connected to collagen fibres. Image taken from: <http://www.uic.edu/classes/bios/bios100/f06pm/integrin.jpg>. B) The depicted integrin in A) requires a specific sequence to interact with such as the peptide sequence “RGD” (arginine-glycine-aspartic acid).

The interaction between cells and their environment is decisive for tissue regeneration. It is unimportant if a wound heals naturally or with the help of implanted devices. For biomaterials it is on the one hand important to suppress unspecific interactions via protein adsorption that can lead to inflammation and foreign body reactions [2]. On the other hand selective binding moieties are crucial for cell attachment and interactions. Such signalling molecules are peptide sequences found in proteins of the ECM. A prominent representative of these sequences is the “RGD” peptide sequence, consisting of arginine, glycine and

aspartic acid [3] (Figure 1). It was found that this sequence can be detected by transmembrane receptors of cells. While several classes of receptors exist such as selectins, syndecans and integrins they all anchor cells within the ECM [4]. By that way cell survival and maintaining a functional tissue are guaranteed [5]. Referring to these receptors, integrins are expressed on most human cells [6, 7]. They are transmembrane protein complexes consisting of an  $\alpha$  and a  $\beta$  subunit [7]. Numerous variations of these subunits exist that can occur in varying combinations. The  $\alpha/\beta$ -heterodimers that are non-covalently associated can specifically bind to ligands present on protein-fibrils in the ECM. According to the key-lock principle, the RGD motive of fibronectin (an ECM protein) coordinates with the amino acid arginine to the  $\alpha$ -subunit while aspartic acid interacts with the  $\beta$ -subunit of the integrin [8]. The interaction relies on the three-dimensional presentation of the peptide sequence that can be influenced by flanking amino acids as well as the overall protein structure exhibiting the adhesion mediating sequences [9, 10]. On the inside of anchored cells the integrins induce structural conformation changes while bound, triggering the actin skeleton of the cell to align according to the adhesion sites. In fibroblasts, this leads to a change in cell shape from spherical geometries to flat and well spread cells [11, 12].

During the last decade electrospun fibres gained much attention as fibrous scaffolds for tissue engineering and regenerative medicine [13-15]. The biocompatibility of such fibres can be improved by presenting proteins or peptides on the fibre surface. Published processes used physical adsorption [16] or covalent attachment [17, 18], but generally these strategies were time consuming as they involved several process steps [19, 20].

In this chapter a one-step preparation method is described that renders protein repellent fibres cell-adhesive by incorporating the model peptide sequence “RGD” into the fibre surface.

## 2 Experimental section

### 2.1 NCO-sP(EO-*stat*-PO) synthesis

A hydroxyl terminated six arm star shaped prepolymer consisting of an ethylene oxide and propylene oxide backbone (ratio 80:20) and a molecular weight of 12 kDa was transferred into an isocyanate terminated prepolymer with isophorone diisocyanate. The detailed synthesis is described by Götz *et al.* [21].

### 2.2 Preparation of NCO-sP(EO-*stat*-PO) coated surfaces

Both glass cover slips and silicon wafers were used for coating substrates. Prior to the coating process they were cleaned thoroughly in an ultrasonic bath, sequentially immersed in acetone, water and isopropanol and sonicated for 5 min each. Freshly UV/ozone activated substrates could be used for an aminosilylation with 0.3 mL of N-[3-(trimethoxysilyl)-propyl]ethylene diamine, filtered with a syringe filter of 0.02  $\mu\text{m}$  pore size, in 50 mL dry toluene for 2 h under nitrogen atmosphere in a glove box. The aminosilylated wafers were washed thoroughly with and stored in dry toluene until further processing.

A solution of 10 mg/mL NCO-sP(EO-*stat*-PO) was prepared in a mixture of water/THF (THF, dried over sodium, Prolabo, Darmstadt, Germany) (9/1, v/v). After 5 min the solution was filtered with a 0.2  $\mu\text{m}$  syringe filter (Whatman, Dassel, Germany) and placed on the substrate. A spin coater “WS-400-B-6NPP/LITE” (Laurell Technologies, North Wales, USA) was applied for creating thin hydrogel films on the mentioned substrates. Effective process parameters were rotation speeds of 2,500 rpm for 40 seconds with an acceleration time of 5 seconds. The resulting films featured a thickness of 30 nm and were stored at ambient conditions before further use.

### 2.3 Electrospinning

Electrospinning was performed with a solution of 6 w/v% NCO-sP(EO-*stat*-PO) and 28 w/v% PLGA RG 504 in a mixture of acetone, DMSO and acidic water. The spinning solution was prepared as follows: first, NCO-sP(EO-*stat*-PO) was dissolved in DMSO and consecutively mixed with an aqueous solution of trifluoroacetic acid (TFA) at a concentration of 20  $\mu\text{L}$  TFA per mL water. The solution was diluted with acetone and briefly mixed. Finally, PLGA was



added and stirred for 10 min until a homogeneous solution was at hand. A common batch of such an electrospinning solution consisted of 143 mg PLGA, 30 mg NCO-sP(EO-*stat*-PO), 450  $\mu$ L acetone, 50  $\mu$ L DMSO and 10  $\mu$ L acidic water. To generate fibres with peptide decorated surfaces, the respective peptides were covalently linked to NCO-sP(EO-*stat*-PO) prior electrospinning. A molar peptide to NCO-sP(EO-*stat*-PO) ratio of 1: 1, 1: 2, 1: 5, 1: 10 and 1: 20 were used for GRGDS (purchased from Bachem, Bubendorf, Switzerland). The peptide was dissolved in 10  $\mu$ L acidic water, diluted with 50  $\mu$ L DMSO and then added to bulk NCO-sP(EO-*stat*-PO). The mixture was stirred and diluted with 450  $\mu$ L acetone after 10 min. Finally, PLGA was added and mixed until a homogeneous solution was at hand.

The solution was spun at a feed rate of 0.5 mL/h through a flat-tip stainless steel spinneret ( $\varnothing = 0.4 \cdot 25$  mm) connected to a high-voltage power supply. An Eltex KNH34 (Germany) high voltage generator was utilised to charge the solutions at 13 kV while the collector remained grounded. The fibres were collected on NCO-sP(EO-*stat*-PO) coated substrates fixed to a rotating mandrel in a distance of 160 mm.

#### **2.4 Cell culture and bioassays**

Cell culture experiments were carried out with human dermal fibroblasts (female patient, 38 years, maximum passage 8). Cells were cultured in a basal medium consisting of DMEM supplemented with 10% foetal bovine serum (Bio Whittaker, Belgium) at 37 °C, 5% CO<sub>2</sub> and 95% humidity. After fabrication, samples were immediately removed from the target and placed in a sterile polystyrene dish. The silicon wafers carrying the electrospun fibres were thoroughly washed with sterile PBS buffer five times to remove any contaminations. The samples were prewetted in culture vials overnight (24 h) with DMEM. After carefully removing the medium, the samples were pre-seeded with 500  $\mu$ L cell suspension (60,000 cells ml<sup>-1</sup>) for 1 h. Afterwards, 2 mL of DMEM were added and samples incubated for 24 h at 37 °C *in vitro*. Alternatively, the samples were directly seeded with 1 mL cell suspension (20,000 cells ml<sup>-1</sup>) and incubated at 37 °C *in vitro*. For the determination of cell survival, a Live/Dead® viability/cytotoxicity kit for mammalian cells (molecular probes) was used according to the manufacturer's protocol. To observe the cell morphology, the cells were fixed with 4 wt% paraformaldehyde incubation before further analysis.

### **2.5 Live/Dead® staining**

A viability staining of cells was performed after one week of cell culture. The Live/Dead® staining kit (Invitrogen, Karlsruhe, Germany) consisted of Calcein AM and Ethidium homodimer-1 and was used according to the manufacturer's protocol. Viable cells convert Calcein AM into green fluorescent Calcein, while the red fluorescent Ethidium homodimer-1 cannot penetrate the cell membrane of viable cells. Dead cells are stained with the red dye as the membrane is disintegrated.

### **2.6 Fluorescent staining of the cytoskeleton**

The cell morphology was visualised with an actin cytoskeleton and cell nucleus staining. Therefore the cells were fixed with 4 wt-% paraformaldehyde (Roth, Karlsruhe, Germany) and permeabilised with 0.1 vol-% Triton X-100 (Sigma-Aldrich, Steinheim, Germany) in PBS buffer. Subsequently diluted staining solutions were made, consisting of tetramethylrhodamine isothiocyanate-conjugated phalloidin (1/500) (Chemicon, Schwalbach, Germany) and 4',6-diamidino-2-phenylindole (DAPI, 1/1000) (Chemicon, Schwalbach, Germany) in PBS. The cells were incubated with these solutions for 1 h each. Finally the samples were washed with PBS buffer.

### **2.7 Microscopy**

Optical and fluorescent microscopy were carried out with the inverted Axiovert 100A Imaging microscope with an AxioCam MRc digital camera (Carl Zeiss, Göttingen, Germany) and were analysed using the AxioVision V4.7 software.

### 3 Results and discussion

#### 3.1 Live/Dead® staining

Pure PLGA fibres, sP(EO-*stat*-PO)/PLGA fibres as well as sP(EO-*stat*-PO)/PLGA fibres containing the adhesion mediating peptide GRGDS were collected on non-adhesive sP(EO-*stat*-PO) coated cover slips. The peptide sequence “GRGES” (glycine-arginine-glycine-glutamic acid-serine) that does not promote cell adhesion due to the minor difference of one –CH<sub>2</sub>– group between aspartic and glutamic acid was used as control sequence. This was spun to investigate the specificity of the RGD sequence. The peptides were applied in a star polymer to peptide ratio of 1: 1. Human dermal fibroblasts were seeded on these scaffolds and after

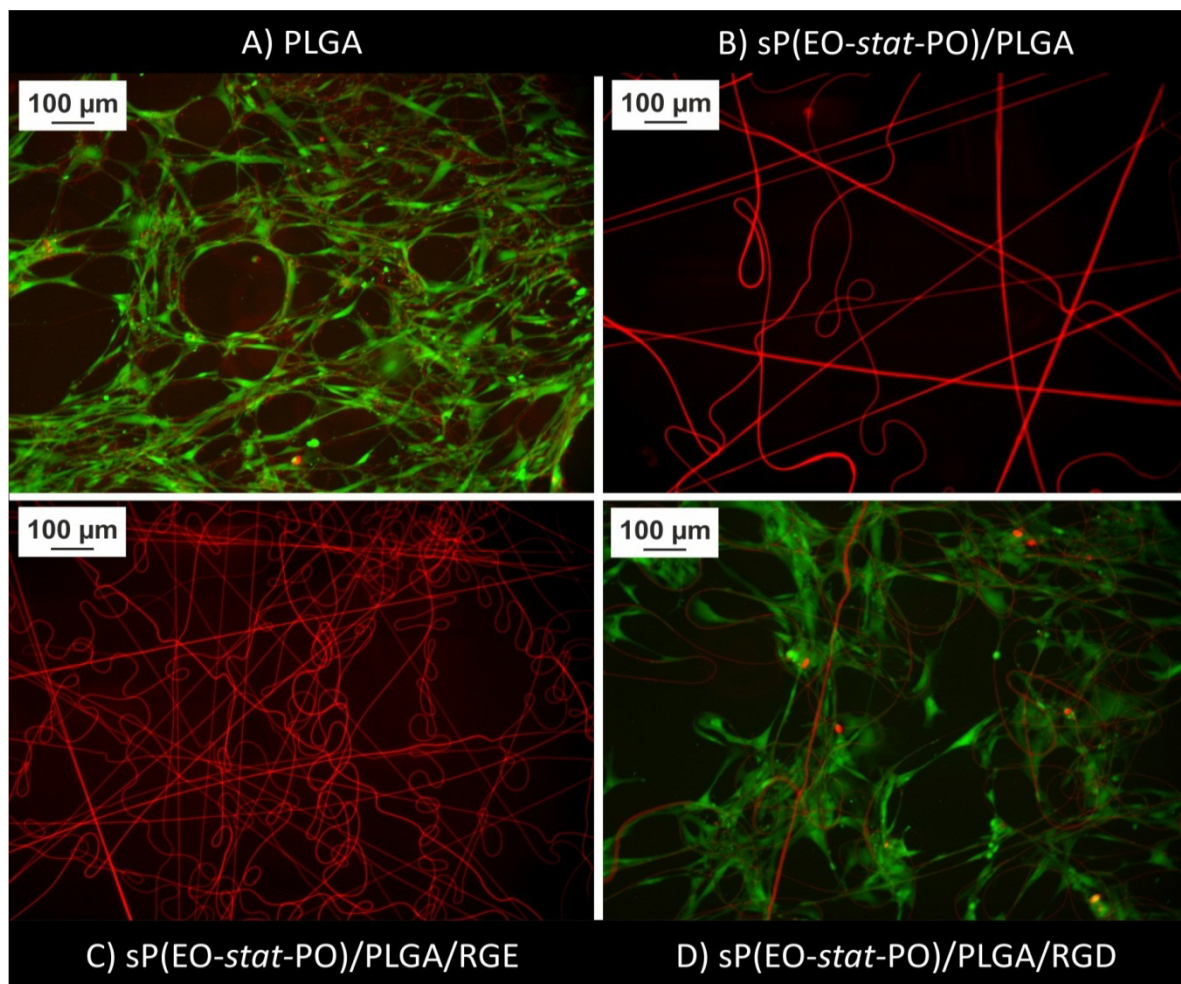


**Figure 2:** Live/Dead® staining of human dermal fibroblasts on electrospun fibres. Viable cells are displayed in green, whereas the red colour represents dead cells besides fibres. Image modified from reference [22] with permission from Nature Publishing Group.

7 days stained with a Live/Dead® staining kit. The samples were immediately observed with fluorescent microscopy. In Figure 2 representative micrographs are shown that depict the varying cell responds to the sample types.

Human dermal fibroblasts readily adhered on pure PLGA fibres which can be attributed to a non-specific binding caused by adsorbed proteins. Nevertheless, the green staining indicates that the cells are vital. On sP(EO-*stat*-PO)/PLGA fibres, as shown in Figure 2 B, hdFs could not adhere as no cells were detected on these samples. The strong hydrophilicity of the fibres and corresponding protein repellence prevent cell attachment. In Figure 2 C and D the peptide containing fibres are presented. The non-cell-adhesive motive GRGES did not induce a cell adhesion in spite of the molecular similarity to GRGDS. The green stain of the cytosol on RGD containing fibres demonstrates the selective cell adhesion on principally non-adhesive fibres. This observation leads to following conclusions: first, the peptide is present on the fibre surface as hdF can only adhere to fibres with an RGD peptide. Second, though the fibre surface is statistically covered with a peptide, its protein repellent properties remain.

### **3.2 Cell morphology and proliferation**

The hdF exhibited a well spread morphology on sP(EO-*stat*-PO)/PLGA fibres bearing GRGDS peptide sequences in a star polymer to peptide ratio of 1: 1. Figure 3 shows fibroblasts after 24 hours of being cultured *in vitro*, fixed and fluorescently stained for actin cytoskeleton in red and cell nuclei in blue. The cells solely adhered on fibres while spreading across the inert hydrogel surface. This situation resembles their proliferative phenotype in their native environment [23].

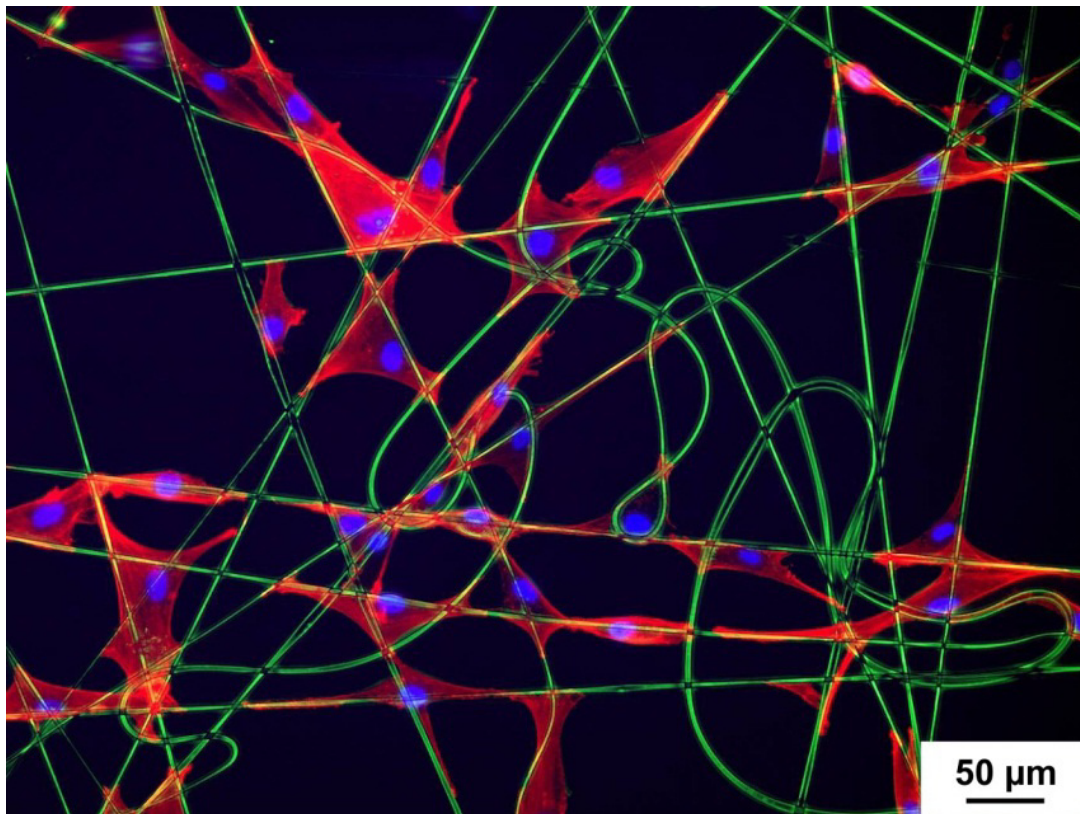


**Figure 3:** Fluorescent micrograph of human dermal fibroblasts with actin fibres stained red and cell nuclei stained blue. The electrospun fibres are displayed green (false colour). Image modified from reference [22] with permission from Nature Publishing Group.

The proliferative character of fibroblasts on sP(EO-*stat*-PO)/PLGA/GRGDS fibres was verified in long term studies over 14 days. A confluent monolayer of cells was observed on the fibre constructs after two weeks. Spatial limitations reduced the proliferation and the experiment was terminated after three weeks. Control samples without cell adhesion mediating peptides did not induce cell adhesion at any time during the experiment. This underlines the non-adhesiveness of the fibres due to the hydrogel-like surface of the fibres.

### 3.3 Adhesion kinetics depending on RGD concentration

The amount of RGD peptide required for successful cell adhesion was determined in an experimental series with GRGDS to NCO-sP(EO-*stat*-PO) ratios of 1: 20, 1: 10, 1: 5, 1: 2 and 1: 1. Pure PLGA meshes served as positive controls. The cells were counted 2 h, 24 h and 48 h after seeding; the results are presented in Figure 4 A. The fibroblasts did not adhere and proliferate as strongly on fibres with a 1: 20 ratio as on fibres with a higher amount of peptide. The fewer cell numbers for this sample type at day two can be allocated to a media change immediately before cell counting as weakly adhering cells were washed off the

meshes. At a molar peptide to sP(EO-stat-PO) ratio of 1: 10, cells adhered well on the samples and were not detached during media changes. There was no significant difference concerning cell attachment between samples with ratios ranging from 1: 10 to 1: 1. The viability of cells was quantified by counting living and dead cells immediately after incubating the cells in a Live/Dead® staining solution. Best viability of 97 % was detected on samples with a peptide to star polymer ratio of 1: 1. A slightly decreased but still very high viability of at least 88 % was found on samples with less RGD-peptide.

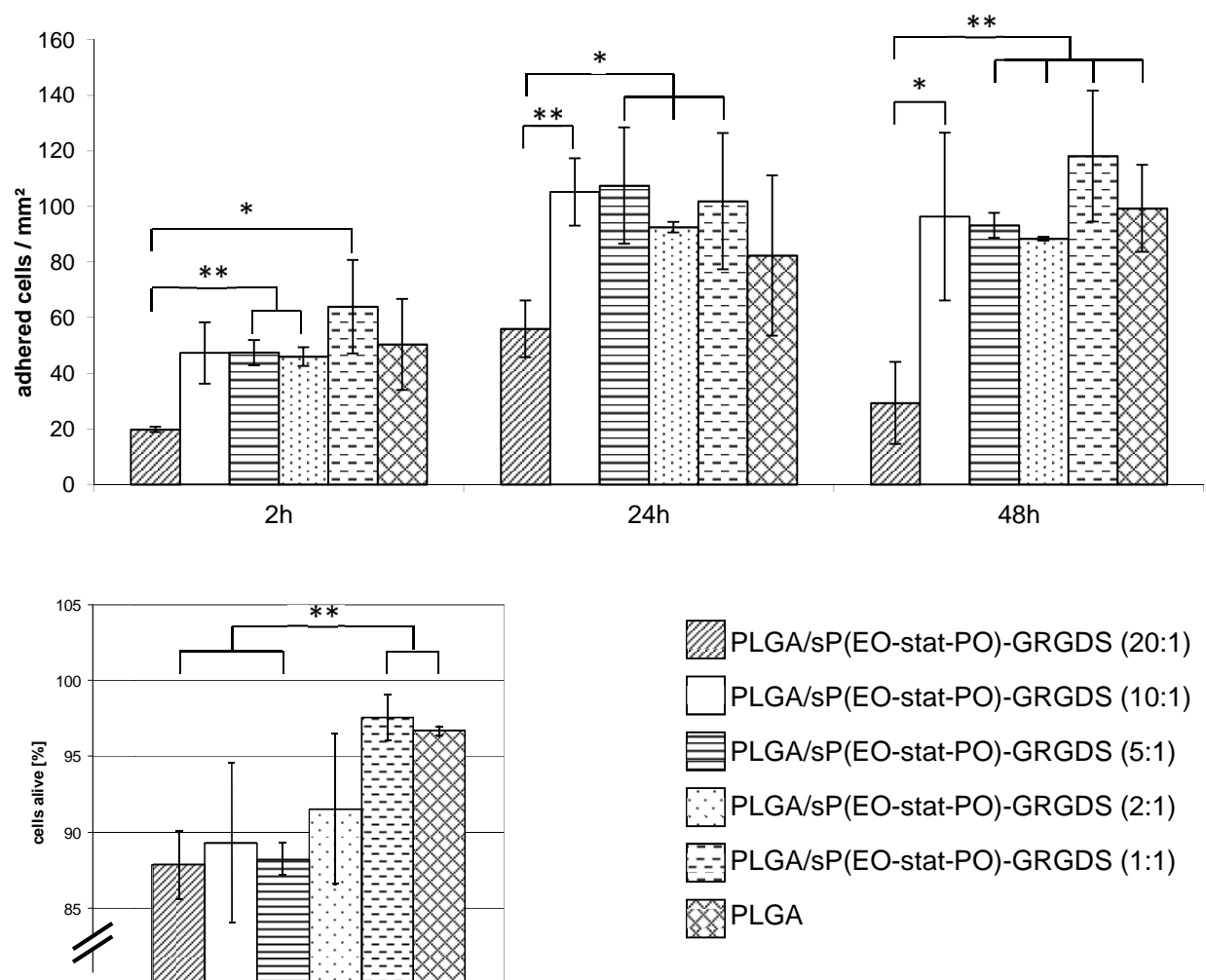


**Figure 4:** Cell adhesion is depending on the amount of GRGDS on electrospun fibre scaffolds. Figure was modified from reference [22] with permission from Nature Publishing Group.

## 4 Conclusion

The generation of biomimetic fibres has been condensed to a one-step preparation method. PLGA, a biocompatible and biodegradable polyester, combined with a functional star-shaped hydrogel additive was electrospun and resulted in protein- and cell-repellent fibres that were modified with a peptide, mediating cell-adhesion. The GRGDS-model-peptide was covalently linked to the NCO-sP(EO-*stat*-PO) additive and was presented on the fibre surface. Fibroblasts specifically attached to the fibre surface exhibiting the RGD-motive. Control fibres with GRGES or no peptides did not lead to cell adhesion. The proliferation and viability of human dermal fibroblasts was high as long term cell culture studies and Live/Dead® stainings revealed.

This toolbox of an inert surface covered with fibres can be widely applied to examine specific cell-fibre interactions. Multiple peptides and cells can be screened that way.

## 5 References

- [1] Stadelmann W. K., Digenis A. G. and Tobin G. R., 'Physiology and Healing Dynamics of Chronic Cutaneous Wounds', *The American Journal of Surgery*, 176, **1998**, 265-385.
- [2] Castner D. G. and Ratner B. D., 'Biomedical Surface Science: Foundations to Frontiers', *Surface Science*, 500, **2002**, 28-60.
- [3] Pierschbacher M. D. and Ruoslahti E., 'Cell Attachment Activity of Fibronectin Can Be Duplicated by Small Synthetic Fragments of the Molecule', *Nature*, 309, **1984**, 30-33.
- [4] Franz S., Rammelt S., Scharnweber D. and Simon J. C., 'Immune Responses to Implants – a Review of the Implications for the Design of Immunomodulatory Biomaterials', *Biomaterials*, 32, **2011**, 6692-6709.
- [5] Gumbiner B. M., 'Cell Adhesion: The Molecular Basis of Tissue Architecture and Morphogenesis', *Cell*, 84, **1996**, 345-357.
- [6] Hynes R. O., 'Integrins - Versatility, Modulation, and Signaling in Cell-Adhesion', *Cell*, 69, **1992**, 11-25.
- [7] Hynes R. O., 'Integrins: A Family of Cell Surface Receptors', *Cell*, 48, **1987**, 549-554.
- [8] Humphries J. D., Byron A. and Humphries M. J., 'Integrin Ligands at a Glance', *Journal of Cell Science*, 119, **2006**, 3901-3903.
- [9] Pankov R. and Yamada K. M., 'Fibronectin at a Glance', *Journal of Cell Science*, 115, **2002**, 3861-3863.
- [10] Haas T. A. and Plow E. F., 'Integrin-Ligand Interactions: A Year in Review', *Current Opinion in Cell Biology*, 6, **1994**, 656-662.
- [11] Folkman J. and Moscona A., 'Role of Cell Shape in Growth Control', *Nature*, 273, **1978**, 345-349.
- [12] Discher D. E., Janmey P. and Wang Y.-I., 'Tissue Cells Feel and Respond to the Stiffness of Their Substrate', *Science*, 310, **2005**, 1139-1143.
- [13] Huang Z. M., Zhang Y. Z., Kotaki M. and Ramakrishna S., 'A Review on Polymer Nanofibers by Electrospinning and Their Applications in Nanocomposites', *Composites Science and Technology*, 63, **2003**, 2223-2253.
- [14] Greiner A. and Wendorff J. H., 'Electrospinning: A Fascinating Method for the Preparation of Ultrathin Fibres', *Angewandte Chemie-International Edition*, 46, **2007**, 5670-5703.
- [15] Lee J., Cuddihy M. J. and Kotov N. A., 'Three-Dimensional Cell Culture Matrices: State of the Art', *Tissue Engineering Part B-Reviews*, 14, **2008**, 61-86.
- [16] Ma Z., Gao C., Ji J. and Shen J., 'Protein Immobilisation on the Surface of Poly-L-Lactic Acid Films for Improvement of Cellular Interactions', *European Polymer Journal*, 38, **2002**, 2279-2284.
- [17] Steffens G. C. M., Nothdurft L., Buse G., Thissen H., Höcker H. and Klee D., 'High Density Binding of Proteins and Peptides to Poly(D,L-Lactide) Grafted with Polyacrylic Acid', *Biomaterials*, 23, **2002**, 3523-3531.
- [18] Ma Z., Gao C., Yuan J., Ji J., Gong Y. and Shen J., 'Surface Modification of Poly-L-Lactide by Photografting of Hydrophilic Polymers Towards Improving Its Hydrophilicity', *Journal of Applied Polymer Science*, 85, **2002**, 2163-2171.
- [19] Patel S., Kurpinski K., Quigley R., Gao H., Hsiao B. S., Poo M.-M. and Li S., 'Bioactive Nanofibers: Synergistic Effects of Nanotopography and Chemical Signaling on Cell Guidance', *Nano Letters*, 7, **2007**, 2122-2128.
- [20] Kim T. G. and Park T. G., 'Surface Functionalised Electrospun Biodegradable Nanofibers for Immobilisation of Bioactive Molecules', *Biotechnology Progress*, 22, **2006**, 1108-1113.
- [21] Götz H., Beginn U., Bartelink C. F., Grünbauer H. J. M. and Möller M., 'Preparation of Isophorone Diisocyanate Terminated Star Polyethers', *Macromolecular Materials and Engineering*, 287, **2002**, 223-230.
- [22] Grafahrend D., Heffels K. H., Beer M. V., Gasteier P., Moller M., Boehm G., Dalton P. D. and Groll J., 'Degradable Polyester Scaffolds with Controlled Surface Chemistry Combining Minimal Protein Adsorption with Specific Bioactivation', *Nature Materials*, 10, **2011**, 67-73.
- [23] Nishida T., Yasumoto K., Otori T. and Desaki J., 'The Network Structure of Corneal Fibroblasts in the Rat as Revealed by Scanning Electron Microscopy', *Investigative Ophthalmology & Visual Science*, 29, **1988**, 1887-1890.



## CHAPTER 6

---

### **Interaction and differentiation of chondrocytes on electrospun fibres modified with cartilage derived peptides**

One step in the development of a scaffold for tissue engineering involves proving that a specific cell type interacts with the scaffold the same *in vitro* as well as *in vivo*. With a focus on articular cartilage, this chapter explores the question whether human articular chondrocytes can survive and interact with NCO-sP(EO-*stat*-PO)/PLGA meshes, either as-spun or chemically modified. Three different peptides associated with cartilage were co-spun and covalently attached to the fibres. This study is comprised of a viability assessment using Live/Dead® staining as well as adhesion and migratory experiments including live cell imaging. Furthermore, the re-differentiation capacity of chondrocytes on the scaffolds is investigated using biochemical analysis and gene expression.

---

This chapter outlines a cooperative project with Travis J Klein, Karsten Schrobback, June Jeon and Dietmar W. Hutmacher.

## 1 Introduction

The human organism has the ability to self-heal damaged tissue. For tissues such as muscle or bone the healing process involves inflammation, cell proliferation and tissue remodelling [1]. The speed of this healing process relies on the optimal supply of cells, nutrients and waste disposal which is best realised in a highly vascularised tissue. Avascular tissues such as articular cartilage lack this healing phenotype and once damaged slowly degrade with the progression of osteoarthritis [2].

Cartilage enables frictionless movement in joints and is shock absorbing to prevent damage and friction between bones. Depending on the composition and function, cartilage can be categorised into three different types: hyaline cartilage found in articular joints; elastic cartilage of the outer ear, containing elastin for increased elasticity; and fibrocartilage which is present in intervertebral discs and the meniscus [3]. As cartilage in joints is prone to degenerate as a consequence of high loads, injury, and disease, possible treatments are intensely studied.

### 1.1 Cartilage structure

Synovial joints consist of numerous components such as tendons, muscles and ligaments that connect the bones (Figure 1). These can slide with low-friction over each other as they are covered with articular cartilage, providing a smooth surface that is additionally lubricated with synovial fluid [4]. Furthermore, chondrocytes are supplied with nutrients from the diffusion of synovial fluid into the cartilage in the absence of vascularisation.

As a connective tissue, cartilage has a low cellular content and mainly consists of extracellular matrix (> 98 %) [5]. The matrix is comprised of collagens (60 %), proteoglycans (25 %), non-collageneous proteins and glycoproteins (15 %) [6]. Besides collagen type II being the most abundant collagen with more than 90 – 95 % of all collagens in cartilage, the types IV, IX, X, and XI can also be found [6]. Collagen fibrils provide structural support in cartilage, particularly concerning tensile stiffness and compression [7]. Proteoglycans such as aggrecan (ca. 90 %) bear highly negatively charged glycosaminoglycan (GAG) side chains which attract cations and water, resulting in a hydrogel complex that contributes to the compressive strength of cartilage [8]. Other matrix proteins [9] and glycoproteins such as

link protein [10] are relevant to organise and maintain the structure of the matrix components [7].

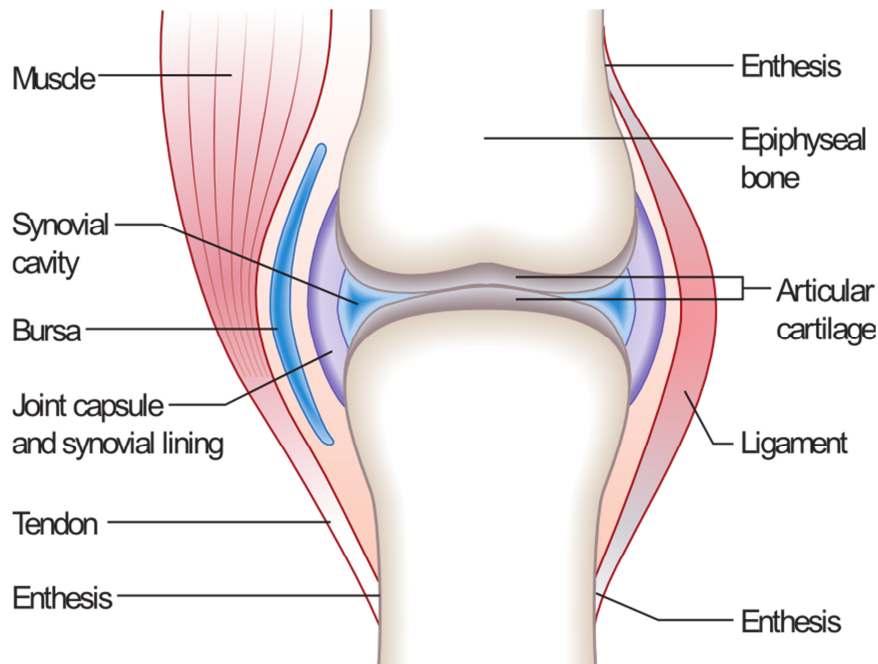


**Figure 1:** Sketch of a synovial joint comprised of bone, cartilage, encapsulated synovial fluid, muscles and tendons (Image taken from [http://en.wikipedia.org/wiki/Synovial\\_joint](http://en.wikipedia.org/wiki/Synovial_joint))

Rather than having a uniform structure, cartilage is highly organised into three different zones. Each of the “superficial”, “middle” and “deep” zone exhibits a characteristic cell shape [11-15], extracellular matrix composition [16, 17] and function [12]. The cells of each zone respond differently to external stimuli and furthermore retain their zone-specific function once they are isolated and cultured *in vitro* [12, 18, 19].

The topmost layer of articular cartilage is the superficial zone. Because it is the site of articulation, lubrication and resistance to shear stresses are the main functions [20]. Chondrocytes in this zone feature a flat morphology and are aligned in the direction of the surface of the tissue [21]. The cells are specialised to synthesise lubricating molecules such as proteoglycan 4 (PRG4, also known as lubricin) [6] rather than to produce extracellular matrix proteins. Only 10-20% of articular cartilage is of the superficial type [18]. As a consequence of the low GAG content in the superficial layer, the compressive modulus is low. Wong and Carter reported compression up to 50 % in the superficial zone [22].

The middle zone in cartilage transitions between the superficial and deep zones. The cells feature a round morphology and mainly generate matrix proteins [18, 20]. With a thickness of about 40 – 60% of the total cartilage tissue and high proteoglycan content, this zone

provides the high compressive strength of cartilage. The collagen fibres are randomly oriented contributing to both shear and compressive strength clearly showing the intermediate character of this layer [23].

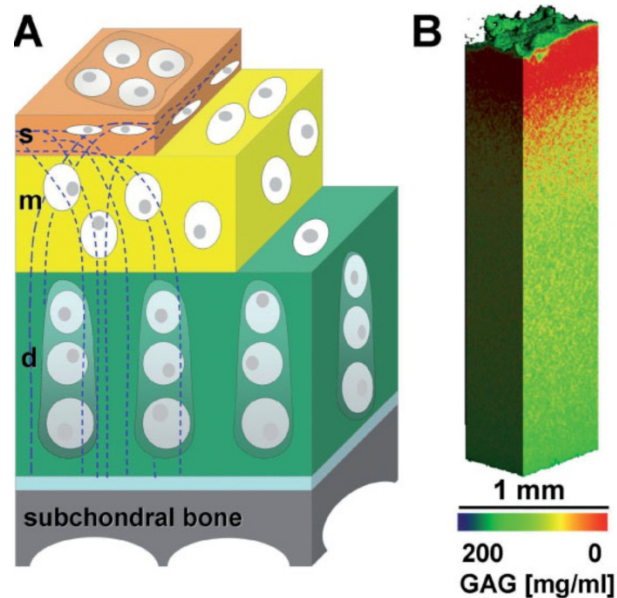


**Figure 2:** A) Sketch of the zonal organisation of cartilage. The topmost layer is the superficial (S) zone with a high density of flattened chondrocytes. The chondrocytes secrete proteoglycan 4 as it is the site of articulation. From the middle (M) to the deep (D) zone, the cells feature a round shape and are aligned in columns. The dashed blue lines represent the orientation of collagen fibres that change from alignment parallel to the surface in the superficial zone to perpendicular in the deep zone. B) The GAG content increases from the superficial zone to the deep zone. The figure was adapted from Klein *et al.* [24] with permission from John Wiley and Sons.

The deep zone is located below the middle layer of cartilage, comprising 30 – 40 % of the articular cartilage [20]. The chondrocytes found in this region are larger, elongated and self-arranged into columns [25]. They exhibit the highest activity of synthesising matrix molecules resulting in a high concentration of proteoglycans and GAGs [18, 26]. Together with hyaluronan and link protein, large proteoglycan clusters are formed that take up large amounts of water and thus increase the resistance to compressive forces [7, 23, 27]. The collagen fibres in this layer are oriented perpendicular to the cartilage surface, contributing to the compressive strength but also anchoring cartilage in the subchondral bone [6].

Between the deep zone of cartilage and bone a so-called subchondral zone links the two tissues. This zone is a calcified layer of cartilage featuring a gradual transition between hydrogel-like cartilage and ossified tissue.

## 1.2 Cartilage damage

As a consequence of its function as a load-bearing tissue cartilage lacks blood vessels, a lymphatic system and neural cells and therefore features no proper healing responses [12]. Hence, the chance of cartilage degeneration increases with age. Jinks *et al.* reported that 50 % of people over 50 suffer from knee pain over the course of a year [28]. Furthermore, osteoarthritis, one main disease of cartilage degeneration, is the main cause of impaired mobility for adults over the age of 65 [29]. Osteoarthritis develops from inflammatory cytokine release, stimulated for example by injurious loading. The state of the art treatment for osteoarthritic defects ranges from microfracture, osteochondral autograft to autologous chondrocyte implantation. However, complete cartilage regeneration is generally not achieved [30]. The best healing results are commonly observed in young patients, although even in these cases the “repaired” cartilage does not feature the same structural composition and mechanical strength compared to the original tissue [31].

## 1.3 Treatment methods for cartilage diseases

Existing treatment methods aim to reduce the pain and increase the mobility of patients. Non-surgical methods range from physical therapies with a focus on exercise to increase joint motion and flexibility, to drug therapies with pain killers, steroidal anti-inflammatory drugs [32] or antibiotics that inhibit matrix degeneration [33, 34]. A minimally invasive approach is the injection of hyaluronan into the damaged site providing lubrication and decreasing the pain in the joint [35].

Surgical treatments are applied for full-thickness defects which are small and localised. The techniques that are conducted in the clinic comprise subchondral drilling [36], abrasion [37] and microfracture [38]. These three therapies are based on the concept of enabling stem cells from the bone marrow to invade the injured site and initiate a healing process. Mosaicplasty (osteochondral autograft transfer (OAT)) [39] is a different strategy that involves transplanting healthy cartilage from non-load bearing sites to the defect site. This method results in more promising tissue formation than microfracture [40]. The autologous chondrocyte transplantation (ACI) is a modern approach of therapy for small defects. Chondrocytes are harvested from a biopsy of non-load bearing cartilage, expanded *in vitro* and reimplanted in the defect [41]. Peterson *et al.* reported that the stiffness of newly formed cartilage in these cases scored values of 90 % compared to native cartilage [42].

Besides positive outcomes such as the high stiffness, the new tissue lacks a zonal collagen fibre orientation and is prone to form fibrocartilage [43]. As a consequence of non-consistent outcomes and possible complications such as tissue hypertrophy [44], the reoperation rate is high (25 %) compared to defects treated with microfracture (10 %) [45].

If a defect affects the majority of a cartilaginous joint, a total joint replacement is often the only option to restore function to the patient [46]. The limited life time of these implants of 10 to 15 years [47] makes this treatment unsuitable for young patients as multiple revision surgeries may be necessary [48].

### **1.4 Tissue engineering of cartilage**

A tissue regenerating method that restores both the structure and function of cartilage is still not available. The cell-based ACI approach provides good prospects for regenerative capabilities of cartilage but could be optimised by incorporating hydrogel scaffolds to provide structural support and to guide cell proliferation and ECM expression [49]. Cultivation of chondrocytes in agarose and alginate hydrogels was already established in the 1980s and 1990s [50, 51]. The structural homogeneity of these hydrogels favours a spherical shape of embedded chondrocytes, similar to their natural morphology. But at the same time the zonal structure of cartilage cannot be mimicked by pure hydrogels.

Fibrous meshes have gained increasing interest for tissue engineering (TE) scaffolds as they may lead to chondrocytes orientating along the fibres. The interaction between scaffold material, often synthetic, and chondrocytes is a crucial aspect for the success of such scaffolds [52-54]. Bioactive molecules that have been applied in cartilage TE are collagen [55], chitosan [56], chondroitin-6-sulfate [57] and silk fibroin [58]. Short peptide sequences that resemble adhesion moieties of the mentioned biologic macromolecules can be used instead for easier processing and reproducibility.

In this chapter the fibrous system introduced in the previous chapters will be examined in terms of its suitability for cartilage regeneration. Briefly, PLGA a biodegradable polyester was used as the fibrous component. This was supplemented with a functional additive NCO-sP(EO-*stat*-PO) which introduced hydrophilicity to the fibres and opened various possibilities to modify the protein and cell repellent fibre surface. Primary human superficial and middle-deep chondrocytes are cultured on these scaffolds to examine the interaction between cells and fibres, particularly cell differentiation on the substrates. Besides unmodified NCO-sP(EO-

*stat-PO*)/PLGA fibres, three peptide sequences derived from the ECM of cartilage were used to induce specific cell-fibre interactions. Therefore, electrospun NCO-sP(EO-*stat-PO*) and PLGA fibres were functionalised with either the collagen II derived sequence CMQGPMGPMGPRG [59], the chondrogenic decorin sequence CGKLER [60] or the collagen II  $\alpha 1$  binding sequence CGWYRGRL [61]. The response of chondrocytes in terms of survival, adhesion, migration, proliferation and gene expression was compared between the various fibrous scaffolds with and without peptides.

## 2 Experimental section

### 2.1 NCO-sP(EO-*stat*-PO) synthesis

A hydroxyl terminated six arm star shaped prepolymer consisting of an ethylene oxide and propylene oxide backbone (ratio 80:20) and a molecular weight of 12 kDa was transferred into an isocyanate terminated prepolymer with isophorone diisocyanate. The detailed synthesis is described by Götz *et al.* [62].

### 2.2 Preparation of NCO-sP(EO-*stat*-PO) coated surfaces

Prior to being coated the glass cover slips were cleaned thoroughly in an ultrasonic bath, sequentially immersed in acetone, water and isopropanol and sonicated for 5 min each. Freshly UV/ozone activated substrates could be used for an aminosilylation with 0.3 mL of N-[3-(trimethoxysilyl)-propyl]ethylene diamine, filtered with a syringe filter of 0.02  $\mu\text{m}$  pore size, in 50 mL dry toluene for 2 h under nitrogen atmosphere in a glove box. The aminosilylated glass slides were washed thoroughly with and stored in dry toluene until further processing.

A solution of 10 mg/mL NCO-sP(EO-*stat*-PO) was prepared in a mixture of water/THF (THF, dried over sodium, Prolabo, Darmstadt, Germany) (9/1, v/v). After 5 min the solution was filtered with a 0.2  $\mu\text{m}$  syringe filter (Whatman, Dassel, Germany) and placed on the substrate. A spin coater “WS-400-B-6NPP/LITE” (Laurell Technologies, North Wales, USA) was used to apply thin hydrogel films on the substrate surfaces; with an acceleration time of 5 seconds, a rotational speed of 2,500 rpm for 40 seconds. The resulting films featured a thickness of 30 nm and were stored at ambient conditions before further use.

### 2.3 Electrospinning

Electrospinning was performed with a solution of 6 w/v% NCO-sP(EO-*stat*-PO) and 28 w/v% PLGA RG 504 in a mixture of acetone, DMSO and acidic water. The spinning solution was prepared as follows: first, NCO-sP(EO-*stat*-PO) was dissolved in DMSO and then mixed with an aqueous solution of trifluoroacetic acid (TFA) at a concentration of 20  $\mu\text{L}$  TFA per mL water. The solution was diluted with acetone and briefly mixed. Finally, PLGA was added and stirred for 10 min until a homogeneous solution was at hand. A common batch of such an electrospinning solution consisted of 143 mg PLGA, 30 mg NCO-sP(EO-*stat*-PO), 450  $\mu\text{L}$



acetone, 50  $\mu$ L DMSO and 10  $\mu$ L acidic water. To generate fibres with peptide decorated surfaces, the respective peptides were covalently linked to NCO-sP(EO-*stat*-PO) prior electrospinning. A molar peptide to NCO-sP(EO-*stat*-PO) ratio of 1: 2 was used for each peptide (CMQGPMGPMGPRG, CGKLER and CGWYRGRL purchased from JPT, Berlin, Germany). The peptides were dissolved in 10  $\mu$ L acidic water, diluted with 50  $\mu$ L DMSO and added to bulk NCO-sP(EO-*stat*-PO). The mixture was stirred and diluted with 450  $\mu$ L acetone after 10 min. Finally, PLGA was added and mixed until a homogeneous solution was at hand.

The solution was spun at a feed rate of 0.5 mL/h through a flat-tip stainless steel spinneret ( $\varnothing = 0.4 \cdot 25$  mm) connected to a high-voltage power supply. An Eltex KNH34 (Germany) high voltage generator was utilised to charge the solutions at 13 kV while the collector remained grounded. The fibres were collected on NCO-sP(EO-*stat*-PO) coated substrates fixed to a rotating mandrel at a distance of 160 mm. Meshes without glass cover slip backing were directly spun onto a rotating mandrel.

#### **2.4 Scanning electron microscopy and optical microscopy:**

To investigate their morphology, the fibres were characterised using scanning electron microscopy (SEM) and optical microscopy. For high-resolution images, the electrospun fibres were deposited onto aluminium foil. Unless otherwise stated, all samples were imaged with a FEI Quanta 200 Environmental SEM (Hillsboro, Oregon, USA) using an accelerating voltage of 10 kV and a working distance of 10-15 mm. All samples for optical microscopy were collected on sP(EO-*stat*-PO) coated glass coverslips. In order to observe the presence of the fluorescent dyes on the fibre surface, images were taken with an exposure time of 5000 ms using an appropriate fluorescence filter. Green fluorescence was observed with an F41-26 filter provided by AHF Analysentechnik (Germany), whereas red fluorescence was documented by filter set 31 of Zeiss (Germany).

#### **2.5 Cell culture**

Primary human articular cartilage was zonally harvested with consent from the femoral condyles of knee replacement surgery patients as described by Jeon, *et al.* [63]. The Queensland University of Technology (QUT) and Prince Charles Hospital (Brisbane, Australia) gave ethical clearance for the sample collection. The obtained cell populations were zonally enriched with superficial and middle-deep chondrocytes, respectively. As the cells have a

“zonal memory”, they will be labelled accordingly to discuss zone specific responses. The chondrocytes were pre-cultured to passage 3 and used at that passage. The expansion was performed in tissue culture polystyrene (TCPS) flasks with expansion medium consisting of Low-Glucose Dulbecco’s Modified Eagles Medium (LG-DMEM) with 10 % foetal bovine serum (FBS) (Hyclone, UT, USA) and additives (GlutaMAX-1, 110 mg/L sodium pyruvate, 10 mM HEPES, 0.1 mM nonessential amino acids, 50 U/mL penicillin, 50 µg/mL streptomycin, 0.5 µg/mL fungizone (all Invitrogen, CA, USA), 0.4 mM L-proline (Sigma, MO, USA), 0.1 mM L-ascorbic acid (WAKO Chemical, Japan)). The chondrogenic differentiation medium consisted of High-Glucose Dulbecco’s Modified Eagles Medium (HG-DMEM) (10313-021) including the additives as in the expansion medium: 10 mM HEPES, 0.1 mM nonessential amino acids, 50 U/mL penicillin, 50 µg/mL streptomycin, 0.5 µg/mL fungizone and 10 ng/mL TGF-β3.

### **2.6 Cell seeding on scaffolds**

The well plates for cell culture were coated with a silicone layer of Sigmacote (Sigma Aldrich) to prevent any unspecific cell attachment. Electrospun meshes (0.5 x 0.5 cm) were placed in the pretreated wells and washed five times thoroughly with sterile PBS buffer. After carefully removing the buffer, the samples were pre-seeded with 20 µL cell suspension (50,000 cells/mL) for 2 hours. Afterwards, 2 mL of DMEM were added and samples incubated till sampling at days 2, 7 and 28 at 37°C *in-vitro*.

### **2.7 Cell staining**

Besides monitoring cells using optical microscopy, cells were stained with fluorescent dyes to visualise their viability and cell structure concerning actin skeleton and nucleus.

#### **2.7.1 Viability staining**

By staining constructs with fluorescein diacetate and propidium iodide, living cells can be discriminated from dead cells as living cells fluoresce green while dead cell nuclei fluoresce red. The cells were rinsed twice in PBS buffer and then incubated with a staining solution containing 0.67 µg/mL fluorescein diacetate (Invitrogen, Carlsbad, CA, USA, Cat. No. F1303) and 5 µg/mL propidium iodide (Invitrogen, Carlsbad, CA, USA, Cat. No. P1304MP) for 5 minutes at 37 °C. The cell substrates were washed again twice with PBS buffer to remove any superficially adsorbed dyes. The staining was immediately recorded on a Nikon Eclipse TE2000-U (Nikon, Tokyo, Japan) microscope.

### **2.7.2 Actin filament and nuclei staining**

Information about the cell morphology was gained via staining the cytoskeleton and cell nucleus. Prior to the staining procedure the samples were washed twice with 2 mL PBS buffer and the cells were fixed with 4% paraformaldehyde in PBS at 37 °C for at least 30 minutes. To successfully stain actin filaments and DNA, the cells were treated with a 10 % Triton X-100 in PBS solution, enabling fluorescent dyes to pass the cell membrane. Finally, the samples were repeatedly rinsed with PBS.

After fixation of the cells, the scaffolds were transferred into a 0.5% BSA/PBS solution. For easier processing the 2-(4-amidinophenyl)-1H-indole-6-carboxamide (DAPI) and phalloidin stainings were performed within the same solution. The staining solution of Phalloidin Rhodamine 415 contained 100 µL phalloidin stock solution, at a concentration of 200 U/mL Phalloidin Rhodamine 415, diluted with 25 mL PBS containing 1 % BSA. The DAPI staining solution was applied at a concentration of 2.5 µg/mL PBS. The samples were finally washed twice in PBS and documented with fluorescent microscopy.

### **2.8 Biochemical analysis**

The activity of the cells was analysed by determining the matrix production. Meshes with superficial and middle-deep chondrocytes were digested in 0.5 mg/mL proteinase K (dissolved in phosphate buffered 2,2',2'',2'''-(Ethane-1,2-diyldinitrilo)tetraacetic acid (EDTA) (PBE)) solution (Invitrogen) overnight at 60 °C. A modified 1,9-dimethylmethylen blue (DMMB) (Sigma) assay was used at pH 1.5 according to a protocol by Enobakhare *et al.* to determine the glycosaminoglycan content in the samples [64]. For the subsequent DNA assay the samples were diluted 1:5 fold in PBE and mixed 1:1 with Quant-iT PicoGreen dsDNA assay kit (Invitrogen) in a black 96 well plate. The GAG content was normalised to the DNA content, representing the number of cells on the samples.

### **2.9 Quantitative real-time polymerase chain reaction (qRT-PCR)**

The mRNA levels of collagen I, collagen II, aggrecan, Ki-67 and lubricin were quantified with qRT-PCR. The RNA was extracted from the meshes cultured for 7 and 28 days using TRIzol (Invitrogen) reagent according to the manufacturer's protocol. Discrete mRNA bands were confirmed with electrophoresis. Any remaining DNA was decomposed with DNase (DNase I, Invitrogen) before the mRNA was transcribed into cDNA with SuperScript<sup>TM</sup> III, a first-strand

synthesis supermix for qRT-PCR (Invitrogen), according to the manufacturer's protocol. The PCR reaction was carried out with an Express SYBR GreenERTM qPCR supermix universal kit (Invitrogen) and a 7900HT fast real-time PCR system (Applied Biosystems, CA, USA). The cycle threshold (Ct) value of each gene was normalised to the housekeeping gene, 18S rRNA, using the comparative Ct method ( $2^{-\Delta\Delta C_t}$ ).

**Table 1:** List of primer sequences used for qRT-PCR.

Gene symbol	Sequence (5'->3')	GeneBank accession #	Amplicon position
COL1A1	F: CAGCCGCTTCACCTACAGC R: TTTTGTATTCAATCACTGTCTTGCC	NM_000088	4335-4417
COL2A1	F: GGCAATAGCAGGTTACGTACA R: CGATAACAGTCTTGCCCCACTT	NM_001844	4454-4532
ACAN	F: GCCTGCGCTCCAATGACT R: TAATGGAACACGATGCCTTTCA	NM_001135	739-844
PRG4	F: GAGTACCCAATCAAGGCATTATCA R: TCCATCTACTGGCTTACCATTGC	NM_005807	3431-3510
Ki-67	F: AATTCAGACTCCATGTGCCTGAG R: CATTGTCCTCAGCCTTCTTTGG		

## 2.10 Statistics

Where applicable, data are presented as mean  $\pm$  standard deviation. A two-sample Student's t-test was performed and any results with  $p < 0.05$  were considered significant. Where significant effects were detected, post-hoc tests were performed with a Bonferroni correction for multiple comparisons.

### 3 Results and discussion

In the course of the experiments two different mesh morphologies were investigated. The cell morphology was monitored by optical and fluorescence microscopy, therefore NCO-sP(EO-*stat*-PO) coated glass cover slips served as backing for the thin electrospun meshes to achieve an adequate optical density for the analysis. For the cell viability and long-term study with SEM-, GAG- and DNA-analysis and gene expression measurements, 10 µm thick electrospun meshes were used in Scaffoldex CellCrown™ inserts.

#### 3.1 Viability

Superficial (S) and middle-deep (MD) chondrocytes were cultured on electrospun meshes consisting of NCO-sP(EO-*stat*-PO), PLGA and a peptide sequence to promote cell adhesion. The peptide sequences resemble binding motifs from collagen II (CMQGPMGPMGPRG), decorin (CGKLER) and a collagen II binding sequence (CGWYRGRL). A mesh without peptides served as a control. Figure 3 depicts the results of a viability test where viable cells are green and dead cells are red. The survival rate of superficial and middle-deep chondrocytes was high for each sample, including peptides. Only single dead cells were monitored in the micrographs A – C and E – G.

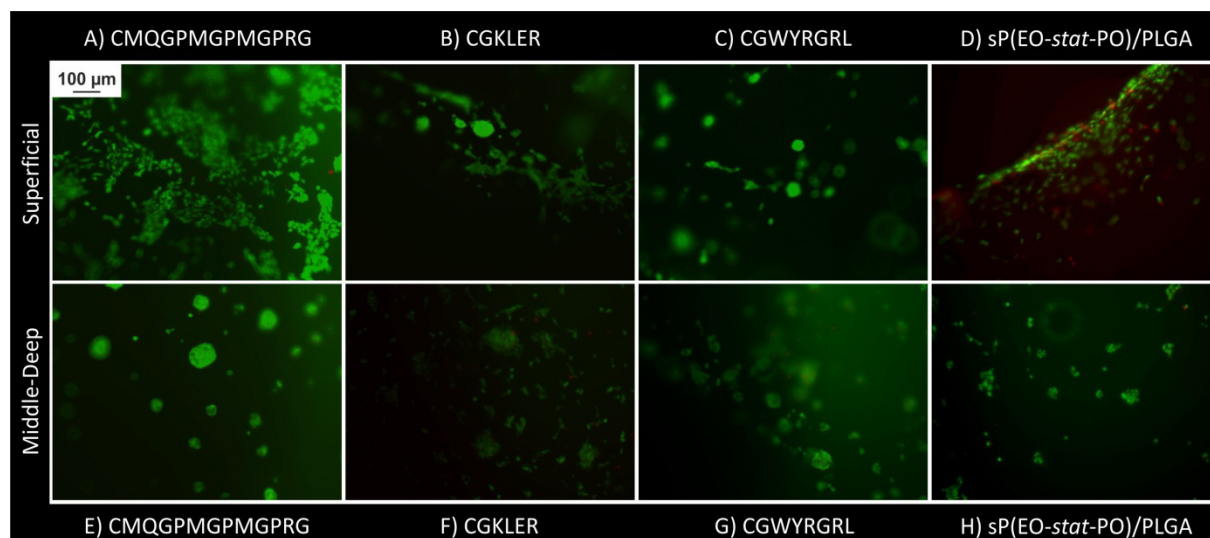


**Figure 3:** Fluorescence images of S and MD chondrocytes after a viability staining. Green indicates viable cells and dead cells are stained red. All meshes with peptides (A-C, E-G) feature a non-toxic environment that leads to cell survival after 7 days of culture. In D) several dead cells are seen, as the superficial chondrocytes cannot interact with the mesh.

Superficial cells on the control mesh without a peptide featured approximately 50 % dead cells, indicating that missing adhesion sequences impact on cell viability. In contrast to the results presented in Chapter 5, where human dermal fibroblasts only adhered to fibres with an RGD-motive, the chondrocytes exhibited at least the potential to survive on non-adhesive meshes. This can be attributed to the different sample type used in this chapter: here, the mesh was clamped into a Scaffdex® CellCrown, featuring a more pronounced 3D-environment for cells compared to the fibres that were deposited on flat surfaces. The washing step during the staining protocol removed the loosely or not-bound cells from fibres on surfaces, whereas cells in 3D-meshes were not removed by this washing step. This could be due to a stronger 3D scaffolding effect of the mesh and thus an increased unspecific adhesion to the meshes.

### **3.2 Adhesion and migration**

#### **3.2.1 Optical and fluorescence microscopy**

An overview of the cell adhesion patterns on the various substrates was seen in optical micrographs. The chondrocytes were cultured on electrospun fibres on a sP(EO-*stat*-PO) surface backing. On day 4 and 7 images of S and MD cells were recorded. Figure 4 shows significant differences in the cell numbers and morphology depending on the substrate. While the collagen II sequence CMQGPMGPMGPRG induced similar adhesion patterns of S and MD cells but only few adherent cells with a mixed morphology of spread and spherical chondrocytes, the samples with the decorin sequence CGKLER exhibited dense cell sheets of both S and MD chondrocytes.

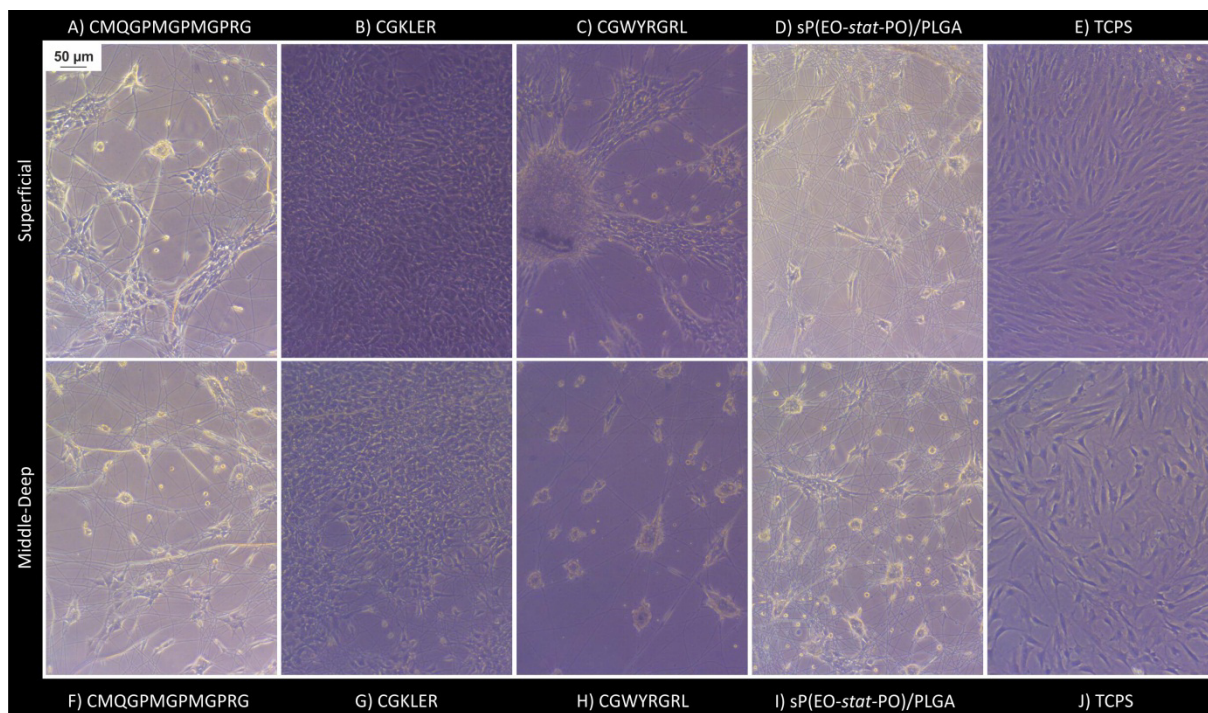


**Figure 4:** Optical micrograph of superficial and middle-deep chondrocytes on electrospun fibres at day 4. The fibres were spun on sP(EO-*stat*-PO) coated glass cover slips and consisted of NCO-sP(EO-*stat*-PO)/PLGA with cell adhesion mediating peptides (A-C, F-H), without peptides (D, I) and control samples on tissue culture plastic.

The CGWYRGRL sequence resulted in a different pattern. Here, S chondrocytes were predominantly well spread while MD cells formed multi-cell spheres across the substrate. Interestingly, the unmodified fibres that did not have adhesive properties towards fibroblasts in Chapter 5 featured some spread and spherical chondrocytes in Figure 4 D and I. The latter were mostly single cells that seemed to be floating on the substrate. As expected the chondrocytes showed a well spread morphology on the TCPS control samples.

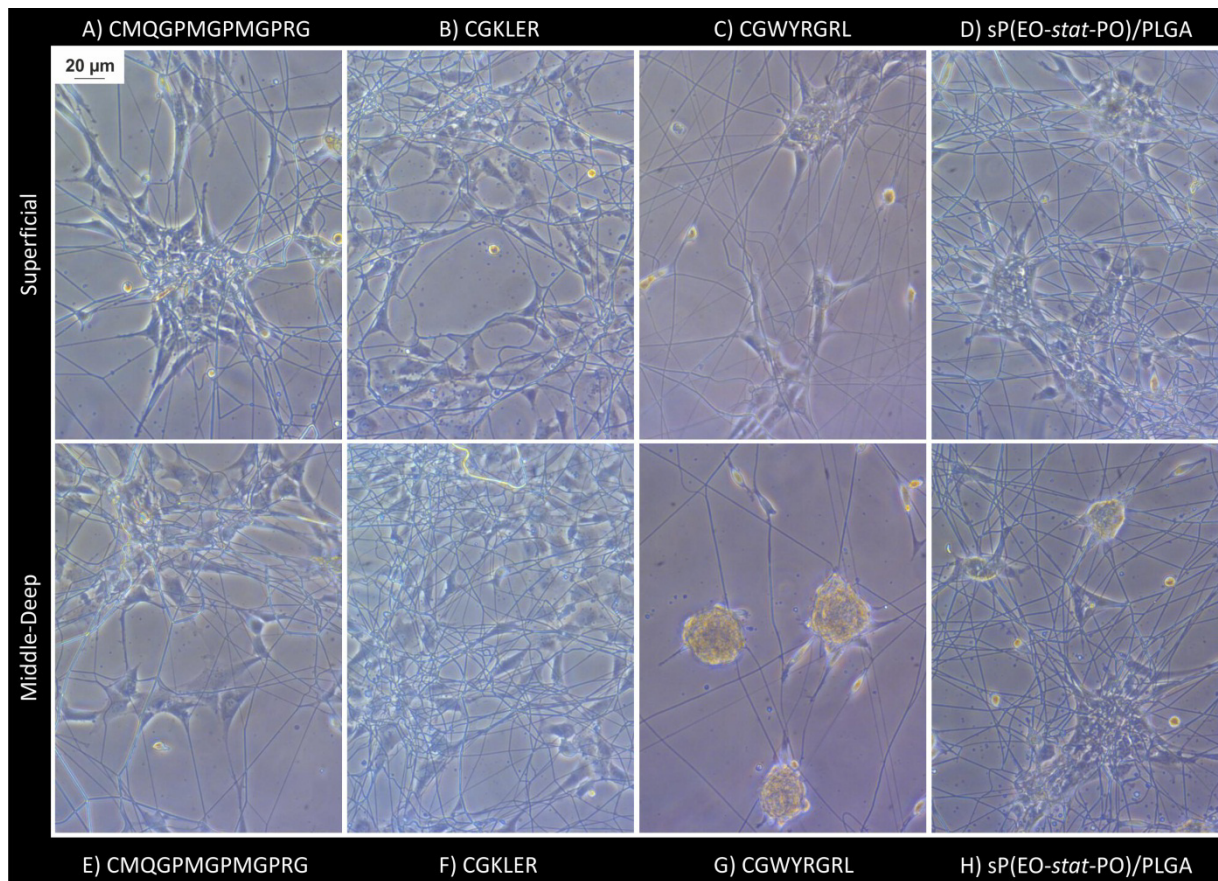


**Figure 5:** Optical micrograph of superficial and middle-deep chondrocytes on electrospun fibres at day 7. The fibres were spun on sP(EO-*stat*-PO) coated glass cover slips and consisted of NCO-sP(EO-*stat*-PO)/PLGA with cell adhesion mediating peptides (A-C, E-G), without peptides (D, H).

In Figure 5 day 7 images with a higher magnification were taken that more closely depict the interaction of cells with fibres. In each case with spread cells the fibres seemed to be pulled into the cell complex which indicates an adhesive interaction of chondrocytes with fibres. Solely MD cells on CGWYRGRL featured only spherical cell clusters that had slightly protruding cells along the fibres underneath the cell cluster (Figure 5). In this case no manipulation of the fibres by cells was observed.

The staining of the cytoskeleton revealed an organised actin skeleton on all substrates. This was observed most significantly on substrates with spread cells. But even in cellular spheres (e.g., Figure 6 C) organised cell skeletal structures are present and support the viability of the cells.



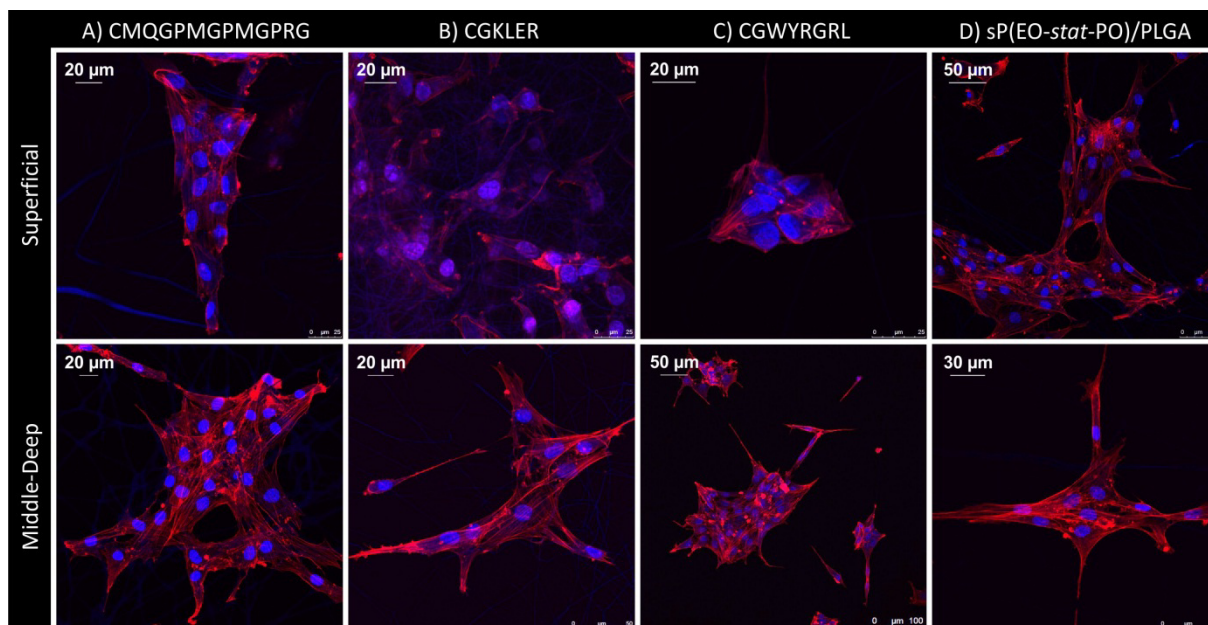


**Figure 6:** Cytoskeleton staining of superficial and middle-deep chondrocytes on NCO-sP(EO-stat-PO)/PLGA fibres after 7 days. The actin skeleton is displayed in red, the nuclei feature a blue staining.

### 3.2.2 Live-cell imaging

Live-cell imaging revealed details on the adhesion and interaction of chondrocytes to the meshes. With this method the *in vitro* development of chondrocytes was monitored over the course of three days. The dependence of the peptide within the meshes as well as the culturing condition was investigated.

S and MD chondrocytes cultured on meshes with a collagen II sequence (CMQGPMGPMGPRG) did not interact with the substrate. For both expansion media and chondrogenic media there is a cluster formation above the mesh, but no attachment of cells onto the mesh.

Chondrocytes on fibres containing the CGKLER-motive derived from decorin strongly interacted with the mesh. In expansion media they migrated through the fibre network, deforming the fibres due to their adhesion forces (Figure 7). The cells tended to form clusters, regardless of which media was used. The proliferative character remained unclear due to the clustering. However, on several samples a cell division was monitored of single cells or small clusters. In chondrogenic media the chondrocytes lost their migratory potential while the preference to form clusters increased.

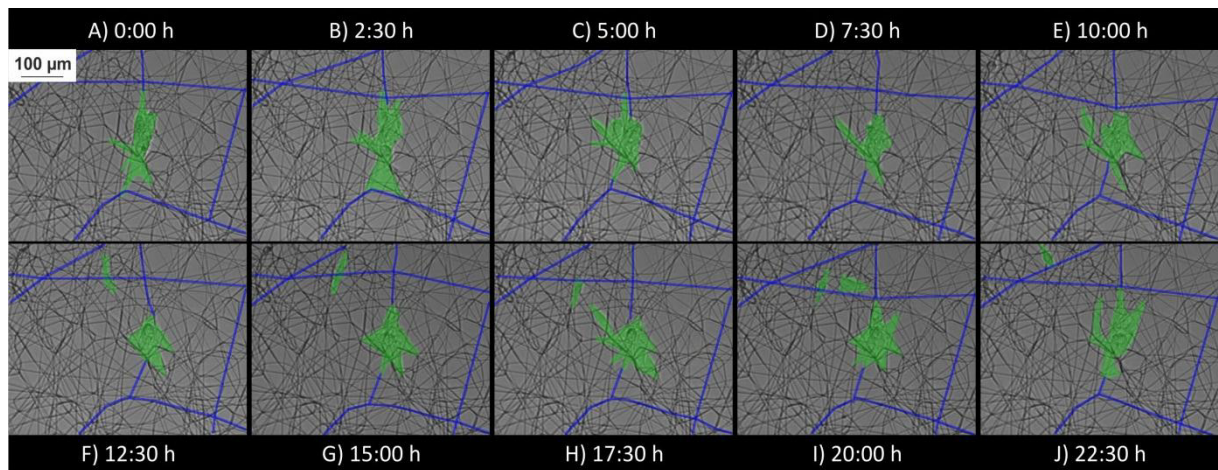


**Figure 7:** Modified Live-cell imaging pictures of S chondrocytes on a sP(EO-*stat*-PO)/PLGA/CGKLER mesh in expansion media. The cells are coloured in green and deformed fibres in blue. The cells adhered to the mesh and deformed fibres while migrating through the fibrous network.

The attachment of chondrocytes to fibres with the collagen II binding sequence CGWYRGRL was strong for chondrocytes from the superficial zone cultured in expansion media. The cell migration was small and the proliferation was unclear as large cell clusters formed. S chondrocytes in chondrogenic media did not interact with these fibres while the MD chondrocytes did not interact in either media. On fibres without peptides, the chondrocytes did not attach but formed clusters. Neither cell migration nor proliferation could be detected. The control on TCPS exhibited strong cell attachment, migration and proliferation for both cell types and media tested.

The findings of optical microscopy on flat surfaces decorated with fibres matched the findings of the live-cell imaging of meshes that were cultured in Scaffdex® 24-well inserts. The results suggest that there is only a definite interaction of the KLER-motif with chondrocytes, while the other peptides seem to induce no direct interaction between cells and fibres. However, there might be an indirect mechanism for cell adhesion as some cells on sP(EO-*stat*-PO)/PLGA fibres that were spreading, appeared to wrap around the fibres as these were the only topographical anchor sites. Interestingly, there were no spreading cells in the corresponding live-cell imaging experiment. This may be a consequence of a more pronounced 3D-environment compared to the culture on surfaces that were decorated with only a few fibres. The 3D situation could have a stronger scaffolding effect as the cells are surrounded by fibres more efficiently.

The similar phenotype of chondrocytes on non-adhesive and CMQGPMGPMGPRG-containing fibres underlines that there is no direct interaction with CMQGPMGPMGPRG-peptides as observed in the live-cell imaging.

### 3.3 Long term cell culture study

In a long-term cell culture study the morphology and matrix expression was analysed. For this experiment the substrates with glass cover slip backing were unsuitable as an environment should be investigated that resembles the natural 3D situation more closely. Therefore, the S and MD chondrocytes were cultured on meshes with a thickness of 30 – 40  $\mu\text{m}$  covering the bottom of a well in a 24 well plate as meshes cultured in Scaffoldex<sup>®</sup> CrownCell inserts were prone to rupture after 3 days and cells may be lost through these ruptures. The cells were kept in expansion media to increase their numbers on the meshes for 7 days. Beginning with day 8, chondrogenic media was used to induce a redifferentiation to a more chondrogenic cell character as primary chondrocytes dedifferentiate towards a mesenchymal phenotype under expansion cell culture conditions. The long term experiment was terminated after 21 days in chondrogenic media.

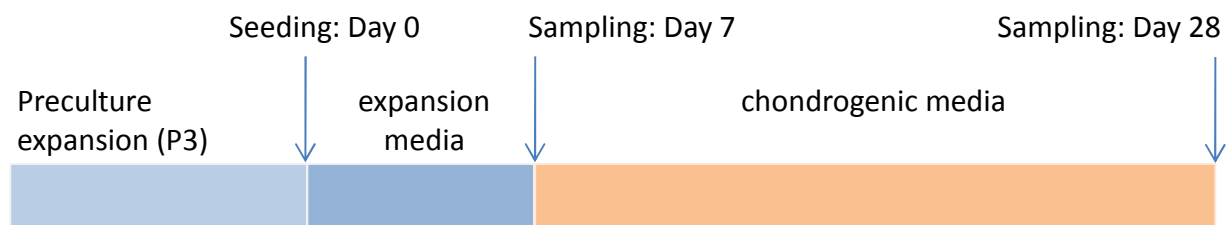


**Figure 8:** Course of the long-term cell culture experiment.

#### 3.3.1 Cell morphology by SEM

The mesh and cell morphology was analysed using SEM. The electrospun fibre diameters were measured at  $1.0 \pm 0.2 \mu\text{m}$  and exhibited similar mesh structures as observed in Chapter 3. The characteristically un-oriented fibres produced by solvent electrospinning showed signs of heat shrinkage once seen by the macroscopic reduction in mesh dimension and secondly the characteristic wave-like pattern of the previously straight and stretched fibres can be seen in the SEM micrographs.

The superficial and middle-deep cells were spread on all samples except for MD chondrocytes on meshes without peptides after seven days. The chondrocytes appeared to attach to the electrospun fibres as they stretched into the mesh. This behaviour was very

strong for samples with CGKLER and CGWYRGRRL motifs. Cells favoured attachment to fibres in grooves in the mesh, especially for the non-adhesive mesh in Figure 9 D. In general, chondrocytes did not adhere as single cells but in groups of several cells to the mesh and had a rough cell surface structure due to proteins on the cell surface.

After 21 days in chondrogenic media the cell structure changed to a mixed phenotype on samples with CGWYRGRRL and without peptides. Besides spread cells, spherical cell clusters were found. A confluent cell sheet grew on samples with the collagen II peptide or decorin derived sequence. For the latter, superficial chondrocyte clusters were found that grew into the fibrous network presenting a well spread morphology and indicating strong interaction with the electrospun fibres. S and MD chondrocytes on CMQGPMGPMGPRG and CGKLER meshes were very active in producing their own ECM fibres and proteins. The binding sequence of collagen II (CGWYRGRRL) predominantly resulted in very spherical cell clusters with rough cell surface but no or very little matrix fibre production. Occasionally, a spherical cell cluster attached slightly to the electrospun fibres, indicated by a flattened cell structure. On meshes without peptides the chondrocytes exhibited a mixed phenotype as well. Here, the spread cells mainly adhered in grooves on the mesh so that the cells were surrounded by fibres and interacting with the fibrous structure rather than by direct interaction through peptides. The results are summarised in Table 2.

**Table 2:** Summary of the observed phenotypes of chondrocytes on electrospun meshes according to SEM micrographs.

	sP(EO- <i>stat</i> -PO)/PLGA Mesh	Middle-Deep Chondrocytes			Superficial Chondrocytes		
		morphology	surface	fibre production	morphology	surface	fibre production
Day 7	CMQGPMGPMGPRG	spread	rough		spherical	rough	
	CGKLER	spread	rough		spread	medium rough	
	CGWYRGRRL	spread	rough		spread	medium rough	
	-	spherical	rough		spread	rough	
Day 28	CMQGPMGPMGPRG	spread	rough	high	spread	rough	high
	CGKLER	spread	rough	high	spread	rough	high
	CGWYRGRRL	mixed	very rough	few	mixed	very rough	
	-	mixed	rough		mixed	only spherical	high

In spite of the artefacts which occurred during the sample drying process (as seen in Figure 9 B and M) it is important to distinguish spherical cells from dead cells. An indication is given by lamellipodia and filapodia that can be easily seen on spread cells, for example in Figure 9 J. However also on samples with spherical cell morphologies, such as in Figure 9 A or Figure 10 C, lamellipodia grew from the round cell clusters into the mesh, indicating viable cells. Whereas on samples without peptides less lamellipodia were observed as depicted in Figure 9 L and Figure 10 L.

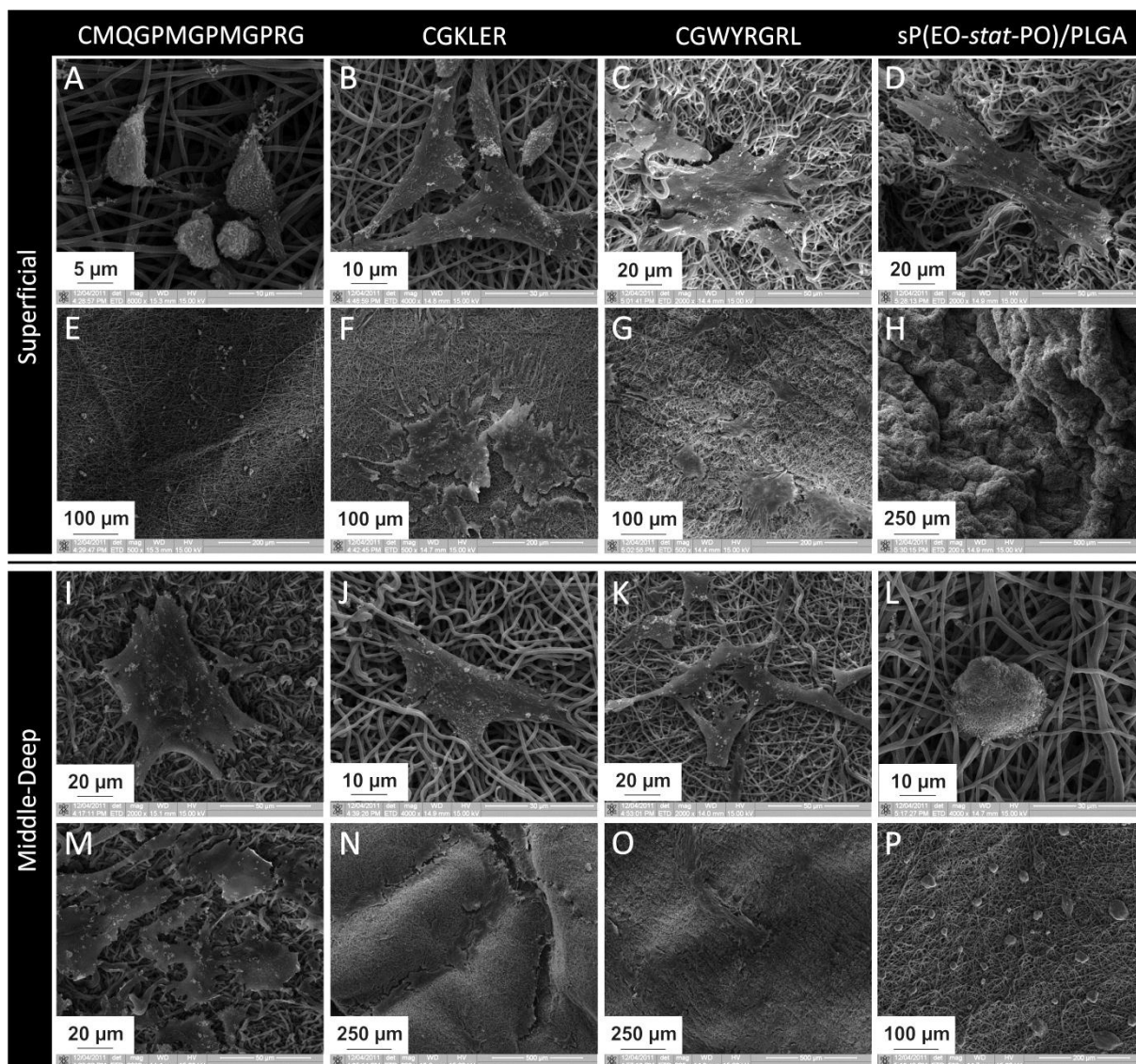


**Figure 9:** SEM images of S and MD chondrocytes on electrospun meshes after 7 days in expansion media.

Comparing the two points in time an overall increase in cell density was observed for all conditions. In particular on samples with the collagen II sequence fibroblastic cells covered the whole mesh.

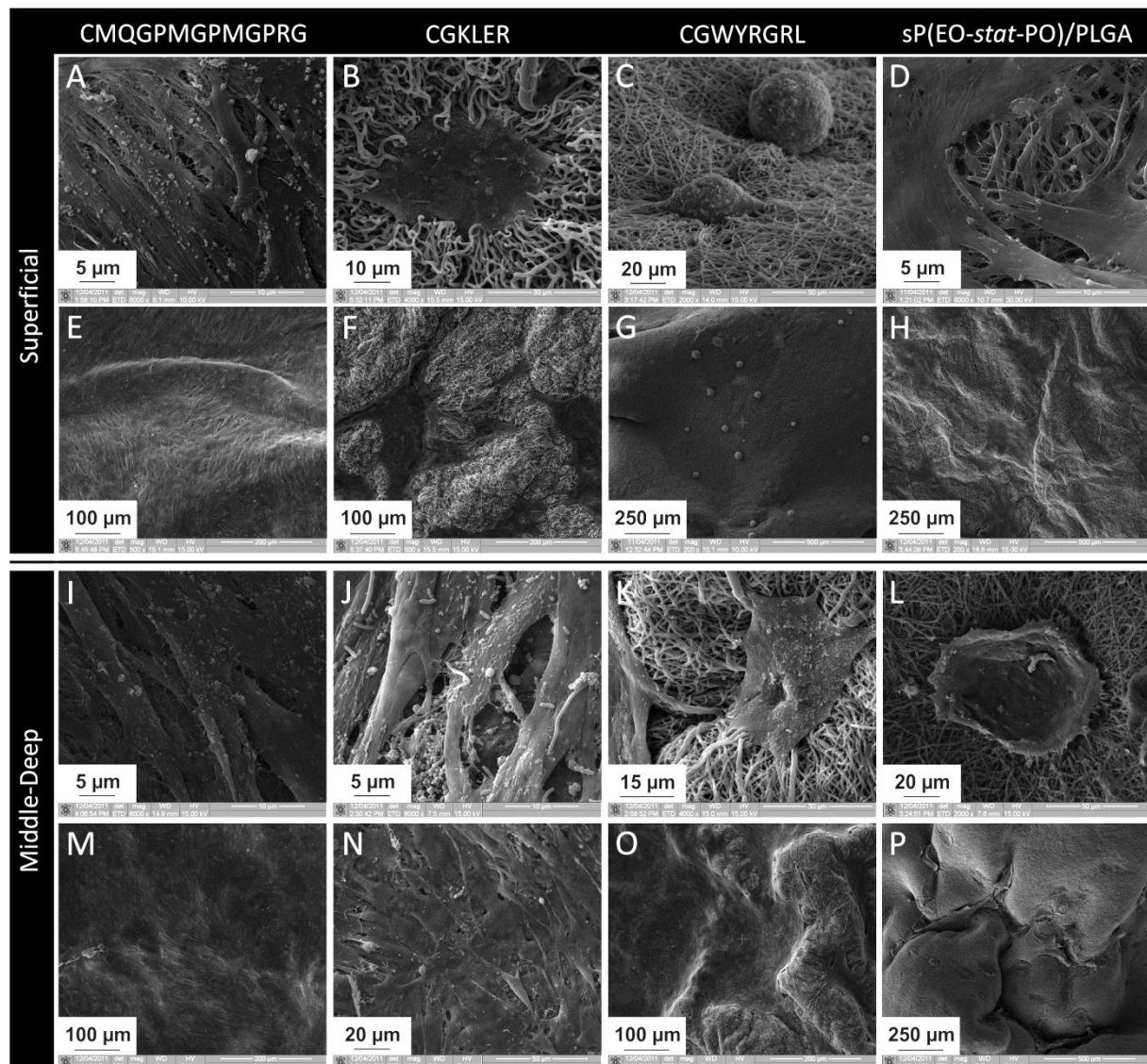


**Figure 10:** SEM images of S and MD chondrocytes on electrospun meshes after 28 days (7 days in expansion media, then 21 days in chondrogenic media).

### 3.3.2 Proliferation and GAG expression

For each sampling on day 7 and day 28 the matrix production of the cells was determined in the form of GAG expression. To correlate the absolute values to the number of cells, the total DNA content was analysed. It was found that after 7 days on meshes in expansion media, the GAG expression was similar to that of chondrocytes expanded on TCPS. On day 28, after 3 weeks in chondrogenic media an increased GAG production was found for all samples as depicted in Figure 11.

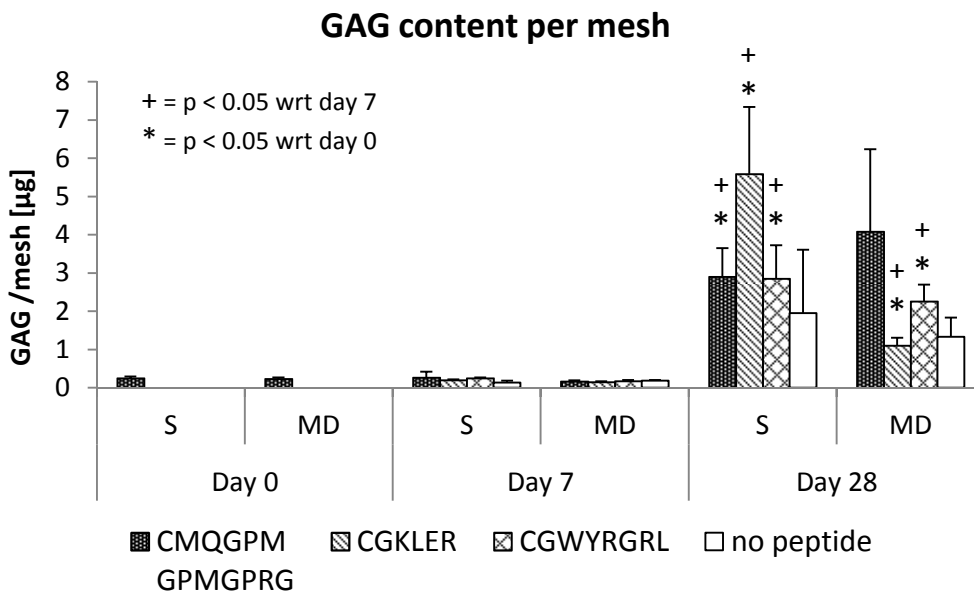


**Figure 11:** After 7 days on meshes in expansion media, the GAG expression was similar to that of chondrocytes expanded on TCPS. 21 days in chondrogenic media induced an increase in GAG production.

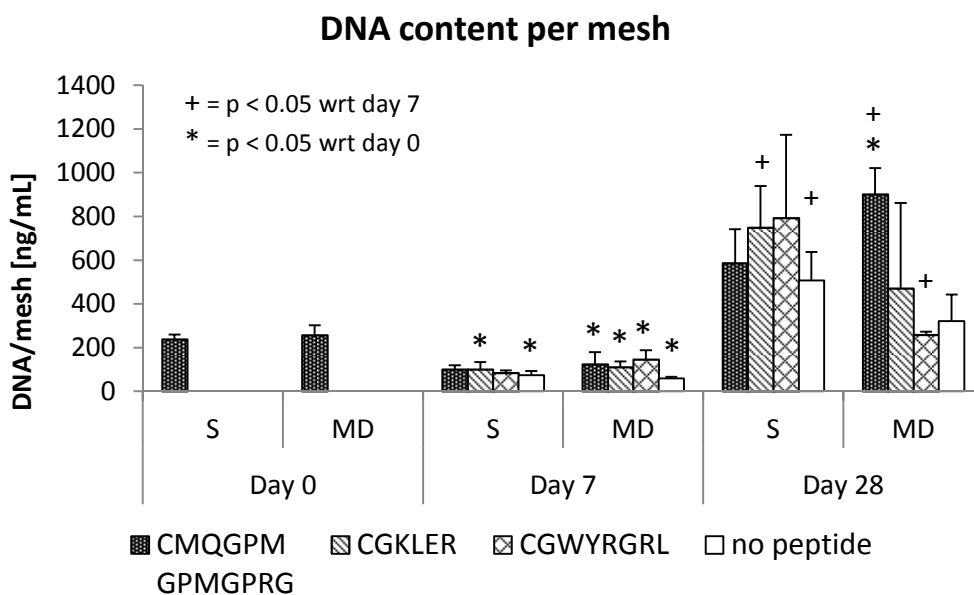


**Figure 12:** The change of DNA content (reflecting the cell number) with cell culture time on examined meshes. The drop from day 0 to day 7 samples can be attributed to a minor number of cells surviving the seeding process and finding suitable adhesion possibilities. The chondrocytes recovered with time and still proliferated while cultured in chondrogenic media.

Figure 12 presents the amount of DNA in the respective sample. To calculate the corresponding number of cells an amount of 7 pg DNA per cell was used. The cell number was reduced from 30,000 seeded cells (day 0) to an average of 15,000 cells after one week

on samples with binding sequences. On meshes without peptides the cell number decreased to 8,000. This observation can be explained by the fact that cells requiring adhesion possibilities to survive but do not find adhesion sites, undergo apoptosis, resulting in a reduced number of cells than seeded. After four weeks, the cell number increased for each sample, as the present cells produced matrix proteins onto which the cells could adhere, finally promoting cell proliferation. The measured GAG content was normalised to the number of cells and the result displayed in Figure 13. The significant differences that were found are time dependent and thus a result of the culturing condition rather than mesh and accordingly peptide dependent.

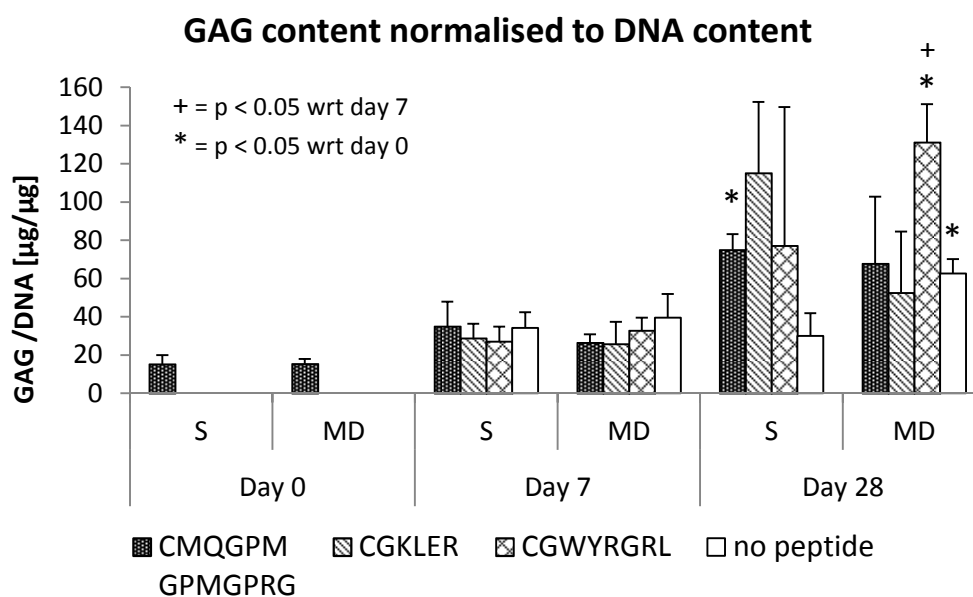


**Figure 13:** The GAG production per DNA content resulted in no significant differences for day 7 compared to day 0. The increase of GAG production was a result of the different culturing condition in chondrogenic media. The different meshes and peptides did not influence the GAG production significantly.

It has to be considered that the measured values were all detected at the low end of the GAG assay where the assay is not very sensitive. The low sensitivity as well as a sample number of three led to the large error bars. Therefore it is difficult to find significant differences between the examined samples.



### 3.3.3 Gene expression

The gene expression of the chondrocytes seeded on various fibrous scaffolds was analysed to determine the chondrogenic character of the cells.

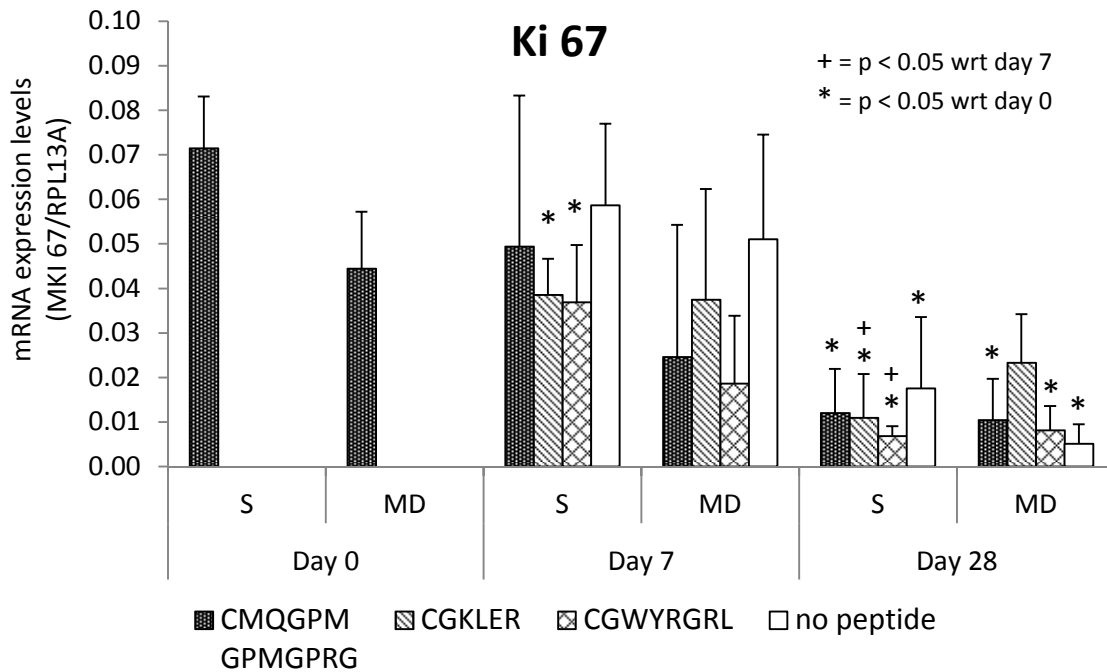


**Figure 14:** mRNA expression levels of the proliferation marker Ki 67.

The Ki-67 protein is associated with cell proliferation and can be detected in cells that are in the active phases of the cell cycle ( $G_1$ , S,  $G_2$  and mitosis) [65]. It is generally used to determine the growth fraction of a given human cell population. Figure 14 gives the mRNA expression levels of Ki-67. Referring to marker levels at day 0, proliferation marker levels decrease only slightly (significantly for S cells on CGKLER and CGWYRGRL) until day 7 as the cell culture medium promoted cell expansion. The change to chondrogenic media until day 28 decreased the proliferative character of the cells significantly. Superficial and middle-deep derived chondrocytes showed the same tendency in mRNA expression for Ki-67. Significant differences between meshes and peptides were not found.

These results correlate with the influences of the cell culture medium used in the long term experiment. The cells were pre-cultured in expansion media on TCPS, transferred to the electrospun meshes and cultured in the same medium for 7 days. This medium promotes cell proliferation whereas the differentiation media used from day 8 was intended to induce redifferentiation into chondrocytes that feature less proliferative activity.

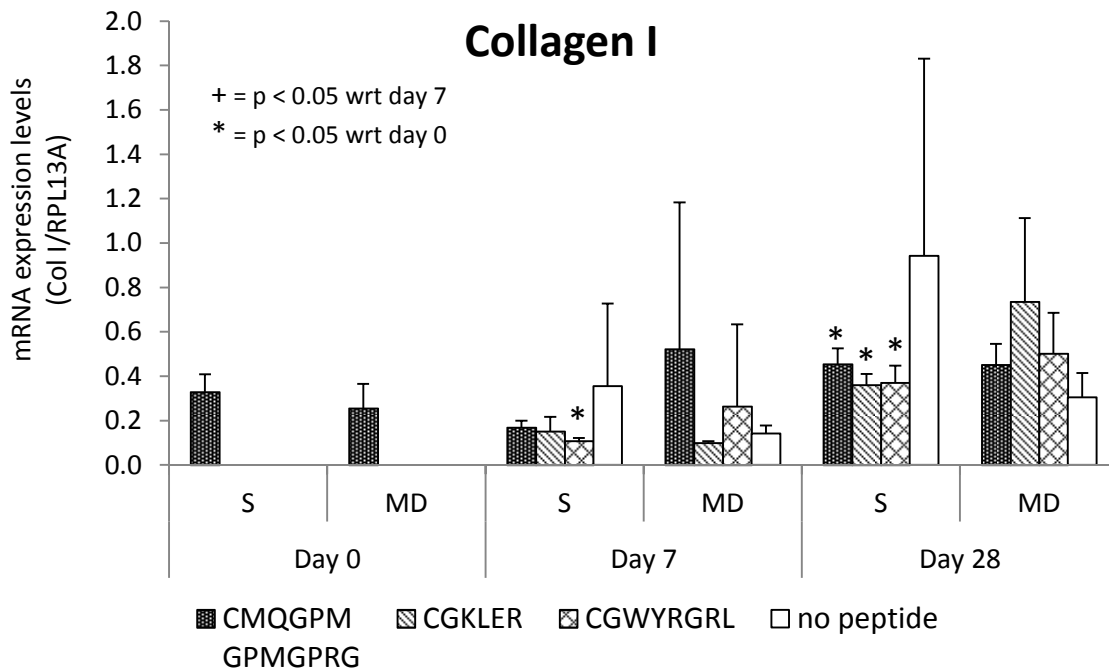


**Figure 15:** Collagen I production according to mRNA expression levels.

Type I collagen is the most abundant structural protein in animals [66]. About 90 % of all collagen is of type I, being present mainly in connective tissue such as tendons, skin, artery walls and fibrocartilage [67]. It is important to mention that cartilage does not consist of collagen type I but mainly of collagen type II. Therefore, the amount of collagen type I expression is a marker for dedifferentiated chondrocytes during expansion culture rather than for re-differentiated cells with a chondrogenic phenotype.

Superficial chondrocytes showed a significant increase ( $p < 0.05$ ) of collagen I expression at day 28 on meshes with peptides. The expression levels of any other sample at day 28 were similar but no statistical significance was found due to the large error bars. For the early sampling day (day 7) the expression levels were about the same compared to the cells after expansion on TCPS. Differences between mesh types cannot be concluded due the large error bars.

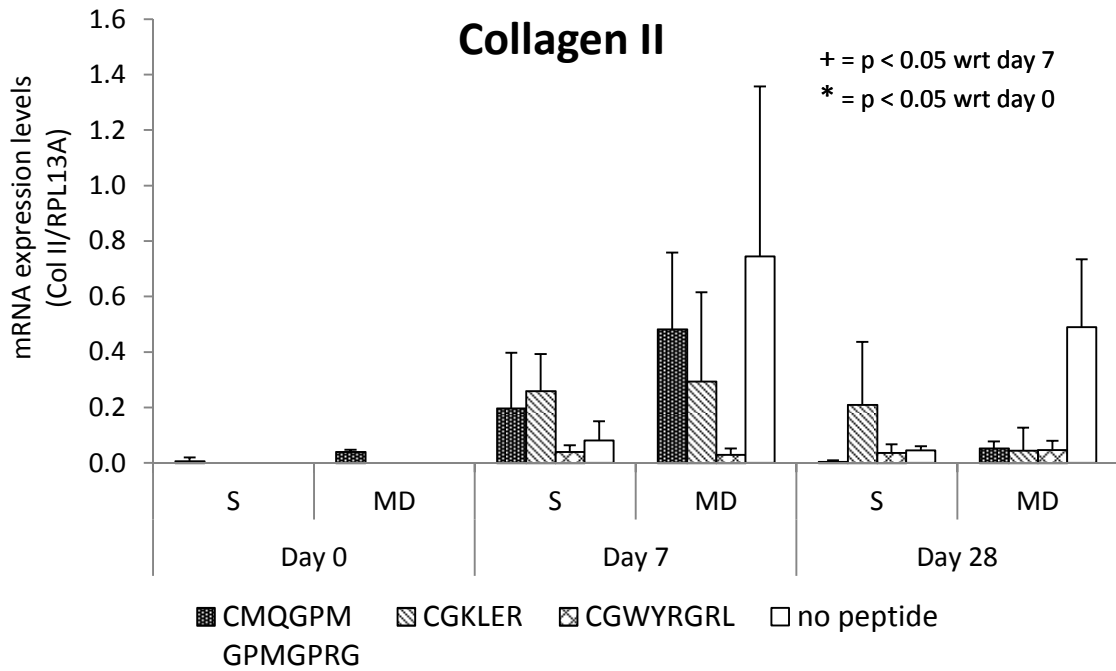


**Figure 16:** Collagen II production of S and MD chondrocytes according to mRNA expression levels.

Collagen type II is the main fibrous structure protein in cartilage that is expressed by chondrocytes. Its expression levels are an important measure in how active S and MD cells are on fibrous scaffolds in cartilage ECM production.

For collagen type II expression levels no significant time dependence was found. Generally the collagen II expression dropped at the late stage of the experiment, which is interesting as the culture medium was expected to promote the production of this protein. As a consequence of the large error bars no relevant significances could be extracted concerning a mesh and peptide dependence.

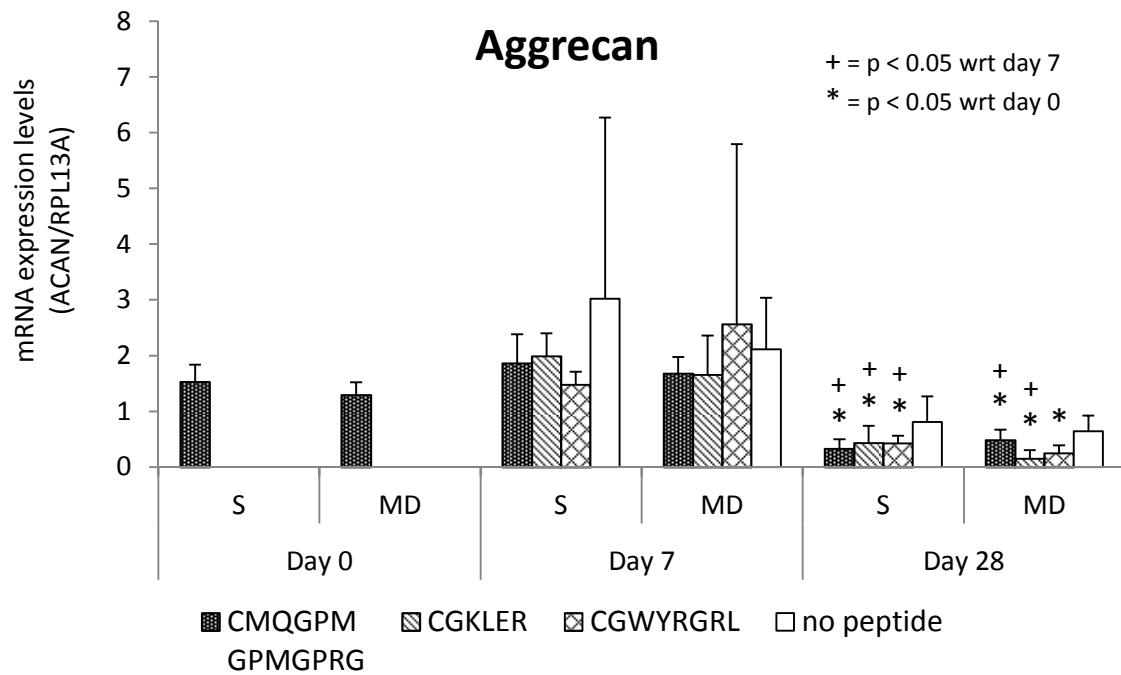


**Figure 17:** Production of the proteoglycan “Aggrecan” according to mRNA expression levels.

Besides a high amount of collagen type II, cartilage contains proteoglycans that are responsible for the highly hydrated nature of cartilage. Aggrecan is such a proteoglycan that is associated to hyaluronan via link proteins forming large molecular complexes that can take up large amounts of water [9]. Thus, the amount of aggrecan production can be correlated to the degree of the chondrogenic character of S and MD chondrocytes.

Superficial and middle-deep cells exhibit the same response in terms of aggrecan expression on the electrospun meshes. From day 0 to day 7 the expression levels remain unchanged but decrease significantly until day 28. The mesh types appear to have no influence on the aggrecan expression.

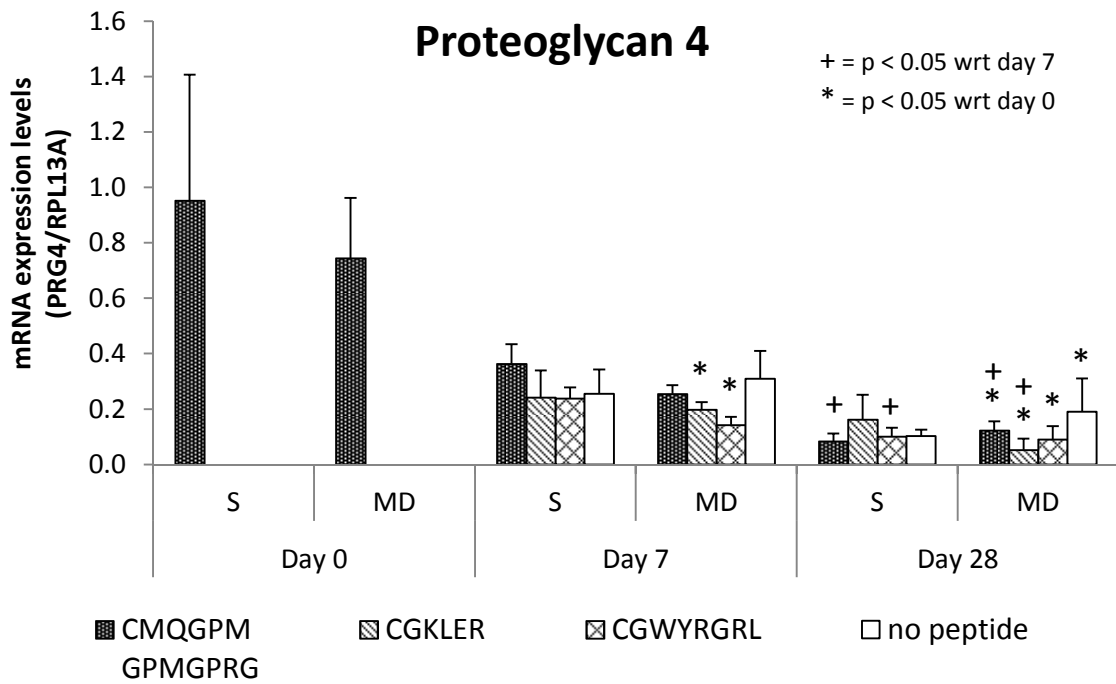


**Figure 18:** Production of proteoglycan 4 “lubricin” in S and MD chondrocytes according to mRNA expression levels.

The articular joints are lubricated by a glycoprotein called “lubricin” or “proteoglycan 4” (PRG4) [68]. It is mainly found in the synovial fluid and superficial layer of cartilage [69]. The mRNA of S and MD chondrocytes were investigated for the PRG4 expression levels to see if the electrospun meshes can induce zone specific cell activity.

The mRNA data revealed no zone specific PRG4 expression levels for both points in time. For S and MD chondrocytes a significant decrease down to 30 % in expression levels was found ( $p < 0.05$ ) until day 7. After three weeks in chondrogenic media the expression levels dropped to 12 %. The PRG4 expression was independent of the peptides used.

### 3.3.4 Discussion of gene expression data

It is known that chondrocytes stop producing aggrecan and collagen II while cultured in 2D expansion environments [70]. Therefore, the production of these proteins on 3D fibrous scaffolds is expected to rise if a re-differentiation process occurs. The observed pattern of a rise in aggrecan and collagen II mRNA expression after 7 days of culture in expansion media and a consecutive decrease after a further 21 days in chondrogenic media is surprising. We can only speculate what may have happened here. The chondrogenic media, including TGF- $\beta$ 3 which is a growth factor promoting chondrogenic differentiation [71], was changed once every seven days. We chose this frequency to monitor a differentiation that is substrate dependent rather than an effect of TGF- $\beta$ 3. At the early stage of the experiment, the provided media may be sufficient for the respective cell number but with increasing cell numbers during the course of the experiment the consumption of media content will increase accordingly. If the TGF- $\beta$ 3 levels have been depleted, the remaining media will be even less potent than expansion media to promote chondrogenic differentiation [72].

Due to the large variation in experimental data, it is difficult to draw conclusions from these measurements. Inhomogeneities which can result from the solution electrospinning process, such as fibre thickness distribution or fibre surface composition, may influence the cell response. Moreover, we cannot provide definite numbers of peptides that are present on the fibre surface, a topic that is currently being investigated.

One hypothesis to explain the observed data is that the surface modification of electrospun fibres is important in the initial stage of the experiment concerning cell attachment and migration. As the cell culture progresses the natural ECM production of the cells increases, cell – ECM contact as well as cell – cell contact gain importance, while the scaffolding function of the synthetic fibres decreases to a minor role. Although the mRNA data suggest that limited chondrogenic differentiation took place, a final conclusion on this hypothesis cannot be drawn from the mRNA data. Follow-up experiments are required to shed further light on this matter.

## 4 Conclusion

In this chapter the viability, morphology and biochemical expression of human articular chondrocytes was investigated on NCO-sP(EO-*stat*-PO)/PLGA based electrospun fibres. The fibres were selectively functionalised with peptide sequences derived from proteins that are characteristic for cartilage. The cell survival proved to be positive for any mesh type, including peptides, whereas the viability on pure NCO-sP(EO-*stat*-PO)/PLGA meshes was lower. The chondrocytes featured a fibroblastic phenotype on the majority of the investigated meshes. Exceptions were fibres modified with CGWYRGRL and unmodified fibres. The strongest cell-scaffold interaction was found for the decorin derived sequence CGKLER where live-cell imaging revealed the motion of well-spread chondrocytes through 3D meshes. The chondrogenic differentiation seemed to be low according to the low amount of GAG production and low amount of mRNA expression of chondrogenic markers such as collagen type II, aggrecan and proteoglycan 4. For conclusive evidence on the chondrogenic differentiation further experiments are necessary that support or reject the presented results. In the follow-up experiments a more frequent media change and thus TGF- $\beta$ 3 supply to the cells could be advantageous and should be adjusted to the expected cell numbers on the meshes. Moreover, with an extended knowledge about the fibre surface and its decoration with peptides the observed influences on the cell response could be assessed in more detail and conclusions drawn on the differentiation process. Finally combinations of the investigated peptides may be of interest, as the cells are surrounded by a cocktail of all proteins in their natural environment.

## 5 References

- [1] Diegelmann R. F. and Evans M. C., 'Wound Healing: An Overview of Acute, Fibrotic and Delayed Healing', *Frontiers in Bioscience*, 9, **2004**, 283-289.
- [2] Buckwalter J. A., 'Articular Cartilage Injuries', *Clinical Orthopaedics and Related Research*, 402, **2002**, 21-37.
- [3] Rogers K., *Bone and Muscle: Structure, Force and Motion* (New York: Britannica Educational Publishing, 2010).
- [4] Neumann D. A., *Kinesiology of the Musculoskeletal System* Elsevier, 2010).
- [5] Poole A. R., Kobayashi M., Yasuda T., Laverty S., Mwale F., Kojima T., Sakai T., Wahl C., El-Maadawy S., Webb G., Tchetina E. and Wu W., 'Type Ii Collagen Degradation and Its Regulation in Articular Cartilage in Osteoarthritis', *Annals of the Rheumatic Diseases*, 61, **2002**, ii78-ii81.
- [6] Buckwalter J. A. and Mankin H. J., 'Articular Cartilage: Tissue Design and Chondrocyte-Matrix Interactions', *Instructional course lectures*, 47, **1998**, 477-486.
- [7] Poole C. A., 'Review. Articular Cartilage Chondrons: Form, Function and Failure', *Journal of Anatomy*, 191, **1997**, 1-13.
- [8] Buschmann M. D., Gluzband Y. A., Grodzinsky A. J. and Hunziker E. B., 'Mechanical Compression Modulates Matrix Biosynthesis in Chondrocyte/Agarose Culture', *Journal of Cell Science*, 108, **1995**, 1497-1508.
- [9] Roughley P. J., 'The Structure and Function of Cartilage Proteoglycans', *European Cells & Materials*, 12, **2006**, 92-101.
- [10] Hardingham T. E., 'Role of Link-Protein in the Structure of Cartilage Proteoglycan Aggregates', *Biochemical Journal*, 177, **1979**, 237-247.
- [11] Clar C., *Clinical and Cost-Effectiveness of Autologous Chondrocyte Implantation for Cartilage Defects in Knee Joints : Systematic Review and Economic Evaluation* (Tunbridge Wells: Gray Publishing on behalf of NCCHTA, 2005).
- [12] Grande D. A., Breitbart A. S., Mason J., Paulino C., Laser J. and Schwartz R. E., 'Cartilage Tissue Engineering: Current Limitations and Solutions', *Clinical Orthopaedics and Related Research*, 367, **1999**, S176-S185.
- [13] Mithoefer K., Williams R. J., Warren R. F., Potter H. G., Spock C. R., Jones E. C., Wickiewicz T. L. and Marx R. G., 'The Microfracture Technique for the Treatment of Articular Cartilage Lesions in the Knee - a Prospective Cohort Study', *Journal of Bone and Joint Surgery-American Volume*, 87A, **2005**, 1911-1920.
- [14] Niikura T. and Reddi A. H., 'Differential Regulation of Lubricin/Superficial Zone Protein by Transforming Growth Factor Beta/Bone Morphogenetic Protein Superfamily Members in Articular Chondrocytes and Synoviocytes', *Arthritis and Rheumatism*, 56, **2007**, 2312-2321.
- [15] Simon T. M. and Jackson D. W., 'Articular Cartilage: Injury Pathways and Treatment Options', *Sports Medicine and Arthroscopy Review*, 14, **2006**, 146-154.
- [16] Schumacher B. L., Block J. A., Schmid T. M., Aydelotte M. B. and Kuettner K. E., 'A Novel Proteoglycan Synthesised and Secreted by Chondrocytes of the Superficial Zone of Articular Cartilage', *Archives of Biochemistry and Biophysics*, 311, **1994**, 144-152.
- [17] Buckwalter J. A. and Mankin H. J., 'Articular Cartilage: Degeneration and Osteoarthritis, Repair, Regeneration, and Transplantation', *Instructional course lectures*, 47, **1998**, 487-504.
- [18] Aydelotte M. B., Greenhill R. R. and Kuettner K. E., 'Differences between Sub-Populations of Cultured Bovine Articular Chondrocytes. Ii. Proteoglycan Metabolism', *Connective Tissue Research*, 18, **1988**, 223-234.
- [19] Frenkel S. R., Toolan B., Menche D., Pitman M. I. and Pachence J. M., 'Chondrocyte Transplantation Using a Collagen Bilayer Matrix for Cartilage Repair', *Journal of Bone and Joint Surgery-British Volume*, 79B, **1997**, 831-836.
- [20] Darling E. M., Hu J. C. Y. and Athanasiou K. A., 'Zonal and Topographical Differences in Articular Cartilage Gene Expression', *Journal of Orthopaedic Research*, 22, **2004**, 1182-1187.
- [21] Roth V. and Mow V. C., 'The Intrinsic Tensile Behavior of the Matrix of Bovine Articular-Cartilage and Its Variation with Age', *Journal of Bone and Joint Surgery-American Volume*, 62, **1980**, 1102-1117.
- [22] Wong M. and Carter D. R., 'Articular Cartilage Functional Histomorphology and Mechanobiology: A Research Perspective', *Bone*, 33, **2003**, 1-13.



- [23] LeBaron R. G. and Athanasiou K. A., 'Ex Vivo Synthesis of Articular Cartilage', *Biomaterials*, 21, **2000**, 2575-2587.
- [24] Klein T. J., Rizzi S. C., Reichert J. C., Georgi N., Malda J., Schuurman W., Crawford R. W. and Huttmacher D. W., 'Strategies for Zonal Cartilage Repair Using Hydrogels', *Macromolecular Bioscience*, 9, **2009**, 1049-1058.
- [25] Newman A. P., 'Articular Cartilage Repair', *The American Journal of Sports Medicine*, 26, **1998**, 309-324.
- [26] Wong M., Wuethrich P., Egli P. and Hunziker E., 'Zone-Specific Cell Biosynthetic Activity in Mature Bovine Articular Cartilage: A New Method Using Confocal Microscopic Stereology and Quantitative Autoradiography', *Journal of Orthopaedic Research*, 14, **1996**, 424-432.
- [27] Ng L., Grodzinsky A. J., Patwari P., Sandy J., Plaas A. and Ortiz C., 'Individual Cartilage Aggrecan Macromolecules and Their Constituent Glycosaminoglycans Visualised Via Atomic Force Microscopy', *Journal of Structural Biology*, 143, **2003**, 242-257.
- [28] Jinks C., Jordan K., Ong B. N. and Croft P., 'A Brief Screening Tool for Knee Pain in Primary Care (Knest). 2. Results from a Survey in the General Population Aged 50 and Over', *Rheumatology*, 43, **2004**, 55-61.
- [29] Hunter D. J., Neogi T. and Hochberg M. C., 'Quality of Osteoarthritis Management and the Need for Reform in the Us', *Arthritis Care & Research*, 63, **2011**, 31-38.
- [30] Temenoff J. S. and Mikos A. G., 'Review: Tissue Engineering for Regeneration of Articular Cartilage', *Biomaterials*, 21, **2000**, 431-440.
- [31] Detterline A. J., Goldberg S., Bach B. R. J. and Cole B. J., 'Treatment Options for Articular Cartilage Defects of the Knee', *Orthopaedic Nursing*, 24, **2005**, 361-366.
- [32] Puett D. W. and Griffin M. R., 'Published Trials of Nonmedicinal and Noninvasive Therapies for Hip and Knee Osteoarthritis', *Annals of Internal Medicine*, 121, **1994**, 133-140.
- [33] Yu L. P., Smith G. N., Brandt K. D., Myers S. L., O'Connor B. L. and Brandt D. A., 'Reduction of the Severity of Canine Osteoarthritis by Prophylactic Treatment with Oral Doxycycline', *Arthritis & Rheumatism*, 35, **1992**, 1150-1159.
- [34] Attur M. G., Patel R. N., Patel P. D., Abramson S. B. and Amin A. R., 'Tetracycline up-Regulates Cox-2 Expression and Prostaglandin E2 Production Independent of Its Effect on Nitric Oxide', *The Journal of Immunology*, 162, **1999**, 3160-3167.
- [35] Lussier A., Cividino A. A., McFarlane C. A., Olszynski W. P., Potashner W. J. and De Medicis R., 'Viscosupplementation with Hylan for the Treatment of Osteoarthritis: Findings from Clinical Practice in Canada', *The Journal of rheumatology*, 23, **1996**, 1579-1585.
- [36] Pridie K., 'A Method for Resurfacing Osteoarthritic Knee Joints', *JBJS*, 41, **1959**, 618-619.
- [37] Johnson L. L., 'Arthroscopic Abrasion Arthroplasty Historical and Pathologic Perspective: Present Status', *Arthroscopy: The Journal of Arthroscopic & Related Surgery*, 2, **1986**, 54-69.
- [38] Steadman J. R., Rodkey W. G. and Briggs K. K., 'Microfracture to Treat Full-Thickness Chondral Defects: Surgical Technique, Rehabilitation, and Outcomes', *The journal of knee surgery*, 15, **2002**, 170-176.
- [39] Hangody L., Kish G., Karpati Z., Udvarhelyi I., Szigeti I. and Bely M., 'Mosaicplasty for the Treatment of Articular Cartilage Defects: Application in Clinical Practice', *Orthopedics*, 21, **1998**, 751-756.
- [40] Gudas R., Kalesinskas R. J., Kimtys V., Stankevicius E., Toliusis V., Bernotavicius G. and Smailys A., 'A Prospective Randomised Clinical Study of Mosaic Osteochondral Autologous Transplantation Versus Microfracture for the Treatment of Osteochondral Defects in the Knee Joint in Young Athletes', *Arthroscopy-the Journal of Arthroscopic and Related Surgery*, 21, **2005**, 1066-1075.
- [41] Brittberg M., Lindahl A., Nilsson A., Ohlsson C., Isaksson O. and Peterson L., 'Treatment of Deep Cartilage Defects in the Knee with Autologous Chondrocyte Transplantation', *New England Journal of Medicine*, 331, **1994**, 889-895.
- [42] Peterson L., Brittberg M., Kiviranta I., Akerlund E. L. and Lindahl A., 'Autologous Chondrocyte Transplantation - Biomechanics and Long-Term Durability', *American Journal of Sports Medicine*, 30, **2002**, 2-12.
- [43] Horas U., Pelinkovic D., Herr G., Aigner T. and Schnettler R., 'Autologous Chondrocyte Implantation and Osteochondral Cylinder Transplantation in Cartilage Repair of the Knee Joint - a Prospective, Comparative Trial', *Journal of Bone and Joint Surgery-American Volume*, 85A, **2003**, 185-192.
- [44] Bartlett W., Skinner J. A., Gooding C. R., Carrington R. W. J., Flanagan A. M., Briggs T. W. R. and Bentley G., 'Autologous Chondrocyte Implantation Versus Matrix-Induced Autologous Chondrocyte Implantation for Osteochondral Defects of the Knee', *Journal of Bone & Joint Surgery, British Volume*, 87-B, **2005**, 640-645.
- [45] Knutsen G., Engebretsen L., Ludvigsen T. C., Drogset J. O., Grontvedt T., Solheim E., Strand T., Roberts S., Isaksen V. and Johansen C., 'Autologous Chondrocyte Implantation Compared with Microfracture in

- the Knee - a Randomised Trial', *Journal of Bone and Joint Surgery-American Volume*, 86A, **2004**, 455-464.
- [46] Felson D. T., Lawrence R. C., Dieppe P. A., Hirsch R., Helmick C. G., Jordan J. M., Kington R. S., Lane N. E., Nevitt M. C., Zhang Y., Sowers M., McAlindon T., Spector T. D., Poole A. R., Yanovski S. Z., Ateshian G., Sharma L., Buckwalter J. A., Brandt K. D. and Fries J. F., 'Osteoarthritis: New Insights. Part 1: The Disease and Its Risk Factors', *Annals of Internal Medicine*, 133, **2000**, 635-646.
- [47] Ong K., Lau E., Suggs J., Kurtz S. and Manley M., 'Risk of Subsequent Revision after Primary and Revision Total Joint Arthroplasty', *Clinical Orthopaedics and Related Research*<sup>®</sup>, 468, **2010**, 3070-3076.
- [48] Julin J., Jämsen E., Puolakka T., Konttinen Y. T. and Moilanen T., 'Younger Age Increases the Risk of Early Prosthesis Failure Following Primary Total Knee Replacement for Osteoarthritis', *Acta Orthopaedica*, 81, **2010**, 413-419.
- [49] Hutmacher D. W., 'Scaffolds in Tissue Engineering Bone and Cartilage', *Biomaterials*, 21, **2000**, 2529-2543.
- [50] Benya P. D. and Shaffer J. D., 'Dedifferentiated Chondrocytes Reexpress the Differentiated Collagen Phenotype When Cultured in Agarose Gels', *Cell*, 30, **1982**, 215-224.
- [51] Hauselmann H. J., Masuda K., Hunziker E. B., Neidhart M., Mok S. S., Michel B. A. and Thonar E. J., 'Adult Human Chondrocytes Cultured in Alginate Form a Matrix Similar to Native Human Articular Cartilage', *American Journal of Physiology - Cell Physiology*, 271, **1996**, C742-C752.
- [52] Shin H. J., Lee C. H., Cho I. H., Kim Y. J., Lee Y. J., Kim I. A., Park K. D., Yui N. and Shin J. W., 'Electrospun Plga Nanofiber Scaffolds for Articular Cartilage Reconstruction: Mechanical Stability, Degradation and Cellular Responses under Mechanical Stimulation in Vitro', *Journal of Biomaterials Science-Polymer Edition*, 17, **2006**, 103-119.
- [53] Ma Z., Gao C., Gong Y. and Shen J., 'Cartilage Tissue Engineering Plla Scaffold with Surface Immobilised Collagen and Basic Fibroblast Growth Factor', *Biomaterials*, 26, **2005**, 1253-1259.
- [54] Chang K.-Y., Cheng L.-W., Ho G.-H., Huang Y.-P. and Lee Y.-D., 'Fabrication and Characterisation of Poly(Gamma-Glutamic Acid)-Graft-Chondroitin Sulfate/Polycaprolactone Porous Scaffolds for Cartilage Tissue Engineering', *Acta Biomaterialia*, 5, **2009**, 1937-1947.
- [55] Lee C. R., Grodzinsky A. J., Hsu H. P. and Spector M., 'Effects of a Cultured Autologous Chondrocyte-Seeded Type Ii Collagen Scaffold on the Healing of a Chondral Defect in a Canine Model', *Journal of Orthopaedic Research*, 21, **2003**, 272-281.
- [56] Hong Y., Song H., Gong Y., Mao Z., Gao C. and Shen J., 'Covalently Crosslinked Chitosan Hydrogel: Properties of in Vitro Degradation and Chondrocyte Encapsulation', *Acta Biomaterialia*, 3, **2007**, 23-31.
- [57] Chen Y.-L., Lee H.-P., Chan H.-Y., Sung L.-Y., Chen H.-C. and Hu Y.-C., 'Composite Chondroitin-6-Sulfate/Dermatan Sulfate/Chitosan Scaffolds for Cartilage Tissue Engineering', *Biomaterials*, 28, **2007**, 2294-2305.
- [58] Xi-Ying L., Yong W., Xiang D., Qiao-Yan D., Ming-Zhong L., Shen-Zhou L., Huan-Xiang Z. and Xue-Guang Z., 'Attachment and Growth of Human Bone Marrow Derived Mesenchymal Stem Cells on Regenerated Antheraea Pernyi Silk Fibroin Films', *Biomedical Materials*, 1, **2006**, 181.
- [59] Kim H. J. and Kirsch T., 'Collagen/Annexin V Interactions Regulate Chondrocyte Mineralisation', *Journal of Biological Chemistry*, 283, **2008**, 10310-10317.
- [60] Salinas C. N. and Anseth K. S., 'Decorin Moieties Tethered into Peg Networks Induce Chondrogenesis of Human Mesenchymal Stem Cells', *Journal of Biomedical Materials Research Part A*, 90A, **2009**, 456-464.
- [61] Rothenfluh D. A., Bermudez H., O'Neil C. P. and Hubbell J. A., 'Biofunctional Polymer Nanoparticles for Intra-Articular Targeting and Retention in Cartilage', *Nat Mater*, 7, **2008**, 248-254.
- [62] Götz H., Beginn U., Bartelink C. F., Grünbauer H. J. M. and Möller M., 'Preparation of Isophorone Diisocyanate Terminated Star Polyethers', *Macromolecular Materials and Engineering*, 287, **2002**, 223-230.
- [63] Jeon J. E., Schrobback K., Hutmacher D. W. and Klein T. J., 'Dynamic Compression Improves Biosynthesis of Human Zonal Chondrocytes from Osteoarthritis Patients', *Osteoarthritis and Cartilage*, **2012**.
- [64] Enobakhare B. O., Bader D. L. and Lee D. A., 'Quantification of Sulfated Glycosaminoglycans in Chondrocyte/Alginate Cultures, by Use of 1,9-Dimethylmethylene Blue', *Analytical Biochemistry*, 243, **1996**, 189-191.
- [65] Scholzen T. and Gerdes J., 'The Ki-67 Protein: From the Known and the Unknown', *Journal of Cellular Physiology*, 182, **2000**, 311-322.
- [66] Sweeney S. M., Orgel J. P., Fertala A., McAuliffe J. D., Turner K. R., Di Lullo G. A., Chen S., Antipova O., Perumal S., Ala-Kokko L., Forlino A., Cabral W. A., Barnes A. M., Marini J. C. and Antonio J. D. S.,

- 'Candidate Cell and Matrix Interaction Domains on the Collagen Fibril, the Predominant Protein of Vertebrates', *Journal of Biological Chemistry*, 283, **2008**, 21187-21197.
- [67] Di Lullo G. A., Sweeney S. M., Körkkö J., Ala-Kokko L. and San Antonio J. D., 'Mapping the Ligand-Binding Sites and Disease-Associated Mutations on the Most Abundant Protein in the Human, Type I Collagen', *Journal of Biological Chemistry*, 277, **2002**, 4223-4231.
- [68] Schumacher B. L., Block J. A., Schmid T. M., Aydelotte M. B. and Kuettner K. E., 'A Novel Proteoglycan Synthesised and Secreted by Chondrocytes of the Superficial Zone of Articular Cartilage', *Arch Biochem Biophys*, 311, **1994**, 144-152.
- [69] Flannery C. R., Hughes C. E., Schumacher B. L., Tudor D., Aydelotte M. B., Kuettner K. E. and Caterson B., 'Articular Cartilage Superficial Zone Protein (Szp) Is Homologous to Megakaryocyte Stimulating Factor Precursor and Is a Multifunctional Proteoglycan with Potential Growth-Promoting, Cytoprotective, and Lubricating Properties in Cartilage Metabolism', *Biochemical and Biophysical Research Communications*, 254, **1999**, 535-541.
- [70] Hicks D. L., Sage A. B., Schumacher B. L., Sah R. L. and Watson D., 'Growth and Phenotype of Low-Density Nasal Septal Chondrocyte Monolayers', *Otolaryngology -- Head and Neck Surgery*, 133, **2005**, 417-422.
- [71] Ebisawa K., Hata K. I., Okada K., Kimata K., Ueda M., Torii S. and Watanabe H., 'Ultrasound Enhances Transforming Growth Factor Beta-Mediated Chondrocyte Differentiation of Human Mesenchymal Stem Cells', *Tissue Engineering*, 10, **2004**, 921-929.
- [72] Clarke D. C., Brown M. L., Erickson R. A., Shi Y. and Liu X., 'Transforming Growth Factor B Depletion Is the Primary Determinant of Smad Signaling Kinetics', *Molecular and Cellular Biology*, 29, **2009**, 2443-2455.



## CHAPTER 7

---

### **Immune response of monocytes and macrophages on 2D and 3D hydrogel surfaces and fibres based on NCO-sP(EO-*stat*-PO)**

This chapter focuses on the response of macrophages to two-dimensional (2D) hydrogel surfaces and three-dimensional (3D) electrospun fibres. Three different fibre densities were investigated, that gradually changed from 2D to 3D morphology. Monocytes could not adhere to 2D surfaces of sP(EO-*stat*-PO) until day 3 and formed cell clusters that migrated over the surface. On 3D fibres fewer clusters were observed, accompanied by reduced migratory activity. The macrophage phenotype is strongly influenced by the substrate morphology rather than surface chemistry.

---

This chapter represents a cooperative project with Matthias Bartneck.

Parts of this Chapter have been published:

Bartneck, M., Heffels, K.-H., Pan, Y., Bovi, M., Zwadlo-Klarwasser, G., *et al.*, 'Inducing Healing-Like Human Primary Macrophage Phenotypes by 3D Hydrogel Coated Nanofibres', *Biomaterials*, 33, **2012**, 4136-4146.

## 1 Introduction

The response of the immune system to implants decides their success. In the field of tissue engineering biomaterials need to cause more than sole passive acceptance and prevention of foreign body reaction. An active incorporation of implants into the living organism is required to regenerate tissue, large defects or even organs. The three-dimensional (3D) implant geometry, bioactivation of implant surfaces as well as supporting effects such as angiogenesis are crucial for this task. Li *et al.* showed that in comparison with a two-dimensional (2D) culture, 3D PLGA scaffolds improved the differentiation and function of stem cell derived hepatocytes [1]. However, the influences of surface bioactivation and scaffold morphology on the response of the human immune system are still largely unknown.

Inflammation occurs as a response of the immune system to an infiltration of alien material into an organism. It is required to stop tissue destruction and initiate the healing process. Immediately after injury immune cells migrate from the blood to the injured tissue causing an acute inflammation. After a few days the acute inflammation is either resolved, turned into a chronic inflammation or the formation of an abscess occurs. The resolution of inflammation is the preferred outcome for a structurally and functionally restored tissue, whereas a chronic inflammation can lead to tissue destruction. Abscesses are accumulations of large amounts of dead immune cells, neutrophils in particular, which disrupt tissue healing.

The immune cells are responsible for protection of the organism; they propagate and control the protection mechanism of inflammation. They originate like all blood cells from hematopoietic stem cells of the bone marrow. Figure 1 presents the differentiation of the two blood cell lineages descending from a common progenitor stem cell. This chapter focuses on macrophages as biomaterial acceptance largely depends on their response. Consequently, it is the most important cell type of the innate immune system that is almost omnipresent in the human body. Macrophages evolve from monocytes by differentiation and are found as tissue resident or mobile cells [2]. Their cellular task as a phagocyte is to engulf and digest cellular debris and pathogens. Furthermore, they communicate with other cells (immune cells, fibroblasts) by releasing cytokines and other inflammation mediators. These cytokines vary depending on the type of cell activation: in the beginning of

inflammation pro-inflammatory signals are released, whereas during the resolution of an inflammation anti-inflammatory mediators are predominantly expressed [3].

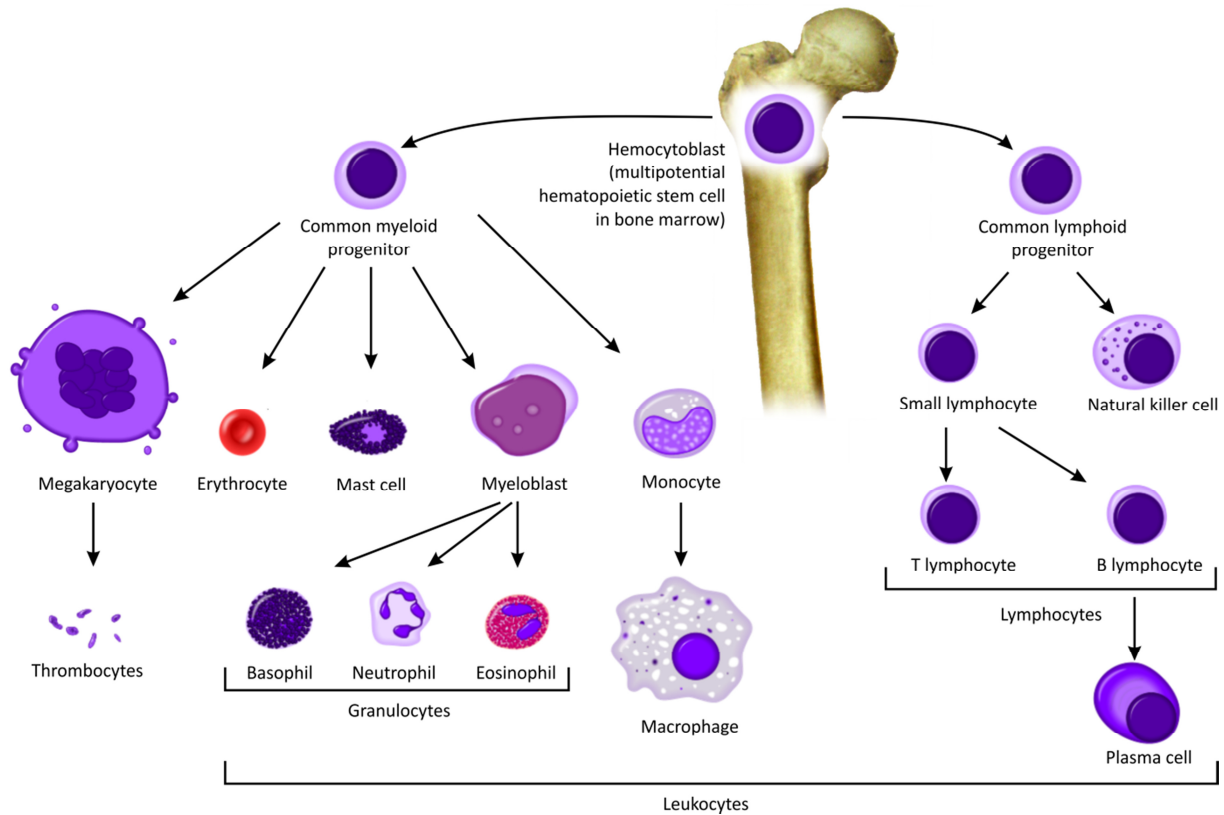


**Figure 1:** Simplified scheme of the human immune cell lineage. (Material from [http://en.wikipedia.org/wiki/File:Hematopoiesis\\_simple.png](http://en.wikipedia.org/wiki/File:Hematopoiesis_simple.png) and <http://doctorology.net/wp-content/uploads/2009/06/femur-tampak-depan.jpg>.)

This leads to a general classification of macrophages in either classically (M1) or alternatively (M2) activated macrophages. The macrophage subpopulations can be identified by surface markers that are expressed according to the cell function. 27E10 is a marker that is expressed on pro-inflammatory macrophages as well as on their myeloid progenitor [4]. Pro-inflammatory activated cells fight bacterial infections and are able to degrade the extracellular matrix (ECM) [5, 6] or polymeric scaffolds [7]. Anti-inflammatory macrophages complement the capacity of M1 cells as they are involved in remodelling the ECM [6, 8] and support wound healing [9]. M2 cells are characterised by scavenger receptors such as clusters of differentiation 163 (CD 163) and stabilin-1. Immune cells use scavenger receptors to detect negatively charged macromolecules such as low-density lipoprotein (LDL). As the name “scavenger” suggests, the detected molecules are taken up into the cytosol and by that way cleaned from the extracellular space. CD 163 recognises haemoglobin while

Stabilin-1 is expressed in the presence of glucocorticoids [10]. An indicator for a declining inflammation is the scavenger receptor “MARCO” which has a collagenous structure and is involved in the uptake of environmental particles [11, 12].

It is important to mention that the subtypes of M1 and M2 may co-exist in a population [6] but even single cells have been found that exhibited markers for both activation patterns [13]. Classically, the surface chemistry of implants is believed to be decisive for macrophage activation [14] but recent studies prove that topographical surface properties also influence macrophage behaviour [15, 16].

This chapter deals with the behaviour of monocytes and macrophages on 2D and 3D geometries that feature the same surface chemistry. As the basis of this study, NCO-sP(EO-*stat*-PO) prepolymer is coated on flat surfaces and covers the surface of electrospun fibres consisting of PLGA and NCO-sP(EO-*stat*-PO). The adhesion and migration of immune cells on these treated substrates as well as the molecular response is presented in a comprehensive overview.



## 2 Experimental section

### 2.1 NCO-sP(EO-*stat*-PO) synthesis

A hydroxyl terminated six arm star shaped prepolymer consisting of an ethylene oxide and propylene oxide backbone (ratio 80:20) and a molecular weight of 12 kDa was transferred into an isocyanate terminated prepolymer with isophorone diisocyanate. The detailed synthesis is described by Götz *et al.* [17].

### 2.2 Electrospinning

Unless otherwise stated the electrospinning was performed with a solution of 6 w/v% NCO-sP(EO-*stat*-PO) and 28 w/v% PLGA RG 504 in a mixture of acetone, DMSO and acidic water. acetone and DMSO was mixed with Trifluoroacetic acid that was diluted in water at 20  $\mu$ L/mL resulting in a (v/v/v) relation of 90/10/2. The solution was spun at a feed rate of 0.5 mL/h through a flat-tip stainless steel spinneret ( $\varnothing = 0.4 \cdot 25$  mm) connected to a high-voltage power supply. An Eltex KNH34 (Germany) high voltage generator was utilised to charge the solutions at 13 kV while the collector remained grounded. The fibres were collected on various targets in a distance of 160 mm.

### 2.3 Scanning electron microscopy and optical microscopy

To investigate their morphology, the fibres were characterised by scanning electron microscopy (SEM) and optical microscopy. For high-resolution images, the electrospun fibres were deposited onto aluminium foil. Unless otherwise stated, all samples were imaged with a FEI Quanta 200 Environmental SEM (Hillsboro, Oregon, USA) using an accelerating voltage of 10 KV and a working distance of 10-15 mm. All samples for optical microscopy were collected on sP(EO-*stat*-PO) coated glass coverslips. In order to observe the presence of the fluorescent dyes on the fibre surface, images were taken with an exposure time of 5000 ms using an appropriate fluorescence filter. Green fluorescence was observed with an F41-26 filter provided by AHF Analysentechnik (Germany), whereas red fluorescence was documented by filterset 31 of Zeiss (Germany).

## 2.4 Surface preparation

Glass cover slips with a diameter of 15 mm were activated using UV/O<sub>3</sub>-treatment and silanised immediately. The cover slips were placed into a mixture of 60 mL dry toluene and 0.2 mL N-[3-(trimethoxysilyl)-propyl]-ethylene diamine for 2 h, followed by washing with dry toluene and storage in dry toluene. The silanised cover slips were dried in a N<sub>2</sub>-stream and immediately used for spin coating with a solution of 1 wt% NCO-sP(EO-*stat*-PO) in water and tetrahydrofuran (THF) 90/10 (v/v). NCO-sP(EO-*stat*-PO) coated glass cover slips were fixed on a conducting surface and used as targets for electrospinning as described earlier in detail by Grafahrend *et al.* [18].

## 2.5 Contact angle measurement

The contact angle at an interface is determined by the equilibration of the present interface clamping. There is a proportional relation between the contact angle and the hydrophobicity of a material. The sessile drop method was performed to determine the contact angle. Droplets of water (2 mL) were deposited on the surfaces and the contour of the droplets was captured by a digital camera. Contact angles were calculated from three independent experiments.

## 2.6 Calculation of fibre density on substrates

Besides parameters such as molecular composition and functionality, the reactivity of electrospun fibres as well as their influence on cells is determined by the amount of reactive groups and hence also depends on the amount of fibres. Quantitative results from Enzyme Linked Immunosorbent Assays (ELISA), fluorescence measurements and degradation are only comparable with the corresponding fibre surface or mass.

A statistical model was developed that approximates parameters of 3D – non woven meshes with stacked 2D fibre layers where the diameter of one fibre corresponds to the thickness of one layer. This model refers to the relation between void space and fibres in an electrospun network but can also be used to gain information about the number and length of fibres on substrates. The void space between fibres was easily determined for substrates with few fibres by processing survey micrographs with the image processing software Gimp 2.2 (<http://www.gimp.org/>).

Grayscale SEM pictures were transformed to black/white images via setting the threshold appropriately for each micrograph so that fibres are white but the background is black. The numbers of black and white pixels, corresponding to background (black) and fibres (white), was counted with the histogram function and applied to the model of Eichhorn *et al.* [19].

The focus was on two of five main parameters that influence fibrous networks. First, there is the mean porosity  $\epsilon$  taken from non-woven meshes and second, the mean coverage  $\bar{c}$  which is defined as the expected numbers of fibres covering a point in the plane of the network. In contrast to  $\epsilon$ ,  $\bar{c}$  varies with mesh thickness, thus can be used as a characterising parameter for the substrates investigated in this work. As  $\bar{c}$  is a mean value, the probability that a point is covered with a discrete coverage  $c$  is given by following the Poisson probability  $P(c)$ :

$$P(c) = \frac{\bar{c}^c e^{-\bar{c}}}{c!} \quad \text{for } c = 0, 1, 2, 3, \dots$$

With the provided area percentage  $p$  that is covered by a discrete amount of fibres,  $\bar{c}$  can be calculated. The easiest possibility is to determine the area not covered by fibres i.e.  $c = 0$ . Hence the Poisson probability can be simplified and reorganised to:

$$\bar{c} = -\ln(p)$$

With  $\bar{c}$  calculated, we can determine any probability for  $c \geq 1$  and thus can state the area covered by fibres.

## 2.7 Cell extraction, cultivation and analysis

The protocols for the detailed handling and analysis of primary human monocytes and macrophages can be found in "Inducing healing-like human primary macrophage phenotypes by 3D hydrogel coated nanofibres." (Reference [20]). So the results of these investigations will only be presented in a summarised version in this chapter.

### 3 Results and discussion

The technology of NCO-sP(EO-*stat*-PO) based hydrogels has been extensively investigated on 2D surfaces [21] and a transfer to 3D fibrous structures was described in the previous chapters. As these 2D and 3D structures feature the same surface chemistry, systematic studies comparing the cellular adhesion, morphology and inflammatory reaction were performed to provide information on the cellular response due to the topographic differences.

#### 3.1 Contact angle determination

The hydrophilic or hydrophobic nature of the 2D and 3D substrates was analysed by contact angle measurements (CA). Flat surfaces of NCO-sP(EO-*stat*-PO) exhibited CAs of 40° while PLGA surfaces were significantly more hydrophobic with CAs of 70°. The fibrous morphology intensified the trends of hydrophilic (NCO-sP(EO-*stat*-PO)) and hydrophobic (PLGA) substrates. While the CA of PLGA fibres increased to 120°, the hydrogel fibres soaked up any water droplet on contact with the mesh within seconds as already presented in chapter 3.

#### 3.2 Cellular response to material morphology

The monocyte attachment was initially inhibited on sP(EO-*stat*-PO) surfaces. Therefore, predominantly clusters of more than 100 cells formed that migrated across the surface. After three days the clusters resolved into smaller clusters and single cells. The migratory activity of single macrophages was elevated, compared to control substrates of TCPS and PLGA surfaces where no clusters formed and the cells showed a circular migratory pattern.

Less cell cluster formation was observed on the fibrous scaffolds with increasing fibre density. At the highest fibre density investigated no cluster formation and no migratory activity was observed. Concerning these findings, no differences between PLGA fibres and sP(EO-*stat*-PO)/PLGA fibres were detected, indicating a morphology driven effect on the cells. The delayed adherence of monocytes to sP(EO-*stat*-PO) surfaces is in accordance with the findings of chapter 5 where fibroblasts could not attach on hydrogel surfaces or fibres.

While the cluster formation of monocytes is known *in vivo* where they form cell agglomerates with T-cells, this is a new observation on a hydrogel *in vitro* [22]. It may be

explained as a survival strategy on this non adhesive material while the cells seek possibilities to adhere.

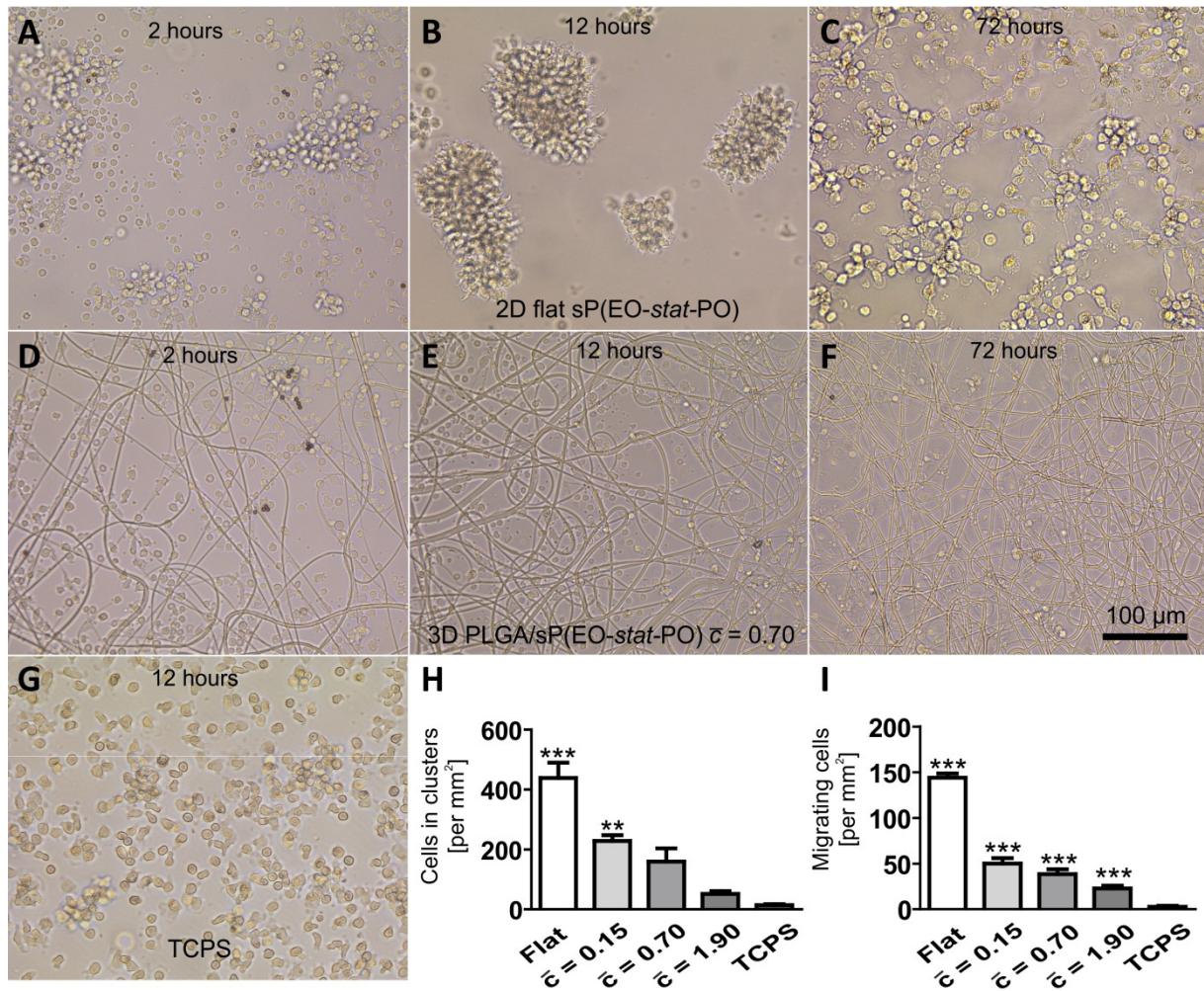


**Figure 2:** Monocyte morphology and migratory activity on protein repellent surfaces. On 2D surfaces consisting of sP(EO-*stat*-PO), monocytes form clusters after 2 h (A) and 12 h (B) that start to resolve after 3 days (C). On sP(EO-*stat*-PO)/PLGA fibres (D-F) the observed cell clusters were smaller and the cells migrated less. On TCPS the monocytes were well dispersed and adhered to the surface. Significant differences related to TCPS control \*P < 0.05, \*\*P < 0.005, \*\*\*P < 0.001 (one way ANOVA). Data represent mean values (n = 8). Figure was reprinted from reference [20] with permission from Elsevier.

*In vitro* monocytes transform into macrophages after three days of cell culture. Accordingly, the substrates were cultured for 7 days to monitor the macrophage behaviour on the different 2D and 3D morphologies. Dense cell layers of mature macrophages were found on flat surfaces with a low migratory activity as on all investigated substrates. But in contrast to fibrous substrates the macrophages exhibited a flattened morphology on 2D surfaces, covering large areas. Fibres instead, caused a cellular alignment especially on fibres with low

and medium density ( $\bar{c} = 0.15$  and  $0.7$ ) while dense 3D networks induce a fusion of cells with fibres ( $\bar{c} = 1.9$ ).

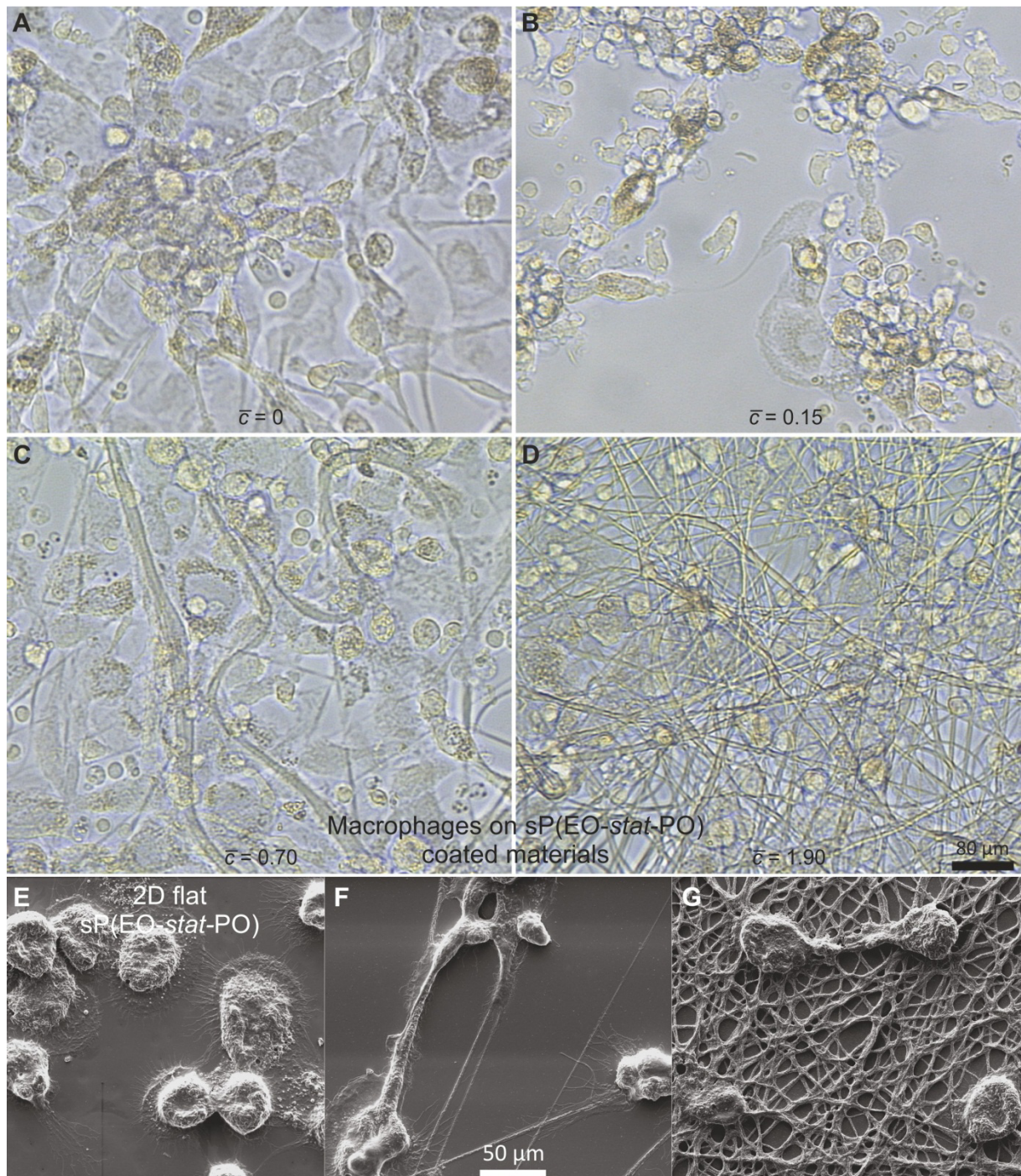


**Figure 3:** The macrophage morphology changed with the substrate roughness. Flattened, spread macrophages appear on 2D surfaces (A, E) while on surfaces with fibres the macrophages adhere to the fibrous structures (B-D, F+G). A-D are optical micrographs, E-G are images of scanning electron microscopy. Figure was reprinted from reference [20] with permission from Elsevier.

### 3.3 Nanofibre degradation

As a leukocyte, the innate task of macrophages comprises degradation of foreign body material. Hence, the degradation of PLGA and NCO-sP(EO-stat-PO)/PLGA in cell culture medium was compared with the degradation in the presence of macrophages (Figure 4). It was found that macrophages rapidly degraded PLGA fibres within a few days while sP(EO-stat-PO) containing fibres degraded much slower. In control samples without macrophages, the degradation proceeded by a hydrolytic mechanism and also exhibited a much slower kinetic. Similar results on hydrolytic fibre degradation were found in chapter 3 with complete fibre degradation after 4 months. Thus, it can be concluded, that the hydrolytic degradation of PLGA and sP(EO-stat-PO)/PLGA fibres plays only a minor role in the presence of macrophages.

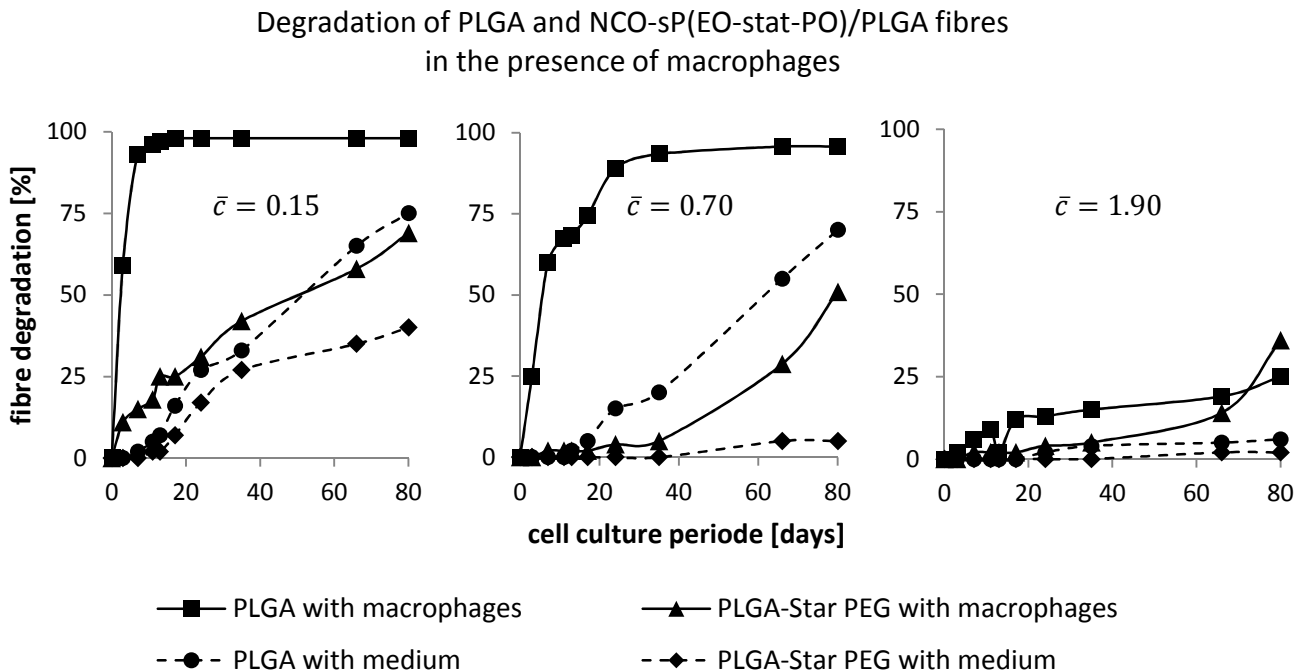


**Figure 4:** Degradation pattern of PLGA and NCO-sP(EO-stat-PO)/PLGA fibres in cell culture medium with and without macrophages. Figure was modified from reference [20] with permission from Elsevier.

### 3.4 Cell surface markers and signalling – Results at a glance

A detailed presentation of the results on cell surface markers and cytokine release as well as their discussion can be found in "Inducing healing-like human primary macrophage phenotypes by 3D hydrogel coated nanofibres." (Reference [20]). However, an overview of these results will be given in the following paragraph.

The macrophage populations on 2D surfaces expressed an anti-inflammatory phenotype, however released pro-inflammatory cytokines. Interestingly, the opposite pattern was found on 3D fibrous meshes where pro-inflammatory surface markers were detected: although the chemokine release indicated a healing phenotype with pro-angiogenic properties. Some markers seemed to require an ideal porosity or roughness of 3D scaffolds to release the maximal pro-angiogenic molecules [23]. The expression of the chemokines IL8 [24] and CXCL9 [25] continually increased from 2D surfaces to 3D substrates. They have been associated with the vascular endothelial growth factor (VEGF) and thus are linked to angiogenesis. This indicates that the provided scaffold morphology is of particular relevance in the design of scaffolds for tissue engineering.

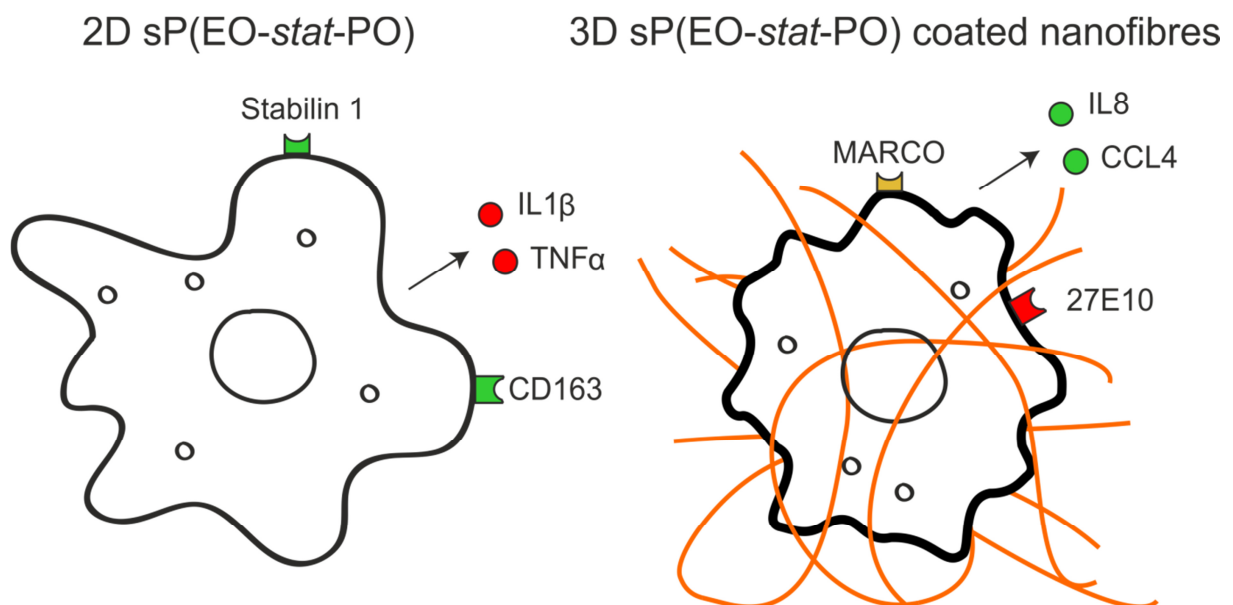


**Figure 5:** Sketch of the most important surface markers expressed and cytokines released of macrophages on 2D and 3D structures. Figure modified from reference [20] with permission from Elsevier.

These *in vitro* findings may also be relevant for *in vivo* situations, because monocytes and macrophages previously showed similar behaviour *in vitro* and *in vivo* [26]. Hence, the correlation between substrate geometry and angiogenesis is expected to be valid *in vivo* as well and has to be considered for future biomaterial and implant designs. Furthermore, the macrophage classification of macrophages through surface marker expression may be insufficient or misleading for the inflammatory response to biomaterials. While scavenger receptors generally have a broad variety of biological activities [10, 27], the cytokine release can act on other cells [28] and even tissues [29], influencing the inflammatory or angiogenic response significantly.



## 4 Conclusion

This study revealed that primary human monocytes and macrophages respond differently to substrates with the same surface chemistry but different morphology. Furthermore, the cytokine release is contrary to the surface marker expression when it comes to the classification of macrophages into pro-inflammatory and pro-angiogenic phenotypes. To examine the inflammatory response to a biomaterial, the cytokine release should be considered as a criterion rather than the surface marker expression. Moreover, this study showed an accelerated degradation on pure PLGA fibres compared to a solely hydrolytic process in contrast to sP(EO-*stat*-PO) containing fibres that were not subject to a similarly fast degradation.

## 5 References

- [1] Li J., Tao R., Wu W., Cao H., Xin J., Guo J., Jiang L., Gao C., Demetriou A. A., Farkas D. L. and Li L., '3d Plga Scaffolds Improve Differentiation and Function of Bone Marrow Mesenchymal Stem Cell-Derived Hepatocytes', *Stem Cells and Development*, 19, **2010**, 1427-1436.
- [2] Finnin M., Hamilton J. A. and Moss S. T., 'Characterisation of a Csf-Induced Proliferating Subpopulation of Human Peripheral Blood Monocytes by Surface Marker Expression and Cytokine Production', *Journal of Leukocyte Biology*, 66, **1999**, 953-960.
- [3] Janeway C. A., Travers P., Walport M. and Shlomchik M. J., *Immunobiology*. 5th Edition edn (New York: Garland Science, 2001).
- [4] Zwadlo G., Schlegel R. and Sorg C., 'A Monoclonal Antibody to a Subset of Human Monocytes Found Only in the Peripheral Blood and Inflammatory Tissues', *The Journal of Immunology*, 137, **1986**, 512-518.
- [5] Katsuda S. and Kaji T., 'Atherosclerosis and Extracellular Matrix', *Journal of atherosclerosis and thrombosis*, 10, **2003**, 267-274.
- [6] Martinez F. O., Sica A., Mantovani A. and Locati M., 'Macrophage Activation and Polarisation', *Frontiers in bioscience : a journal and virtual library*, 13, **2008**, 453-461.
- [7] van Apeldoorn A. A., van Manen H.-J., Bezemer J. M., de Bruijn J. D., van Blitterswijk C. A. and Otto C., 'Raman Imaging of Plga Microsphere Degradation inside Macrophages', *Journal of the American Chemical Society*, 126, **2004**, 13226-13227.
- [8] Gratchev A., Kzhyshkowska J., Utikal J. and Goerdts S., 'Interleukin-4 and Dexamethasone Counterregulate Extracellular Matrix Remodelling and Phagocytosis in Type-2 Macrophages', *Scandinavian Journal of Immunology*, 61, **2005**, 10-17.
- [9] Badylak S. F., Valentin J. E., Ravindra A. K., McCabe G. P. and Stewart-Akers A. M., 'Macrophage Phenotype as a Determinant of Biologic Scaffold Remodeling', *Tissue Engineering Part A*, 14, **2008**, 1835-1842.
- [10] Kzhyshkowska J., Gratchev A. and Goerdts S., 'Stabilin-1, a Homeostatic Scavenger Receptor with Multiple Functions', *Journal of Cellular and Molecular Medicine*, 10, **2006**, 635-649.
- [11] Palecanda A., Paulauskis J., Al-Mutairi E., Imrich A., Qin G., Suzuki H., Kodama T., Tryggvason K., Koziel H. and Kobzik L., 'Role of the Scavenger Receptor Marco in Alveolar Macrophage Binding of Unopsonised Environmental Particles', *The Journal of Experimental Medicine*, 189, **1999**, 1497-1506.
- [12] Arredouani M. S., Franco F., Imrich A., Fedulov A., Lu X., Perkins D., Soininen R., Tryggvason K., Shapiro S. D. and Kobzik L., 'Scavenger Receptors Sr-Ai/li and Marco Limit Pulmonary Dendritic Cell Migration and Allergic Airway Inflammation', *The Journal of Immunology*, 178, **2007**, 5912-5920.
- [13] Pettersen J. S., Fuentes-Duculan J., Suarez-Farinas M., Pierson K. C., Pitts-Kiefer A., Fan L., Belkin D. A., Wang C. Q. F., Bhuvanendran S., Johnson-Huang L. M., Bluth M. J., Krueger J. G., Lowes M. A. and Carucci J. A., 'Tumor-Associated Macrophages in the Cutaneous Scc Microenvironment Are Heterogeneously Activated', *J Invest Dermatol*, 131, **2011**, 1322-1330.
- [14] Brodbeck W. G., Voskerician G., Ziats N. P., Nakayama Y., Matsuda T. and Anderson J. M., 'In Vivo Leukocyte Cytokine Mrna Responses to Biomaterials Are Dependent on Surface Chemistry', *Journal of Biomedical Materials Research Part A*, 64A, **2003**, 320-329.
- [15] Bartneck M., Schulte V. A., Paul N. E., Diez M., Lensen M. C. and Zwadlo-Klarwasser G., 'Induction of Specific Macrophage Subtypes by Defined Micro-Patterned Structures', *Acta Biomaterialia*, 6, **2010**, 3864-3872.
- [16] Paul N. E., Skazik C., Harwardt M., Bartneck M., Denecke B., Klee D., Salber J. and Zwadlo-Klarwasser G., 'Topographical Control of Human Macrophages by a Regularly Microstructured Polyvinylidene Fluoride Surface', *Biomaterials*, 29, **2008**, 4056-4064.
- [17] Götz H., Beginn U., Bartelink C. F., Grünbauer H. J. M. and Möller M., 'Preparation of Isophorone Diisocyanate Terminated Star Polyethers', *Macromolecular Materials and Engineering*, 287, **2002**, 223-230.
- [18] Grafahrend D., Calvet J. L., Klinkhammer K., Salber J., Dalton P. D., Möller M. and Klee D., 'Control of Protein Adsorption on Functionalised Electrospun Fibers', *Biotechnology and Bioengineering*, 101, **2008**, 609-621.
- [19] Eichhorn S. J. and Sampson W. W., 'Statistical Geometry of Pores and Statistics of Porous Nanofibrous Assemblies', *Journal of the Royal Society Interface*, 2, **2005**, 309-318.

- [20] Bartneck M., Heffels K.-H., Pan Y., Bovi M., Zwadlo-Klarwasser G. and Groll J., 'Inducing Healing-Like Human Primary Macrophage Phenotypes by 3d Hydrogel Coated Nanofibres', *Biomaterials*, 33, **2012**, 4136-4146.
- [21] Groll J., Fiedler J., Engelhard E., Ameringer T., Tugulu S., Klok H. A., Brenner R. E. and Moeller M., 'A Novel Star Peg-Derived Surface Coating for Specific Cell Adhesion', *Journal of Biomedical Materials Research Part A*, 74A, **2005**, 607-617.
- [22] Green D. M., Trial J. and Birdsall H. H., 'Tnf- $\alpha$  Released by Comigrating Monocytes Promotes Transendothelial Migration of Activated Lymphocytes', *The Journal of Immunology*, 161, **1998**, 2481-2489.
- [23] Rosenkilde M. M. and Schwartz T. W., 'The Chemokine System – a Major Regulator of Angiogenesis in Health and Disease', *APMIS*, 112, **2004**, 481-495.
- [24] Martin D., Galisteo R. and Gutkind J. S., 'Cxcl8/Il8 Stimulates Vascular Endothelial Growth Factor (Vegf) Expression and the Autocrine Activation of Vegfr2 in Endothelial Cells by Activating Nfkb through the Cbm (Carma3/Bcl10/Malt1) Complex', *Journal of Biological Chemistry*, 284, **2009**, 6038-6042.
- [25] Sahin H., Borkham-Kamphorst E., Kuppe C., Zaldivar M. M., Grouls C., Al-samman M., Nellen A., Schmitz P., Heinrichs D., Berres M.-L., Doleschel D., Scholten D., Weiskirchen R., Moeller M. J., Kiessling F., Trautwein C. and Wasmuth H. E., 'Chemokine Cxcl9 Attenuates Liver Fibrosis-Associated Angiogenesis in Mice', *Hepatology*, 55, **2012**, 1610-1619.
- [26] Schwarzer E., De Matteis F., Giribaldi G., Ulliers D., Valente E. and Arese P., 'Hemozoin Stability and Dormant Induction of Heme Oxygenase in Hemozoin-Fed Human Monocytes', *Molecular and Biochemical Parasitology*, 100, **1999**, 61-72.
- [27] Onofre G., Kolackova M., Jankovicova K. and Krejsek J., 'Scavenger Receptor Cd163 and Its Biological Functions', *Acta medica (Hradec Kralove) / Universitas Carolina, Facultas Medica Hradec Kralove*, 52, **2009**, 57-61.
- [28] Zimmermann H. W., Seidler S., Nattermann J., Gassler N., Hellerbrand C., Zerneck A., Tischendorf J. J. W., Luedde T., Weiskirchen R., Trautwein C. and Tacke F., 'Functional Contribution of Elevated Circulating and Hepatic Non-Classical Cd14<sup>+</sup>Cd16<sup>+</sup> Monocytes to Inflammation and Human Liver Fibrosis', *PLoS ONE*, 5, **2010**, e11049.
- [29] Mullarky I. K., Szaba F. M., Berggren K. N., Kummer L. W., Wilhelm L. B., Parent M. A., Johnson L. L. and Smiley S. T., 'Tumor Necrosis Factor Alpha and Gamma Interferon, but Not Hemorrhage or Pathogen Burden, Dictate Levels of Protective Fibrin Deposition During Infection', *Infection and Immunity*, 74, **2006**, 1181-1188.



## CHAPTER 8

---

### ***In vivo* Biocompatibility of NCO-sP(EO-stat-PO)/PLGA/Prolene®- meshes for the treatment of diaphragmatic hernias**

Until now in this dissertation the properties and functionality of the electrospun fibres have been examined *in vitro*. These biocompatible meshes are promising to be used *in vivo* for tissue engineering research. This chapter involves a treatment application to support the remodelling of diaphragm tissue. The medical condition of diaphragmatic hernia was studied in a rabbit model comparing the performance of a polypropylene microfibre mesh (Prolene®, Ethicon, Norderstedt, Germany) and a Prolene® mesh decorated with electrospun fibres. The mechanical properties were analysed regarding the required airtightness of the constructs for the surgery. Furthermore, the biocompatibility of the unmodified electrospun meshes proved to be in the range of the Prolene® control meshes. First investigations on drug delivery opportunities were conducted to design an improved fibrous scaffold.

---

This chapter represents a cooperative project with Gabriele Böhm and Jochen Salber.

Parts of this chapter have been published:

Böhm G., Ushakova Y., Alizai H. P., Braunschweig T., Lente C., Heffels K. H., Groll J., Neumann U. P. and Junge K., 'Biocompatibility of PLGA/sP(EO-stat-PO)-Coated Mesh Surfaces under Constant Shearing Stress', *European Surgical Research*, 47, **2011**, 118-129.

## 1 Introduction

The inherent structure of electrospun meshes, with thin fibres and high porosity makes them suitable for tissue engineering (TE) applications [1]. Their structure resembles the native fibrous environment of cells, the extracellular matrix, especially of connective tissue. *In vivo* studies conducted into diabetic ulcer treatment [2], bone regeneration [3] and vascular reconstruction [4] where electrospun fibres played a crucial role in the treatment concept as a supporting scaffold. Additionally, such scaffolds act as a carrier for growth factors and drugs.

A hernia is a medical condition where organs of the abdominal cavity protrude through the wall of this cavity. The standard treatment comprises straight-forward suturing of these hernias or, in the case of large ruptures, additional foils or meshes are applied to seal the abdominal wall. The diaphragmatic hernia is one of several kinds of hernias that are generally acquired prenatal.

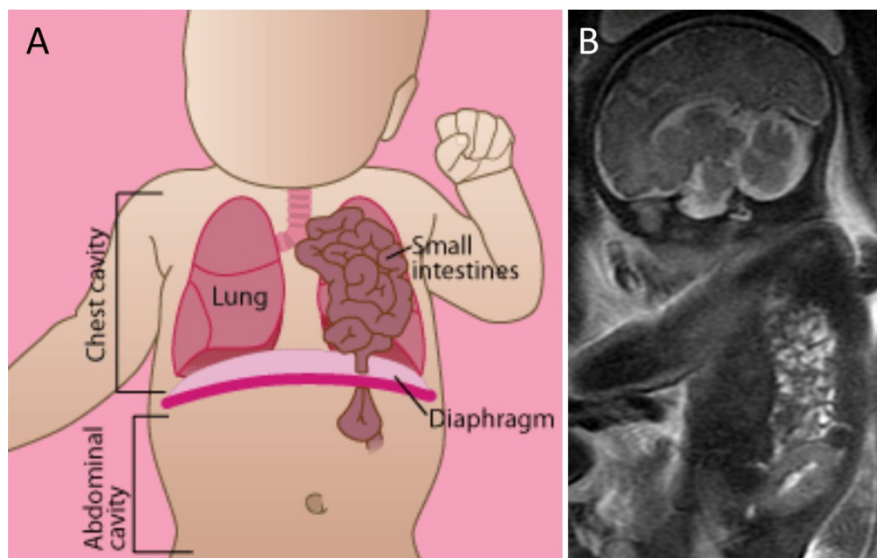


**Figure 1:** A) Sketch of a diaphragmatic hernia. The small intestine moved into the chest cavity through a hernia of the diaphragm. Image taken from: <http://www.codysfoundation.com/CDHinfo/index.htm>. B) Magnetic resonance image of a new-born with a diaphragmatic hernia. Bright contrast represents the small intestine in the chest cavity. Image taken from: <http://www.childrenshospital.org/gallery/Gallery45/02Fetal-MRI-diaphragmatic-her.jpg>.

This condition is associated with a high mortality of new-borns if left untreated [5-7], but due to the improved perioperative care the mortality rate was reduced to less than 50 % [8]. While small hernias can be sutured, for large defects prosthetic patches are required to reconstruct the dome of the diaphragm [9]. Such patches need to be easily insertable,

biocompatible and promote tissue ingrowth. But even today, the recurrence rate is still above 50 % in the first 3 years after the initial treatment [10, 11].

The “gold-standard” are foils of expanded poly(tetrafluor ethylene) (e-PTFE) that are strong and seal the defect well. On the other hand these are not elastic enough to adapt their shape completely to the movement of the diaphragm. Furthermore, the foils are poorly integrated into the growing tissue. Meshes made from biological sources such as Surgisis® (porcine small intestinal submucosa) feature better tissue ingrowth but do not influence the recurrence rate [9]. The ideal implant should tackle these issues and feature improved biocompatibility, flexibility, tissue integration, improved wound healing and reduced scar formation.

This chapter involves the development of an improved implant to be used as a diaphragmatic patch. The key technology is a fibrous mesh of NCO-sP(EO-*stat*-PO) and PLGA produced by electrospinning that has already been presented in the previous chapters. Their biocompatibility plus the possibility of versatile modifications to address cells specifically suggests proper tissue integration. In a first step the electrospun fibres will be combined with a Prolene® mesh made of polypropylene (PP) while the long term aim is the generation of a fully resorbable mesh [12, 13]. Here, the focus will be on the scaffold production and the hypothesis that the presented scaffolds are at least equally biocompatible as unmodified meshes.

## 2 Experimental section

### 2.1 NCO-sP(EO-*stat*-PO) synthesis

A hydroxyl terminated six arm star shaped prepolymer consisting of an ethylene oxide and propylene oxide backbone (ratio 80:20) and a molecular weight of 12 kDa was transferred into an isocyanate terminated prepolymer with isophorone diisocyanate. The detailed synthesis is described by Götz *et al.* [14].

### 2.2 Plasma activation

Prolene® meshes provided by Ethicon (Norderstedt, Germany) were cut into 25 · 10 cm pieces to fit on aluminium drums to collect the electrospun fibres. The microfibre meshes were treated with ammoniac plasma (400 mbar NH<sub>3</sub>, 400 W, 120 s) on each side prior to any coating and electrospinning experiments.

### 2.3 Electrospinning

Unless otherwise stated the electrospinning was performed with a solution of 6 w/v% NCO-sP(EO-*stat*-PO) and 28 w/v% PLGA RG 504 in a mixture of acetone, DMSO and acidic water. Acetone and DMSO was mixed with Trifluoroacetic acid that was diluted in water at 20 µL/mL resulting in a (v/v/v) relation of 90/10/2. The solution was spun at a feed rate of 0.5 mL/h through a flat-tip stainless steel spinneret ( $\varnothing = 0.4 \cdot 25$  mm) connected to a high-voltage power supply. An Eltex KNH34 (Germany) high voltage generator was utilised to charge the solutions at 13 kV while the collector remained grounded. The fibres were collected on various targets in a distance of 160 mm.

### 2.4 Coating of composite meshes

Finally, the scaffolds were placed in an aqueous bath of 1 % NCO-sP(EO-*stat*-PO) to apply an airtight seal of hydrogel on the constructs. While the scaffolds of Series A were left in the gelling solution, resulting in a dense hydrogel layer, the meshes of Series B were dipped in an aqueous bath of 1 % NCO-sP(EO-*stat*-PO) but were taken out of the coating solution after one minute. Excessive coating solution was removed from the construct to achieve a thin coating around the fibres. A scheme of the production process is presented in Figure 2.



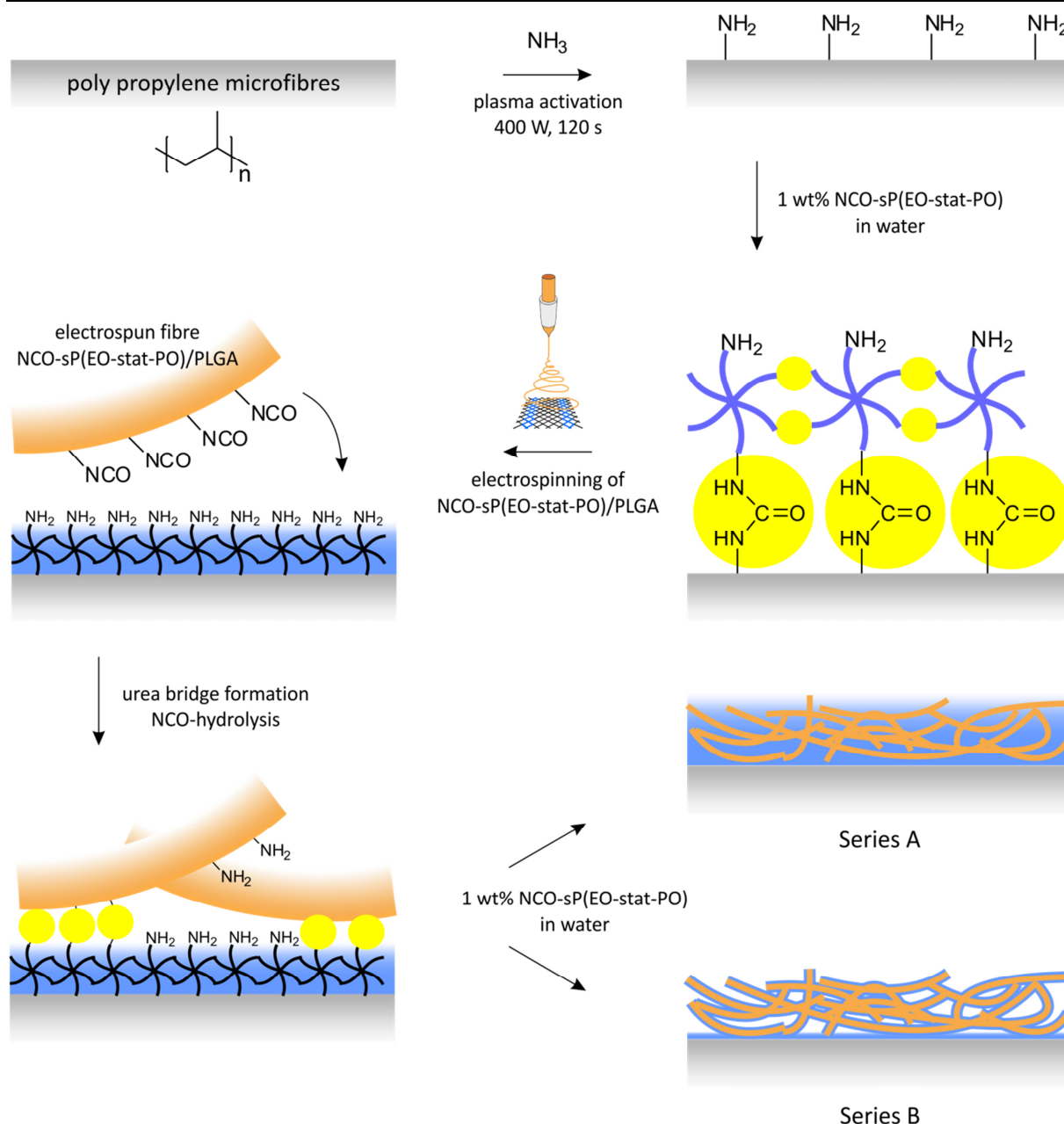


**Figure 2:** Scheme of the composite scaffold production for the treatment of diaphragmatic hernia. Polypropylene meshes serve as basis microfibre meshes that were first modified in an ammoniac plasma to be coated with a thin hydrogel layer of NCO-sP(EO-*stat*-PO). Followed by electrospinning NCO-sP(EO-*stat*-PO)/PLGA fibres on the microfibrils and a second coating with NCO-sP(EO-*stat*-PO) an airtight construct results. Meshes of Series A were kept in the final gelling solution until a gel formed while meshes of Series B were simply dipped into the gelling solution.

## 2.5 Scanning electron microscopy

The fibres were characterised by scanning electron microscopy. For high-resolution images, the electrospun fibres were deposited onto aluminium foil. all samples were imaged with an

S-4800 Ultra High Resolution Scanning Electron Microscope (Hitachi) using an accelerating voltage of 10 kV and a working distance of 10-15 mm.

## 2.6 Air-permeability test

The perfusion of air through electrospun meshes was investigated with a custom made apparatus that is displayed in Figure 3. A constant gas flux was led through a manometer (WIKA, Klingenberg, Germany) and consecutively through a sample chamber with a circular opening that was covered with the non-woven meshes. The maximal pressure that caused the sP(EO-*stat*-PO/PLGA meshes to break was recorded.

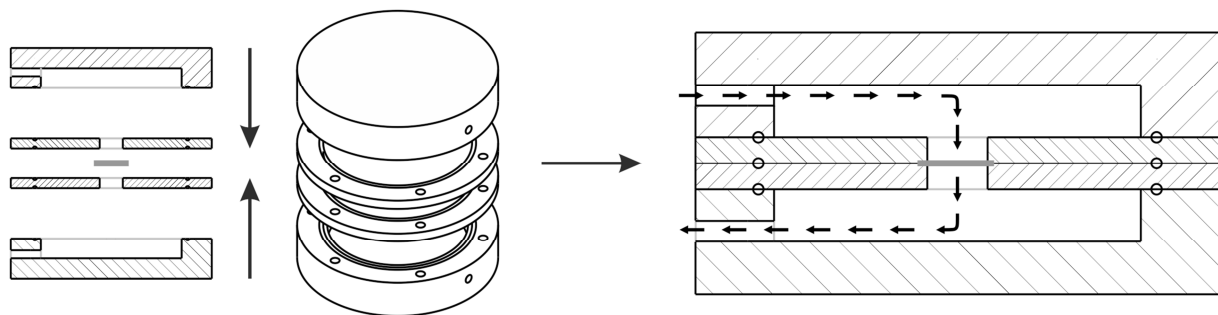


**Figure 3:** Sketch of a custom made apparatus that was used to measure the perfusion of gases through electrospun membranes (displayed in the centre of the apparatus). The membrane was clamped between the inner discs, end cap elements with gas in- and outlets closed the apparatus.

## 2.7 Release of Ilomastat

The matrix metalloproteinase (MMP) inhibitor “Ilomastat” was mixed into the electrospinning solution. The as-spun fibres were cut into pieces of 2 g each and were placed in phosphate buffered saline (PBS) at pH 7.4 and stirred at 37 °C. The release profile of Ilomastat was recorded by measuring its fluorescence at a wavelength of 354 nm with a Varian Cary-Eclipse Fluorescence spectrometer (Darmstadt, Germany) after varying points in time.

## 2.8 Packaging and sterilisation

The composite scaffolds of PP-meshes and electrospun fibres including a hydrogel coating were placed in petri dishes, double wrapped and sealed in Tyvek® Roll with STERRAD® Chemical Indicator. The samples were  $\gamma$ -sterilised at BGS (Beta-Gamma-Service GmbH & Co. KG, Weil am Rhein, Germany) with a dose of 29 kGy.

### 3 Results and discussion

Before porous meshes can replace foils in the treatment of diaphragmatic hernias, airtight sealing has to be guaranteed. The method that is used here relies on the addition of a nanofibre web in combination with a sealing hydrogel. A prerequisite for a stable implant is the covalent attachment of the electrospun fibres on the polypropylene meshes. This was achieved by activating the PP-fibre surface in ammonia plasma, generating amino groups on the microfibre surface. The isocyanates of NCO-sP(EO-*stat*-PO)/PLGA fibres interact with these amino groups, forming urea bridges so that the electrospun fibres are immobilised on the PP-mesh (Figure 2).

#### 3.1 Electrospinning on non-conductive meshes

The technique of electrospinning is based on depositing charged fibres on a conductive collector. This collector is generally designed in a way that charges can be dissipated and do not accumulate, thus metallic targets are commonly used. Direct spinning on non-conductive materials, such as meshes made of PP, resulted in poor fibre deposition as charges accumulated on the PP mesh and consecutively inhibited further fibre deposition due to the repulsion of charges with the same polarity. To circumvent this disadvantage the PP-meshes were fixed on an aluminium plate with a hook-and-loop fastener as depicted in Figure 4A.

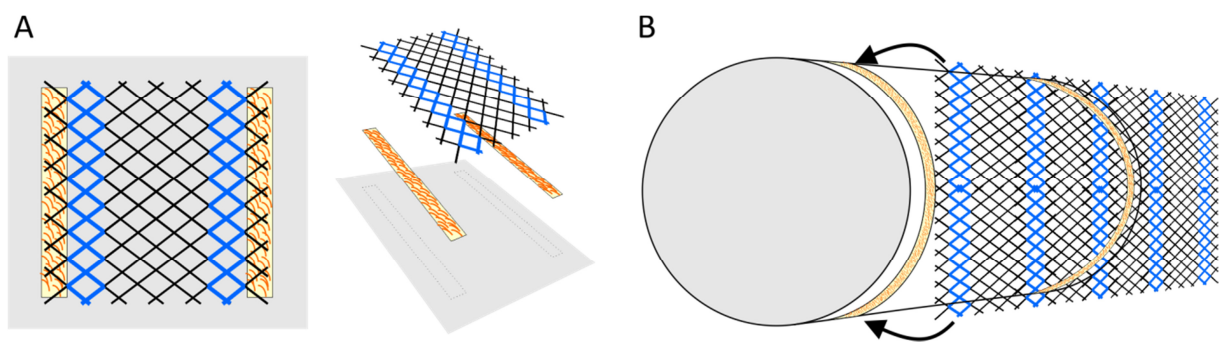


**Figure 4:** Target configurations for spinning onto non-conductive polypropylene meshes. A) In Series A the mesh (3 · 3 cm) was fixed with a hook-and-loop fastener onto an aluminium plate (5 · 5 cm). For Series B an aluminium drum (10 · 25 cm) was used as backing target.

The electric charges were supposed to be dissipated by the conductive backing so that a dense fibrous network could be deposited on the PP mesh. An experiment with sample dimensions of 3 · 3 cm (Series A) revealed that a proper fibre deposition only took place in the centre of the fixed mesh (Figure 5A). The charges were solely transferred to the

electrode where the mesh was in close contact with the backing. On the sites with the hook-and-loop fastener the insulation was too high to allow sufficient charge conduction.

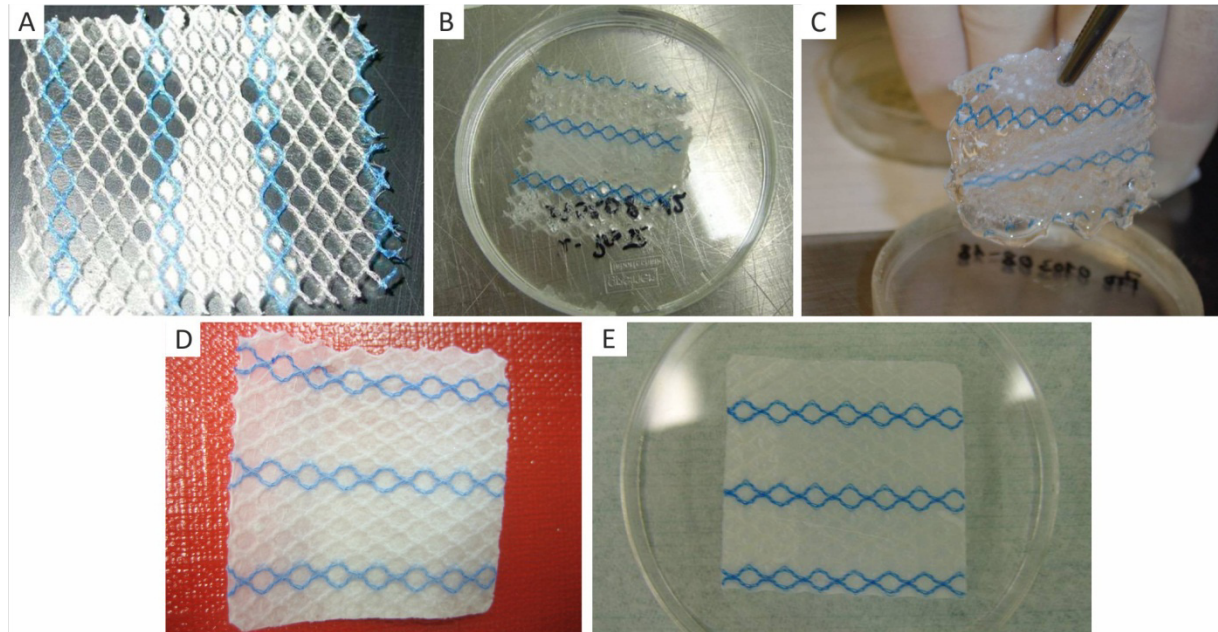


**Figure 5:** Electrospun fibres on a Prolene® mesh. The microfibre mesh was fixed to an aluminium plate as shown in **Figure 4**, the spun fibres were deposited where the mesh was in close contact with the conductive backing. On the sides of the sample the hook-and-loop fastener prevented that the deposited charges were transferred to the electrode. Figure was modified from reference [15] with permission from S. Karger AG, Basel.

To minimise these edge effects, a rotating aluminium drum of 10 cm in width and a circumference of 25 cm was applied as a backing target (Series B, Figure 4B). While using the same fixating method, only the sides of the PP mesh were affected with minor fibre deposition due to insulation effects. The microfibre mesh was decorated with electrospun fibres on both sides of the Prolene® mesh by simply detaching the mesh from the fastener and fixing it again from the other side.

The 10 · 25 cm meshes were cut into pieces of 3 · 3 cm, featuring homogeneous layers of electrospun fibres on both sides of the PP mesh. Figure 5D and Figure 6 display the morphology of these scaffolds. To achieve airtight sealing of the still very porous scaffolds of Series A (Figure 5A), a hydrogel was cast on the electrospun fibres from a solution of 1 wt% NCO-sP(EO-*stat*-PO) in water. The electrospun fibres served as an anchor for the hydrogel, sealing the void between the macropores of the PP mesh. The more homogeneous spinning of Series B allowed less hydrogel to be used for the sealing process. Here, only a thin layer was cast on the nanofibres instead of a scaffold encapsulating gel in Series A.

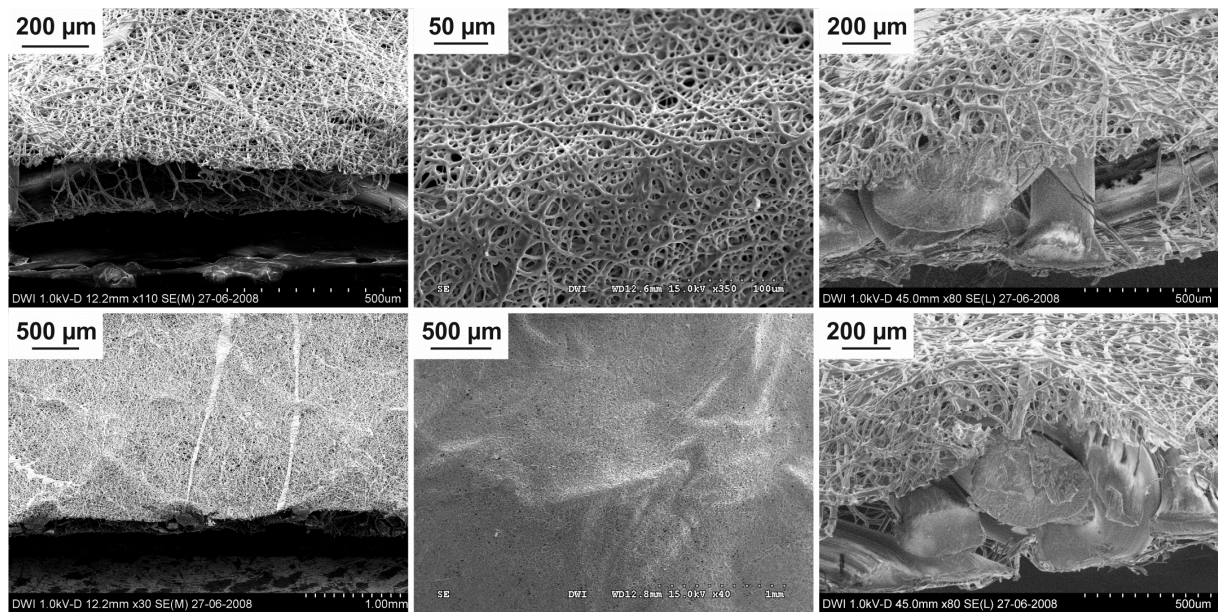


**Figure 6:** SEM-images of composite scaffolds consisting of Prolene®-meshes and electrospun fibres of NCO-sP(EO-*stat*-PO)/PLGA fibres produced by spinning on the rotating drum. Figure was modified from reference [15] with permission from S. Karger AG, Basel.

### 3.2 Airtight sealing of electrospun fibres

The extent to which electrospun fibres can seal hernias hermetically was examined. Therefore, an experimental setup was designed where the applied pressure and air flux through an electrospun mesh could be measured (Figure 3). It was found that dry electrospun membranes of NCO-sP(EO-*stat*-PO)/PLGA permit an air flux accompanied by an increased over-pressure on the membrane. Furthermore, once the non-woven meshes were wetted, the membrane inhibited any air flux. This barrier lasted as long as the increasing pressure on the membrane could be compensated by the strength of the membrane. This effect can be explained by the hydrophilic nature of the electrospun fibres: The water is homogeneously distributed within the fibrous network and surface tension forces retain the water meniscus within the fibres. As no pores or voids remain, the wetted mesh is impenetrable to gases. Figure 7 displays the linear dependence of the force the membrane can withstand to the mesh thickness. A wetted mesh with a thickness of 18 µm is sufficient to resist the maximal diaphragmatic pressure of  $171 \pm 8$  cm H<sub>2</sub>O ( $167.7 \pm 7.8$  mbar) that is exerted by the diaphragm in young adult humans [16]. Hence, the membranes with a thickness of 50 µm that were used in the rabbit model met the strength requirements.

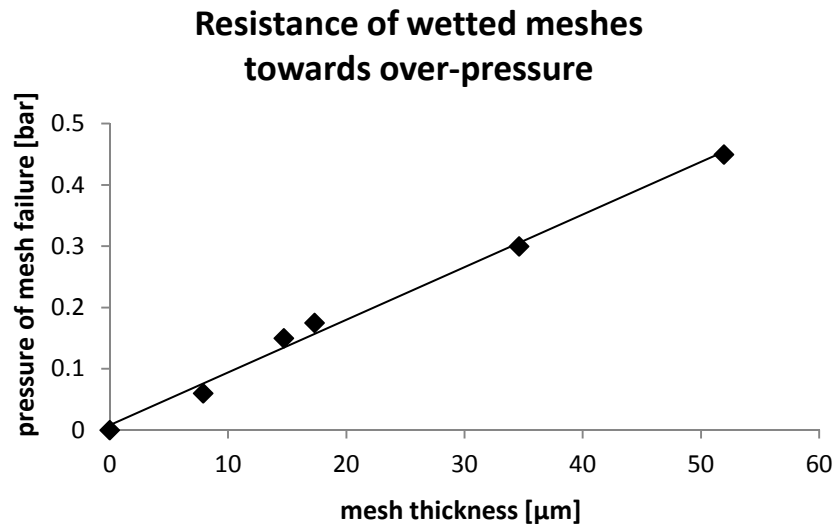


**Figure 7:** The strength of electrospun meshes towards air pressure on a circular surface of 1 cm<sup>2</sup>. The maximal pressure at the point of mesh failure is depicted in relation to the mesh thickness.

### 3.3 Biocompatibility *in vivo*

The *in vivo* biocompatibility experiments have been performed in cooperation with the Department of Surgery of the University Hospital in Aachen with Dr. Gabriele Böhm as the executing surgeon. The results of these experiments will be presented briefly, a detailed description can be found in “Biocompatibility of PLGA/sP(EO-*stat*-PO)-Coated Mesh Surfaces under Constant Shearing Stress” by Böhm *et al.* [15].

The scaffolds were wetted and placed on a circular defect of the diaphragm, which was 1 cm in diameter. With their hydrophilic surface, the meshes easily adopted the shape of the backing diaphragm and were sewed centrally above the defect. After four months *in vivo*, the meshes were explanted and it was revealed that the meshes were incorporated in the newly formed tissue. Interestingly, regarding the samples of Series A, with a dense, encapsulating hydrogel layer, thick granulomas formed between the mesh and diaphragm (Figure 8), whereas in Series B that included only a thin hydrogel layer on the electrospun fibres no granuloma formation was observed in any case.

As granulomas are accumulations of macrophages this indicates that an inflammation accompanied with the attempt of the organism to encapsulate the alien material occurred [17]. Regarding the results from chapter 7 where flat surfaces of sP(EO-*stat*-PO) led to the release of pro-inflammatory cytokines, similar cellular pathways may have occurred *in vivo*. The scaffolds of Series A featured a smooth surface and no fibrous structure. These

observations are comparable to those from chapter 7 where different morphologies induced different cell responses in spite of the same surface chemistry. The analogy can be drawn further as the fibrous material did not induce a massive pro-inflammatory reaction.

The size of the defect shrank significantly to less than 25 % during the *in vivo* placement of the scaffolds of Series B. The histologic examination revealed that the defect was filled with scar tissue which is comprehensible as no peptides were used that induce guided diaphragm muscle tissue regrowth. It is important to mention that the biocompatibility of the modified PP meshes has similar qualities compared to unmodified PP meshes and the inflammatory reaction was low to moderate according to the histologic examination.

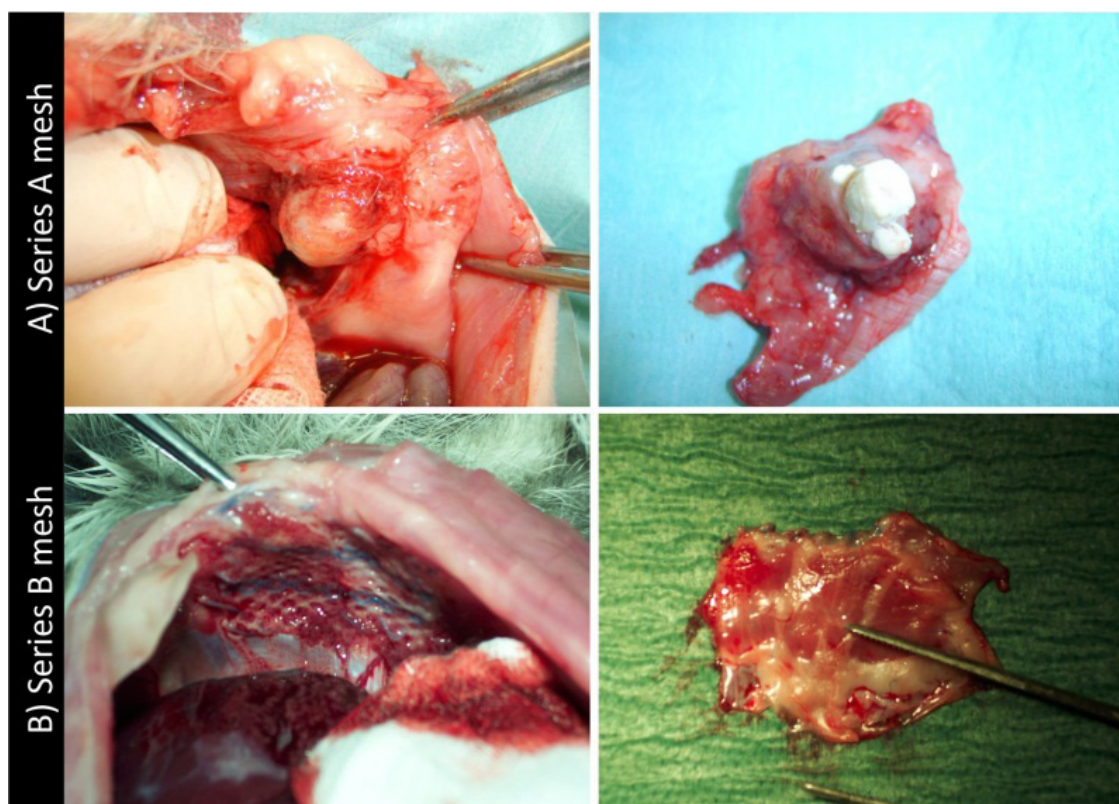


**Figure 8:** Explantation of diaphragm hernia meshes 4 months after implantation. Figure was modified from reference [15] with permission from S. Karger AG, Basel.

### 3.4 Series C: MMP-Inhibitor release

The *in vivo* trial with scaffolds of Series B resulted in defect closure with scar tissue formation. To support tissue regeneration rather than “repair” with scar tissue, a matrix metalloproteinase (MMP) inhibitor was incorporated in the third scaffold generation to minimise the scar tissue formation [18]. Ilomastat (GM6001) was used as a model drug for MMP-inhibitors (Figure 9).

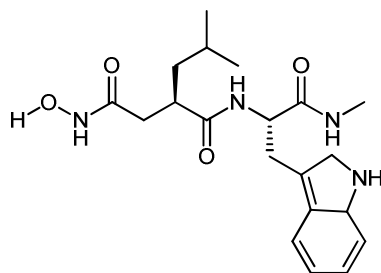


**Figure 9:** Structure of matrix metalloproteinase inhibitor “Ilomastat”.

To examine the release profile of Ilomastat, 2 wt% of the drug was mixed into the spinning solution and spun as the meshes of Series B. Because isocyanate reactive groups are missing, the drug did not bind covalently to NCO-sP(EO-*stat*-PO) molecules and a release from spun fibres is possible.

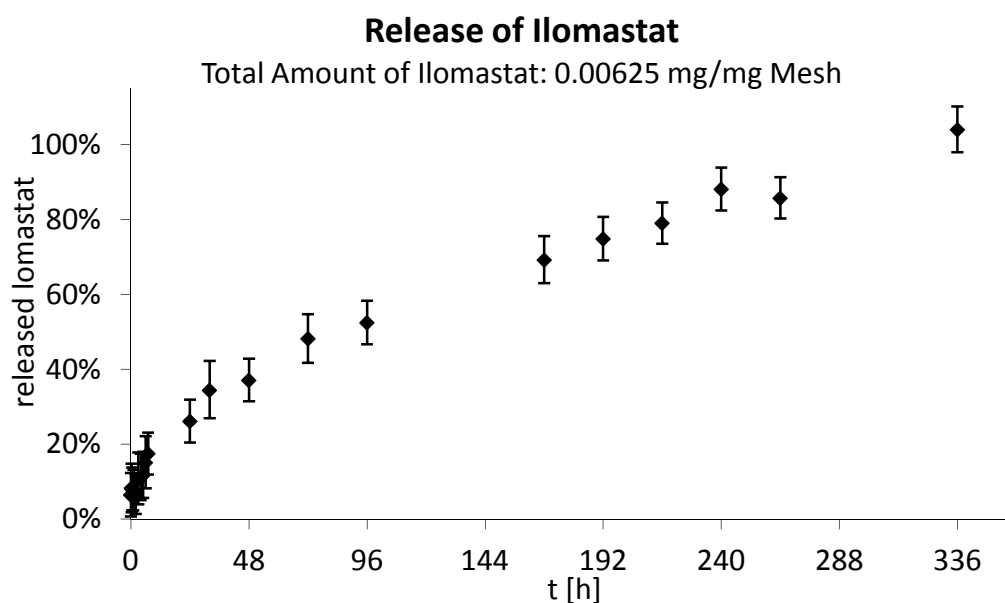


**Figure 10:** Release rate of Ilomastat from electrospun fibres loaded with 6.25  $\mu\text{g}/\text{mg}$  mesh.

The release profile in PBS at 37 °C revealed an initial burst release up to 20 % of the drug loading with a subsequent, almost linear progression for two weeks when the total amount of Ilomastat is found in solution. The MMP-inhibitor should be released from the scaffold within the first two weeks after the surgery to develop its optimal efficiency. As Figure 10 states, the release profile meets the recommendations, thus Ilomastat can be used for this application.

The *in vivo* experiments with meshes including Ilomastat are currently evaluated and will be reported as soon as possible.



## 4 Conclusion

In this chapter the previously presented electrospun meshes consisting of NCO-sP(EO-*stat*-PO) and PLGA were analysed *in vivo* with respect to their biocompatibility. Their performance in rabbits concerning the closure of diaphragm hernias did not show any negative effects in comparison with control meshes made of polypropylene. The prospect to enhance the current treatment is promising as in future studies the fibres can be modified with drugs and peptides to result in guided tissue regeneration with suppressed scar formation.

## 5 References

- [1] Sill T. J. and von Recum H. A., 'Electrospinning: Applications in Drug Delivery and Tissue Engineering', *Biomaterials*, 29, **2008**, 1989-2006.
- [2] Choi J. S., Leong K. W. and Yoo H. S., 'In Vivo Wound Healing of Diabetic Ulcers Using Electrospun Nanofibres Immobilised with Human Epidermal Growth Factor (Egf)', *Biomaterials*, 29, **2008**, 587-596.
- [3] Shin M., Yoshimoto H. and Vacanti J. P., 'In Vivo Bone Tissue Engineering Using Mesenchymal Stem Cells on a Novel Electrospun Nanofibrous Scaffold', *Tissue Engineering*, 10, **2004**, 33-41.
- [4] Tillman B. W., Yazdani S. K., Lee S. J., Geary R. L., Atala A. and Yoo J. J., 'The in Vivo Stability of Electrospun Polycaprolactone-Collagen Scaffolds in Vascular Reconstruction', *Biomaterials*, 30, **2009**, 583-588.
- [5] Clark R. H., Hardin Jr W. D., Hirschl R. B., Jaksic T., Lally K. P., Langham Jr M. R. and Wilson J. M., 'Current Surgical Management of Congenital Diaphragmatic Hernia: A Report from the Congenital Diaphragmatic Hernia Study Group', *Journal of Pediatric Surgery*, 33, **1998**, 1004-1009.
- [6] Skari H., Bjornland K., Frenckner B., Friberg L. G., Heikkinen M., Hurme T., Loe B., Mollerlokken G., Nielsen O. H., Qvist N., Rintala R., Sandgren K., Serlo W., Wagner K., Wester T. and Emblem R., 'Congenital Diaphragmatic Hernia: A Survey of Practice in Scandinavia', *Pediatric Surgery International*, 20, **2004**, 309-313.
- [7] Tsao K. and Lally K. P., 'The Congenital Diaphragmatic Hernia Study Group: A Voluntary International Registry', *Seminars in Pediatric Surgery*, 17, **2008**, 90-97.
- [8] Moyer V., Moya F., Tibboel R., Losty P., Nagaya M. and Lally K. P., 'Late Versus Early Surgical Correction for Congenital Diaphragmatic Hernia in Newborn Infants', *Cochrane database of systematic reviews (Online)*, **2002**, CD001695.
- [9] Grethel E. J., Cortes R. A., Wagner A. J., Clifton M. S., Lee H., Farmer D. L., Harrison M. R., Keller R. L. and Nobuhara K. K., 'Prosthetic Patches for Congenital Diaphragmatic Hernia Repair: Surgisis Vs Gore-Tex', *Journal of Pediatric Surgery*, 41, **2006**, 29-33.
- [10] Lawrence Moss R., Chen C. M. and Harrison M. R., 'Prosthetic Patch Durability in Congenital Diaphragmatic Hernia: A Long-Term Follow-up Study', *Journal of Pediatric Surgery*, 36, **2001**, 152-154.
- [11] Hajer G. F., vd Staak F. H. J. M., de Haan A. F. J. and Festen C., 'Recurrent Congenital Diaphragmatic Hernia; Which Factors Are Involved?', *Eur J Pediatr Surg*, 8, **1998**, 329,333.
- [12] Junge K., Rosch R., Krones C., Klinge U., Mertens P., Lynen P., Schumpelick V. and Klosterhalfen B., 'Influence of Polyglecaprone 25 (Monocryl) Supplementation on the Biocompatibility of a Polypropylene Mesh for Hernia Repair', *Hernia*, 9, **2005**, 212-217.
- [13] Harrell A., Novitsky Y., Cristiano J., Gersin K., Norton H., Kercher K. and Heniford B., 'Prospective Histologic Evaluation of Intra-Abdominal Prosthetics Four Months after Implantation in a Rabbit Model', *Surgical Endoscopy*, 21, **2007**, 1170-1174.
- [14] Götz H., Beginn U., Bartelink C. F., Grünbauer H. J. M. and Möller M., 'Preparation of Isophorone Diisocyanate Terminated Star Polyethers', *Macromolecular Materials and Engineering*, 287, **2002**, 223-230.
- [15] Böhm G., Ushakova Y., Alizai H. P., Braunschweig T., Lente C., Heffels K. H., Groll J., Neumann U. P. and Junge K., 'Biocompatibility of Plga/Sp(Eo-stat-Po)-Coated Mesh Surfaces under Constant Shearing Stress', *European Surgical Research*, 47, **2011**, 118-129.
- [16] Tolep K., Higgins N., Muza S., Criner G. and Kelsen S. G., 'Comparison of Diaphragm Strength between Healthy Adult Elderly and Young Men', *American Journal of Respiratory and Critical Care Medicine*, 152, **1995**, 677-682.
- [17] Mukhopadhyay S., Farver C. F., Vaszar L. T., Dempsey O. J., Popper H. H., Mani H., Capelozzi V. L., Fukuoka J., Kerr K. M., Zeren E. H., Iyer V. K., Tanaka T., Narde I., Nomikos A., Gumurdulu D., Arava S., Zander D. S. and Tazelaar H. D., 'Causes of Pulmonary Granulomas: A Retrospective Study of 500 Cases from Seven Countries', *Journal of Clinical Pathology*, 65, **2012**, 51-57.
- [18] Wong T. T. L., Mead A. L. and Khaw P. T., 'Prolonged Antiscarring Effects of Ilomastat and Mmc after Experimental Glaucoma Filtration Surgery', *Investigative Ophthalmology and Visual Science*, 46, **2005**, 2018-2022.

## Summary

This thesis concerned the design and examination of a scaffold for tissue engineering applications. The template for the presented scaffold came from nature itself: the intercellular space in tissues that provides structure and support to the cells of the respective tissue, known as extracellular matrix (ECM). Fibres are a predominant characteristic feature of ECM, providing adhesion sites for cell-matrix interactions. In this dissertation a fibrous mesh was generated using the electrospinning technique to mimic the fibrous structure of the ECM. Two base polymers were explored: a biodegradable polyester, poly(D,L-lactide-co-glycolide); and a functional PEG-based star polymer, NCO-sP(EO-*stat*-PO). This topic was described in three major parts: the first part was materials based, concerning the chemical design and characterisation of the polymer scaffolds; the focus was then shifted to the cellular response to this fibrous scaffold; and finally the *in vivo* performance of the material was preliminarily assessed.

The first steps towards an electrospun mesh started with adjusting the spinning parameters for the generation of homogeneous fibres. As reported in **Chapter 3** a suitable setup configuration was on the one hand comprised of a spinning solution that consisted of 28.5 w/v% PLGA RG 504 and 6 w/v% NCO-sP(EO-*stat*-PO) in 450  $\mu$ L acetone, 50  $\mu$ L DMSO and 10  $\mu$ L of an aqueous trifluoroacetic acid solution. On the other hand an ideal spinning behaviour was achieved at process parameters such as a flow rate of 0.5 mL/h, spinneret to collector distance of 12-16 cm and a voltage of 13 kV. The NCO-sP(EO-*stat*-PO) containing fibres proved to be highly hydrophilic as the functional additive was present on the fibre surface. Furthermore, the fibres featured a bulk degradation pattern as a consequence of the proportion of PLGA. Besides the morphologic similarity to ECM fibres, the functionality of the electrospun fibres is also decisive for a successful ECM mimicry. In **Chapter 4**, the passive as well as active functionality of the fibres was investigated. The fibres were required to be protein repellent to prevent an unspecific cell adhesion. This was proven as even 6.5 % sP(EO-*stat*-PO) in the PLGA fibres reduced any unspecific protein adsorption of bovine serum albumin and foetal calf serum to less than 1 %. However, avidin based proteins attached to the fibres. This adhesion process was avoided by an additional fibre surface treatment with glycidol. The active functionalisation of NCO-sP(EO-*stat*-PO)/PLGA fibres was investigated with two fluorescent dyes and biocytin. A threefold, chemically orthogonal, fibre

modification was achieved with these dyes. The chapters about the chemical and mechanical properties laid the basis for the *in vitro* chapters where a specific fibre functionalisation with peptides was conducted to analyse the cell adhesion and biochemical expressions. Beginning with fibroblasts in **Chapter 5** the focus was on the specific cell adhesion on the electrospun fibres. While NCO-sP(EO-*stat*-PO)/PLGA fibres without peptides did not allow any adhesion of fibroblasts, a fibre modification with GRGDS (an adhesion mediating peptide sequence) induced the adhesion and spreading of human dermal fibroblasts on the fibrous scaffolds. The control sequence GRGES that has no adhesion mediating qualities did not lead to any cell adhesion as observed on fibres without modifications. While the experiments of Chapter 5 were a proof-of-concept, in **Chapter 6** a possible application in cartilage tissue engineering was examined. Therefore, primary human chondrocytes were seeded on fibrous scaffolds with various peptide sequences. Though the chondrocytes exhibited high viability on all scaffolds, an active interaction of cells and fibres was only found for the decorin derived sequence CGKLER. Live-cell-imaging revealed both cell attachment and migration within CGKLER-modified meshes. As chondrocytes undergo a de-differentiation towards a fibroblast-like phenotype, the chondrogenic re-differentiation on these scaffolds was investigated in a long term cell culture experiment of 28 days. Therefore, the glycosaminoglycan production was analysed as well as the mRNA expression of genes coding for collagen I and II, aggrecan and proteoglycan 4. In general only low amounts of the chondrogenic markers were measured, suggesting no chondrogenic differentiation. For conclusive evidence follow-up experiments are required that support or reject the findings. The success of an implant for tissue engineering relies not only on the response of the targeted cell type but also on the immune reaction caused by leukocytes. Hence, **Chapter 7** dealt with primary human macrophages and their behaviour and phenotype on two-dimensional (2D) surfaces compared to three-dimensional (3D) fibrous substrates. It was found that the general non-adhesiveness of NCO-sP(EO-*stat*-PO) surfaces and fibres does not apply to macrophages. The cells aligned along the fibres on surfaces or resided in the pores of the meshes. On flat surfaces without 3D structure the macrophages showed a retarded adhesion kinetic accompanied with a high migratory activity indicating their search for a topographical feature to adhere to. Moreover, a detailed investigation of cell surface markers and chemokine signalling revealed that macrophages on 2D surfaces exhibited surface markers indicating a healing phenotype while the chemokine release suggested a

pro-inflammatory phenotype. Interestingly, the opposite situation was found on 3D fibrous substrates with pro-inflammatory surface markers and pro-angiogenic cytokine release. As the immune response largely depends on cellular communication, it was concluded that the NCO-sP(EO-*stat*-PO)/PLGA fibres induce an adequate immune response with promising prospects to be used in a scaffold for tissue engineering.

The **final chapter** of this thesis reports on a first *in vivo* study conducted with the presented electrospun fibres. Here, the fibres were combined with a polypropylene mesh for the treatment of diaphragmatic hernias in a rabbit model. Two scaffold series were described that differed in the overall surface morphology: while the fibres of Series A were incorporated into a thick gel of NCO-sP(EO-*stat*-PO), the scaffolds of Series B featured only a thin hydrogel layer so that the overall fibrous structure could be retained. After four months *in vivo* the treated defects of the diaphragm were significantly smaller and filled mainly with scar tissue. Thick granulomas occurred on scaffolds of Series A while the implants of Series B did not induce any granuloma formation. As a consequence of the generally positive outcome of this study, the constructs were enhanced with a drug release system in a follow-up project. The incorporated drug was the MMP-inhibitor Ilomastat which is intended to reduce the formation of scar tissue.

In conclusion, the simple and straight forward fabrication, the threefold functionalisation possibility and general versatile applicability makes the meshes of NCO-sP(EO-*stat*-PO)/PLGA fibres a promising candidate to be applied in tissue engineering scaffolds in the future.

## Zusammenfassung

Diese Dissertation beschäftigte sich mit der Entwicklung und Untersuchung eines Gerüsts zur Geweberegeneration. Der interzelluläre Raum, der in Geweben für die Gewebestruktur verantwortlich ist, wurde als Vorbild aus der Natur für das entwickelte Gerüst verwendet. Fasern sind in dieser extrazellulären Matrix (EZM) ein charakteristischer Bestandteil, die Adhäsionssequenzen für Zell-Matrix-Interaktionen enthalten und zur strukturellen Organisation der Gewebe beitragen. In der vorliegenden Arbeit wurden Faservliese mit Hilfe des elektrostatischen Verspinnens hergestellt, um die natürlichen Fasern der EZM zu imitieren. Zwei Polymere bildeten die chemische Grundlage für diese Fasern: Ein bioabbaubarer Polyester, Poly(D,L-Laktid-co-Glykolid) (PLGA) und ein funktionales auf Polyethylenglykol basierendes, sternförmiges Polymer, NCO-sP(EO-*stat*-PO). Der erste Teil des in drei Hauptteile untergliederten Themas beschäftigte sich mit dem chemischen Design und der Fasercharakterisierung im Sinne der Materialeigenschaften. Der zweite Teil betrachtet die Auswirkungen der Fasern auf zellulärer Ebene, während der dritte Teil einen ersten Eindruck über die *in vivo* Reaktion auf die Materialien vermittelt.

Die ersten Schritte in Richtung eines elektrostatisch gesponnenen Vlieses begannen mit der Erforschung geeigneter Einstellungen für eine homogene Faserproduktion. **Kapitel 3** thematisiert geeignete Spinnparameter, zu denen auf der einen Seite eine spinnfähige Lösung gehörte, die aus 28.5 w/v% PLGA RG 504 und 6 w/v% NCO-sP(EO-*stat*-PO) in 450 µL Aceton, 50 µL DMSO und 10 µL trifluoressigsaurer wässriger Lösung besteht. Auf der anderen Seite wurden Prozessparameter gefunden, wie zum Beispiel eine Flussrate von 0.5 mL/h und ein Kollektor-Abstand von 12-16 cm, die bei einer Potentialdifferenz von 13 kV ein stabiles Spinnverhalten garantierten. Fasern mit dem Additiv NCO-sP(EO-*stat*-PO) zeigten eine äußerst starke Hydrophilie, da das Additiv während des Spinnprozesses an die Faseroberfläche segregierte. Des Weiteren sind die Fasern dank des PLGA-Anteils nach einem Volumenabbaumechanismus unter physiologischen Bedingungen degradierbar. Neben der morphologischen Ähnlichkeit zwischen natürlichen Fasern der EZM und elektrogewebenen Fasern ist die Funktionalität der synthetischen Fasern entscheidend für eine erfolgreiche Imitation der EZM. **Kapitel 4** betrachtet deswegen sowohl die passive als auch aktive Funktionalität der Fasern. Unter passive Funktionalität fällt das proteinabweisende Verhalten, welches eine unspezifische Zelladhäsion verhindert. Es wurde

gezeigt, dass ein Anteil von 6.5 % sP(EO-*stat*-PO) in den PLGA-Fasern ausreicht, um die unspezifische Adhäsion von Albumin aus Rinderserum und fötalem Kälberserum auf weniger als 1 % zu senken. Dennoch adhärten avidinbasierte Proteine auf den Fasern, was jedoch durch eine Behandlung mit Glycidol unterbunden werden konnte. Die aktive Funktionalisierung wurde exemplarisch mit zwei Fluoreszenzfarbstoffen und Biocytin untersucht. Mit diesen Modellmolekülen wurde eine dreifache, chemisch orthogonale Fasermodifizierung erreicht.

Die Kapitel über die chemischen und mechanischen Eigenschaften haben die Grundlage für *in vitro* Zellversuche gelegt, bei denen eine Faserfunktionalisierung mit Peptidsequenzen durchgeführt wurde, um eine spezifische Zelladhäsion zu erreichen und die biochemische Reaktion der Zellen zu untersuchen. In **Kapitel 5** lag der Fokus auf der spezifischen Adhäsion von humanen dermalen Fibroblasten an den elektrogesponnenen Fasern. Während NCO-sP(EO-*stat*-PO)/PLGA Fasern ohne Peptide keine Zelladhäsion zuließen, induzierte eine Fasermodifikation mit GRGDS, einer adhäsionsvermittelnden Peptidsequenz, sowohl die Adhäsion als auch Ausbreitung der Fibroblasten auf den Fasern. Eine Kontrollsequenz ohne adhäsionsvermittelnde Eigenschaften (GRGES), führte, wie auch Fasern ohne Peptide, zu keiner Zelladhäsion. Die Experimente von **Kapitel 6** gingen über das reine Machbarkeitskonzept von Kapitel 5 hinaus, indem eine mögliche Anwendung im Bereich der Knorpelregeneration untersucht wurde. Daher wurden primäre humane Chondrozyten auf Faservliesen ausgesät, die mit unterschiedlichen Peptiden modifiziert wurden. Trotz einer allgemein sehr guten Vitalität der Zellen auf allen Fasertypen, zeigten die Chondrozyten nur auf Vliesen mit der aus Decorin abgeleiteten CGKLER-Sequenz eine aktive Interaktion. Diese konnte mit dem Live-Cell-Imaging-Verfahren anhand der Zelladhäsion und Zellmigration beobachtet werden. Da Chondrozyten in der 2D-Expansionszellkultur einer Dedifferenzierung in Richtung eines Fibroblasten ähnlichen Zelltypen unterliegen, wurde eine 28-tägige Studie durchgeführt, um das Redifferenzierungsverhalten auf den Fasergerüsten zu untersuchen. Dazu wurde sowohl die Glykosaminoglykanproduktion analysiert als auch die mRNA Expression der Gene, die die Kollagen I und II, Aggrecan und Proteoglykan 4 Produktion regulieren. Die chondrogenen Marker wurden in diesen Versuchen nur geringfügig ausgeschüttet, was in Anbetracht der großen Varianzen in den Messwerten auf keine Redifferenzierung schließen lässt. Für eine abschließende Beurteilung werden Folgeexperimente empfohlen, die die gemachten Beobachtungen bestärken oder

widerlegen. Der Erfolg eines Implantats zur Geweberegeneration beruht nicht nur auf der gewünschten Reaktion des Zielzelltyps, sondern auch auf der Immunreaktion des Organismus, welche durch Leukozyten gesteuert wird. Folglich beschäftigte sich **Kapitel 7** mit dem Verhalten und den Phänotypen primärer humaner Makrophagen auf dreidimensionalen Fasergerüsten und zweidimensionalen Oberflächen im Vergleich zueinander. Bei den Versuchen zeigte sich, dass die generelle Nicht-Adhäsivität von NCO-sP(EO-*stat*-PO) Oberflächen für Makrophagen nicht zutrifft. Die Zellen richteten sich an den Fasern auf den Oberflächen aus oder saßen in den Poren der Vliese. Auf flachen Oberflächen ohne dreidimensionale Struktur wiesen die Makrophagen ein verzögertes Adhäsionsverhalten auf und migrierten stark über die Oberfläche auf der Suche nach topographischen Unebenheiten, um dort adhärent zu werden. Des Weiteren zeigte eine detaillierte Untersuchung der Oberflächenmarker und der Zytokinausschüttung, dass Makrophagen auf 2D-Oberflächen gemäß der Oberflächenmarker einen entzündungshemmenden Phänotypen aufwiesen, während die Zytokinausschüttung einen entzündungsfördernden Phänotypen suggerierte. Interessanterweise bot sich das entgegengesetzte Bild auf 3D-Faseroberflächen. Hier wurde die Erkenntnis gewonnen, dass die Morphologie einen größeren Einfluss auf die Zellreaktion hat als die Oberflächenchemie. Da die Immunantwort eines Organismus auf ein Implantat stark von der interzellularen Kommunikation abhängt, wurde gefolgert, dass die NCO-sP(EO-*stat*-PO)/PLGA Fasern eine adäquate Immunantwort hervorrufen mit vielversprechenden Aussichten, die Fasergerüste im Bereich der Geweberegeneration einzusetzen.

Das **letzte Kapitel** der Dissertation berichtet über eine erste *in vivo* Studie der hier vorgestellten Fasern. Mit den Fasern wurde ein bestehendes Behandlungskonzept für Hernien des Zwerchfells erweitert und die Leistungsfähigkeit in einem Kaninchenmodell überprüft. Zwei Gerüsttypen wurden untersucht, die sich in der Oberflächenmorphologie maßgeblich unterschieden: In Serie A wurden die elektrogewebten Fasern in ein Gel aus NCO-sP(EO-*stat*-PO) gebettet, während die Fasern in Serie B nur mit einer dünnen Gelschicht bedeckt wurden, so dass die topografische Faserstruktur erhalten blieb. Nach 4 Monaten *in vivo* waren die behandelten Zwerchfelldefekte signifikant kleiner und überwiegend mit Narbengewebe gefüllt. Die ausgeprägte Granulombildung bei Fasergerüsten der Serie A konnte in der darauffolgenden Studie (Serie B) minimiert werden. Das gute Abschneiden



dieser Studien wurde zum Anlass genommen, die Vliese weiterzuentwickeln und eine Medikamentenfreisetzung (Ilomastat) zu integrieren, um die Narbenbildung zu minimieren.

Zusammenfassend beschreibt diese Dissertation einen einfachen und direkten Weg, Fasern für eine gezielte Geweberegeneration zu erzeugen, die dreifach funktionalisierbar und vielseitig anwendbar sind. Dies macht Fasergerüste auf der Basis von NCO-sP(EO-*stat*-PO)/PLGA zu einem vielversprechenden Kandidaten um in der Geweberegeneration eingesetzt zu werden.

## Acknowledgement

***Yesterday is history. Tomorrow is a mystery.  
Today is a gift. That is why it is called the present.***

Alice Morse Earle, 1851-1911

The projects of this thesis were conducted in three cities over four years, a truly eventful time. It was in Aachen in 2008, when I started to delve into this topic that began with my diploma thesis. If somebody had asked me, where will you be in three or four years, I would have guessed still in Aachen. However, now in Würzburg, I look back at a very eventful time, having changed my desk and lab countless times, having visited many cities and met a lot of people who became colleagues, project partners and friends. Many of them contributed to this interdisciplinary thesis and now it is time to say a heartfelt “thank you” to them.

First of all, my gratitude goes to Prof. Jürgen Groll for giving me the opportunity to work on this fascinating topic in both Germany and Australia. I appreciate all our fruitful discussions and his unwavering faith in me.

I would also like to thank Prof. Meinel for being my co-corrector and Prof. Möller for the time I spent at the DWI in Aachen. A big thank you goes to my cooperation partners in Aachen: Meike Beer for the fibroblast cell culture and giving me the first induction in cell culture, Dr. Matthias Bartneck for your endless motivation and fun in our cooperation and Dr. Jochen Salber and Dr. Gabriele Böhm for the *in vivo* experiments. Thank you Michaela Meuthrath for all the “stars” you synthesised and sent to me, also thank you Wilfried Steffens for all your constructions in the workshop. Furthermore, my gratitude goes to my research students Florian Störmann, Matthias Kuhlmann, Yoanna Tsvetkova and Tobias Maurell Lopez for their contribution to the experimental work.

From my time in Brisbane, I would like to thank Prof. Dietmar Hutmacher for the invitation to the Medical Device Domain and the warm welcome. Moreover, thank you Dr. Travis Klein for supervising my cartilage project and being an open door for all my concerns. I thank Dr. June Jeon for the help with the chondrocyte cell culture and Dr. Karsten Schrobback for the introduction to the qRT-PCR experiments. Thanks to all members of the Cartilage Regeneration Lab and the rest of the Medical Device Domain for the time you spent with me in the lab and on the beach. Special thanks to Toby Brown for proofreading my thesis.

From my time in Würzburg, I would like to acknowledge Dr. Andrea Ewald for all cell related discussions, Judith Friedlein for the assistance with the SEM measurements and Isabell Biermann for being the “good soul” of the lab. Harald Hümpfer and Anton Hofmann, thank you for the help you gave in all technical matters. Furthermore, I have to thank all cooperation partners whose projects did not make it into this thesis: Antje Appelt, Kathrin Hahn, Ulrike Kriegebaum, Dr. Christian Linz, Samuel Schmidt and Katharina Werner. My gratitude goes to you for your enthusiasm and endurance with the experiments. Thanks to all members of the “AG Groll” in Aachen and Würzburg, for the life and joy you brought to the lab to make it a pleasant time.

To all my friends, I send a heartfelt “thank you” for the necessary distraction from the scientific life with music, games and discussions.

It is invaluable to know I have a safety net if something goes wrong. Therefore, I would like to give special thanks to my family for their love, encouragement and support. Without your faith in me, I would not be where I am today.

## List of publications

1. Bartneck M., Heffels K.-H., Pan Y., Bovi M., Zwadlo-Klarwasser G. and Groll J., 'Inducing Healing-Like Human Primary Macrophage Phenotypes by 3d Hydrogel Coated Nanofibres', *Biomaterials*, 33, **2012**, 4136-4146.
2. Grafahrend D., Heffels K. H., Beer M. V., Gasteier P., Moller M., Boehm G., Dalton P. D. and Groll J., 'Degradable Polyester Scaffolds with Controlled Surface Chemistry Combining Minimal Protein Adsorption with Specific Bioactivation', *Nature Materials*, 10, **2011**, 67-73.
3. Böhm G., Ushakova Y., Alizai H. P., Braunschweig T., Lente C., Heffels K. H., Groll J., Neumann U. P. and Junge K., 'Biocompatibility of Plga/Sp(Eo-stat-Po)-Coated Mesh Surfaces under Constant Shearing Stress', *European Surgical Research*, 47, **2011**, 118-129.
4. Grafahrend D., Heffels K. H., Möller M., Klee D. and Groll J., 'Electrospun, Biofunctionalised Fibers as Tailored *in vitro* Substrates for Keratinocyte Cell Culture', *Macromolecular Bioscience*, 10, **2010**, 1022-1027.
5. Heffels K. H., Gasteier P., Grafahrend D., Salber J., Möller M., Groll J., An easy route to biofunctional electrospun fibres with reactive star shaped PEO-*stat*-PPO based molecules for tissue engineering, *BIOMaterialien*, 9, **2008**, 100.

## Conferences

1. Karl-Heinz Heffels, Michael Schmitz, Gabriele Böhm, Meike V. Beer, Martin Möller and Jürgen Groll, Hernia meshes enhanced with nanofibres for treatment of diaphragm defects, **WITE: Strategies in Tissue Engineering**, May 23-25, 2012, Würzburg. [Oral Presentation]
2. Karl-Heinz Heffels, Jürgen Groll, Bioactivation and 3D Morphology as Tools to Control the Cellular Answer to Hydrogels, **Biomedica 2012**, April 18-19, 2012, Liège. [Oral Presentation]
3. Karl-Heinz Heffels, Dirk Grafahrend, Meike V. Beer, Peter Gasteier, Martin Möller, Gabriele Boehm, Paul D. Dalton and Jürgen Groll, Bioactivation and functionalisation of degradable polyester scaffolds, **Cellular Nano-Sciences**, Juli 3-6, 2011, Heidelberg. [Oral Presentation]
4. Karl-Heinz Heffels, Gabriele Böhm, Meike V. Beer, Martin Möller and Jürgen Groll, *Application of Nanofibre Meshes for Treatment of Diaphragm Hernia*, **IHBI Inspires 2010**, November 25-26, 2010, Gold Coast. [Poster]
5. Karl-Heinz Heffels, Gabriele Böhm, Meike V. Beer, Martin Möller and Jürgen Groll, Application of nanofibre meshes for treatment of diaphragm hernia, **TERMIS-AP 2010**, September 15-17, 2010, Sydney. [Oral Presentation]
6. Meike V. Beer, Karl-Heinz Heffels, Dirk Grafahrend, Martin Möller, Jürgen Groll, *Hydrogel coated electrospun fibres: ECM mimicry through specific cell adhesion*, **Biomedica 2010**, March 17-18, 2010, Aachen. [Poster]
7. G. Böhm, Y. Ushakova, B. Hermanns-Sachweh, T. Braunschweig, J. Groll, K.-H. Heffels, M. Möller, V. Schumpelick, *Biocompatibility of PLGA / sP(EO-stat-PO)-coated mesh surfaces under constant shearing stress*, **Biomedica 2010**, March 17-18, 2010, Aachen. [Poster]

8. K.-H. Heffels, P. Gasteier, D. Grafahrend, J. Salber, P. D. Dalton, M. Möller, J. Groll, *An easy route to biofunctional electrospun fibres with reactive star shaped PEG based molecules for tissue engineering*, **1. Neujahrs – Symposium RWTH Aachen**, January 09, 2009, Aachen. [Poster]
9. K.-H. Heffels, P. Gasteier, D. Grafahrend, J. Salber, P. D. Dalton, M. Möller, J. Groll, *An easy route to biofunctional electrospun fibres with reactive star shaped PEG based molecules for tissue engineering*, **Aachen-Dresden International Textile Conference**, December 04-05, 2008, Dresden. [Poster]
10. D. Grafahrend, R. Lösel, J. Lleixà Calvet, K. Klinkhammer, K.-H. Heffels, P. Gasteier, J. Groll, J. Salber, P.D. Dalton, M. Möller, D. Klee, *Biofunctionalised electrospun fiber scaffolds showing reduced unspecific protein adsorption*, **International Colloquium Biointerface „Detection and Control of Surface-indicated Biomolecular and Cellular Functions“**, June 22 – 25, 2008, Kerkrade, The Netherlands [Poster].
11. K.-H. Heffels, P. Gasteier, D. Grafahrend, J. Salber, M. Möller, J. Groll, *An easy route to biofunctional electrospun fibres with reactive star shaped PEO-stat-PPO based molecules for tissue engineering*, **World Biomaterials Congress**, 2008, Amsterdam [Oral Presentation].

## Curriculum Vitae

Karl-Heinz Heffels

born 23 May 1983 in Geilenkirchen

### OCCUPATION

05/2011 – 09/2012 University of Würzburg  
Department for functional materials in medicine and dentistry

09/2010 – 04/2011 Queensland University of Technology, Brisbane, Australia  
Institute of Health and Biomedical Innovation

09/2008 – 08/2010 RWTH Aachen University, DWI e.V.

### ACADEMIC STUDIES

09/2008 – 09/2012 University Würzburg  
PhD studies in chemistry

04/2006 – 08/2006 Norwegian University of Science and Technology, Trondheim  
Research visit, Erasmus-scholarship  
Department of Chemistry

04/2003 – 07/2008 RWTH Aachen University  
Chemistry studies

### SCHOOL

08/1993 – 06/2002 Kreisgymnasium in Heinsberg

### AWARDS AND SCHOLARSHIPS

09/2010 – 04/2011 DAAD PhD student scholarship for a research visit in Australia

05/2008 – 06/2008 Travel award to the World Biomaterials Conference 2008 in  
Amsterdam of „Deutsche Gesellschaft für Biomaterialien e.V.“

04/2006 – 07/2006 ERASMUS scholarship for one research semester in Norway